Silicate weathering in soils:
A solution for soil pH management?

Jostein Soldal

Master of Science Thesis

Department of Earth Science

University of Bergen

September 2015

Abstract

N_2O released form agricultural soils is mainly a product of denitrification; a key microbial process in the N cycle. The relative rate of N_2O released from this process depends of the soil pH, where the relative amount of N_2O to denitrified N (N_2O/N_2+N_2O) increase in more acidic soils. pH management in soils is mainly based on carbonate based liming, which will release CO_2 to the atmosphere during dissolution or at later acidification. Use of non-carbonate rock powders for pH management in agriculture can thus significantly decrease greenhouse gas emissions if they increase soil pH sufficiently. Mafic minerals have basic reactions and dissolve slower than dolomite and calcite. This thesis presents laboratory dissolution experiments examining the dissolution mechanisms in soils and compare dissolution rates and pH increase capacity of a set of rock samples, including the effect of mineral and organic acids.

The work was divided in two parts. Part one was examination of olivine and anorthosite dissolution in soils using a scanning electron microscope after 1.5 years of soil incubation. The purpose of the examination was to identify and quantify visible dissolution structures, and examine if the observed dissolution features were most likely to increase or inhibit further dissolution.

The purpose of the experiments in part two was to measure and compare the pH increase, dissolution rates and heavy metal leaching of olivine, anorthosite, dolomite, nepheline syenite, larvikite, eclogite and norite under acidic conditions. The acids used were HNO_3, HCl, oxalic acid, acetic acid (+ HCl) and a combination of peat soil and HCl. The experiments were conducted in stirred, open batch reactors at room temperature with initial pHs from 1 to 3, where pH was allowed to increase freely upon reaction with minerals.

Fractures, etch-pits and silica-layers were present on both olivine and anorthosite grains after 1.5 y in peat soil. In addition some olivine grains display serpentinization features and Al oxide-layers. The olivine grains were generally far more weathered than the anorthosite grains, and they also increased the soil pH more (pH 4.4 vs 4.0) respectively. The formation of silicate layers can probably inhibit dissolution, however it seems as the silicate layers break up and flake off over time, and they are typically not found on the same surfaces as acid pitting was found. Fractures and etch-pits will increase the grain surface area, however it is uncertain if the formation of etch-pits increase the reactive surface area, particularly in anorthosite.

Olivine, nepheline syenite and norite gave the highest pH increase of the silicates (but lower than dolomite). Dissolution rates were decreasing with increasing pH. Organic acids or peat soil slurry had a significant effect compared to HCl, however the effect of chelating agents was different between the

rock types, and the relative order of dissolution rates between rocks were not altered by adding acids with chelating effects. Oxalic acid and peat soil seem to increase the dissolution and solubility of heavy metals as Ni more than major elements as Mg or Ca. High concentrations of Ni in norite and olivine and leachates might lead to restrictions in use for agricultural purposes.

Acknowledgements

The work presented in this thesis was carried out at the Centre for Geobiology (GCB) at the University of Bergen from 2013-2015 and has been funded by the Mitigation of Greenhouse gas emissions from cropped soils by mafic mineral applications (MIGMIN) project. I would like to thank the industrial partners for providing sample materials and funding of the project: Titania AS, Larvik Granite, Lundhs, Franzefoss Minerals, YARA, OMYA and Oslo Kommune. I'd also thank Sibelco Europe, Nordic Mining and Prof. Marina Bleken at NMBU for providing rock samples.

I very much want to thank my supervisors Pål Tore Mørkved and Ingunn Hindenes Thorseth for excellent guidance along the way. I also want to thank Pål Tore for the opportunity to attend two MIGMIN project meetings.

My gratitude also goes to a number of people at the University of Bergen and Institute for Energy Technology (IFE) who have assisted in technical analyses during this investigation. I would like to thank Maria Dimitru for help in preparation of sample material for major element analyses and to Ole Tumyr for running the XRF-analyses. Siv Hjortnes Dundas and Hildegunn Almelid are thanked for preforming numerous ion concentration analyses. Dr. Romain Meyer conducted the rock-digestion and trace element analyses on the sample material. Dr. Mali Husby Rosnes preformed the BET specific surface area measurements. The XRD analyses were preformed by Dr. Farhana Huq at IFE. Egil Erichsen and Irene Heggstad were very helpful during my many hours with the scanning electron microscope.

Table of contents

1 Introduction

This thesis is a part of the "Mitigation of Greenhouse gas emissions from cropped soils by mafic mineral applications" (MIGMIN) project, with collaborators from the University of Bergen (UIB), Institute for energy technology (IFE) and Norwegian University of life science (NMBU). The project involves laboratory and field experiments investigating practical amendments, mineral/rock sample characteristics and greenhouse gas (GHG) mitigation possibilities. This thesis includes several laboratory experiments on silicate minerals in connection with a field-experiment conducted at NMBU, Ås.

1.1 Greenhouse gas emissions from agriculture

Nitrogen it is an essential component in many biomolecules, including proteins, DNA and chlorophyll and is one of the vital elements for sustaining life on this planet. Even though nitrogen gas (N_2) composes approximately 78% of the atmosphere it is mostly not accessible to organisms. Nitrogen gas has to be converted into ammonia (NH_3) to become available for primary producers, such as plants. Transformation of nitrogen into its different oxidation forms is very important for productivity in the biosphere and is very dependent on activities by microorganisms. The major reactions in terms of nitrogen transformation are nitrogen fixation, nitrification, denitrification, anaerobic ammonium oxidation (anammox) and ammonification (Fig 1.1). There are two natural processes of making nitrogen gas (N_2) bioavailable, microbial nitrogen fixation and lightning. Converting nitrogen gas demands a lot of and hence only a few groups of prokaryotes can execute this process. Nitrogen can also be fixed through industrial processes such as Haber-Bosch process (mainly to produce N fertilizers) or as a byproduct of combustion (e.g. in engines). Nitrogen fertilizer is applied to cropped soils worldwide and massively increases the amount of bioavailable nitrogen. The use of fertilizers in agriculture leads to a higher rate of denitrification and thus elevated levels of emitted greenhouse gases from cropped soils, especially nitrous oxide (N_2O). N_2O in soils is produced during microbial redox transformations and one of the limiting factors is the abundance of bioavailable nitrogen in the soil. The use of fertilizers in agriculture is still increasing, especially in developing countries, and will most likely prolong for some time with present population growth and urbanization (Vitousek et al., 1997). A constant harvest of cropped fields demands refill of nutrients as the natural weathering of rocks incorporated in the soil is not fast enough to sustain nutrient requirements to the annual food production.

73% of the total N_2O emissions in Norway are from agricultural systems and hence a reduction of N_2O emissions from cropped land can be a valuable contribution in the effort to reduce climate gas (Bye et al., 2014). Emissions of N_2O from agriculture is a result from food production and mitigation of these gases is difficult because the production systems are very complex and methods that reduce individual sources of N_2O often enhances others (Smith et al., 2007). Emissions of N_2O is controlled by a wide range of physical, chemical and biological factors and previous attempts to reduce emissions seemed only to work under certain conditions (Stehfest and Bouwman, 2006). Denitrification is an anaerobic microbial process that removes bioavailable nitrates by converting nitrates into nitrogen gas (N_2) (Fig 1.1). Denitrification is thus closing the N cycle, and all N fixed from the atmosphere will at some point be denitrified if reactive N is not accumulated in the biosphere. One of the intermediate steps produce nitrous oxide (N_2O) and nitric oxide (NO), which both are considered greenhouse gases contributing to air pollution, although nitrous oxide contributes much more. The reactions are performed by a wide diversity of procaryotes, e.g. Thiomicrospira denitrificans live in anaerobic and aerobic soil and are capable denitrification.

Denitrification: $\mathbf{NO_3^- \rightarrow NO_2^- \rightarrow NO + N_2O \rightarrow N_2}$

One factor that have been considered a key variable is soil pH. Nömmik (1956) discovered that acidic environments have an increasing effect on denitrification and hence N_2O emissions, however all mechanisms involved were not fully understood, including the pH effect on the $N_2O/(N_2O+N_2)$ product ratio. New research from the NMBU Nitrogen group have discovered that high pH lowers the $N_2O/(N_2O+N_2)$ production ratio, implying that elevating soil pH is crucial in order to reduce N_2O emissions (Bergaust et al., 2010; Liu et al., 2010; Raut et al., 2012; Qu et al., 2014).

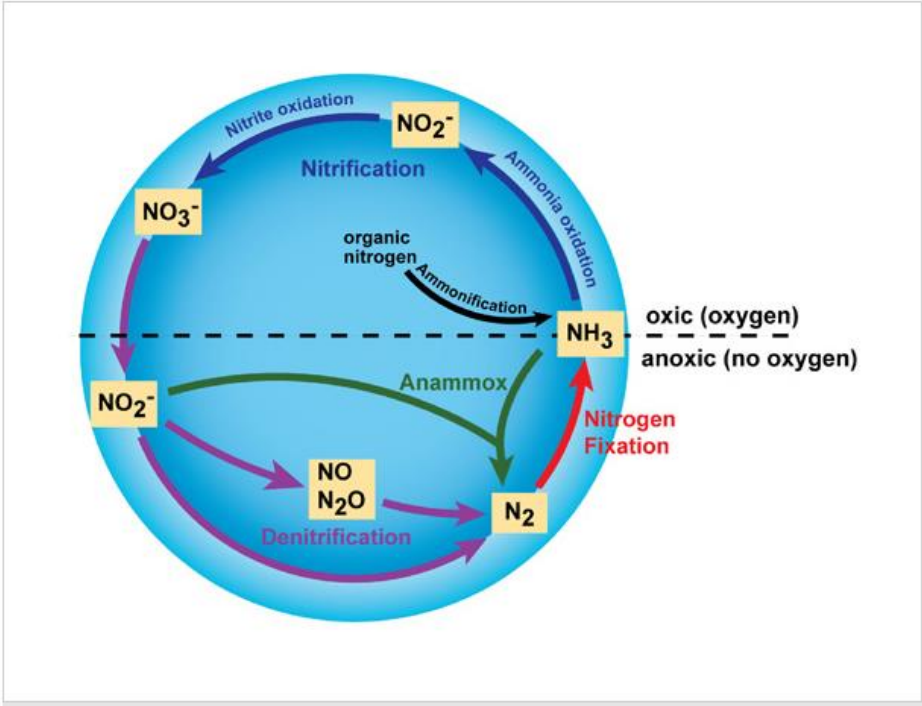

Fig 1.1 Illustration of the nitrogen cycle, showing the reaction path from fixation of nitrogen gas (N_2) to ammonia (NH_3) and all the way around back to nitrogen gas (N_2). It is worth noting that the top half of the circle represent oxic conditions and the bottom half anoxic conditions (Bernhard, 2010).

The pH is important for several soil processes, such as nutrient bioavailability, microbial activity and root growth and the optimal pH for most cropped soils is typically 6.5-7 (Gregory, 2012). Presently limestone ($CaCO_3$) and dolomite ($MgCa(CO_3)_2$) is applied to most moderately acidic cropped fields to increase pH in terms of improving crop quality. However, the fast pH increase caused by weathering of carbonates effects several biological processes and enhance N_2O emissions on a short term (Baggs et al., 2010). Application of fertilizers and limestone/dolomite to soils occurs at such a rate that there will be a constant imbalance in the soil. Dissolution of carbonates increase pH by the consumption of H^+ ions in the formation of bicarbonate.

$$CaCO_3 + 2H \leftrightarrow HCO_3^- + H^+ + Ca^{2+} \leftrightarrow H_2CO_3 + Ca^{2+} \leftrightarrow CO_{2(g)} + H_2O + Ca^{2+}$$

This reaction implies that liming potentially might cause release of CO_2 to the atmosphere if acidic conditions reoccur in the soil. On the other hand, it has a great potential for C sequestration if pH is maintained high enough. What happens with the bicarbonate in the soil solution determines whether C emission or sequestration happens (Sanderman, 2012). For C sequestration to be possible, bicarbonate must be transported to a stable long time reservoir, such as the ocean or groundwater. On the contrary, if bicarbonate is exposed to continuous acidification in the initial soil or migrates to other open acidic environments, it might cause a net release of atmospheric CO_2.

In order to reduce emissions from agriculture it is proposed that another rock/mineral is applied for neutralizing acidic soils. One option is silicates of mafic composition, as these have relatively high dissolution rates. Most mafic silicates are rich in cations such as Ca^{2+}, Mg^{+2} and Fe^{+2}, which in addition to be important nutrients for soil biology has a the potential to trap CO_2 as thermodynamically very stable carbonate minerals (Lackner, 2002)**.** A mafic mineral/rock could possibly achieve a similar slightly basic environment as limestone/dolomite, without the fast initial increase, and because of a lower dissolution rate obtain the high pH for a longer time.

1.2 Silicate minerals and rocks

The vast majority of mineral and rocks on the Earth's surface are silicates, composing 95 % of the continental crust. Chemical weathering of minerals is a fundamental processes in the geological cycle as it effects a large variety processes including element cycling, porosity in soil reservoirs, ore deposits, soil formation and soil fertility (Wilson, 2004; Brantley, 2008b). Dissolution kinetics are complex and hence a lot of research have been done in order to get a better understanding, e.g. (Lasaga, 1984; Lasaga and Blum, 1986; Swoboda-Colberg and Drever, 1993; Oelkers et al., 1994; Golubev et al., 2005). This thesis includes dissolution experiments on various silicate rocks and therefore a brief overview of silicate mineral structure and dissolution kinetics is given in the following sections.

1.2.1 Geochemical composition

Silicate rocks are classified into four main groups: ultramafic, mafic, intermediate and felsic rocks. Classification are mainly based on silica (SiO_2) content, where felsic rocks contain about 66-76% silica, intermediate about 52-66%, mafic about 45-52% and ultramafic about 38-45%. The amount of silica is related to crystallization temperature of a melt (Fig. 1.2). A high crystallization temperature correlates with an ultramafic composition and elevated concentrations of Mg, Ca and Fe. While a low crystallization temperature correlates with a felsic composition and elevated concentrations of Na, Al and K. The amount of silica also reflects the relative rock/mineral stability observed at surface conditions where high concentrations of silica correspond to high stability and slow dissolution rates and low silica concentration indicate lower stability and a higher dissolution (Marshak and Prothero, 2008).

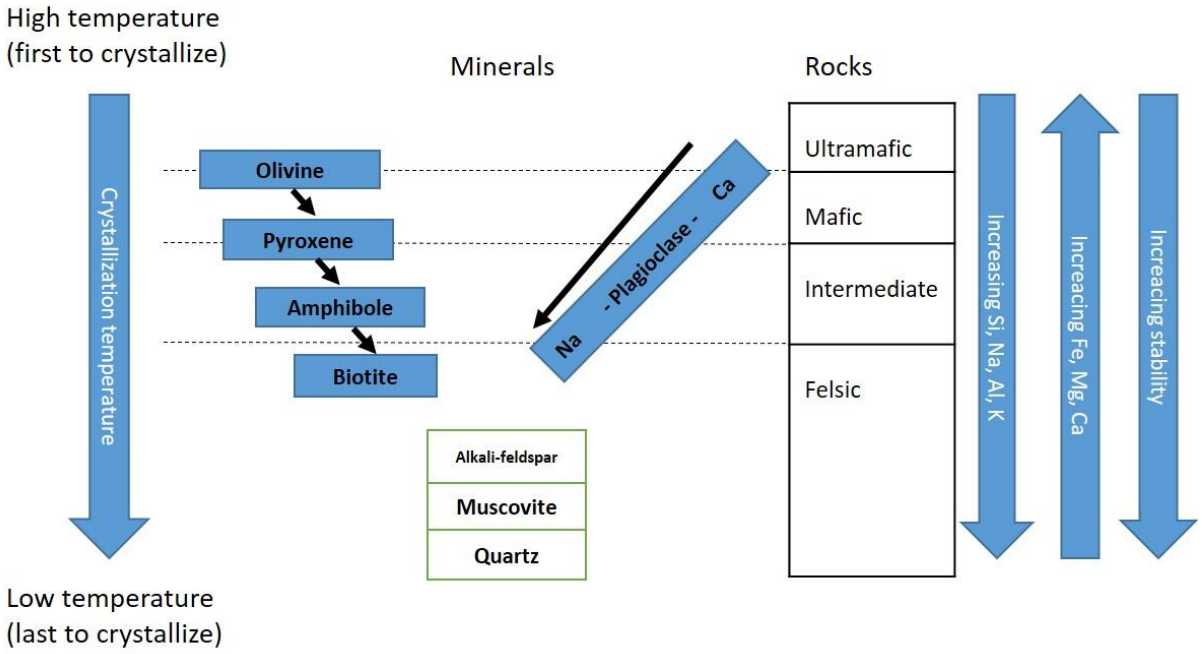

Fig. 1.2 Illustration of how crystallization temperature is related to element concentrations and rock/mineral relative stability observed at surface conditions. Figure modified from Marshak and Prothero (2008)

1.2.2 Internal structure

The SiO_4 tetrahedron is the fundamental building block in all silicate minerals. It is composed of a Si^{4+} ion in the centre surrounded by four O^{2-} ions at the corners. The oxygen ions are capable of binding to several Si ions, changing the silicate structure. The degree of polymerization by sharing O ions between Si ions, is the basis of the classification of the silicate minerals (Table 1.1).

Table 1.1 Classification of main rock forming silicate minerals based on numbers of shared oxygen per tetrahedron. Modified from Nesse (2009).

Silicate Class	**Number of O^2-shared per Tetrahedron**	**Z:O Ratio**	**Structural Configuration**	**Common mineral**
Orthosilicates	0	1:4	Isolated tetrahedra	Olivine, garnet
Chain silicates-				
- Single chain	2	1:3		Pyroxenes
- Double chain	2 or 3	4:11		Amphiboles
Sheet silicates	3	2:5	Sheets of tetrahedra	Biotite, muscovite
Framework minerals	4	1:2	Framework of tetrahedra	Quartz, feldspars

The degree of polymerization is linked to the relative abundance of silicon during mineral growth, thus a high grade of polymerization requires high levels of silicon. Increased grade of silica polymerization increases the structure stability, hence making the minerals more sustainable to chemical weathering (e.g. Kump et al., 2000). One complicating factor is the substitution of Si with Al in the tetrahedral structure, which causes a valence electron deficiency. To compensate there has to be an additional cation substitution in order to achieve electron charge neutrality. For example in plagioclase feldspar the coupled substitution between albite ($NaAlSi_3O_8$) and anorthite ($CaAl_2Si_2O_8$), Ca^{2+} substitute for Na^+ and Al^{3+} for Si^{4+}, making the structure less stable.

1.2.3 Chemical weathering

Minerals may dissolve congruently, which means that the mineral is totally dissolved into solution, (e.g.carbonates), or they may dissolve incongruently (e.g. aluminum silicates), which means that a secondary mineral or product mineral phase (e.g. clay) is formed. Silicate weathering is a slow process and its effect on river and groundwater chemical compositions are very gradual, compared to carbonate dissolution. However, because of the high abundance in the continental crust it is estimated that silicate weathering contribute to 45% of total dissolved solids in rivers and is an important CO_2 sink (Stumm and Wollast, 1990). During the last decades numbers of studies have been done on silicate dissolution, both experimentally and naturally (e.g. Swoboda-Colberg and Drever, 1993; Ullman et al., 1996; Oelkers, 2001b; Wilson, 2004).

Based on dissolution rates obtained from laboratory experiments, Lasaga et al. (1994) calculated the mean lifetime of 1 mm diameter crystals of various minerals at 25°C and pH 5 (Table 1.2). These calculations are in good agreement with the relative mineral stability obtained from field observations (Fig. 1.2) and illustrate a large variation in dissolution rates for various silicates.

Mineral dissolution mechanisms are very complex reactions and are not yet completely understood. There are many influencing factors and minerals may dissolve differently and at different rates depending on their internal crystal structure, chemical composition and the properites of the reacting solutions (e.g. Oelkers and Schott, 2001; Lüttge et al., 2013).

Table 1.2 Mean lifetime of 1mm crystals at 25°C and pH 5, retrieved from Lasaga et al. (1994) and references within.

Mineral	Log rate (mol/m^2/s)	Life time (years)
Quartz	-13.39	34,000,000
Kaolinite	-13.28	6,000,000
Muscovite	-13.07	2,600,000
Epidote	-12.61	923,000
Microcline	-12.50	921,000
Prehnite	-12.41	579,000
Albite	-12.26	575,000
Sanidine	-12.00	291,000
Gibbsite	-11.45	276,00
Enstatite	-10.00	10,100
Diopside	-10.15	6,800
Forsterite	-9.5	2,300
Nepheline	-8.55	211
Anorthite	-8.55	112
Wollastonite	-8.00	79

One basic mechanism describing element leaching on mineral surfaces is proton-promoted dissolution, where metal-oxygen bonds are broken and replaced by proton-oxygen bonds (Furrer and Stumm, 1986). It is suggested that the metal-proton exchange continues until no viable structure remains. The last of these exhanges destroy the structure and in most cases is irreversible. The last exchange is also the slowest and is the rate controlling step. Not all bond must be broken in order to destroy all mineral structures. For instance, Oelkers (2001a) showed that a forsterite structure, containing Mg-O and Si-O bonds, can be destroyed at low pH by only breaking the Mg-O bonds. A summary of various dissolution mechanisms at acidc conditions is illustrated in Fig. 1.3. Proton-promoted dissolution may not adequtly describe complex surface dissolution mechanisms, but it gives an idea about how it happens.

Crystal defects and orientation of the crystal structure can cause dissolution rate variations in similar minerals. Imperfections in the crystal structure such as line- and planar defects may cause variations in the dissolution kinetics. Different crystal faces may have different activation energies/dissolution rates, e.g. olivine (Awad et al., 2000). Adsorption of molecules on the mineral surface can diminish or enhance dissolution rates depending on the adsorbed molecule.

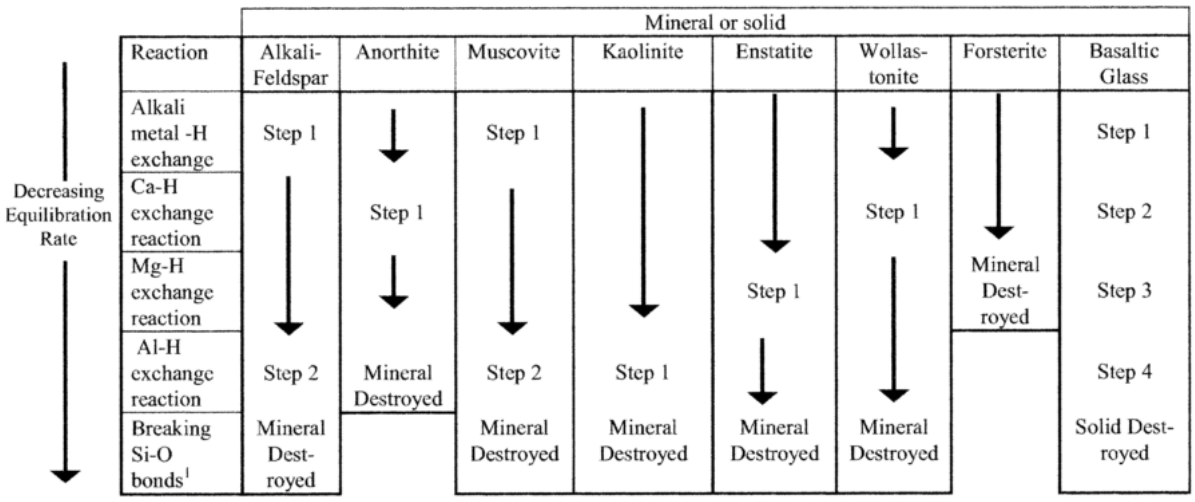

Fig. 1.3 Summary of dissolution mechanisms of some silicate minerals and basaltic glass at acidic conditions. Instead of Si-H exchange H_2O adsorption is likely involved in the breaking of Si-O bonds (Dove and Crerar, 1990). Figure retrieved from Oelkers (2001b).

The solution properties also have a great influence on mineral weathering. One important factor influencing dissolution rates is pH. Aluminum silicates have a distinct minimum dissolution rate at around neutral pH and increasing rates as the solution becomes more acidic and basic. It is also imminent that the effect of pH varies between the minerals, e.g. for forsterite and albite (Rimstidt et al., 2012; Gudbrandsson et al., 2014). The activity of leached cations in a solution is also predicted to effect the dissolution rates of various silicates such as pyroxenes, amphiboles and feldspars (Brantley, 2008b). Cation concentrations are not assumed to have an effect on forsterite and anorthite dissolution, because complete leaching of Al and Ca (anorthite) or Mg (forsterite) leaves the Si tetrahedra without any bridging oxygens.

The presence of organic acids and microbes may also influence mineral dissolution rates, but the impact is debated (Drever and Stillings, 1997; Meheruna and Akagi, 2006). Drever and Stillings (1997) and Declercq et al. (2013) imply that concentrations of organic acids in soil solutions are generally insufficient to cause a significant increase in dissolution rates, however higher concentrations may be present in microenvironments. Density of bacteria are rarely high enough to have an impact on dissolution rates except in microenvironements, where they might increase or inhibit further dissolution (Ullman et al., 1996). The extent of microbial activity also depends on mineral composition. From an in situ micocosms experiment where minerals were exposed to bacteria, Bennett et al. (1996) observed that surfaces of a microcline (K-rich feldspar) were more deeply weathered than an albite (Na-rich feldspar). This difference in dissolution is most likely because the bacteria were K limited and thus attacked the microcline.

The many factors effecting silicate dissolution and rate-limiting processes may be difficult to anticipate as they may vary. Numerous laboratory studies have been done to understand silicate dissolution mechanics, however there are difficulties in correlating dissolution rates from different laboratory experiments with weathering rates observed in natural environments (Fischer et al., 2012; Futter et al., 2012; Hellmann et al., 2012; Lüttge et al., 2013).

1.3 Rock-flour applications

The use of silicates as a nutrient supply in agriculture is widely investigated and regarded as a necessary asset to accommodate future food production (Harley and Gilkes, 2000). The agronomic effect of rock-flour depends on several factors, e.g. mineral and soil characteristics, the main implication for rock-flour is to enhance mineral dissolution for increased nutrient release (Van Straaten, 2006). It has also been suggested that geoengineering using olivine could sequester CO_2 by the formation of $MgCO_3$. Schuiling and Krijgsman (2006) suggested that applications of olivine to acidic soils could cause precipitation of Mg-carbonates to capture CO_2. Hangx and Spiers (2009) investigated the effect of coastal spreading of olivine, and concluded that a grain size of <10µm is needed to obtain adequate dissolution rates, but it is not a viable method for CO_2 sequestration. There are uncertainties in the effect of mineral carbonation (Power et al., 2013) The primary idea of the MIGMIN project is to replace limestone/dolomite with silicate rocks and thus reduce the direct emissions from carbonate dissolution.

This thesis includes several laboratory dissolution experiments of different silicate minerals/rocks in connection with large-scale field experiments performed at NMBU. The chosen materials are relevant for the mining industry, in order to possibly create an alternative use of excess mine tailings. The materials originate from different locations in Norway and an additional intension is to have the shortest possible transport distance of the material to applicable agricultural system. From here on the common denomination is material, even though there also are both mineral and rock samples.

The thesis can be divided into two parts:

Part one is a follow up of a currently unpublished laboratory microcosm experiment, where olivine, anorthosite, dolomite and quartz (control) were incubated in two different acidic soils (Mørkved, personal communication). The purpose of the study was to experimentally examine N_2O and CO_2 emissions from soils by the use of alternative pH management, using silicates instead of carbonates. As the experiments showed significant effect on pH and N_2O emissions from soils, it strengthens the

hypothesis that mafic silicate minerals can dissolve fast enough to be used for soil pH management (increase) and that this will reduce N_2O emissions. For the current study, olivine and anorthosite grains were extracted from the microcosms soils and examined for surface dissolution features. Part two is dissolution experiments done under different pH conditions and different types and concentrations of organic and inorganic acids.

1.4 Objectives

Part 1

- Examine and quantify the occurrence of dissolution features on soil incubated olivine and anorthosite mineral surfaces by scanning electron microscope (SEM).
- Examine if any observed dissolution features indicate that dissolution most likely progress at similar or increased rates (e.g. through increase of surface area) or if inhibition (e.g. through precipitation of secondary products) was most likely.

Part 2

- Compare and quantify the pH increasing capacity and dissolution rates of the different silicate materials potentially available for application at an agronomically relevant scale.
- Investigate the potential chelating effects of organic acids on dissolution rates of the same materials.
- Quantify and compare heavy metal release from the same set of materials.
- Propose silicate materials best suited for field experiments.

2 Materials and methods

2.1 Minerals and rocks

Most of the materials used in this study are supplied from different industrial companies, meaning that the materials are chosen based on industry relevance and availability. Experiments are done in order to get a understanding of dissolution kinetics and how dissolution of certain mineral effect pH under laboratory conditions and to relate the results to natural dissolution in soil.

The materials used are from a variety of locations and were from the same sites for all experiments (Table 2.1). However due to the time shift between experiments and the dependence of other activities, materials were subsampled and prepared in several batches and thus are not necessarily identical. The specific materials were selected to represent different groups of mafic rocks with different expected dissolution rates. In addition dolomite was included as a reference material as it is commonly used in agriculture.

Table 2.1 Overview of rock and minerals, source locations and company.

Samples	**Location**	**Company**
Olivine	Åheim	Sibleco Europe
Anorthosite	Gudvangen	
Norite	Sokndal	Titania AS
Larvikite	Larvik	Larvik Granite/Lundhs
Eclogite	Engbøfjellet	Nordic Mining AS
Dolomite	Ballangen	Franzefoss Minerals
Nepheline syenite	Stjernøy, Alta	Franzefoss Minerals/ Sibelco Europe
Basaltic glass	Knipowich ridge, North Atlantic	Center for Geobiology (UIB archive)

Most of the materials used are excess masses from some kind of mineral production, except olivine (Green lightening product), dolomite (agricultural dolomite) and basaltic glass (no commercial production). Most materials did not have pre-treatment before they were delivered and the grains sizes varied from very fine to quite coarse. As these masses do not have a specific marked, many companies have vast amounts piling up. Experiments conducted on these materials are an initial stage

of finding a beneficial application area of these masses. Eight different materials were included in different parts of the experiments.

2.1.1 Olivine

Olivine was provided by Sibelco Europe from an active peridote quarry in Almklovdalen, Åheim, Norway. The olivine crystals are representative from a dunitic mantel rock (Moore and Qvale, 1977; Medaris Jr, 1984). Olivine is a mafic mineral forming a solid solution series with two endmembers forsterite (Mg_2SiO_4) and fayalite (Fe_2SiO_4), with naturally occurring olivine generally richer in magnesium (Johnson et al., 2004). The olivine from Åheim contains approximately Fo_{89}-Fa_{11} component and have traces of enstatite, talc, chlorite and antigorite (Martinez et al., 2014). Further information considering the peridote body and Almklovdalen can be found in e.g. Cordellier et al. (1981) and Carswell et al. (2003). The product delivered is called Green Lighting and is mainly used as slag conditioner, foundry, reactionary and abrasives. DEBIO has approved olivine sand as an ecological fertilizer for agricultural applications (Vold, 2006).

2.1.2 Anorthosite

Anorthosite is collected from an open crop in Gudvangen, which is a part of the Gudvagen-Mjølfell massif in western Norway, and crushed to rock flour at IFE, Kjeller. Anorthosite is an igneous rock composed of 90-100 volume % plagioclase feldspar. Plagioclase is in a solid solution series with two endmembers albite ($NaAlSi_3O_8$) and anorthite ($CaAl_2Si_2O_8$). According to Wanvik (2010) the general anorthite content in the Sogn massifs varies between 60-78 %. The site operated by Gudvangen Stein AS consists of white rock, which is a low An-anorthosite, but aluminium rich. Anorthosite has a varied spectrum of industrial application including abrasives, building materials, silicon production, ceramics, mineral wool, etc. (Wanvik, 2000). The high Al_2O_3 content in Sogn-Voss region anorthosite is also an alternative source of aluminium ore for the Norwegian aluminium industry (Wanvik, 2000).

2.1.3 Norite

The Norite is a cyclone fraction provided by Titania AS from the Tellnes orebody quarry in Sokndal. The Tellnes orebody is an ilmenite norite lens emplaced in the Åna-Sira massif-type anorthosite, belonging to the Rogaland anorthosite province (Wilmart et al., 1989). By definition norite rock consists of >90% plagioclase and orthopyroxene. Titanium has several industrial applications among others in paints,

varnishes, paper and in cosmetic products. Further information regarding the Tellnes orebody can be found in e.g. Charlier et al. (2007) and Wilmart et al. (1989).

2.1.4 Larvikite

The larvikite sample is drill dust from the production of "Emerald Pearl" from the Kålstad quarry in Larvik, provided by Larvik Granite and Lundhs AS. Larvik town is situated close to the centre of the main larvikite plutonic complex, the complex has a ring-shaped structure defined by several different intrusions (Heldal et al., 2008). Quarrying has been carried out in several places of the pluton, but the area around Larvik has developed to be a permanent and sizeable industry, and Kålstad quarry is one of these areas. Larvikite is mainly composed of feldspar, and may have minor Ca-pyroxene, olivine and amphibole, among others. Larvikites are seen as a very attractive dimension stones. More information regarding the larvikite plutonic complex can be found in e.g. Heldal et al. (2008).

2.1.5 Eclogite

Eclogite is provided by Nordic Mining from Engbøfjellet, western Norway. Engbøfjellet eclogite forms a 2.5km long E-W trending lens and is a part of the Hegreneset complex (Korneliussen et al., 1998). The eclogite is belived to have originated from the a Proterozoic gabbroic intrusion, enrichment of Fe and Ti comes from crystal fractionation processes and the transformation to eclogite happened during the Caledonian orogeny (Korneliussen et al., 1998). During the metamorphic processes ilmenite has been replaced by rutile. The Engbøfjell eclogite body is subdivided into two major eclogite types, 1) the ferro eclogite is Fe_2O_3, TiO_2 and garnet rich, > 14% Fe_2O_3, >3 % TiO_2 and 25% garnet. 2) The leuco- and transitional eclogite is Fe_2O_3 and TiO_2 poor. The Engbøfjellet eclogite is going to be mined for titanium in rutile by Nordic Mining and the excess material is planned to be deposited at the bottom of Førdefjorden (Agency, 2015).

2.1.6 Dolomite

Dolomite is provided by Franzefoss Minerals. The product delivered is commercial dolomite called Environmental-Lime (Miljøkalk) and is applied in areas of agriculture, construction, watercourse liming, etc. The dolomite products are mined in Ballangen, Nordland. While lime products are from Hole (Toten) and Hamar. The dolomite in Ballangen is a part of Evenes nappe complex in Northern Nordland (Roberts and Zwaan, 2007). This commercial dolomite is used as a reference point for the other samples during the experiments.

2.1.7 Nepheline syenite

Nepheline syenite is excess material from the production of nepheline syenite from Stjernøya quarry in Finnmark, provided by Sibelco Europe. The nepheline syenite body is a part of the Lillebukt Alkaline complex situated on the southern central part of Stjernøya. The Lillebukt Alkaline Complex is further a part of the Seiland Igneous Province, which is a part of the Kalak Nappe Complex (Gautneb et al., 2009; Roberts et al., 2010). Metagabbros are the host rock and makes a major part of Stjernøya, the nepheline syenite is one of many intrusions penetrating the host rock (Gautneb et al., 2009). Nepheline syenite (Altagro) is approved by DEBIO as an ecological fertilizer for agricultural applications (Vold, 2006).

2.1.8 Basaltic glass

Basaltic glass is a sample from the University of Bergen archive collected the Knipovich Ridge in the North Atlantic. The sample was gathered on a cruise with the G. O. Sars with the Center of Geobioloigy (UIB) using a ROV. The Knipovich Ridge is an Ultra-slow spreading ridge located in the northernmost part of the Mid Atlantic ridge system, and have thus no direct industrial relevance here. Basalts mainly consist of pyroxene and plagioclase, however as basaltic magma comes in contact with cold seawater the chemical species do not have the time to get arranged into their mineral phase and the outer 1-2 cm freezes to an amorphous glass rind. Because basaltic glass has a mafic composition, was available at experiment start and dissolution mechanisms have been previously studied (Oelkers and Gislason, 2001), it was partly included in the experiment as a reference point.

2.1.9 Soil

The soil used in this thesis is from a meadow with no liming and with pH 4.1 in Fureneset in Fjaler, western Norway. The soil is classified as a Sapric Histosol (Mørkved, Personal communication), organic soil, for details see (Sognnes et al., 2006). After the soil incubation experiment by Pål Tore Mørkved mineral grains of olivine and anorthosite was extracted from this soil. This was the soil mixed with an HCl solution and used as an acid solution in experiment 3.

2.2 Experiments

The experiments included in the thesis are summarized in Table 2.2.

Table 2.2 Overview of experiments conducted and their objectives.

Experiment	**Objective**
Grain dissolution quantification	Examination and quantification of dissolution features on anorthosite and olivine grains with electron after 1.5 years of soil incubation experiment by (Mørkved, personal communication).
Dissolution rate experiment 1	Observe pH increase by dissolution of anorthosite, olivine and dolomite. Used as a precursor for experiment 2
Dissolution rate experiment 2	Observe pH increase and element release by dissolution of olivine, eclogite, larvikite, basaltic glass, norite and dolomite, as a preparation for selection of minerals for a field experiment at NUBM at Ås.
Dissolution rate experiment 3	Observe pH increase, calculate dissolution rates and heavy metal leaching by dissolution of olivine, dolomite, eclogite, nepheline syenite, larvikite and norite.

2.2.1 Part 1: Grain dissolution quantification

In the microcosm experiment by Pål Tore Mørkved two soils were split into 120 ml serum for aerobic incubation and into large beakers for later subsampling. Water content was adjusted to 80% water filled pore space and added KNO_3 to 10 mM in soil solution. To reduce water loss the soils were covered during incubation, but not capped to avoid anaerobic conditions. Water content was adjusted 2-3 days before measurements and controlled by weighing. Soils were stored at 20^{o}C (Mørkved, personal communication).

After incubation for approximately 1.5 years anorthosite and olivine mineral grains (200-450 µm) were extracted from the soil and prepared for observations by SEM. To see if any dissolution features had developed during incubation fresh, unaltered grains were examined for comparison. Grains were classified based on distribution and observations of dissolution features (Table 2.3).

Grains for examination were chosen randomly and x-ray micro analysis with SEM verified the mineral identity. On a few occasions mica grains were found and excluded from further examination. If any

interesting areas, such as possibly leached/chemically altered layers were observed, a more thorough chemical analysis was done in the area. Images were taken as documentation and a compilation can be found in appendix D.

To separate mineral grains and from bulk peat soil 1 gram of soil was dissolved in 3 ml distilled ionised (DI) water and 4 ml Nycodense in a 15 ml centrifuge tube (VWR). The tubes were centrifuged with a Heraeus Multifuge 3SR+ (Thermo Scientific) at 5000 rpm (approx.5310.5 g) for 10 min at 20°C. Excess water was removed using a pipette, the top layer of soil was removed with a spatula and the bottom soil containing the minerals were transferred to a petri-dish. Minerals were gently washed with DI-water and organic material and excess water were removed using an automatic pipette. Grains were washed with increasing concentrations of ethanol; first 50%, then 75% and finally three times with 96%, where the ethanol reacted with the sample for 5 min before it was filtered off the last time. Untreated mineral grains and grains from the dissolution experiments were washed using a vacuum based filter-setup with 0.2µm nylon filters (VWR). Then the filters with material were transferred to petri-dishes for drying.

pH measurements in the soil were done in two solutions (0.01 M $CaCl_2$ and distilled water). Soils were dried (80°C) for 30 hours (h) and two gram dry soil was mixed with 5ml solution. The mix settled for 30 min before pH was measured.

For trace element analyses from the soil, two grams dry soil were mixed with 9 ml distilled water and 9 ml $CaCl_2$ and set on a shaking table (250rpm) for 2 h (room temperature). Tubes are centrifuged (5000 rpm) for 20min and liquids filtered with 0.2µm nylon filters with disposable syringes into acid washed tubes (Falcon Blue Max).

Table 2.3 Order and description of the dissolution grade quantification scale applied.

Dissolution grade	Observation
0	Show no or negligible visible dissolution.
1	Dissolution feature visible on particle surface (<20% of area)
2	Dissolution feature is prominent and visible on larger part of the particle surface (20-50%), however less than 3. Some parts are also not affected.
3	The particle surface is dominated (>50%) by the dissolution features.

2.2.2 Part 2: Dissolution rate experiments

The goal of the dissolution rate experiments in order to investigate how pH is effected by mineral dissolution under different conditions. The release of cations were used for dissolution rate calculations. Three experiments were done, each as an improvement of the previous.

The factors that were changed between the experiments were:

- types of minerals/rocks
- pre-treatment of the materials
- types of acid
- acid concentration
- solid/solution ratio

Three dissolution experiments were conducted in order to the find the most efficient method to answer the objectives of the study. The first experiment was in order to get an impression of how pH increases with silicate dissolution and methodical approach. Experiment 2 was scaled up from the first, using materials relevant for a field experiment at NMBU (Ås) and including organic acids. Experiment 3 was the largest and final experiment.

2.2.2.1 Preparation of the materials

Experiment 1 did not have any specific sample preparation, the samples were delivered air dried and sieved into fractions of 200-450 µm and <63 µm.

For experiment 2 and 3 the materials were sieved (Laboratory Test Sieves) into a fraction between 63-125µm. Because the norite sample contains very fine particles (<63µm), an olivine fraction was sieved below 63µm. The materials were sieved with mainly tap water, but distilled water and 96 % ethanol were used in the final step. Materials were then dried (50°C) in aluminium beakers overnight and stored at room temperature.

For experiment 3 there was additional material cleaning. The materials were soaked in 96 % ethanol in 50 ml polypropylene conical tubes (Falcon Blue Max™) for 24 h, thereafter put in an Ultrasonic cleaner (VWR) bath for 15 min. Then the tubes were centrifuged with a Haraeus Multifuge 3R+ (Thermo Scientific) at 4000 rpm (5377.6 g) for 10 min and the ethanol was gently poured out. The tubes were then filled with ethanol, shaken, centrifuged and liquid poured of, this was repeated two times with ethanol and two times with DI water. Tubes with material were then dried (50° C) overnight and additionally at 105°C for 3h. The dry grains were stored in 50 ml tubes at room temperature.

2.2.2.2 Experiment 1

One gram of material (olivine, anorthosite and dolomite) was weighed into 15 ml acid washed narrow-mouth HDPE bottles (Thermo Scientific) and 10 ml of the acid solution (0.1 M and 0.01 M nitric acid) was added, this gave a total of 10 treatments. pH measurements were done after 15 min, 1, 3, 7, 24, 48, 125, 173 and 219 h. The first two days the tubes were hourly shaken by hand (as the instrument was no available), on the third day they were placed on a rotary shaker (150 rpm) at 20°C. At the end of the experiement, materials were rinsed with DI water, dried (60°C) overnight and stored.

2.2.2.3 Experiment 2

The main objective for experiment 2 was to compare pH trajectories for all materials as preparation of a field experiment at NMBU, Ås.

The materials were two olivine fractions (<63µm and 63-125µm), dolomite, eclogite, larvikite, norite and basaltic glass. One gram of each material was weighed into 50 ml acid washed centrifuge tubes (Falcon Blue Max) and 20 ml acid solution (0.1 M nitric acid, 0.01 M nitric acid and 0.01 M oxalic acid) was added to each tube. Three parallels of most of the treatments were made, the exceptions were the blank solution (two parallels), coarse grained dolomite (one parallel) and fine grained dolomite (only mixed with oxalic acid), totally 64 samples. The absence of dolomite parallels were due to lack of material. One parallel was only for pH-measurements, the two others were sampled for fluids to analyses. pH measurements were done after 1, 2, 4, 8, 24, 48, 51, 168 and 240 h. Fluid sampling were taken from parallel 2 after 8 h and parallel 3 after 240 h. Bottles were stored on a rotary table (150 rpm) at 20°C. Samples for analyses used as indication for expected concentrations and are not shown.

To allow sampling of fluids the tubes were centrifuged (5000 rpm) for 10 min. Then the supernatant was gently poured over to 30ml disposable syringes (BD) and filtered with 25mm syringe filters with 0.2µm nylon membranes (VWR) to new acid washed tubes. In total 36 samples were filtered for analysis, including both parallels. After fluid extractions the rest material was rinsed four times with DI water. Water was added to the tubes, shaken by hand, centrifuged (5000 rpm) for 5 min and water was gently poured out. The samples were dried at 60°C overnight and stored.

2.2.2.4 Experiment 3

Previous experiments showed that the rock samples reacted differently to unlike acids and therefore two other acid solutions were included in this experiment. The initial pH was raised to 3 and an increased sample/solution ratio was used. An increased sample/solution ratio (1/100) will delay equilibrium and observations can be done over a larger time interval than previous experiments.

The materials were two olivine fractions (<63µm and 63-125µm), dolomite, nepheline syenite, larvikite, eclogite and norite. The acid solutions used were 0.001 M HCl, 0.001 M oxalic acid, 0.001 M acetic acid (+ HCl) and a peat soil slurry (20 grams/ per 500 ml) (+ HCl). 500 ml 0.001 M acetic acid was titrated with 80 µl 6 M HCl and 500 ml peat soil slurry was titrated with 250 µl 6 M HCl to reach pH 3. Five grams material was mixed with 500 ml acid solution in acid washed 1000 ml naglene wide mouth HDPE bottles (Thermo Scientific), totally 32 treatments (including four blanks with the acid solutions), and lasted for 792 h. Bottles were positioned in a rotary table (85 rpm) between sampling. Sampling for chemical analysis and pH were done at 1 (only pH), 8, 24, 48, 72, 120, 168, 240, 433, 600 and 792 h. Six of the solution sampled were analysed for major elements (8, 24, 48, 72 and 120, 792h).

Fluid was sampled using 10 ml disposable syringes (BD) and filtered with 25mm syringe filters with 0.2µm nylon membrane (VWR) into 15 ml tubes (TTP) for pH-measurements and acid washed 15 ml polypropylene conical tubes (Falcon Blue Max) for chemical analyses. 4.4 ml was sampled each time (except peat soil solutions); 1 ml for pH, 3 ml for chemical analyses and 0.4 ml is anticipated to be lost in the filter. The total loss was 45 ml (9%) from each treatment. Sampling peat soil solution was done with a 5 ml pipette, 1.5 ml for pH and 3 ml for analysis, totally 46.5 ml (9.3%). Peat soil solutions sampled were not filtered before after experiment end (792 h), because the first plan was to do digestion analysis, but this was changed and all samples were sent to the same analysis.

At experiment end 100 ml of each solution was filtered (as described above) into acid washed 125 ml *Naglene HDPE* bottles (*Thermo Scientific*), acidified with 3 ml concentrated distilled nitric acid and stored. The peat soil solutions were filtered with *500 mL Rapid-Flow Bottle Top Filters* with *0.2µm aPES membrane* filters (Thermo Scientific), using vacuum to gather solution in a 500 ml glass bottle. Filter and glass bottle was rinsed with 10 M nitric washing acid and DI water, the glass bottle was reused. Material is rinsed two times with DI water and twice with 96% ethanol. Tubes are centrifuged as above. Solution is gently poured out of the tubes and refilled, to mix sample and material a *VV3* dispersion machine (VWR) is used. Tubes and material was dried at 70^{o}C for 24 h and stored.

An overview of the dissolution experiments is illustrated in Table 2.4.

Table 2.4 Overview of materials, acid solutions, sampling and analyses. Fluid samplings were done at different times during the experiment (see experiment descriptions). In experiment 2 pH measurements was taken at each time point. In experiment 3, 32 samples were taken at each time point. Specific surface area measurements were done on olivine, norite, larvikite, eclogite and nepheline syenite from HCl and oxalic acid solutions, after experiment 3.

	Experiment 1	**Experiment 2[1]**	**Experiment 3**
Duration (hours)	219	240	792
Fluid samplings for element analyses	No	2	6
pH measurement[1] time points	10	10	12
Specific surface measurements	-	-	12
Treatments	10	18	32
Acid solutions	0.1 M HNO_3	0.1 M HNO_3	0.001 M HCl
	0.01 M HNO_3	0.01 M HNO_3	0.001 M oxalic acid
		0.01 M oxalic acid	0.001 M acetic acid (+ HCl)
			20 grams (per 500 ml) peat soil (+ HCl)
Materials	Olivine	Olivine	Olivine
	Anorthosite	Dolomite[2]	Dolomite
	Dolomite	Larvikite	Larvikite
		Eclogite	Eclogite
		Norite	Norite
		Basaltic glass	Nepheline syenite

[1]Three parallels was made of most treatments (see experiment 2 description) [2] Not sieved or cleaned

2.3 Analytical methods

The analytical methods used and their objectives are summarized in Table 2.5. Most of the analyses were done at the University of Bergen, except XRD that was done at the Institute for Energy Technology (IFE).

Table 2.5 Overview of methods used and objectives.

Method	**Target**
X-ray fluorescence spectrometry (XRF)	Major elements
X-ray diffraction spectrometry (XRD)	Bulk rock mineral determination
Inductively coupled plasma mass spectrometry (ICP-MS)	Trace elements concentrations
Inductively coupled plasma optical emission spectrometry (ICP-OES)	Major cation analysis
Brunauer-Emmett-Teller (BET) specific surface area	Specific surface area quantification
Scanning electron microscope (SEM)	Characterization of dissolution features

2.3.1 Solid phase analysis

2.3.1.1 SEM

Mineral grains were mounted on aluminum stubs with duplex carbon tape and coated with carbon with a Turbo Carbon Coater (Agar Scientific). Approximately 25-50 coarse grains were mounted on each stub.

Examinations were done on a ZEISS Supra 55VP field emission scanning microscopy equipped with NORAN System SIX (Thermo Scientific) energy dispersive spectrometer (EDS) system for chemical analysis. Secondary electron imaging was used with intensity 5kV and a working distance of 3-10mm. Chemical analysis were done at 15kV and working of distance 8-12mm.

2.3.1.2 X-ray fluorescence spectrometry (XRF)

Materials were crushed into fine powder using a silica based mortar mill with the frequency set to 30 (1/s) for 20 min. The coarse olivine sample was crushed manually using an agate-mortar. Approximately 2 grams of each sample were weighed into a white-china crucible and heated (1000°C) for 2.5 h in a EFL 11/14B muffle furnace (Carbolite), to burn off all volatiles (organic material, water, carbonates) and to oxidize all the material. Loss of ignition (LOI) was calculated and used to determine how much volatiles that is lost during heating. LOI is calculated by this formula:

$$\text{LOI } \% = \frac{(A - B)}{C} x\ 100\%$$

A is the crucible weight and sample weight before heating, B is the weight of A after heating and C is the sample weight before heating.

Dried material (0.96 gram) was mixed with spectromelt A-10 (6.72 grams), which lowers the melting point and binds the material together. This mix was melted into a homogeneous melt and cooled into glass disks. Standard reference materials (SRM) BCR-2 and GSP-1 were used as calibration and quality control during analysis.

Major element composition of the materials were analysed on a PW1404 X-ray fluorescence spectrometer (Philips).

2.3.1.3 X-ray diffraction spectrometry (XRD)

The mineralogy of the material was determined with XRD. Materials were prepared as described for experiment 3 (except anorthosite).

The XRD analysis were done on a D8 Advance diffractometer (Burker) operated at 40kV and 40mA with Cu Kα radiation and data analysis by the EVA software (Burker).

2.3.1.4 Inductively coupled plasma mass spectrometry (ICP-MS)

Trace element concentration in the bulk material was determined with ICP-MS.

For rock digestion 100 mg material were weighted into 10ml Teflon beakers and dissolved in 4 ml 22M concentrated hydrofluoric acid (HF) was added. The containers were closed on a kept on a PicoTrace hot plate in a fume hood (100°C) for 48 h, and than evaporated (100°C). Residues were re-dissolved in 4 ml of 14M concentrated HNO_3 and DI water and stored in a fume hood (110°C). Residues were re-dissolved in 5 ml 14M HNO_3 and kept at 125°C until complete dissolution, at least 24 h. 1 ml of each sample was diluted with 0.375 ml 14 M HNO3 and 48.635 ml DI water in centrifuge tubes with conical

tips. The final ratio was 20mg sample/50mL solution. Standard reference material (SRM), BCR2, BIR1, BHV02 and PCC1 (Jochum et al., 2005), were digested in parallel with samples and were analysed in between samples

Trace element analyses were performed on an ELEMENT XR™ High Resolution ICP-MS (Thermo Scientific).

2.3.1.5 Brunaur-Emmett-Teller (BET)

Material was prepared as for experiment 3. Prior to the measurements the materials were activated at 120°C for 2 h in a dynamic vacuum.

Gas adsorption measurements were done on a BELSORP-max instrument equipped with a low pressure transducer and a turbomolecular pump, allowing measurements with high precision from very low pressures ($p/p_0 = 10^{-8}$). The nitrogen gas used for gas adsorption measurements were of 99. 9995% or higher purity, purchased from Yara Praxair.

2.3.2 Fluid analysis

2.3.2.1 pH

In experiment 1 and 2 and in the incubation soil, pH was measured directly using a 826 pH mobile (Metrohm), LL primatode NTC pH-meter. For experiment 3, liquid was extracted and measured using and measured in centrifuge tubes with 826 pH mobile (Metrohm), LL flat membrane electrode, and a 728 stirrer (Metrohm) and a magnet (circulation in solution). Three-point calibrations with buffer solutions pH 4, 7 and 9 (Metrohm Ion analysis Buffer solutions) were done in advance of measurement rounds.

2.3.2.2 Inductively coupled plasma optical emission spectrometry (ICP-OES)

Solutions were acidified to 2 % of HNO_3. Instrument calibration was done using a Geo-matrix standard composed of a selection of single elements. Scandium were used as an internal standard during measurements. Standard reference materials (SRMs) were sps-sw-2 (synthetic fresh water) and Perkin Elmer 1000. Detection limits in ppm were Al: 0.01, Ca: 0.01, Mg: 0.0003, K: 0.09, Na: 0.7, Mn: 0.0005, Fe: 0.003, Si: 0.01, Ni: 0.001 and Cr: 0.001.

The analyses were performed on an iCAP™ 7600 ICP-OES (Thermo Scientific).

2.4 Dissolution rate calculations

Since the pH and chemical composition continuously changed in the experiment, dissolution rates (r = mol/m^{2}s) were calculated from the difference in element concentration over time intervals based on the rate equation used by Hellevang et al. (2010),

$$r_t = \frac{2V_{t-1}}{(m_t + m_{t-1})S_{BET}} * \frac{\Delta C}{\Delta t}$$

where V is volume of solution, C is element concentration, m is mass of sample, S_{BET} is initial surface area of sample, and t is time. Subscripts $_t$ and $_{t-1}$ denotes time of sampling and time at previous sampling. The equation was modified on the following basis to be applicable to this data set. Because of lack of information about mass changes, the "m_t+m_{t-1}" was comprised to m_t and as a consequence of this "$2V_{t-1}$" was comprised to V_{t-1}. Aliquots were extracted from the sample solutions during the experiment and were taken into account. Rate calculations was done using the following equation:

$$r_t = \frac{V_{t-1}}{(m_t)S_{BET}} * \frac{\Delta C}{\Delta t}$$

3 Results

The results are divided into three parts: characterization pf start solid material used, material dissolution in soils and dissolution rate experiments.

3.1 Rock characterization

3.1.1 Bulk rock and trace-element analysis

The bulk geochemical composition of the materials are listed in Table 3.1 and the minerals detected by XRD in Table 3.2. All trace element concentrations for the starting material were presented in appendix C.

Table 3.1 Bulk geochemical composition of the materials.

	Ol 63-	Ol 63-125	Norite	Nepheline syenite	Larvikite	Eclogite	Dolomite	Anorthosite	
Na_2O	0,00	0,00	2,78	5,33	6,36	2,28	0,00	3,43	wt%
MgO	46,24	48,97	5,94	4,16	1,26	5,57	15,93	0,40	wt%
Al_2O_3	0,85	1,21	14,06	17,52	17,91	13,36	0,00	30,16	wt%
SiO_2	40,15	42,58	34,42	44,99	57,23	42,95	1,42	48,79	wt%
P_2O_5	0,01	0,01	0,36	0,15	0,38	0,07	0,04	0,02	wt%
K_2O	0,02	0,09	0,76	5,21	4,26	0,15	0,01	0,31	wt%
CaO	0,24	0,18	5,45	7,91	3,55	9,35	25,60	13,77	wt%
TiO_2	0,01	0,02	16,01	2,20	1,37	5,89	0,02	0,12	wt%
MnO	0,10	0,11	0,13	0,32	0,19	0,34	0,00	0,01	wt%
Fe_2O_3	6,47	6,70	19,07	9,86	5,97	20,06	0,10	0,85	wt%
LOI[b]	4,19	1,84	0,95	1,64	0,27	0,00	53,22	1,02	wt%
Sum XRF	98,27	101,70	99,92	99,29	98,75	100,03	96,34	98,89	wt%
Cr	936,1		341,3	66,2	30,9	9,8			mg/kg
Ni	2307		483	28	11	12			mg/kg
SSA[a]	8.4	1.6	6.9	0.2	1.2	0.07	0.1		m^2/g

[a] SSA: specific surface area. [b] LOI: Loss of ignition

Table 3.2 XRD analysis. Identified mineral phases are ranged from highest to lowest (using XRF results and previous studies) for each material. Quantitative abundance calculations are not done.

Olivine	**Norite**	**Nepheline syenite**	**Larvikite**	**Eclogite**	**Dolomite**	**Anorthosite**
Forsterite	Anorthite	Nepheline	Albite intermediate	Omphacite	Dolomite	Anorthite
Cr-chlorite	Mg-Fe silicate (pyroxene)	Orthoclase	Magnetite	Almandine calcian	Calcite	
Enstatite	Illmenite Geikielite	Hornblende Biotite	Quartz	Rutile Quartz	Magnesioferrite Quartz Wustite	

Based on their silica (SiO_2) content most samples were classified with ultramafic composition (below 45% SiO_2), except larvikite which have an intermediate composition (52-63 % SiO_2) and anorthosite which have a mafic composition (45-52% SiO_2).

Olivine 63- and olivine 63-125 were from the same sample; sieved into different grain size fractions. The rock mainly contained Mg (46.2-49.0 wt.% MgO), Fe (6.5-6.7 wt% Fe_2O_3) and SiO_2 (40.1-42.6 wt%) (Table 3.1). The forsterite content has been calculated to $Fo_{0.93}$-$Fa_{0.07}$. Olivine 63- had a higher LOI (probably due to higher water content in the more fine grained sample) and approximately 2 wt.% lower concentrations of MgO and SiO_2 than olivine 63-125, the Fe_2O_3 percent were fairly close for the two grain sizes. There were thus no significant differences in the composition between the two size fractions. The XRD data of olivine identified the mineral phases of forsterite, Cr-chlorite and enstatite (Table 3.2). Forsterite was the main mineral phase and there is most likely lower abundances of enstatite and Cr-chlorite detected in the XRD. Thin-sections using a microscope or abundancy calculations from the XRD data could be done to get more exact information on mineralogical composition. Olivine has consists of 936.1 mg/kg chromium (Cr), 2307 mg/kg nickel (Ni), the highest values of Ni and Cr of the analysed samples. The measured specific surface area for olivine 63- is 8.4 m^2g^{-1} and for olivine 63-125 is 1.6 m^2g^{-1}. The XRF and XRD analysis are in good agreement with characterization done by Martinez et al. (2014).

The norite material mainly consistsed of Al (14 wt% Al_2O_3), SiO_2 (34 wt%), Ti (16 wt% TiO_2) and Fe (19 wt% Fe_2O_3) (Table 3.1),. Other elements such as Na (Na_2O), Mg (MgO) and Ca (CaO) were present in concentrations between 2.78 and 5.94 wt% (Table 3.1) The XRD analysis identified mineral phases of anorthite, orthopyroxene (Mg-Fe pyroxene), ilmenite and geikilite (Table 3.2). Anorthite and orthopyroxene constitutes the majority proportion, while ilmenite and geikilite are less abundant due to the 16.01 wt% of TiO_2. The norite sample consist of 341.3 mg/kg Cr and 483 mg/kg nickel. The

measured specific surface area is 6.9 m^2g^{-1}. The norite have an $An_{0.27}$ which is some lower than the average Rogaland anorthosite complex, which is $An_{0.4\text{-}0.55}$ (Wanvik, 2010), but the norite was from a ilmenite-norite lens which could explain the slightly lower number. The SiO_2, TiO_2, Al_2O_3, MgO and CaO wt. % from this study and Wilmart et al. (1989) have deviations from -2,96 to 2,31 wt. %.

The nepheline syenite material mainly consistsed of Al (17.5 wt% Al_2O_3) and SiO_2 (45 wt%) (Table 3.1),. Other elements such as Na (Na_2O), Mg (MgO), K (K_2O), Ca (CaO) and Fe (Fe_2O_3) had concentrations between 4.16 to 9.86 wt%. The XRD analysis identified the mineral phases orthoclase, nepheline, hornblende and biotite (Table 3.2). Orthoclase and nepheline were the majority proportion, while hornblende and biotite are present in minor concentrations. Nepheline syenite contains 66.2 mg/kg Cr and 28 mg/kg Ni. The measured specific surface areas were 0.16 m^2g^{-1}. The XRF analysis showed lower concentrations of SiO_2, Al_2O_3 and Na_2O and higher concentrations of CaO, Fe_2O_3 and MgO compared to analysis of neheline syenites by Gautneb et al. (2009). The XRD analysis identified mineral phases of nepheline, orthoclase, hornblende and biotite, which correlates with analysis done by Heier (1964), where orthoclase and nepheline are the major components.

The larvikite material mainly consisted of Al (18 wt% Al_2O_3) and SiO_2 (57 wt%) (Table 3.1),. Other elements such as Na (Na_2O), K (K_2O), Ca (CaO) and Fe (Fe_2O_3) have concentrations between 3.55 and 6.36 wt%. XRD analysis identified the mineral phases Albite intermediate, magnetite and quartz low. Albite intermediate (or plagioclase intergrowth) is most likely the main proportion of the sample, while magnetite and quartz are present in minor concentrations (Table 3.2). The larviktie contains 30.9 mg/kg Cr and 11 mg/kg Ni, having the lowest concentration of Ni of the materials. The measured specific surface area is 1.2 m^2g^{-1}. The calculated feldspar content of the larviktie is $An_{0.18}Ab_{0.57}Or_{0.25}$, indicating a main proportion of albite in the sample. Previous analysis received from Larvik Granite and Lundhs show the presence of 88% feldspar, 4 % pyroxene, 2% amphibole, 1% biotite, 3% olivine and 2% magnetite, indicating that there may be some minor mineral phases the analysis did not detect.

The eclogite material mainly consisted of SiO_2 (43 wt%), Al (13 wt% Al_2O_3) and Fe (20 wt% Fe_2O_3) (Table 3.1),. Other elements such as Mg (MgO), Ca (CaO) and Ti (TiO) have concentrations of 5.57-9.35 wt%. XRD analysis identified the mineral phases omphacite, garnet, rutile and quartz. Omphacite and garnet were the main mineral phases, while rutile and quartz are accessory minerals (Table 3.2). Eclogite contained 9.8 mg/kg Cr and 12 mg/kg nickel, having the lowest concentration of chromium of the materials. The measured specific surface area is 0.07 m^2g^{-1}, the lowest surface area of the analysed samples. The eclogite were classified as a ferro eclogite by Korneliussen et al. (1998), based on the high concentrations of Fe_2O_3 (20 wt. %) and TiO_2 (5.9 wt. %), which also indicates a >25% garnet content.

The dolomite material mainly consisted of Mg (16 wt% MgO) and Ca (26 wt% CaO) (Table 3.1),. The SiO_2 concentration is 1.42 wt% and other elements have concentrations below 0.2 wt%. XRD analysis identified the mineral phases dolomite, calcite, magnesioferrite, quartz and wustite (Table 3.2). Based on XRF analyses; dolomite and calcite are most likely the main mineral phases, while the other minerals are present as accessory minerals. Trace element analyses were not done on dolomite. The measured specific surface area is 1.2 m^2g^{-1}.

The anorthosite sample mainly consist of SiO_2 (49 wt%), Al (30 wt % Al_2O_3) and Ca (14 wt% CaO), and a minor concentration of Na (3 wt% Na_2O) (Table 3.1),. XRD analysis only found the mineral phase of anorthite (Table 3.2). The calculated anorthite content from XRF data is 0.69 which corresponds to high labradorite.

3.2 Dissolution in soils investigated by scanning electron microscopy

Minerals with similar composition may weather at different rates and display different dissolution features even though they are exposed to similar chemical and physical conditions. However, similar alteration features are reoccurring on several of the mineral grains. To make a semi quantitative assessment of the degree of dissolution of soil incubated mineral particles, observed dissolution features are rated from 0-3, depending on abundance of the features on each grain (Table 2.3). The grading was based on following observations: grade 0 show no or negligible dissolution features (Fig. 3.1A), grade 1 have observable dissolution features covering less than 20% of the visible grain (Fig. 3.1B), grade 2 have a larger parts of the grain cover by dissolution features (approximately 20-50%) (Fig. 3.1C), grade 3 is a grain dominated by a dissolution feature covering >50% of the grain (Fig. 3.1D).

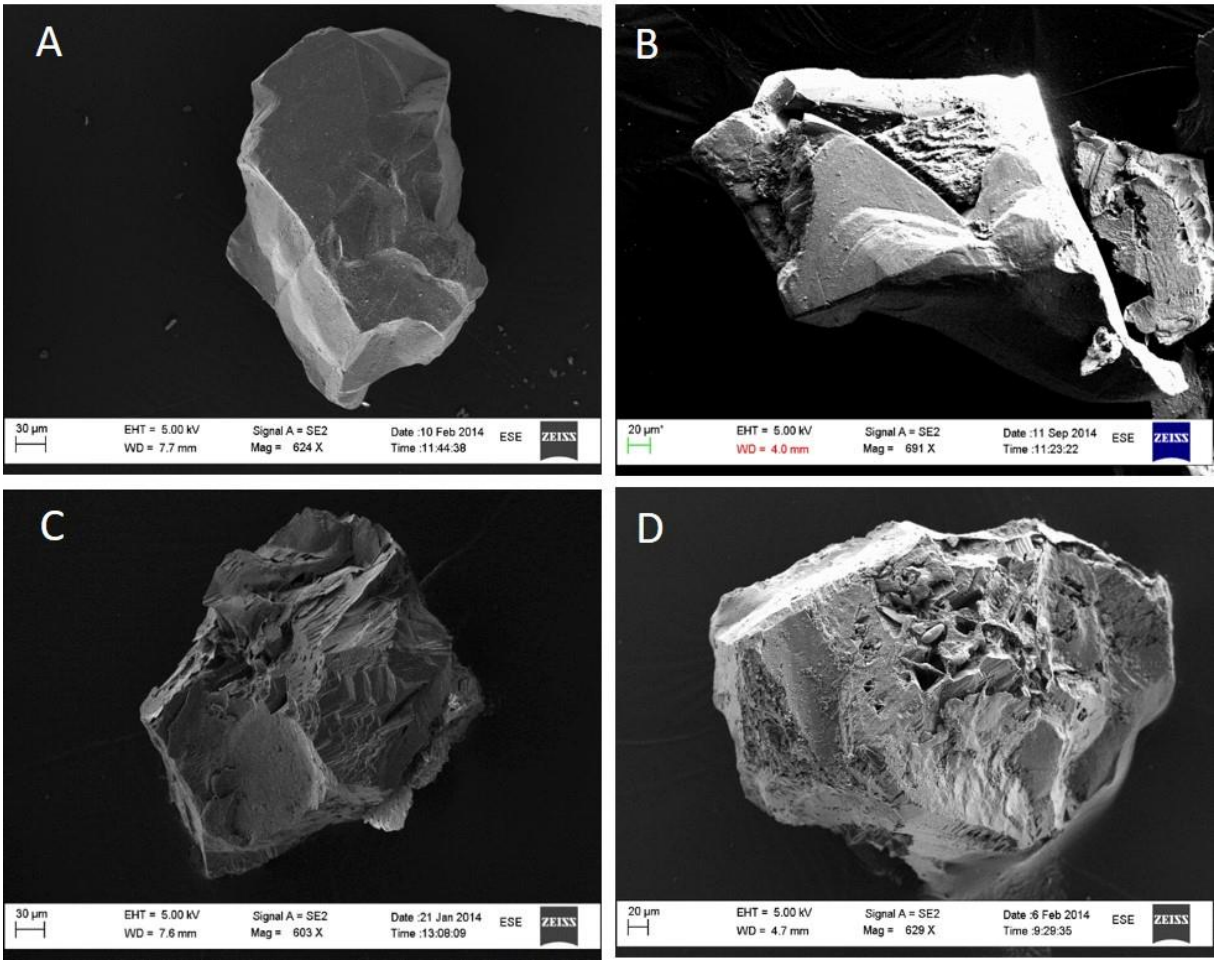

Fig. 3.1 Examples of olivine grains from grade 0 (A) to grade 3 (D), using etch pits as a quantitative measure. A) grade 0 dissolution, B) grade 1 dissolution, C) grade 2 dissolution, D) grade 3 dissolution.

Dissolution features are surface characteristics related to weathering of mineral grains. The extent of dissolution features varies between the grains, why this happens is depending on several factors, among them; exposed crystal face, mineral defects and dislocations. Some of the observed features are fractures, etch pits and silica layers (Fig. 3.2A). Olivine grains have more cone shaped etch-pits while anorthosite etch pits along its lamellae structures (Fig. 3.2B).

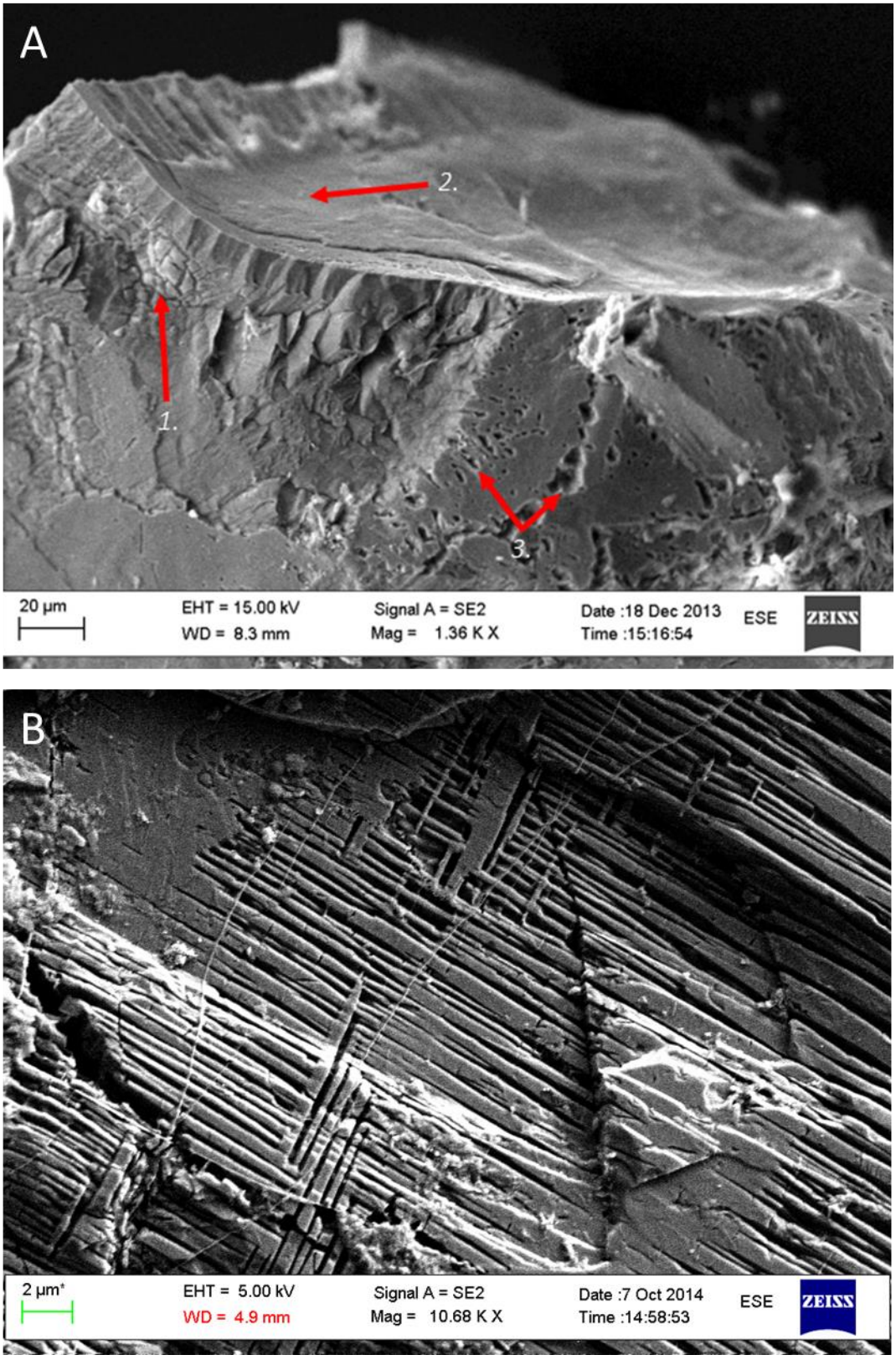

Fig. 3.2 An olivine grain displaying different dissolution features after incubation in organic soil. 1. Fracturing (probably due to hydration/dehydration. 2. Silica layer, 3. Etch pits from acid dissolution. Note that the silicate layer was on a different surface from the fracturing and pitting. B) An Anorthosite grain displaying lamellae etch-pit dissolution features.

Energy-dispersive X-ray spectrometry (EDS) analyses were done on each grain for mineral identification, on a few occasions mica grains were found and excluded from further examination. If any interesting area, such as possibly leached/chemically altered layers were observed a more thorough analysis were done in the area (Fig. 3.3).

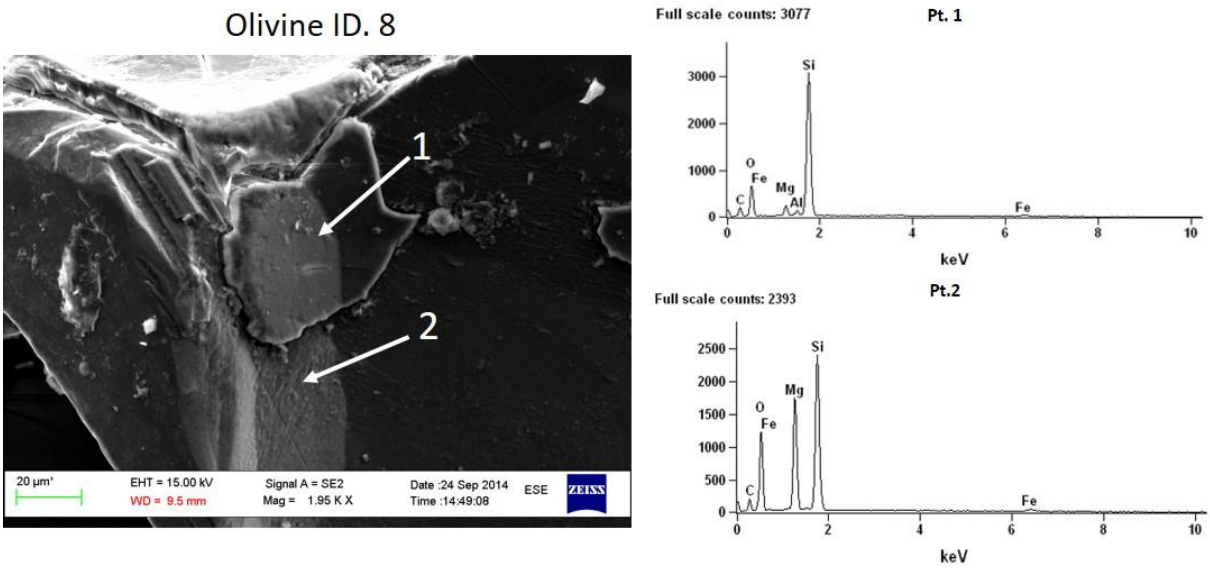

Fig. 3.3 Olivine (ID. 8) where arrows indicate where the EDS analysis were done. On the right are two measurement results from the two locations. Pt. 1 shows an area depleted for all elements except Si and is an example of a leached /chemically altered layer. Pt. 2 shows a fresh olivine surface.

21 grains of olivine and anorthosite were examined after being exposed to weathering for 1.5 years in a soil incubation experiment. The dissolution features observed are cracks, etch-pits, silica layers, serpentinization and secondary minerals. The grains are given a particle ID from 1 to 21 and all images taken are found in appendix D**.**

3.2.1 Olivine

The most frequent observed structures on olivine are cracks (H) and etch pits (P), which was found on almost all samples (Fig. 3.4). 7 out of 21 grains had degree 3 pitting, 7 had degree 2 pitting, 1 out had degree 1 pitting and 6 grains had no visible pitting. 3 out of 21 grains had degree 3 of cracks, 15 had degree 2 cracks and 3 had degree 1 cracks. The abundance of dissolution structures varied quite a lot from grain to grain. The formation of silica layers (leached/chemically altered surface layers) was observed on four of the olivine grains; the extent varied from a small area to half the grain. Serpentinization and the formation of Al-hydroxides was rarely observed, serpentinization was

observed on two grains and Al-hydroxides on one, but may be important for the olivine dissolution mechanics. One interesting feature was that silica layers and pitting structures did not occur on the same grains. Images of the dissolution features observed on olivine are illustrated in Fig. 3.5 and Fig. 3.6.

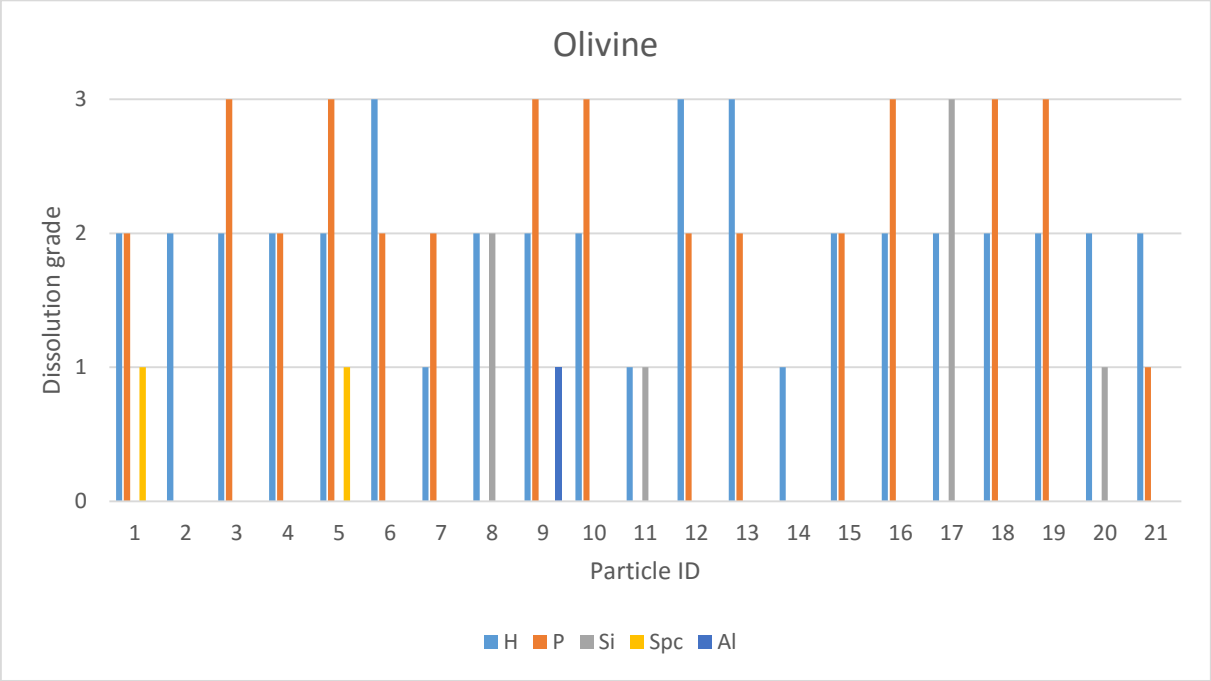

Fig. 3.4 Dissolution grade of olivine grains after 1.5 years weathering in a soil incubation experiment. On olivine 5 different dissolution structures are identified and graded from 1-3 after their abundance. Dissolution structure abbreviations, H=cracking, P = etching pits, Si = silica layers, Spc = serpentinization and Al = aluminium layer.

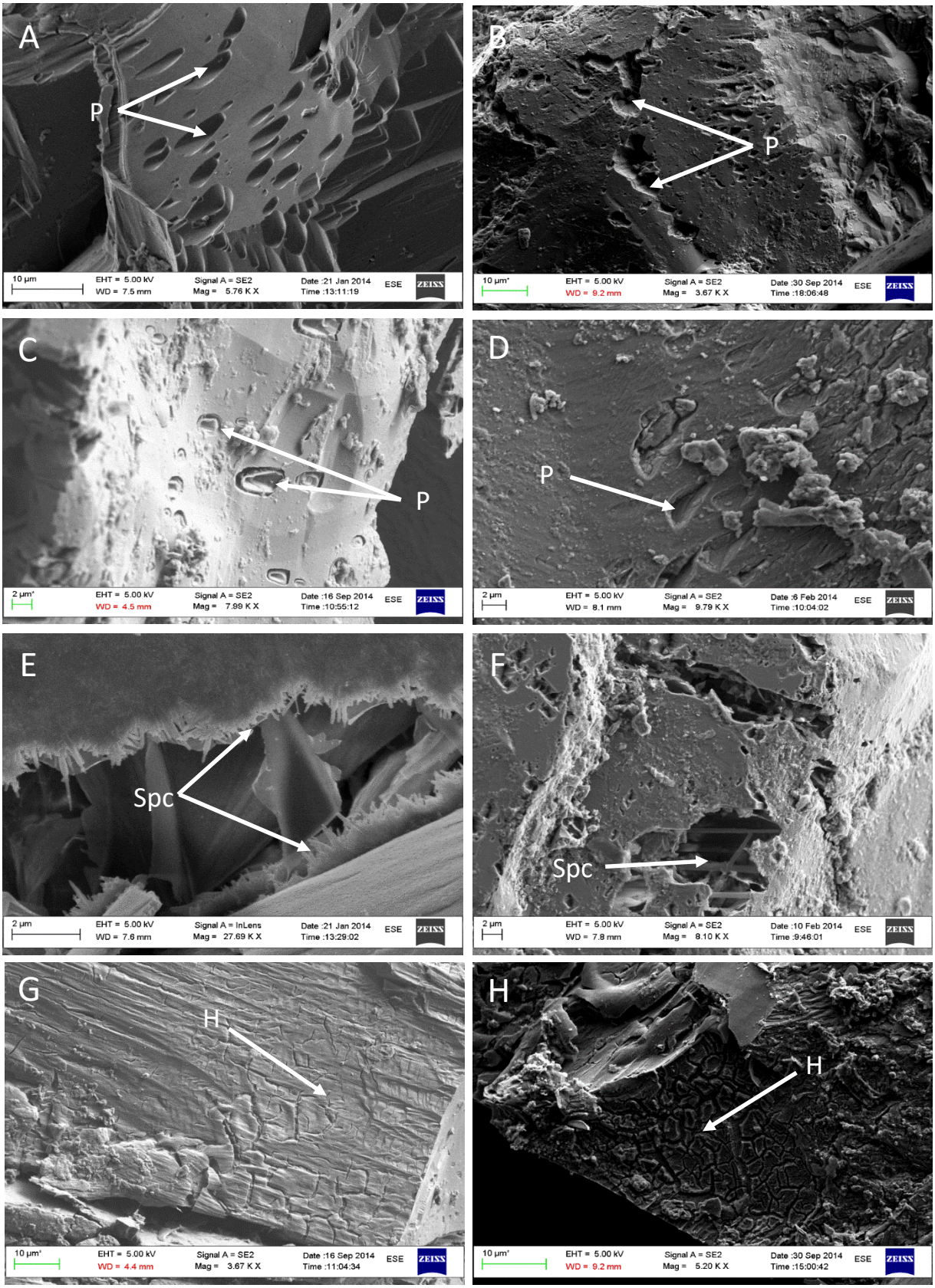

Fig. 3.5 Images of the dissolution structures observed on olivine grains. A-D illustrate different variations of etch-pits (P). E and F illustrate serpentinization structures (Spc). G and H are of fractures (H). More images of these grains can be found in appendix D. A and E = Olivine ID 1, B = Olivine ID 21, C and G = Olivine ID 13, D = Olivine ID 3, F = Olivine ID 5, H = Olivine ID 18.

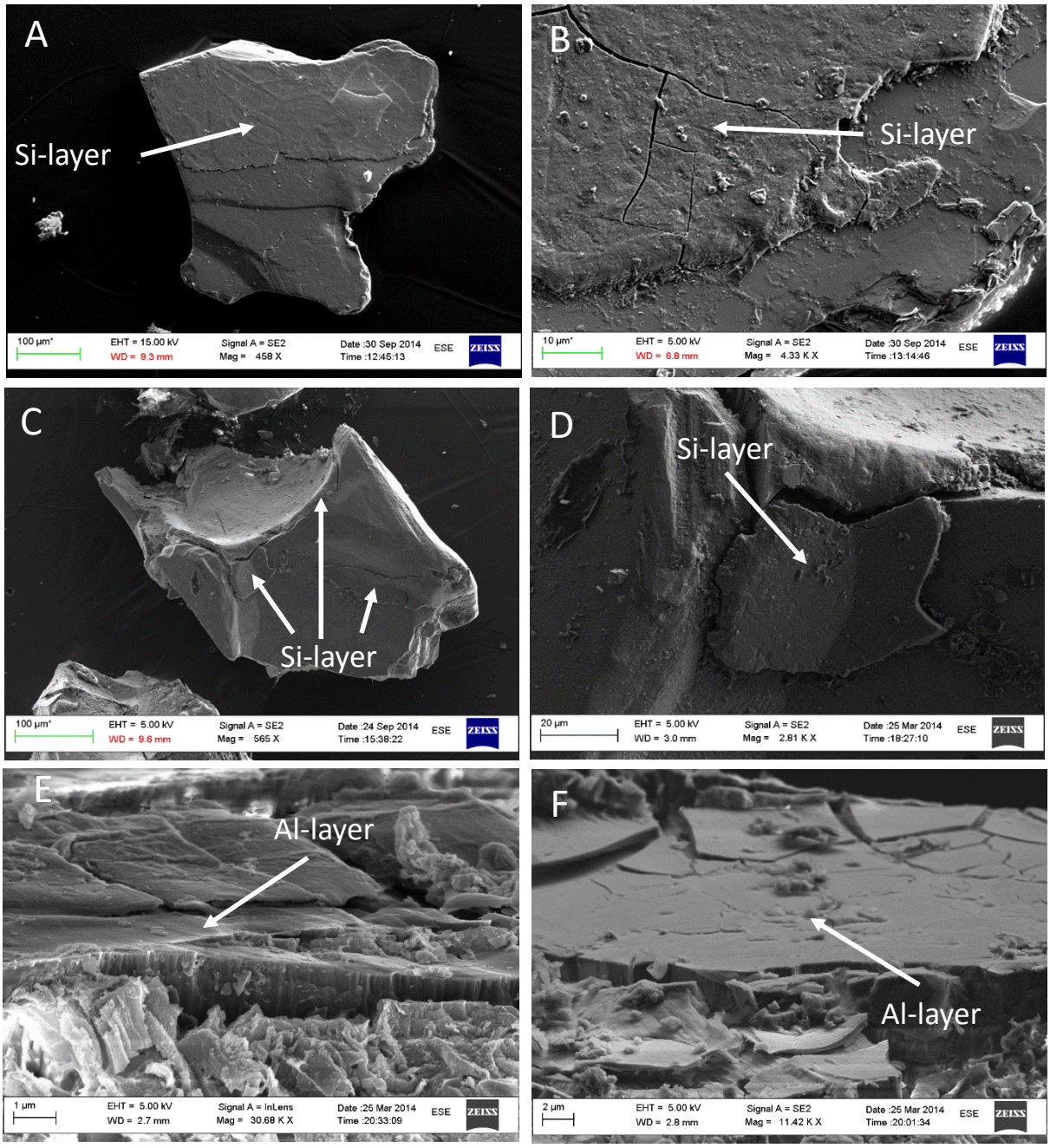

Fig. 3.6 A-D illustrate silica layers. E and F illustrate aluminium layers. More images of these grains can be found in appendix D. A and B = Olivine ID 1, C and D = Olivine ID 8, E and F = Olivine ID 9.

3.2.2 Anorthosite

Cracks (H) and etch pits (P) are also the most frequent observed structures on anorthosite grains (Fig. 3.7). 2 out of 21 grains had degree 2 cracks, 14 out of 21 had degree 1 and 5 grains had no visible cracks. 4 grains had degree 2 pitting, 9 grains had degree 1 pitting and 9 had no visible pitting structures. Etch pits on anorthosite grains appear as etching along lamellae layers, in contrast to the cone shaped etching structures on olivine. There was a general low abundance of dissolution structures on the anorthosite grains compared to the olivine. Silica layers (Si) was found on three of the anorthosite grains. Images of the dissolution features observed on anorthosite are illustrated in Fig. 3.8 and Fig. 3.9.

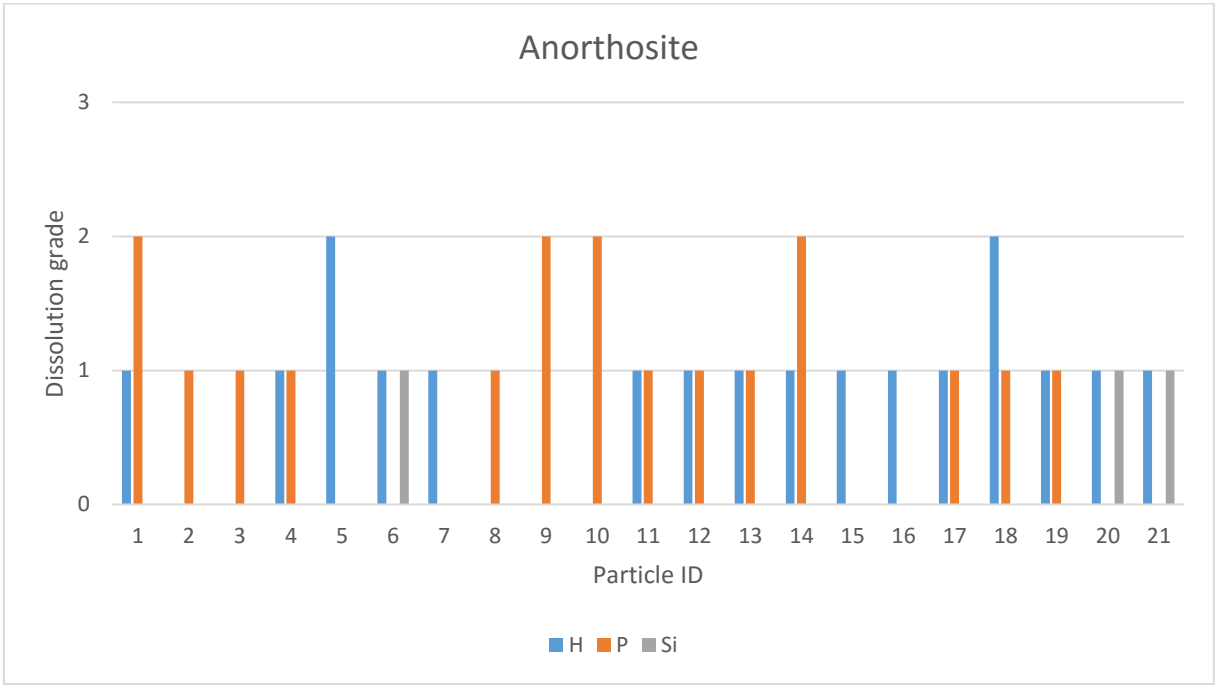

Fig. 3.7 Dissolution grade of anorthosite grains after 1.5 years weathering in a soil incubation experiment. On anorthosite 3 different dissolution structures are identified and graded from 1-3 after their abundance. Dissolution structure abbreviations, H=cracking, P = etching pits and Si = silica layers.

The olivine grains have a wider range of dissolution features appearing and in general a higher overall dissolution. Features observed on anorthosite grains are cracks (H), etch pits (P) and silica-layers, on olivine we in addition found serpentinization (Spc) and Al-hydroxides (Al). Anorthosite does not have any dissolution features at degree 3, while olivine has 6 grains illustrating degree 3 cracks and 1 degree 3 silica layer. How the silica layer effects dissolution is discussed in 4.1.2.

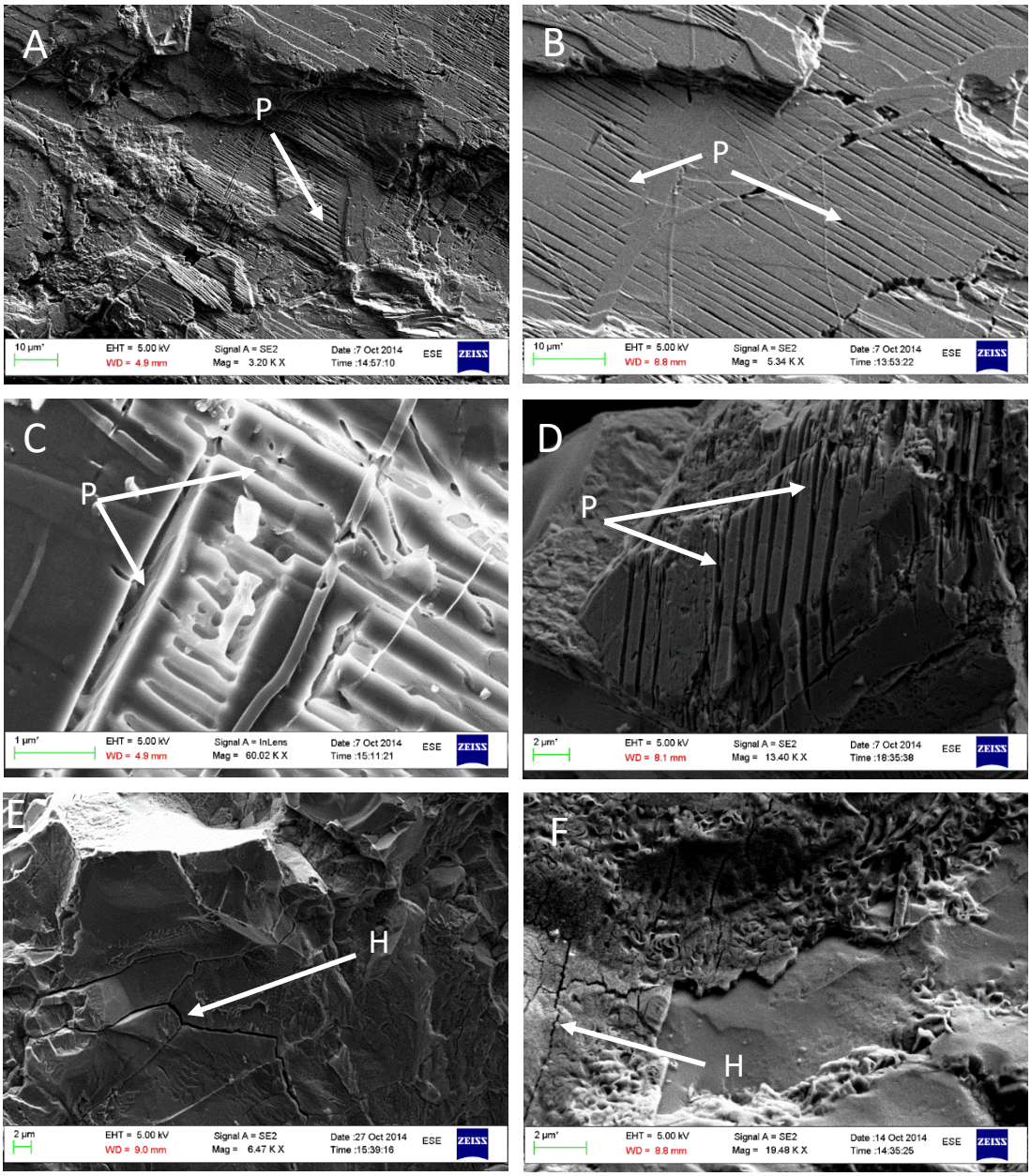

Fig. 3.8 A-D illustrate observed lamellae etching structures (P). E and F illustrate fractures (H). More images of these grains can be found in appendix D. A, B and C = Anorthosite ID 1, D = Anorthosite ID 4, E = Anorthosite ID 9, F = Anorthosite ID 5

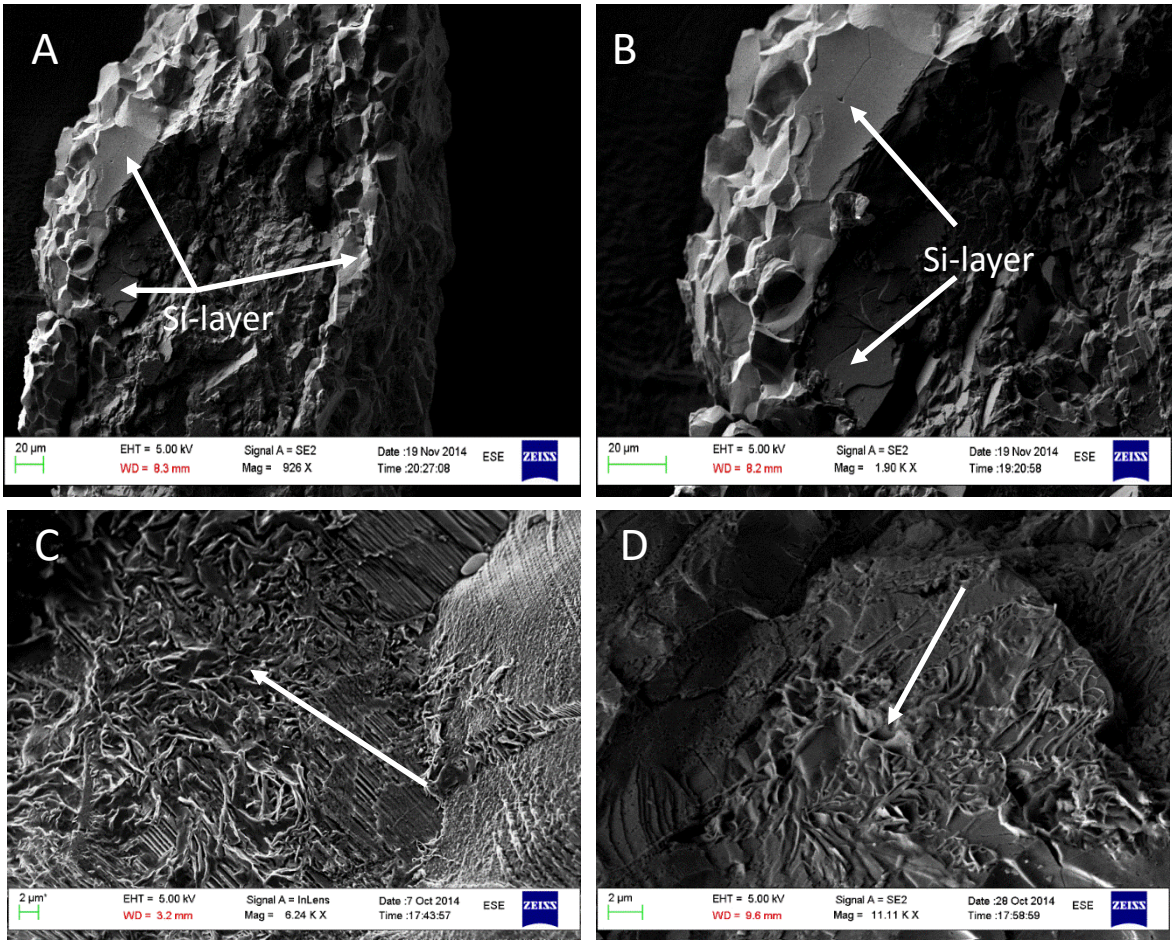

Fig. 3.9 A and B illustrate silica layers on anorthosite grains. C and D illustrate some possible secondary minerals. More images of these grains can be found in appendix D. A and B = Anorthosite ID 21, C = Anorthosite ID 3, D = Anorthosite ID 15.

3.2.3 pH and trace elements in soils after incubation

pH and trace elements were measured in soil from the incubation experiment (Table 3.3) where minerals for SEM were extracted. Measurements were done in a $CaCl_2$ (0.01 M Calsium Chloride) solution and in distilled water. The pH measurements from the $CaCl_2$ solution is in average 0.24 pH units lower than values measured in distilled water, due to ion exchange releasing adsorbed H^+ to the water, and will be used in the following. Minerals examined in SEM were olivine 250-450µm grain fraction (Ol 450) Fjaler with an end pH of 4.07 (0.01 M $CaCl_2$) and 4.44 (distilled water). Anorthosite 250-450 µm grain fraction (An 450) Fjaler with an end pH of 3.66. Chromium concentrations in the soil are all lower than the blank sample measured (13.9 mg/kg). Nickel concentrations are highest in the soil with olivine, Ol 63 have 1794 µg/g and Ol 450 have 1991.8 µg/g. Soil with quartz and anorthosite have nickel concentrations from 200 to 218 µg/g and dolomite have 52.3 µg/g.

Table 3.3 pH values measured in the soil (Mørkved, personal communication) soil mineral incubation experiment. Minerals examined in SEM are Ol 450 (olivine 250-450µm) and An 450 (anorthosite 250-450µm) from the Fjaler organic soil.

Sample	$CaCl_2$ – pH	DI water – pH	Nickel (mg/kg)	Chromium (mg/kg)
Quartz	3.71	4.17	217.7	12.9
Dolomite	5.13	5.44	52.3	13.0
Ol 63	5.17	5.56	1793.9	12.9
Ol 450	**4.07**	**4.44**	1991.8	12.9
An 63	3.73	4.13	205.9	13.0
An 450	**3.66**	**4.03**	200.7	12.9
Blank sample			55.6	13.9

3.3 Dissolution rate experiments

Three dissolution experiments were conducted, where each experiment had several improvements/changes from the previous.

3.3.1 Dissolution rate experiment 1

Experiment 1 was done as an initial assessment of the dissolution effect on pH change of the olivine and anorthosite used in the soil incubations (above). 0.1 M and 0.01 M nitric acid (HNO_3) concentrations were used (Fig. 3.10). In the 0.1M HNO_3 solution, dolomite (Dol) 200-450 and olivine (Ol) 200-450 have a fast pH increase the initial 24 h before increase levels off, but continue to have a small increase throughout the experiment and have a final pH between 6 and 6.5. Anorthosite (An) 200-450 and olivine (Ol) 400-450 have a steady pH increase up until 125h before the increase flattens (Fig. 3.10). An 63- remained in the same range around pH 3.2 after 24 h. There were no pH change in the Ol 200-450 and An 200-450 treatments after 125 h. Ol 200-450 reached pH 3.4 and An 200-450 pH 3.3.

In the 0.01M HNO_3 solution the Ol 63- treatment reached a pH just below 10 within 17 min which it keeps throughout the experiment, except for a small decrease on the last measurement. This is not in accordance with the pH curves in experiment 2 and is most likely a technical artefact. Dol 200-450 levels on a pH around 6.5 after 7h, but have decrease at the final measurement of the experiment. An 63- levels at a pH around 5.5 after 7h, but increase throughout the experiment have a final pH 7. Ol 200-450 and An 200-450 have a slower, but longer lasting reactions. Ol 200-450 increases throughout the experiment and have a final pH of 7.5. An 200-450 levels around pH 4, but there were some variations following measurements.

In the weaker acid (0.01M) the pHs obtained are generally higher than in the stronger acid solution (0.1M).

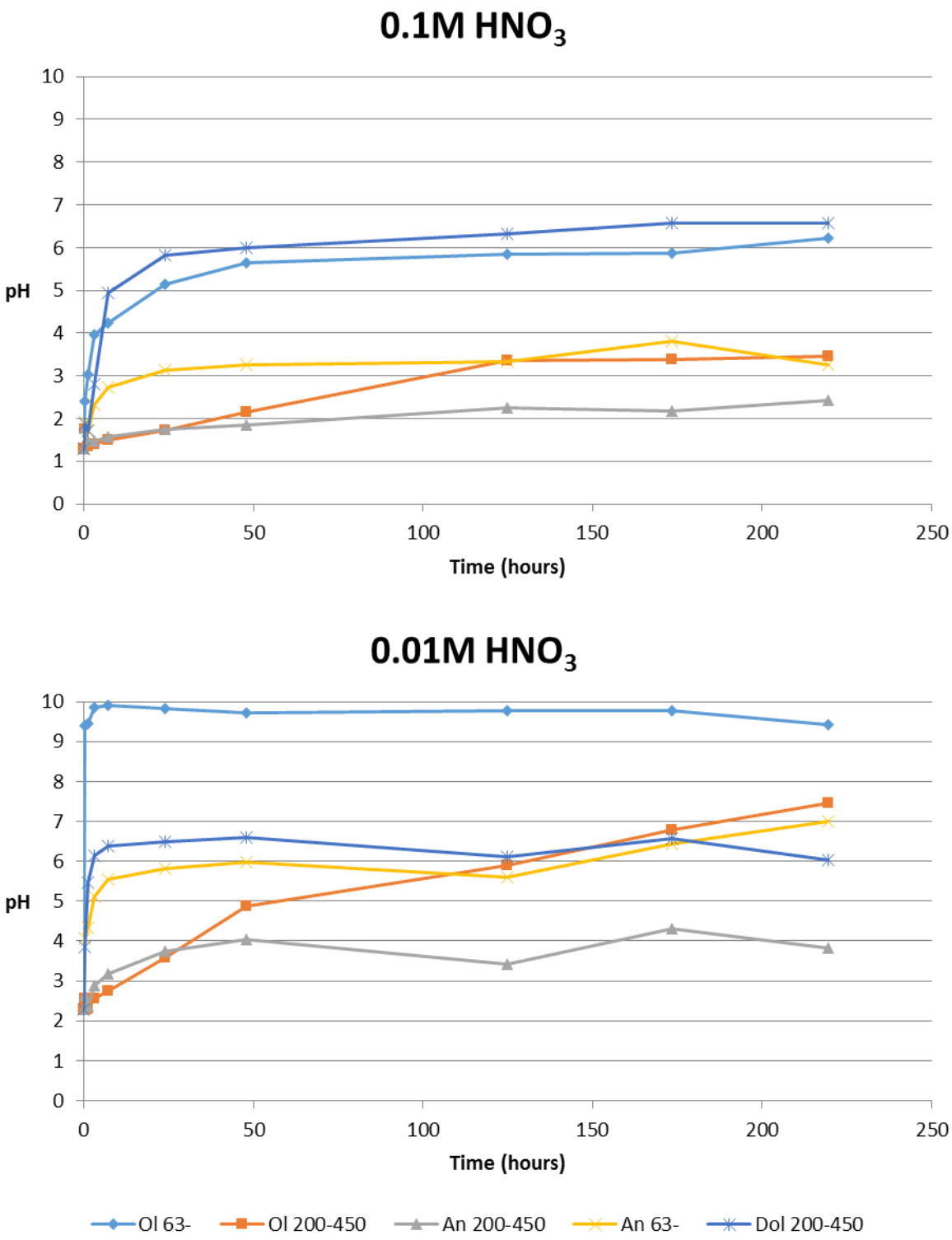

Fig. 3.10. pH evolutions in 0.1 M and 0.01 M HNO_3 for the materials. In 0.1M HNO_3 Ol 63- and Dol 200-450 end on pH 6-7, An 63- and Ol 63-125 on pH ~5 and An 200-450 on pH 2.4. In 0.01M HNO_3 Dol 200-450 end on a lower pH than in the 0.1 M HNO_3. Ol 63-, Ol 63-125 and An 63- end 3-4 pH units higher and An 63- approximately 1 unit higher than in the 0.1 M HNO_3.

3.3.2 Experiment 2

This experiment was done in preparation for a field experiment at NMBU, Ås, aiming to asses how the different materials increase pH under acidic conditions thus inform the selection of materials for use in the field experiments. Since the pH increase in experiment 1 was very rapid we added one treatment with higher concentrations 0.01 M HNO_3, and increased the water to mineral ratio. In addition, one oxalic acid treatment was included to see if this had different effect on H^+ consumption in the different rocks.

One common feature for the treatments was a fast pH increase the first 48 h, after this point all reaction rates decrease significantly. Hence in contrast to experiment 1 were most of the materials continued to increase pH throughout the experiment at a slow rate.

In the 0.1 M HNO_3 the solution starts at pH 1, the Dol 200-250 has the highest initial rate of pH increase (Fig. 3.11), with pH 6.7 after 48 h and continues to rise to pH 7.4 over the next 192 h. Ol 63- ended at the second highest value at pH 4.4, followed by Ol 63-125 at pH 3.2. The basaltic glass and norite treatments had similar pH development and ended at pH 2.5. Larvikite and eclogite treatments also had a similar pH development, however with some small pH changes and a final pH of 1.2.

In the 0.01 M HNO_3 the solution starts at pH 2, the Ol (63- and 63-125), Dol 200-250 and norite ended at pHs from 7.2-8.3 (Fig. 3.11). Larvikite, eclogite and basaltic glass. Ol 63- ended at the highest pH 8.3, followed by Dol 200-250 at pH 7.8, and norite and Ol 63-125 at pH 7.2. Ol 63-125 has a lower initial rate than the other samples in the top, but continue to rise after the others have stabilized. In the bottom all samples follow a similar reaction path and ended on pH around 3.6.

In the 0.01 M oxalic acid treatment Dol 63-, Dol 200-250 and Ol 63- ended at pH 8-9. Dol 63- levelled out after 48 h and stayed on the level until a dip on last measurement (Fig. 3.11). Ol 63- and Dol 200-250 have a high initial rate, but also continue to increase during the whole experiment. Ol 63-125 end at pH 6.9 and norite at pH 5.9, in both treatments the pH increase is highest during the first 48 h, but continue with a minor increase the rest if the experiment. Basaltic glass ended at pH 4.8 closely followed by larvikite on pH 4.2. Eclogite ended at pH 2.5.

The lowest maximum pHs were found in the 0.1 M HNO_3 acid solution. In the 0.01 M HNO_3 Dol 200-250, Ol (63- and 63-125) and norite all end with a pH above 7, while eclogite, larviktie and basaltic glass ended on approximately the same pH of 3.6. In the 0.01 M oxalic acid the pHs at experiment end are spread over a large range. Dol 200-250, larvikite, basaktic glass end at a higher pH than in the 0.01 M nitric acid, Ol (63- and 63-125) end on approximately the same pH and eclogite and nepheline syenite end on a lower pH.

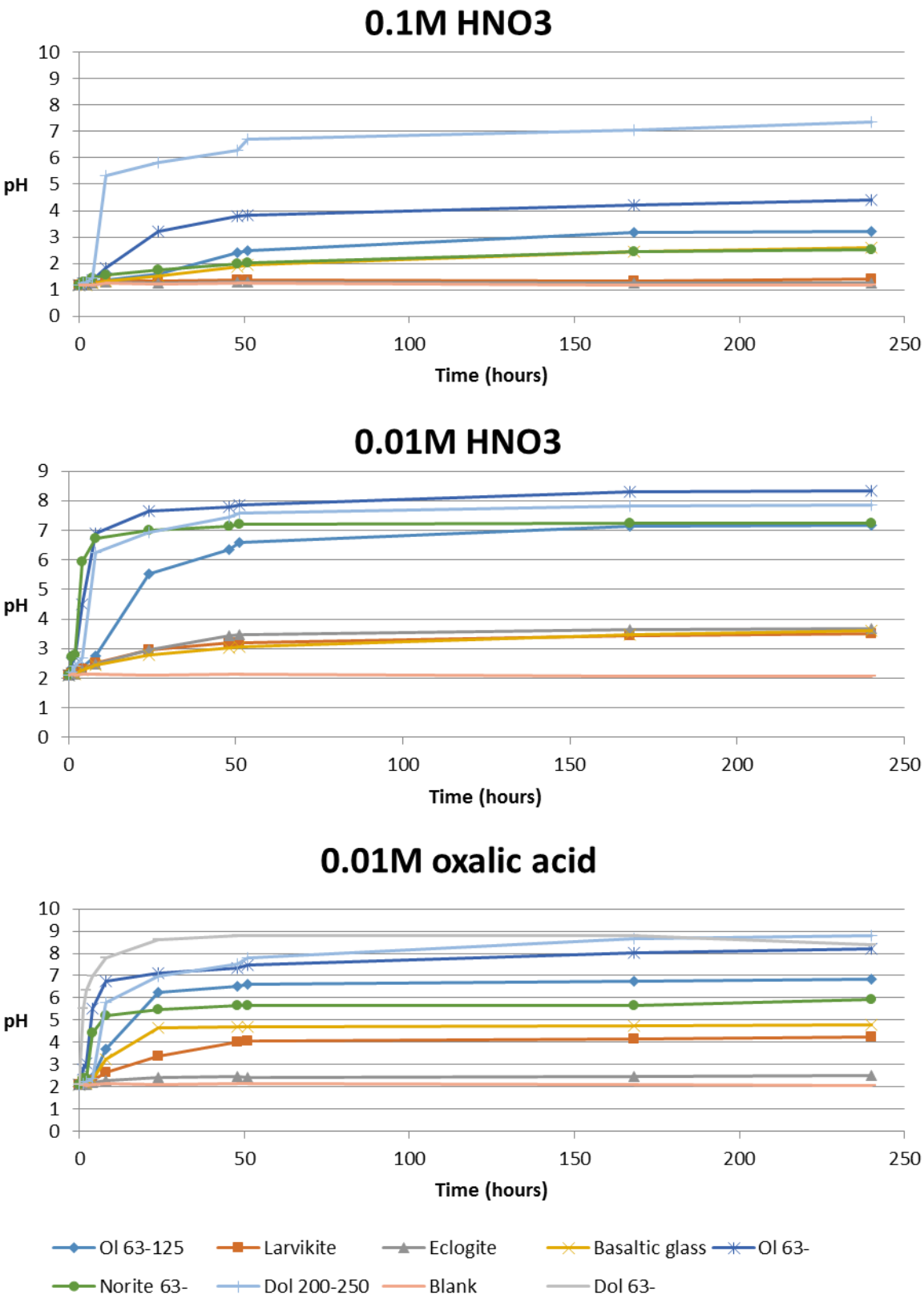

Fig. 3.11 pH development in 0.1 M and 0.01 M HNO_3 and 0.01 M oxalic acid solutions for the materials. The end pHs are lowest for all materials in the 0.1 M HNO_3. In 0.01M HNO_3 most materials end above pH 7, basaltic glass, eclogite and larvikite end below pH 4. In the 0.01 M oxalic acid olivine and dolomite end on approximately the same pH as in 0.01M nitric acid, norite and eclogite on a lower pH, larvikite and basaltic glass on a higher pH.

3.3.3 Experiment 3

In experiment 3 the focus was to assess the dissolution rates and the H^+ consumption capacity in the different materials chosen for the ongoing field experiment. Four different acid solutions were included to compare dissolution rates of the different materials with different potential ligand effects: Hydrochloric acid (HCl) , oxalic acid, acetic acid (+ HCl) and peat soil (+ HCl) (Fig. 3.12). A main difference to the above experiments was that the liquid volume was larger (to decrease the chance of saturation of some elements, that could inhibit dissolution), the acid solution was more dilute (to approach field conditions and reduce dissolution rate). And the choice of materials included those of the previously mentioned field experiments.

In the HCl solution most of the samples end with a pH between 7-8, except eclogite and larvikite. Ol 63-125 and eclogite continue to increase pH significantly after 100 h, but the largest increase happens within the first 100 h. Norite, dolomite, nepheline syenite and Ol 63- have small changes in pH after 100 h, except for a 0.5 pH decrease on the last measurement interval for nepheline syenite.

In the oxalic acid treatment the final pHs are quite similar to the ones in the HCl treatment (Fig. 3.12). Most samples end at pH 7 to 8, except eclogite and larvikite that end just beneath pH 6. Dolomite, norite, olivine 63- and larvikite almost reach their final pHs within the first 100 h, having only a slight increase throughout the experiment. Nepheline syenite, olivine 63-125 and eclogite have a slower initial pH increase and continue to increase for a longer time than the other samples.

In the the acetic acid (+ HCl) treatment (Fig. 3.12), all materials end at pH 7-8, except olivine (63-125) on pH 6.8, and eclogite on pH 4.7 and larvikite on pH 4.3. Ol 63-125 have a slower initial rate but continues to increase pH throughout the experiment. Eclogite and larvikite both have rather slow initial rates and level out shortly after 100 h, eclogite end on pH 4.7 and Larvikite on pH 4.3.

In the peat soil solution (Fig. 3.12) there were more variation in reaction rates and end pHs. Dolomite, Ol (63-), nepheline syenite and Ol (63-125) all continue to increase pH after 100 h at a low rate, norite does not change pH after 100 h. Eclogite and larvikite decrease in pH after 100 h before the pH stabilises after 240 h, and both increase to pH 3.8 in the last measurement. Dolomite and olivine (63-) increase pH the most, dolomite end at pH 7.3 and olivine (63-) at pH 6.8. Olivine (63-125) and nepheline syenite end at a similar pH around 5.65 and norite ends at pH 4.5.

In the HCl, oxalic acid and acetic acid (+ HCl) solutions all materials, except larvikite and eclogite, end on a pH approximately between 7 and 8. Which correlated with observations done in 0.01 nitric acid in experiment 2 (Fig. 3.11).

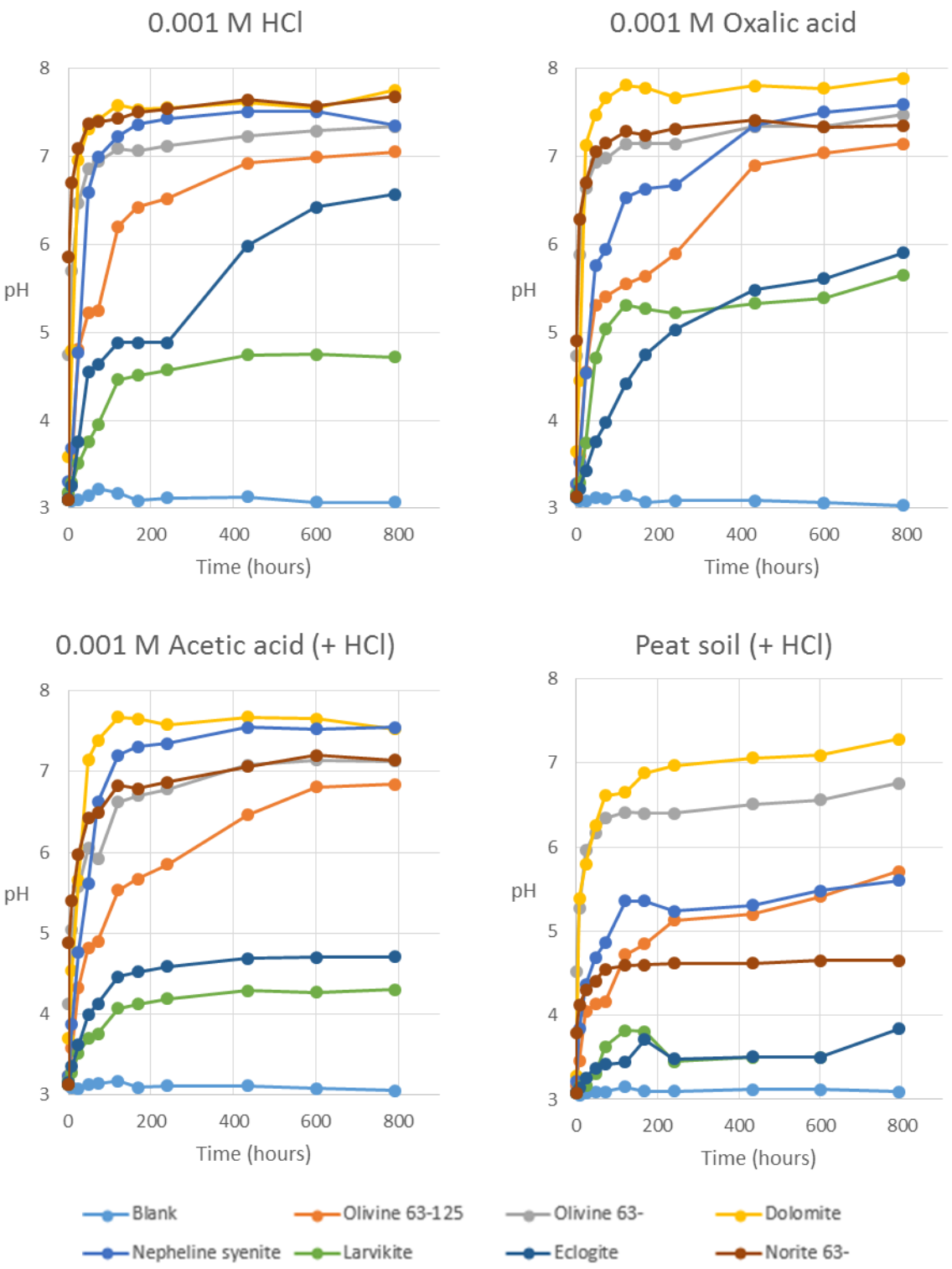

Fig. 3.12 pH evolutions in 0.001 M HCl, 0.001 M oxalic acid, 0.001 M acetic acid (+ HCl) and peat soil (+ HCl). Eclogite and larivkite in average end 1-2 pH units lower than the other materials. The end pHs in HCl, acetic acid (+ HCl) and oxalic acid are fairly similar, except larvikite and eclogite were 1 pH unit lower in the acetic acid (+ HCl). In the peat soil (+ HCl) solution all materials (except dolomite) have end pHs approximately 1-2 units lower than in the other acid solutions.

3.4 Release of elements to solution

Element concentrations were plotted against time to get an overview of element release from the different samples to solution (see all plots in appendix A). In Fig. 3.13 the Mg^{2+}, Si^{4+}, Cr^{3+} and Ni^{2+} concentrations and pH are plotted against time (hours) for the Ol 63-125 treatments.

For all treatments the amount of element dissolved from the material with the highest concentrations were Mg from olivine (ranging from 428ppm in soil and 11 ppm in HCl) and Ca^{2+} for the other samples (ranging from 105ppm to 6 ppm) (Table 3.4). The one exception is for eclogite in oxalic acid were Mg has the highest concentration.

The concentration of released elements varies between the acid treatments (Table 3.4). The peat soil (+ HCl) treatment resulted in the highest concentrations of leached elements for olivine, dolomite and larvikite. While the acetic acid (+ HCl) treatment resulted in the highest leached concentrations for nepheline syenite, eclogite and norite. For Ol 63- the Mg concentrations in peat soil (+ HCl) are 24 times larger than in oxalic and acetic acid (+ HCl) treatments, also the concentrations in oxalic and acetic acid (+ HCl) treatment are 10 ppm larger than in the HCl (Fig. 3.13). Dolomite, nepheline syenite and norite have the fourth highest concentrations of leached Ca in oxalic acid, third in HCl and second in acetic acid (+ HCl). For larvikite the HCl, oxalic acid and acetic acid (+ HCl) treatments results in a similar Ca concentration. For eclogite the Ca concentration in HCl and acetic acid (+ HCl) are in the same range while oxalic acid has a lower concentration.

The amount of leached Cr and Ni (ppm) varied between the materials and different acid treatments. Cr and Ni had the highest concentrations in the first hours of the experiment and decreased as pH increased for the HCl and acetic acid treatments. The Cr concentrations that exceed drinking water limits (3.4 ppb) were Ol (63- and 125) in peat soil (+ HCl), larvikite in oxalic acid and peat soil (+ HCl) and norite in peat soil (+ HCl). The Ni concentrations that exceed drinking water limits (1.7 ppb) were Ol 63-125, larvikite and norite in all acid solutions, Ol 63- in oxalic acid, acetic acid and peat soil (+ HCl), eclogite in oxalic acid and nepheline syenite in peat soil (+ HCl). The highest concentrations of Cr and Ni were from Ol (63- and 63-125) and norite. The solution concentrations are classified using the Norwegian classification system for fresh waters from the Norwegian Environmental agency (Weideborg et al., 2012).

Table 3.4 Net release (ppm) of Mg^{2+} from olivine and Ca^{2+} for the other materials for the different acid treatments are included.

	HCl- Mg^{2+} or Ca^{2+}	Oxalic acid - Mg^{2+} or Ca^{2+}	Acetic acid (+ (HCl) - Mg^{2+} or Ca^{2+}	Peat soil (+ HCl) - Mg^{2+} or Ca^{2+}
Ol 63-	14.7	25.1	25.8	**428.7**
Ol 63-125	10.7	20.9	21.6	**44.6**
Nepheline syenite	27.3	6.4	**46.0**	30.1
Dolomite	26.6	12.5	44.5	**105.1**
Larvikite	5.9	5.3	6.5	**9.4**
Eclogite	15.8	1.5	**17.6**	13.0
Norite	33.0	5.7	**36.5**	19.3

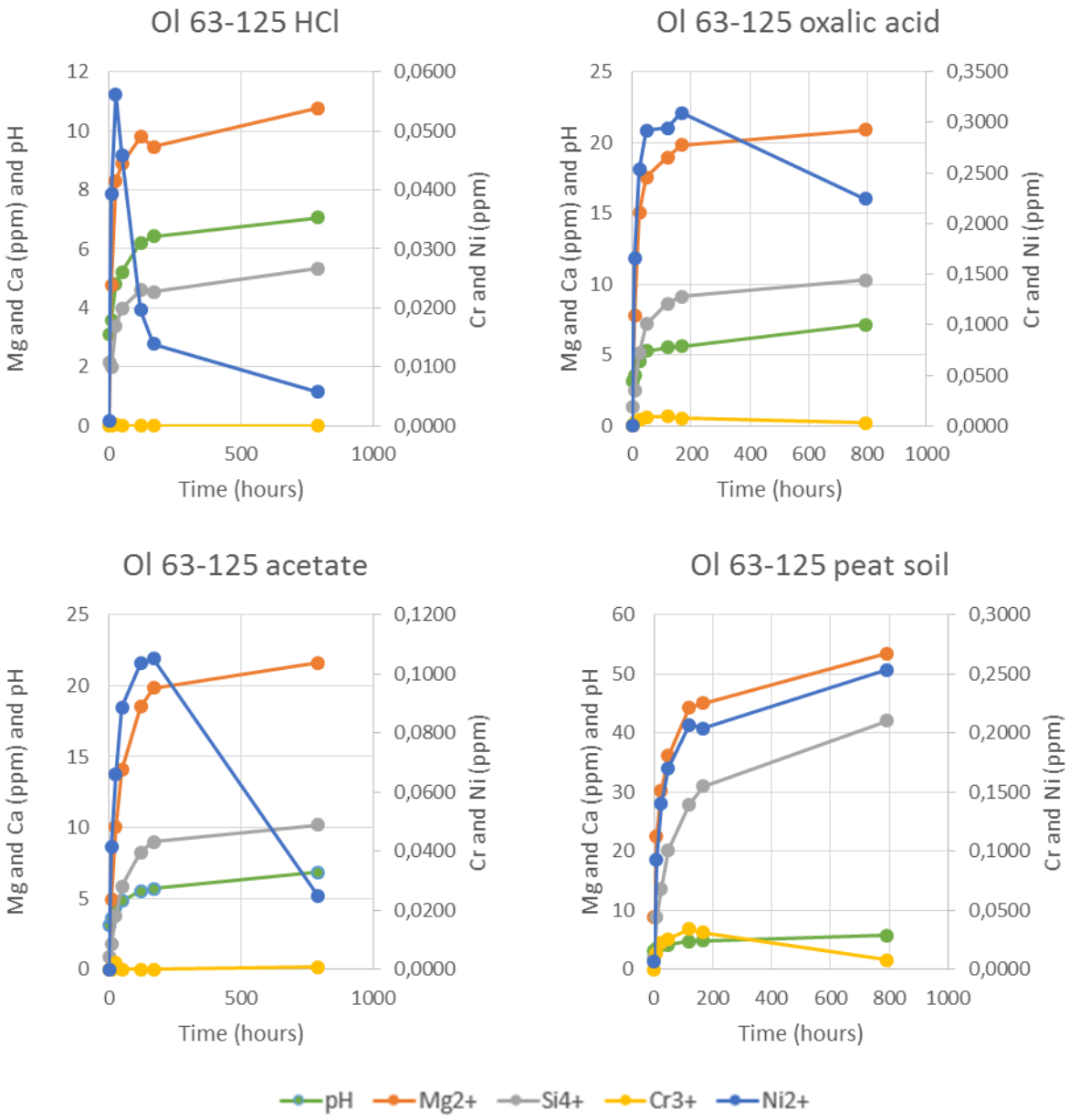

Fig. 3.13 Element concentrations for Mg^{2+}, Si^{4+}, Cr^{3+} and Ni^{2+} (ppm) and pH plotted against time, for the Ol 63-125 treatments. The highest pH in the peat soil was 5.7. See appendix A for the other plots.

3.5 Dissolution rates

The initial cation dissolution rates (moles Mg or Ca/m^2/s) varied between the materials over 2 orders of magnitude (Fig. 3.14). Dolomite, nepheline syneite and eclogite had initial rates (at least for some acid treatments) around 10^{-8} mol/m^2/s. Olivine mainly $10^{-9}$to $10^{-9.5}$ M/m^2/s, whearas larvikite and norite had rates of $10^{-9.4}$ to 10^{-10} mol/m^2/s.

For Ol (63- and 63-125) the different acid solutions do not significantly increase or decrease the dissolution rates. Except for Ol 63- in peat soil (+ HCl) were the dissolution rates are 1 log unit faster than in the other acid solutions. Dolomite and nepheline syenite had significantly lower dissolution rates in the oxalic acid solutions, compared to the other acid solutions. For nepheline syenite the peat soil (+ HCl) solution also caused lower dissolution rates, but not as low as in oxalic acid. For eclogite and norite oxalic acid and peat soil (+ HCl) caused lower dissolution rates than the other acid solutions. For larvikite the dissolution rate in oxalic acid was slightly faster than in the other acid solutions. Dolomite, nepheline syenite and norite all have a significant drop in dissolution rates as pH exceeds 7.

Oxalic acid treatments caused lower dissolution rates in dolomite, nepheline syenite, eclogite and norite, compared to dissolution rates in HCl and acetate (+ HCl). The peat soil (+ HCl) caused lower dissolution rates in nepheline syenite, eclogite and norite, compared to HCl and acetic acid (+ HCl). The dissolution rates in HCl and acetic acid (+ HCl) are relatively similar for all materials.

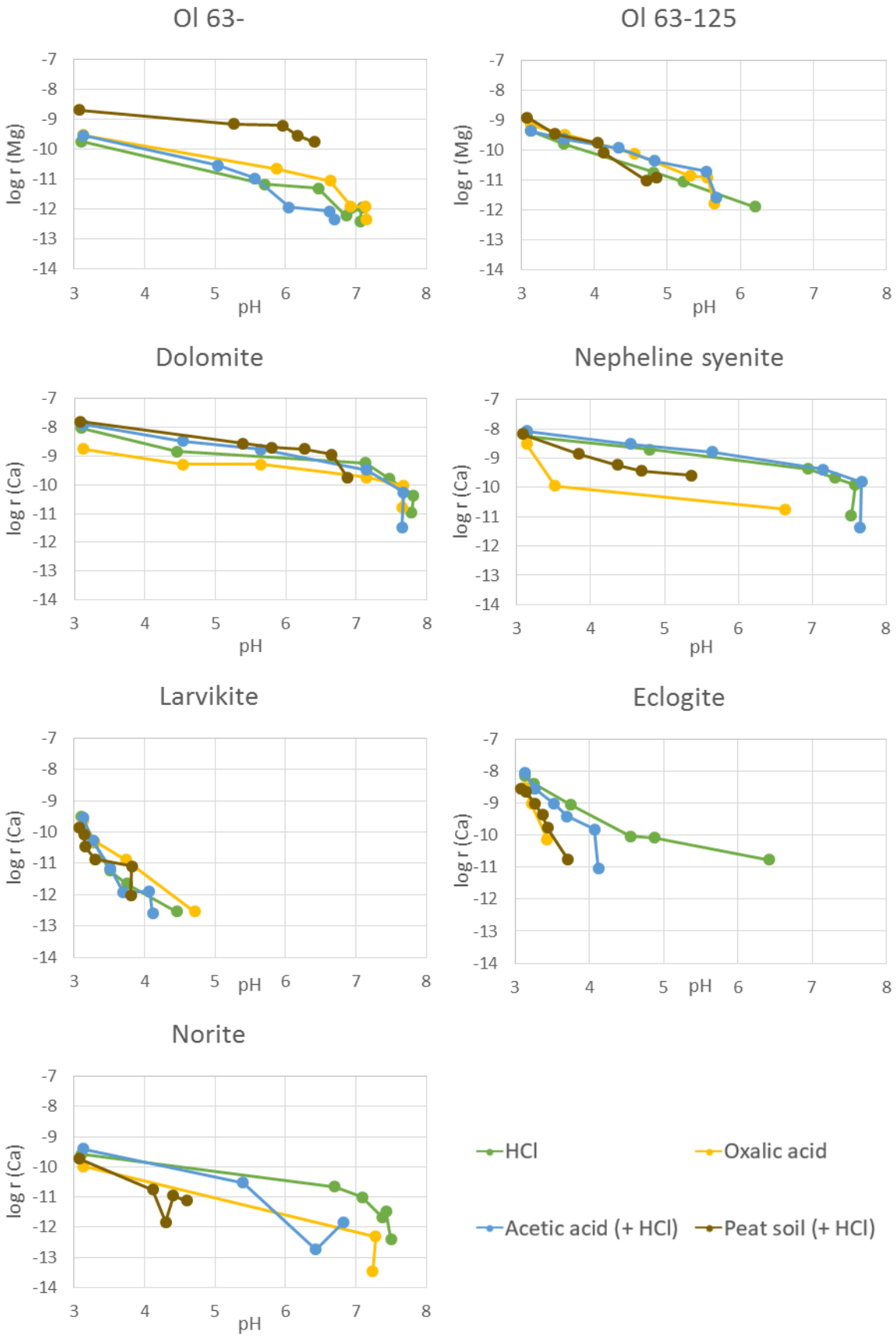

Fig. 3.14 Log dissolution rates plotted against pH for experiment 3. r = mol/m²/s

There was a non-stoichiometric dissolution from all materials (Fig. 3.15). Dissolution of Ol (63- and 63-125), larvikite, eclogite and norite shifted closer to a stoichiometric dissolution (element ratio in start material I Fig.) as the experiment evolved, except Ol 63- in peat soil (+ HCl) which shift away from stoichiometry. Dissolution of dolomite and nepheline syenite shifted away from stoichiometry as the experiment evolved. All materials had a higher release of Mg or Ca compared to Si release (Mg for dolomite).

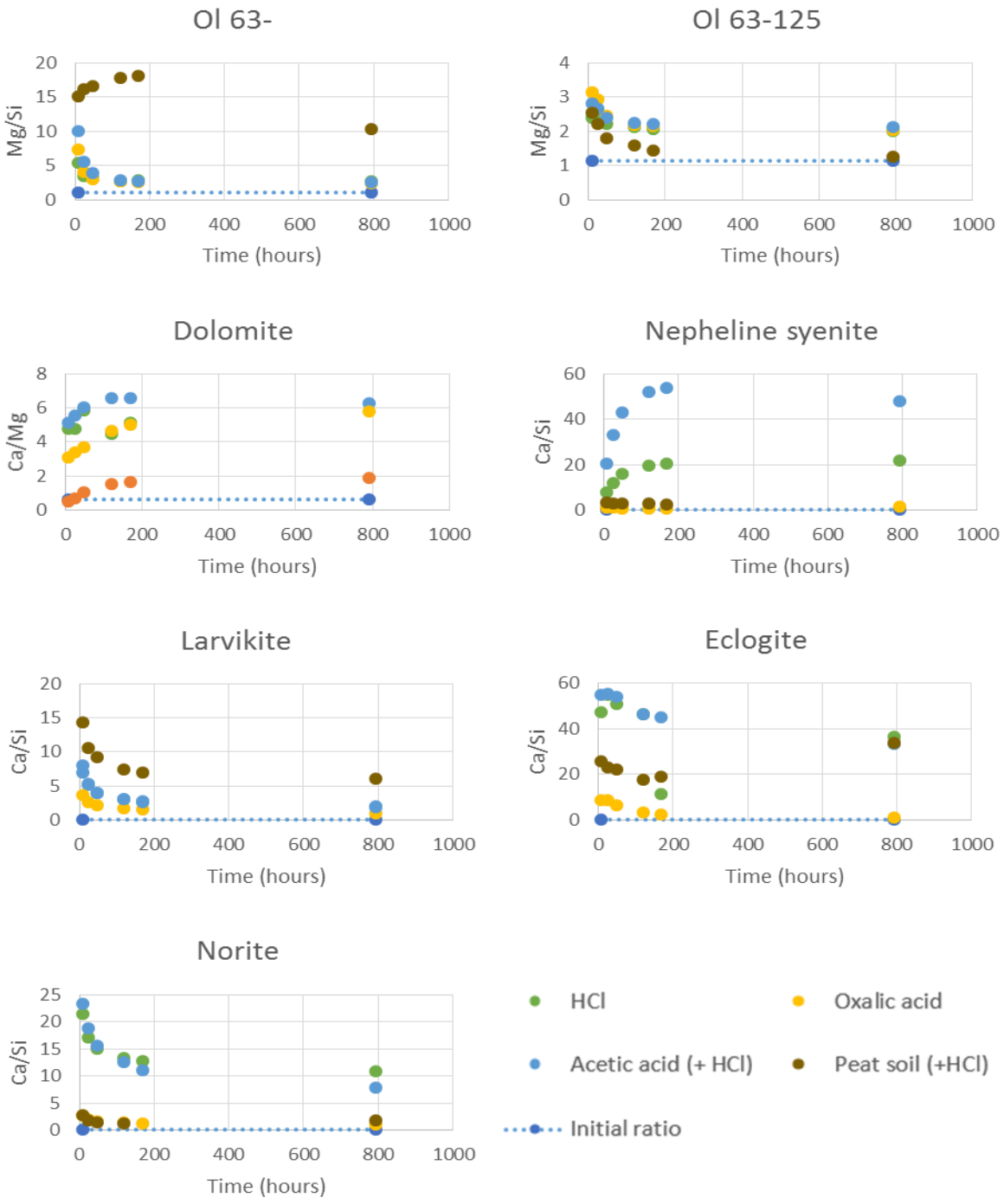

Fig. 3.15 Stoichiometry of dissolution rates from experiment 3. Mg/Si ratios were used for olivine, Ca/Mg for dolomite and Ca/Si for the other materials.

Specific surface measurements were done on Ol (63- and 63-125) nepheline syenite, eclogite and norite (from HCl and oxalic acid solutions) after experiment 3 (Table 3.5). The difference in percentage is calculated from specific surface measurements done prior to the experiment (Table 3.1). All samples, except norite have an increased specific surface area. There difference varies greatly, from a decrease of 23 % to an increase of 252 %. HCl and oxalic acid solutions have resulted in quite similar surfaces for olivine (63-125), olivine (63-) and norite. For nepheline syenite and eclogite the oxalic acid solution have resulted in a much higher surface area than the HCl solution, especially nepheline syenite.

Table 3.5 Specific surface measurements done on samples after experiment 3. The difference (%) is calculated from measurements done on the material in advance of the experiment.

Sample	Acid solution	Original SSA[a] (m^2g^{-1})	SSA (m^2g^{-1}) after exp. 3	Difference (%)
Ol 63-125	HCl	1.59	2.81	77
	Oxalic acid		2.74	73
Ol 63-	HCl	8.42	8.86	5.2
	Oxalic acid		9.66	15
Nepheline syenite	HCl	0.16	0.20	23
	Oxalic acid		0.57	253
Eclogite	HCl	0.07	0.13	104
	Oxalic acid		0.17	157
Norite	HCl	6.93	5.41	-22
	Oxalic acid		5.30	-23

SSA = specific surface area

Based on that some of the materials had a large increase in surface area after experiment 3, Olivine (63-125), nepheline syenite and eclogite were examined with SEM for dissolution features. Material from the experiment were compared to fresh/unaltered material, with an increase between 72-252% in surface area differences were expected. However, no prominent features were observed on any of the grains.

4 Discussion

4.1 Quantification of olivine and anorthosite dissolution in soil by SEM

The SEM studies (Fig. 3.4 and Fig. 3.7) reveals that the olivine grains were generally more weathered than the anorthosite after the soil incubation. The different dissolution features will be discussed in terms of formation and how they influence mineral dissolution.

4.1.1 Etch-pits

Etch-pits are the most common dissolution features on both the olivine and anorthosite grains. Etch-pits were observed on 71% of the olivine grains and 62% of the anorthosite grains. Etch-pits observed on the olivine grains have several different shapes and sizes (Fig. 3.5 A-D). At the same crystallographic planes the pit shapes are similar, but they vary in size and depth. Etch-pits on the anorthosite grains have a different morphology than pits developed on the olivine grains. On anorthosite the etch-pits appear as an elongated network on the mineral surface. The distribution of etch-pits on the anorthosite grains are different, but the morphology are similar. Frequent observations of etch-pits imply that it is an important feature in weathering of olivine and anorthosite grains.

Olivine etch-pits are formed at low temperatures and acidic pH at near surface conditions and not inherited by pre-weathering alterations or processes deeper in the crust (Awad et al., 2000; Velbel and Ranck, 2008). No pitting (or other dissolution features) were observed on the non-incubated olivine grains confirming that this is a feature directly connected to dissolution in acidic soil. The different etch-pit shapes on the olivine can be related to the crystallographic axis. It is suggested that the basic etch-pits are cone shaped and the cones may bind together creating a variety of conical and funnel shapes, and also that the basic etch-pit shape is dependent on the crystallographic axis (Velbel, 2009). The formation of etch-pits increased evidently the specific surface area on the grain in the soil. As the size of the etch-pit increase with increasing weathering (Velbel, 2009), it can be expected that the variation in degree of pitting and size of etch pits between grains is a direct measurement of variation in dissolution rate at different microsites in soil. The variation in etch-pit size on the same crystallographic plane could be related to specific microenvironments on the grain surface, or maybe

crystal defects increased dissolution at specific sites. Anyhow, olivine etch-pits may be considered as a feature that verifies dissolution at surface conditions and is a direct measure of dissolution.

Formation of the anorthosite etch-pit can be related to leaching of Ca-rich lamellae, leaving the more resistant Na-rich layers. Inskeep et al. (1991) observed a 30-50% Ca depletion and a slight Na enrichment on a labrodorite mineral surface weathered at pH 3.7 for 415 days. The results of the present study show that the extent of these lamellae etch-pits varies greatly and in some cases almost covers the entire grain. If these structures are the result of the dissolution of Ca-rich lamellae a chemical variation on the grain surface is expected. This was examined with SEM-EDS analysis and using the backscatter lens (Fig. 4.1) in the SEM.

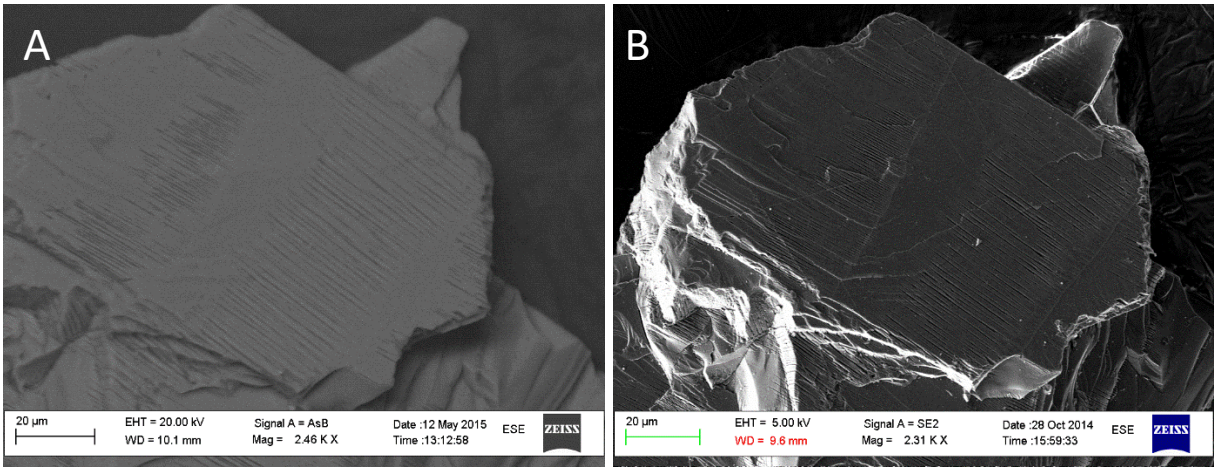

Fig. 4.1 These images show lamellae etch-pit structures on an anorthosite grain, A) backscatter and B) secondary electron image. From the backscatter image no chemical differences can be observed.

Both images are of the same lamellae etch-structures; Fig. 4.1 A shows a backscatter image and Fig. 4.1 B a secondary electron image. The etching structures are visible in both images, but no chemical differences can be observed on the backscatter image. The lack of chemical diffrensiation in the backscatter image could indicate that the observed structures are a part of the crystal structure or that there has been a more homogeneous weathering. It is thus likely that the observed etching structures follow the mineral structure, and that the weathering has not progressed far enough to be detected as chemical differenciation with backscatter imaging. It is suggested by Lasaga and Blum (1986) that etch pit formation is induced by dislocations. The density of dislocations on mineral grains and surfaces varies, and could partly explain the different extent of etch pits observed on the individual grains. On the unweathered anorthosite grains there are minor structures that resemble the etch pits structures found, but they are not very abundant. Some crystal structures may have been interpreted as etch pits but this will most likely not significantly effect the overall classification.

The formation of etch pits on olivine and anorthosite after 1.5 years of soil weathering is the most frequent observed dissoltion structure. Etch-pits will increase the specific surface area of the mineral grains and potentially enhance further weathering, particularily in olivine were selective leaching of the most reactive ions os not expected. However, the specific surface area is not necessarily propositional to reactive surface area (Hodson, 2006), making it difficult to predict exactly how these structures will effect further mineral dissolution.

4.1.2 Silica coatings

Silica layers are observed on both olivine and anorthosite grains, appearing as flakes covering an apparently fresh mineral surface, and were identified with EDS analysis during SEM examination. The layers appear more frequently and generally cover more of the olivine grains than the anorthosite grains, which may be connected to the higher degree of dissolution of the olivine

These layers are an important process in mineral dissolution: secondary mineral formation. Formation of silica layers is thought to decrease the dissolution rate among others due to the inhibition of diffusion of ions to and from the surface, hence it has drawn a lot of attention and research e.g. (Pokrovsky and Schott, 2000; Weissbart and Rimstidt, 2000; Liu et al., 2006; Hellmann et al., 2012; Ruiz-Agudo et al., 2012; Schott et al., 2012; Ruiz-Agudo et al., 2014). The oldest and commonly accepted theory is based on several complex processes assuming non-stoichiometric dissolution and interdiffusion of protons and cations (Schott et al., 2012). Schott et al. (2012) and Weissbart and Rimstidt (2000) did experiments on wollastonite ($CaSiO_3$) and concluded that Ca has a much higher dissolution rate than Si and leached/surface altered layers cannot be formed by stoichiometric dissolution. The Ca-H exchange leads to the formation of amorphous silica layer that grows until the total removal of Ca, and the residual silica structure collapses into a more condensed structure (Schott et al., 2012). The theory of proton-promoted dissolution and subsequent residual silica is challenged by a model of coupled dissolution described by among others Ruiz-Agudo et al. (2014). They argued that several observations done on leached/altered surface layers cannot be explained by proton-cation exchange and rather propose a model on interfacial dissolution-precipitation process. Coupled dissolution is based on an initial stoichiometric dissolution of the mineral, however not all elements are released to solution, but an interstitial boundary layer of supersaturated fluid is produced which under the right conditions can precipitate a secondary layer on the mineral surface (Ruiz-Agudo et al., 2012).

Etch-pit structures and silica layers were not observed on grain surfaces (Fig. 3.2A), which might indicate that also the formation of leached layers are dependent on the crystallographic axis. Regarding the leached layer formation theories it is difficult to suggest which is the most likely because of the lack chemical data. However, the results show that the silica layers appear as a layer on top of the fresh mineral surface, which might indicate a precipitation process as indicated by Ruiz-Agudo et al. (2014) instead of a structural collapse.

With the purpose to use rock-flour in agriculture it would be most convenient to avoid the formation of these dissolution prohibiting silica layers. However, as the formation requires quite specific weathering conditions to occur and the formation process is still debated, it is difficult to counteract the formation by any practical measures. The observed silica layers seems to crack and spall of the surface (Fig. 4.2) and may thus only temporarily inhibit dissolution if this is not an effect of the sample handling. If the fresh mineral surface creates a new silica-layer this will cause the overall dissolution to be very slow. From the observations 20% of the olivine and 14 % of the anorthosite grains have silica layers that may significantly inhibit dissolution. Although an inhibitory effect cannot be excluded, this is most likely minor in the studied system.

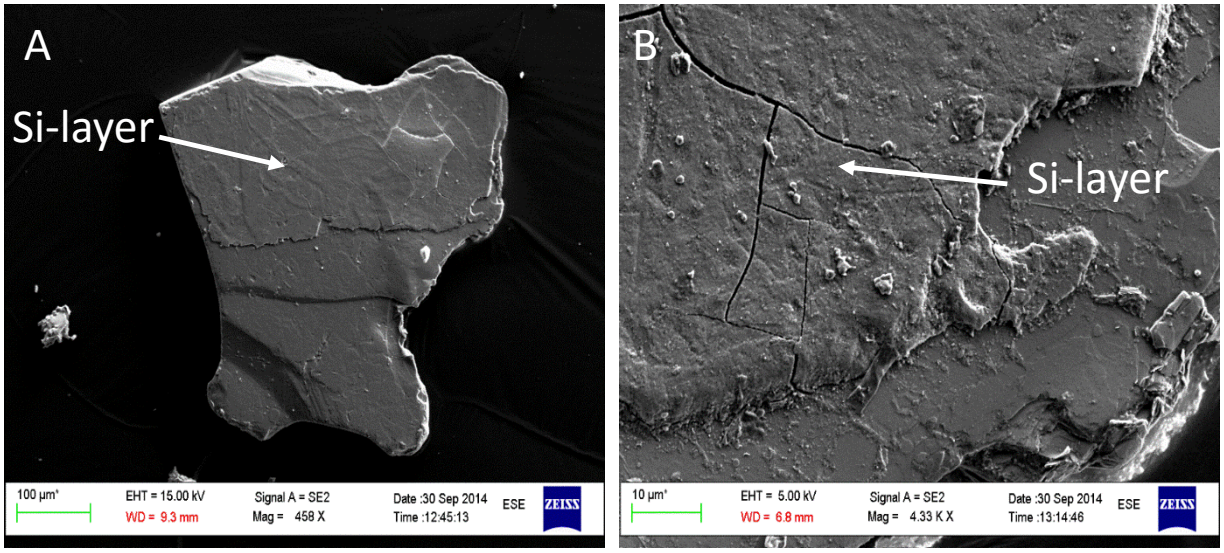

Fig. 4.2 A) Top half of this olivine grain is cover by a silica layer. B) displays the boundary between the silica layer and fresh olivine. It looks like the silica layer over time fractures and break up from the mineral surface.

4.1.3 Fractures and secondary minerals

During soil weathering, a grain surface is exposed to several processes that may cause cracks to appear. Cracks are observed on all grains, both on olivine and anorthosite, and results in increasing surface area. Cracks may appear as a result of hydration and/or dehydration reactions, increasing and decreasing the volume. Cracks will preferentially evolve along weak zones on the mineral surface, for instance in zones with crystal defects. Fractures are observed on all mineral grains, however fractures are also observed on the unweathered grains, which might have been created during mineral crushing. It was difficult to differentiate between fractures that were created by crushing and dissolution

Serpentine crystals were observed on two olivine grains (Fig. 4.3). According to stability diagrams in e.g. Faure (1998) the dissolution of Mg-silicates will change the solution composition in terms if $[Mg^{2+}]/[H^{+}]$ and $[H_4SiO_4]$, until the they reach the solubility limit of a secondary phase. In the soil incubation experiments that the olivine was sampled from there were no flow and the soils were kept at a constant soil humidity. From EDS analysis of the observed crystals Si was detected, which indicates that they were most likely serpentine and not brucite ($Mg(OH)_2$), but the EDS analysis might go deeper than the crystal thickness.

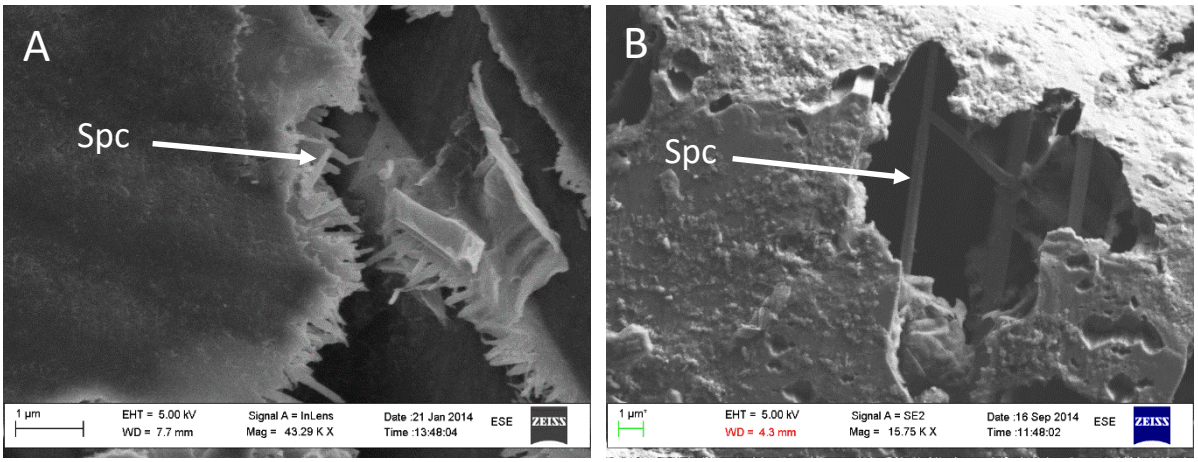

Fig. 4.3 Serpentine crystals from A) olivine ID 1 and B) olivine ID 5. See appendix D for more images.

Serpentinization is generally linked to high temperature reactions, but are also shown to occur at low surface temperatures (Okland et al., 2012). It is thus likely that there is significant formation of serpentine on olivine grains in soil. Fracturing of the mineral surface can also be linked to

serpentinization processes, as the adsorption of water may lead to serpentinization and volume increase, which further may lead to fractures on the mineral surface.

An aluminium layer was also identified on one olivine grain using EDS analysis. Since the aluminium leaching from olivine should be negligible it most likely derives from another source, this could be from the soil or the glass bottle that contained the soil samples. The aluminium layer is most likely the result of precipitation of an Al hydroxide, such as gibbsite ($Al(OH)_3$) or diaspore (AlO (OH)).

Secondary products from anorthosite dissolution is typically a clay mineral such as gibbsite, kaolinite or phyrophyllite (e.g. Faure, 1998). Which product that is formed depends on the solution composition. Some structures that resembled clay minerals on the anorthosite grains were observed, however similar structures were observed on fresh grains (Fig. 4.4). It is therefore not certain weather this was a result of weathering during incubation in soils. The formation of clay minerals would probaly decrease the overall weathering and hence the pH management effect.

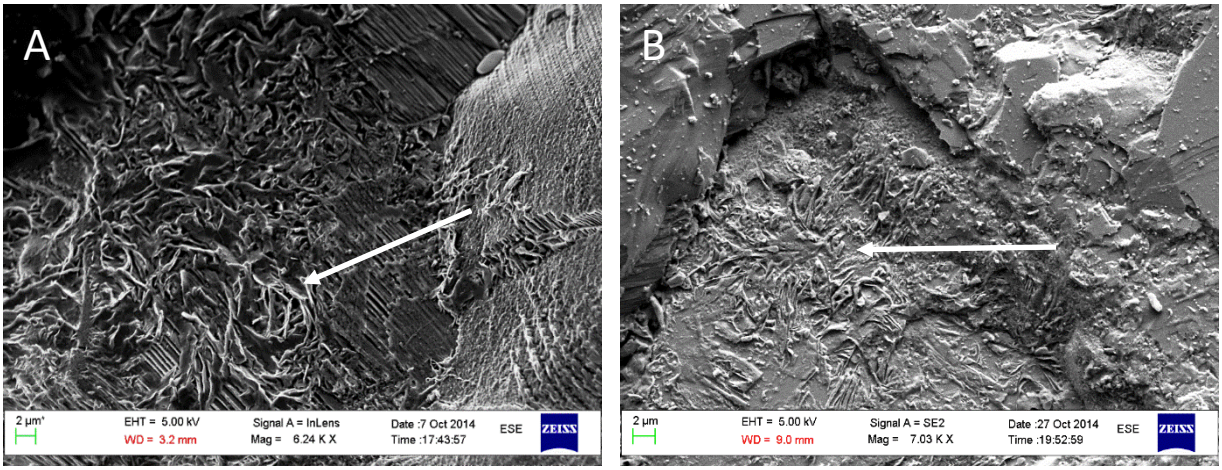

Fig. 4.4 A) weathered anorthosite grain displaying structures that resemble clay minerals, however B) similar structures were observed on fresh anorthosite grains. A = anorthosite ID 1.

4.1.4 Quantification of dissolution based on SEM

The dissolution quantification shows that after 1.5 year of soil incubation the olivine grains were more dissolved than the anorthosite grains. This also correlates with pH measured from the incubation soil, were olivine dissolution results in a higher pH (pH 4.44) than anorthosite dissolution (pH 4.03). The pitting structures are an important part of dissolution in terms of increasing pH as they are the most abundant dissolution features. Even though the grains have been exposed to soils for 1.5 years there is still great potential for further weathering. The silica layers may deacrease the dissolution rates at some grains, but it is most likely not a limiting factor. However, the pH increase in the soil has most likely reduced to dissolution rates.

The reason some grains are more dissolved than others is most probably related to inhomogeneous mixing of soil and mineral grains, where the direct contact between soil and mineral grains might be different from grain to grain. Since the soils were unsaturated with water the thickness and extent of water films in the system will limit diffusion and thus ion concentrations. It is therefore likely that the microenvironments control dissolution rates greatly. From dissolution experiment 1 we also found that olivine dissolution results in higher pH than anorthosite dissolution (Fig. 3.10). This proves that laboratory experiment can provide useful information considering rock samples buffer capacities in soils.

4.2 Dissolution rates in acidic solutions

4.2.1 Dissolution stoichiometry

All materials showed a non-stoichiometric dissolution and release more Mg or Ca than Si compared to their parent materials (Fig. 3.15). This is in accordance with observations by Oelkers (2001b) who find an initial preferential release of Mg or Ca at acidic conditions. We observe that dissolution in organic acids in general were closer to stoichiometric dissolution than in the inorganic acid. Other authors have found that it may take a substantial amount of time before a stoichiometric dissolution is achieved and the time may also vary with rock/mineral material. E.g Chen and Brantley (1998) achieved a steady state dissolution after 2700 h for diposide and anthophyllite at acid pH, Stillings and Brantley (1995) achieved stoichiometric dissolution after 500-1000 h for microcline, albite and bytownite, and over 3000 h for oligiclase at pH 3. Calculations/measurements of dissolution rates may lead to ambiguities in the pH effect if it is done before a stoichiometric dissolution is achieved, (Oelkers and Schott, 2001) as a greater pH increase can be expected in the initial phase.

Most dissolution rate studies use the Si release, because this is conncected to breaking of the crystal structure. However, some metal-oxygen bonds break faster than others and may be removed far before the mineral structure is destroyed (Oelkers, 2001b). In this thesis the experiments were relatively short, much of the pH change and dissolution happened in the initial phase. When we did not have stoichiometric dissolution, Si release would not represent this phase of the dissolution. There is no single element that represents dissolution for all materials.

Since a main objective of these experiments were to assess and compare the pH trajectories during dissolution of silicates, the dissolution rates in this thesis was calculated by using the fastest releasing elements and not the element considering mineral structure breaking, which were Mg for olivine and Ca for the other samples. It can be argued that Ca is not the best choice for all samples for all samples as the Ca content varies between the samples (Table 3.1), but Ca was the fastest dissolving elements from all materials where it was used and therefore used as a measure for dissolution. There were some irregularities in the Si release rates which makes them unsuitable for comparing the ligand effect, e.g. in the HCl solution Ol 63-125 only had one positive dissolution rate using Si. However, by combining the dissolution rates based on Si release for all acid treatments it was possible to compare the dissolution rates to previous studies.

4.2.2 Comparison of dissolution rates of the different materials with literature data

The olivine dissolution rate measurements (based on Mg release) are generally lower than those in the literature, and the difference increase with higher pH (Fig. 4.5). The fast initial pH increase in the experiments might explain why the difference increase with elevating pH. A probable reason for the increasing difference with increasing pH is the increasing concentration of Mg and other cations in solution, which might inhibit dissolution, however no geochemical modelling have been done to verify this. We could also hypothesize that there were inhibitory silica layers on the grain surfaces as the experiments progressed or that the grains were dissolved to such a degree that the reactive surface changed, however no such evidence was seen in SEM or by BET.

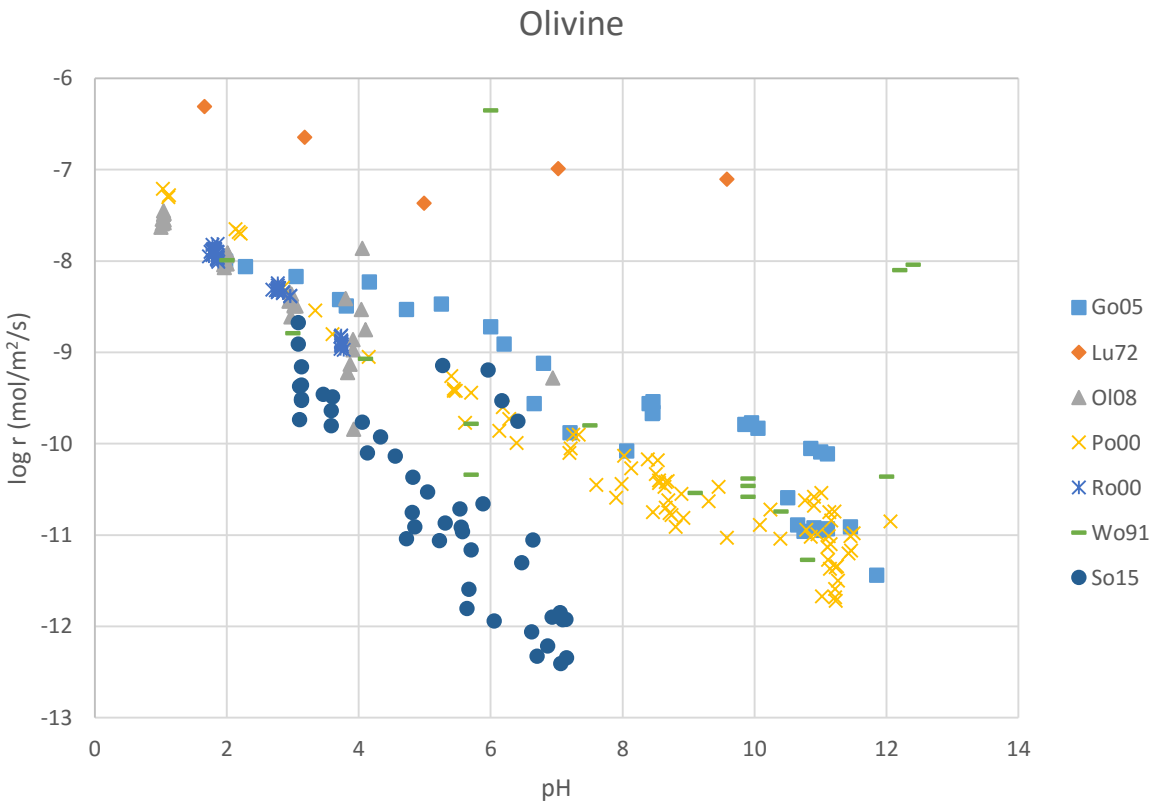

Fig. 4.5 Compilation of olivine dissolution rates (r= Mg Mol/m²/s) at 25⁰C from several authors retrieved from a review by Rimstidt et al. (2012). These rates are based on Mg release to solution. From this dataset all rates calculated for olivine (Mg) are included, without distinguishing between grains size or different acids. Except for dissolution rates from Lu72 most of them are fairly close to each other creating a decreasing trend as pH increases. In general the calculated dissolution rates (So15) are lower than all others. The difference in dissolution rates increases at higher pH. Go05 = (Golubev et al., 2005), Lu72 = (Luce et al., 1972), Ol08 =(Olsen and Rimstidt, 2008), Po00= (Pokrovsky and Schott, 2000), Ro00 = (Rosso and Rimstidt, 2000), Wo91 = (Wogelius and Walther, 1991) and So15 = This study.

The dissolution rates of dolomite were found by adding the dissolution rates for Ca and Mg, and these are compared to results from Pokrovsky et al. (2005) (Fig. 4.6). The rates used from Pokrovsky were done on Cap de Bouc (III) dolomite in open mixed flow reactors at pH from 1 to 12. Dissolution rates in this experiment were 1-2 orders lower, but had a similar decrease with elevating pH until pH 7, and the dissolution rates had an abrupt dip. The sudden drop in the observed dissolution rates are most likely the result of the solution reaching equilibrium or a saturated state.

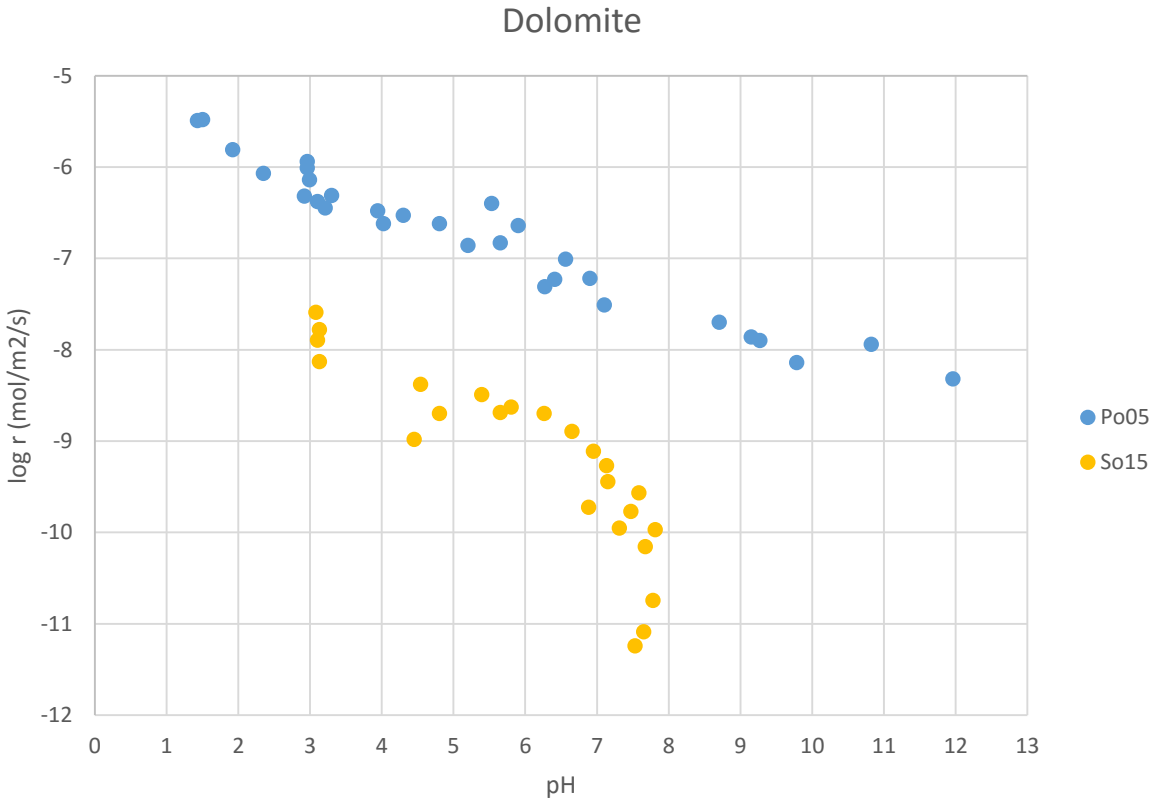

Fig. 4.6 Dolomite dissolution rates (log r Ca+ r Mg) plotted against pH. External dissolution rates were calculated from Cap de Bouc (III) dolomite at 25°C, in an open mixed flow reactor. Po05= (Pokrovsky et al., 2005) and So15= this study.

Nepheline syenite dissolution rates (based on Si release) are compared to nepheline dissolution rates from Tole et al. (1986) and Hamilton et al. (2001) (Fig. 4.7) and although there are large variations, there is reasonable agreement with the rates below pH 6, whereas the rates from Tole were an order of magnitude or more higher. The higher dissolution rates by Tole et al. (1986) compared to Hamilton et al. (2001) have been explained by a higher K content in the nepheline structure (Hamilton et al., 2001). In nepheline syenite, orthoclase and biotite all contain K, so it is difficult to say how this concentration effects these dissolution rates. Nepheline is used for comparison because it is expected to have faster dissolution rates than the other major minerals in nepheline syenite; orthoclase, biotite and hornblende (Palandri and Kharaka, 2004).

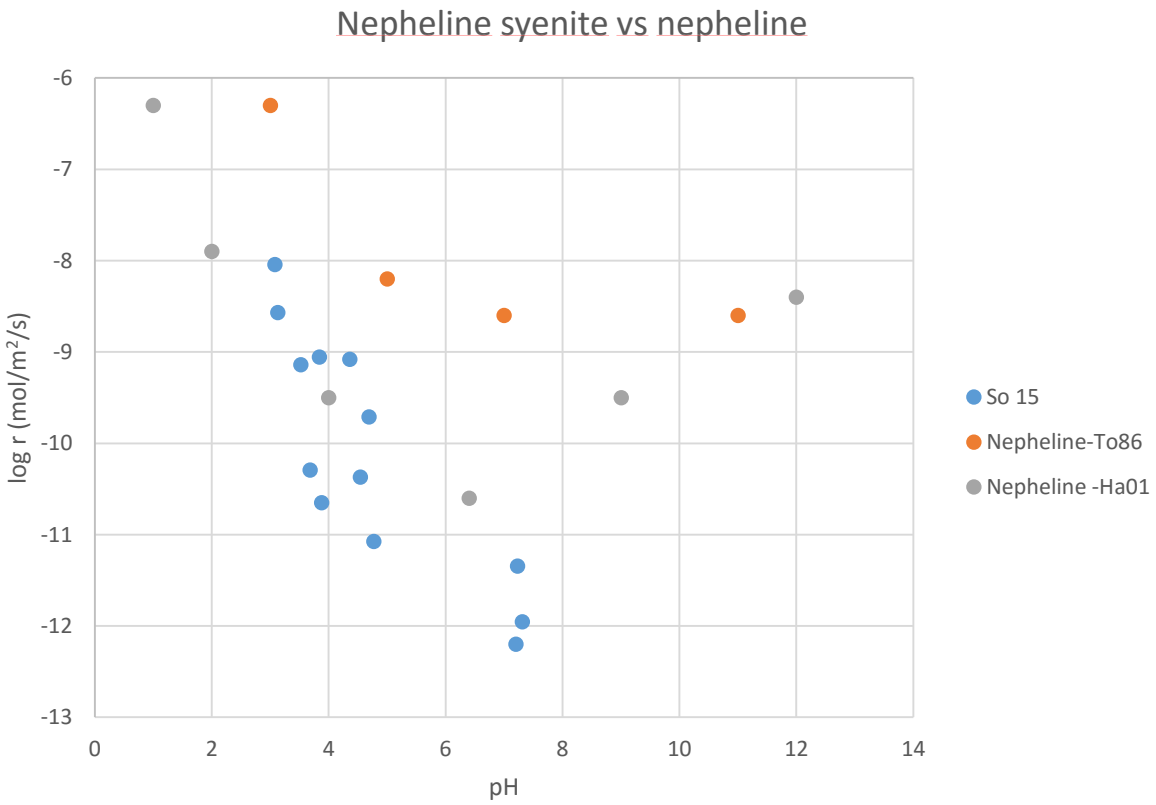

Fig. 4.7 Dissolution rate of nepheline syenite from Si release. Comparisons was done to nepheline dissolution rates, as nepheline is the main component in nepheline syenite. To86= (Tole et al., 1986), Ha01= (Hamilton et al., 2001), So15= This study.

Larvikite dissolution rates (based on Si release) are compared to anorthite from Gudbrandsson et al. (2014) and Oelkers and Schott (1995) and albite from Hamilton et al. (2001) (Fig. 4.8). Larvikite contains of albite intermediate (Table 3.2), which most likely includes the presence of k-feldspar, albite and anorthite. Larviktie dissolution rates are lower than those of anorthite and closer to the albite dissolution rates. Larvikite dissolution rates have a small decrease with elevated pH compared to anorthite, but larger than albite. Comparisons of the dissolution rates indicates that that albite and k-feldspar are the main contributors to Si release, but also influenced by anorthite. This also correlates with the amount of the different part calculated form the XRF data, $An_{0.18}Ab_{0.57}Or_{0.25}$.

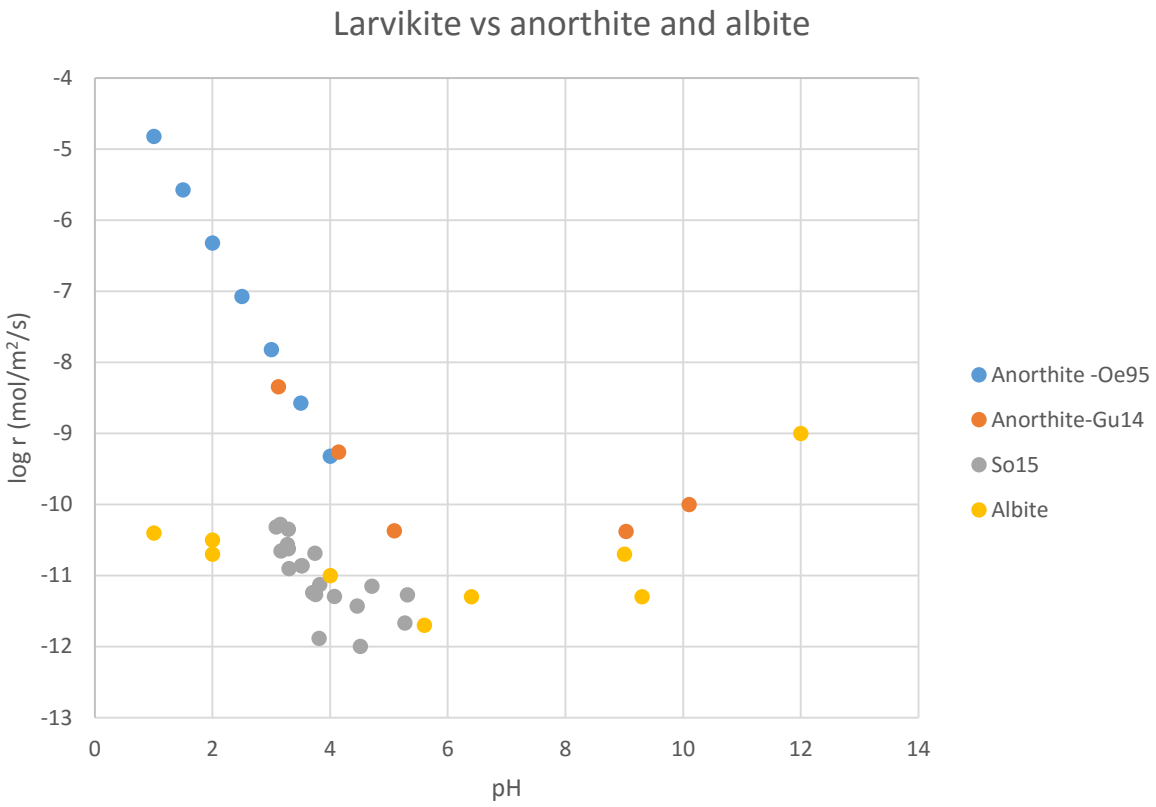

Fig. 4.8 Larvikite dissolution rates compared to anorthite (Oe95 and Gu14) and albite. Oe95 = Oelkers and Schott (1995), Gu14= Gudbrandsson et al. (2014), albite from Hamilton et al. (2001), So15 = this study.

Eclogite dissolution (based on Si release) are compared to augite (Sverdrup, 1990) and jadeite glass (Hamilton et al., 2001) (Fig. 4.9). Eclogite is mainly composed of omphacite, however no dissolution rates for omphacite were found and because omphacite composition is between augite and jadeite those were used for comparison. The eclogite dissolution rates are comparable to augite and jadite at pH 3-4 pH. Above pH 4 a lack of data and variation in eclogite rate estimates makes comparison difficult. Eclogite also most consits of a large fraction (>25%) of garnet, which will probably reduce the apparent dissolution rate of eclogite.

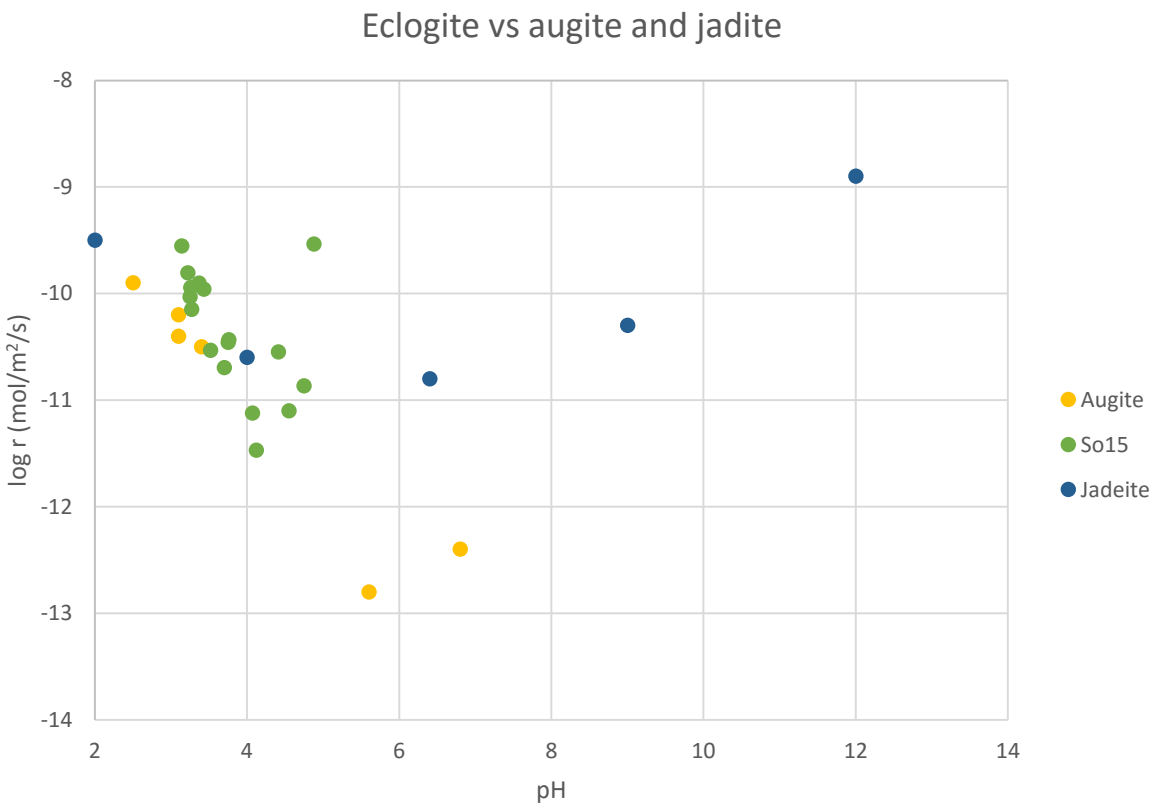

Fig. 4.9 Eclogite Si release compared to augite and jadeite dissolution rates compiled from a compilation of dissolution rates by Brantley (2008a), augite = (Sverdrup, 1990), jadeite = (Hamilton et al., 2001) and So15= this study.

Norite dissolution rates (based on Si release) are compared to anorthite dissolution rates from Gudbrandsson et al. (2014) and Oelkers and Schott (1995) (Fig. 4.10). The main minerals in norite are anorthite and orthopyroxene, and anorthite is used for comparison because of an expected higher dissolution rate than orthopyroxene (Palandri and Kharaka, 2004). The norite dissolution rates are somewhat lower than the anorthite dissolution rates from the literature in the pH range we have for data comparison, but not as low as the larvikite dissolution rates.

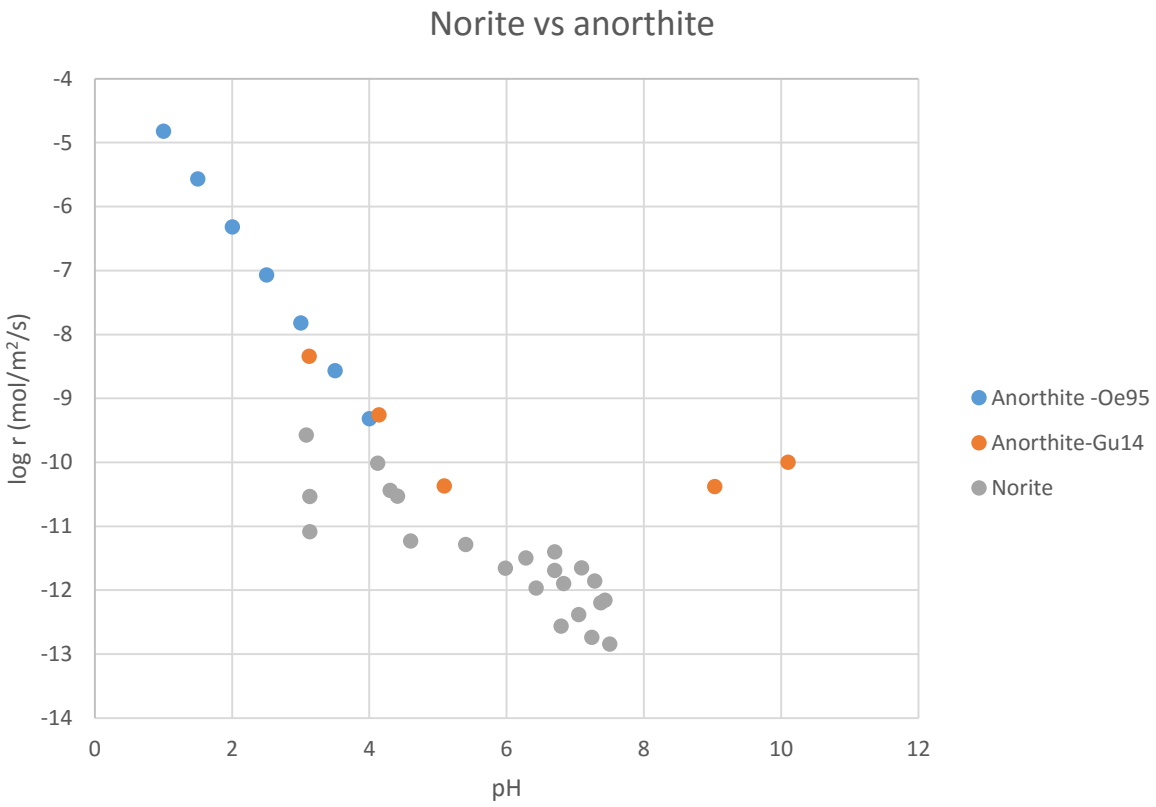

Fig. 4.10 Norite dissolution rates of Si compared to anorthite dissolution rates, retrieved from Oe95 = Oelkers and Schott (1995) and Gu14= Gudbrandsson et al. (2014), norite = this study.

Nepheline syenite, larvikite, eclogite and norite are comparable to previous studies of the relevant minerals, however these materials all contain several minerals (Table 3.2) which will affect the Si release. Since these materials contain several minerals it is very likely that the exposed surface area of the fastest dissolving mineral will be smaller than the measured area. It is also possible that there were other interactions between the minerals that could have further reduces the mineral specific dissolution rates. Although there have not done any attempt to investigate this further, it is thus likely that the real dissolution rate of these fastest releasing minerals would be higher than the overall rate measured of the material containing them. Another factor that could lower dissolution rates in the experiment is the dissolution stoichiometry (Fig. 3.15). In general there are lower dissolution rates of Si compared to Mg or Ca in all materials (Appendix B), and preferential release of these cations may reduce the apparent dissolution as measured by Si. It is therefore realistic with lower overall dissolution rates from materials containing several minerals. Thus we can assume that the rates of these materials are realistc when comparing to literature data.

Olivine and dolomite dissolution rates were, however several orders lower than in previous studies (Fig. 4.5 and Fig. 4.6). One reason for this could be that the experimental design was not able to accurately measure the relatively fast dissolution rates expected of dolomite and olivine. This may be due to diffusion barriers as the stirring were relatively gentle to avoid mechanical weathering resulting in locally increased pH or ion concentrations at the mineral surfaces. Such an effect would be more pronounced in fast reacting materials.

Another factor that may have a lower the dissolution rates is ion concentrations. High Ca concentrations are proven to have a negative effect on dolomite dissolution at pH >7 (Pokrovsky and Schott, 2001) but not at acidic conditions (Gautelier et al., 1999), high Mg concentrations have a negative effect on pyroxene dissolution (Oelkers and Schott, 2001). Anorthite dissolution rates are found to be independent of Al, Si and Ca concentrations (Oelkers and Schott, 1995), however albite (Oelkers et al., 1994) and k-feldspar (Gautier et al., 1994) are strongly effected by Al concentrations. Olivine (forsterite) dissolution rates are found to be independent of aqueous Mg and Si concentrations (Oelkers, 2001a).

Saturation state of the solution with respect to primary and secondary mineral phases may also effect the weathering rates (Welch and Ullman, 1996). As this study have done batch experiments without any fluid flow-through, it is reasonable to assume that these experiments have been more saturated than experiments conducted using flow-through reactors, and that this will affect the later stages of the experiment.

4.3 The chelating effect of organic acids

One of the initial hypotheses was that organic acids, due to their chelating effects could increase dissolution rates, which potentially could be very important in soils due to the relative complex set of such acids often found there. The use of different acids in the experiments have resulted in different net cation release (Table 3.4).

The olivine fractions net release of Mg depends in the acid treatment in the following order: HCl < oxalic acid ≈ acetic acid (+ HCl) < peat soil (+ HCl) (Table 3.4). The Mg release from the olivine fractions were similar, except for a relatively high release of Mg to peat soil (+ HCl) from Ol 63-, which could be a result of a fast dissolution of very fine grains. However, these differences are difficult to see from olivine dissolution rates in the different acid solutions (Fig. 3.14), except in the peat soil (+ HCl) for Ol 63- where the rates are ~ 1 log unit higher than the other dissolution rates. These observations are in agreement with previous studies were organic acids are not assumed to have an effect on dissolution rates at pH 3, but at pH>4.2 oxalic acid may significantly increase the dissolution rates (Olsen and Rimstidt, 2008; Declercq et al., 2013).

The dolomite net release of Ca depends on the acid treatment in the following order: Oxalic acid < HCl < acetic acid (+ HCl) < peat soil (+ HCl). At pH 3 the dissolution rates from, HCl, acetic acid (+ HCl) and peat soil (+ HCl) solutions causes dissolution rates ~ 1 log unit higher than with oxalic acid. At pH > 7, the dissolution rates in HCl, acetic acid (+ HCl) and oxalic acid are very similar and all have a prominent dip in rates at pH 7.7. A high amount of dissolved Ca in solution can strongly inhibit dolomite dissolution above pH 7 (Pokrovsky and Schott, 2001) and may explain the observations. The increased dissolution rates with acetic acid (+ HCl) is also observed by Pokrovsky et al. (2009) and the inhibition with oxalic acid is observed by DeMaio and Grandstaff (1996).

For the nepheline syenite the Ca release most likely comes from the dissolution of hornblende as it is the only Ca containing mineral (Table 3.2). Nepheline syenite net release of Ca depends in the acid treatment in the following: oxalic acid < HCl < peat soil (+ HCl) < acetic acid (+ HCl). The dissolution rates in acetic acid (+ HCl) was slightly higher than in HCl and they followed a similar path as pH increases and both have an abrupt dip as the pH 7.6. The dissolution rates in oxalic acid was significantly lower than dissolution rates in the other acid solutions. The observed dip in dissolution rates could be caused by the increased concentration of Ca in solution, similar to what occurred in dolomite. Barman et al. (1992) reported an increased hornblende dissolution in the presence of 0.5 M oxalic acid. However, at a concentration of 0.001 M oxalic acid we observe a significantly inhibiting effect.

For larvikite the Ca release most likely comes from anorthite. For larvikite we found the following order of net release Ca into acid solution: oxalic acid < HCl < acetic acid (+ HCl) < peat soil (+ HCl), however, the difference were negligible. The dissolution rates in all acids treatments were similar at pH 3. Welch and Ullman (1996) suggest that organic solutions may have a large effect on aluminium rich minerals because of an apparent preferential adsorption at Al-sites and resulting ligand promoted dissolution. Organic acids have been hown a higher effect on dissolution rates at pH 5 than at pH 3.5 on microcline and labradorite (Van Hees et al., 2002). From the results there are no evidence suggesting an enhanced Ca release from larvikite with the presence of organic acids, this might be related to the low pHs in the larvikite acid solutions and organic acids might have an impact when pH exceeds 5.

For eclogite the Ca release is most likely from omphacite (and/or Ca-almandine). For eclogite we found the following order of net release Ca into acid solution: Oxalic acid < peat soil (+ HCl) < HCl < acetic acid (+ HCl). At pH 3 the dissolution rates in HCl and acetic acid (+ HCl) are the same, the dissolution in peat soil (+ HCl) and oxalic acid are also similar, but slightly lower than dissolution rates in HCl and acetic acid (+ HCl). With increasing pH, the HCl solution caused the highest dissolution rate, followed by acetic acid (+ HCl). Dissolution rates in peat soil (+ HCl) and oxalic acid decrease fast.

For norite the Ca release most likely comes from the anorthite. For norite we found the following order of net release Ca into acid solution: oxalic acid < peat soil (+ HCl) < HCl < acetic acid (+ HCl). At pH 3 dissolution rates in all acid solutions are similar. When pH increase the dissolution rates in HCl decrease slower than in the other acids. The second highest dissolution rates are in acetic acid (+ HCl), followed by oxalic acid and peat soil (+ HCl) has the lowest. Previous studies have showed that the presence of oxalic acid increase dissolution rates of anorthite (Amrhein and Suarez, 1992). The reason why the results for Ca dissolution rates do not show any effect of organic acid could be because the organic acids have an apparent preferential adsorption of Al sites and resulting ligand promoted dissolution (Welch and Ullman, 1996).

The net Mg release from olivine indicate that oxalic acid and acetic acid (+ HCl) have an enhancing effect on release from olivine (Table 3.4). The dissolution rates however do no show a similar trend (Fig. 3.14). Dolomite, nepheline syenite, eclogite and norite dissolution are slightly enhanced by acetic acid (+ HCl) and inhibited by oxalic acid. Larvikite dissolution seems to be unaffected by organic acids. Observations indicate that organic acids might have both enhancing and inhibiting effects on cation dissolution of various silicate rocks. The observation that silicate rocks reacts differently to organic acids is also done by Varadachari et al. (1994) and Barman et al. (1992). Comparing the results in this study to previous studies there are some similarities both also some anomalies. Dissolution rates might be affected both by pH and solution composition (Oelkers and Gislason, 2001; Oelkers and Schott,

2001), as the experiments were done without a constant pH and no flow/exchange of solution, it is likely that these factors have influenced the calculated dissolution rates. Declercq et al. (2013) argues that inconsistency with previous studies might be a result of the dissolution experiment only lasting a few hours, and that the Mg and Si release during the first hours can be inconsistent with longer-term steady state rates.

4.4 The buffer capacity of acids

When experiment 3 was designed we decided to have the same molar concentration of all acids. The amount of soil added to the peat soil slurry was a more arbitrary choice. On the other hand we wanted the same starting pH for all acid treatments to be able to compare dissolution rates at the same pH.

To achieve this we had to add HCl to the acetic acid solution and peat soil and the amount of total acid added to these solutions changed (Table 4.1). Thus the HCl, acetic acid and oxalic acid treatments had the same molarity (0.001M), however oxalic acid at this pH were partly undissociated, "retaining" half of its protons as $HC_2O_4^-$. From 0.001 M acetic acid only 12% dissociates at this molarity and the solution was also titrated to 0.94 mM HCl to reach pH 3. This means that the oxalic acid and acetic acid (+ HCl) solutions have undissociated protons, which will be released when pH increases. The same apply to the peat soil. We do not know the composition of acids in the peat soil and therefore it is not possible to calculate the amount of undissociated protons. The amount of HCl added to titrate the peat soil to pH 3 was 300% (Table 4.1) more than in the amount HCl in water to reach pH 3. This shows the high buffer capacity of the peat slurry. This should not affect the dissolution rates as these depends on pH. However, as pH increase the pH trajectory in the different acid treatments con not be directly compared, as the amount of protons to be consumed increase pH of the system is different between the acid treatments (Table 4.2).

Table 4.1 Amount of moles H^+ added to the solutions.

Acid Solution	**HCl**	**Oxalic acid**	**Acetic acid (+ HCl)**	**Peat soil (+ HCl)**
H^+ added	1.00E-03	1.97E-03	1.98E-03	3.00E-3

Table 4.2 Acid consumption (moles H^+/per sample) for the samples in the different acid solutions. The calculations were based on concentrations of added acid, acid dissociation constants and start and final pH.

	Mol H^+ consumption in HCl	Final pH HCl	Mol H^+ consumption in Oxalic acid	Final pH oxalic acid	Mol H^+ consumption in acetic acid (+ HCl)	Final pH acetic acid (+ HCl)
Ol 63-	1.00E-03	7.34	1.95E-03	7.47	1.98E-03	7.13
Ol 63-125	1.00E-03	7.05	1.96E-03	7.14	1.97E-03	6.84
Nepheline syenite	1.00E-03	7.35	1.97E-03	7.56	1.98E-03	7.55
Dolomite	1.00E-03	7.75	1.97E-03	7.89	1.98E-03	7.53
Larvikite	9.81E-04	4.72	1.93E-03	5.65	1.19E-03	4.3
Eclogite	1.00E-03	6.57	1.94E-03	5.9	1.19E-03	4.3
Norite	1.00E-03	7.68	1.97E-03	7.35	1.98E-03	7.14

For Ol 63- treatments the amount of H^+ (mol) consumed was proportional to Mg (mole) released (Fig. 4.11). There were approximately two moles H^+ consumed for one mole Mg released. This also correlates with the amount of Mg released into solution being twice the amount in acetic acid (+ HCl) and oxalic acid compared to HCl.

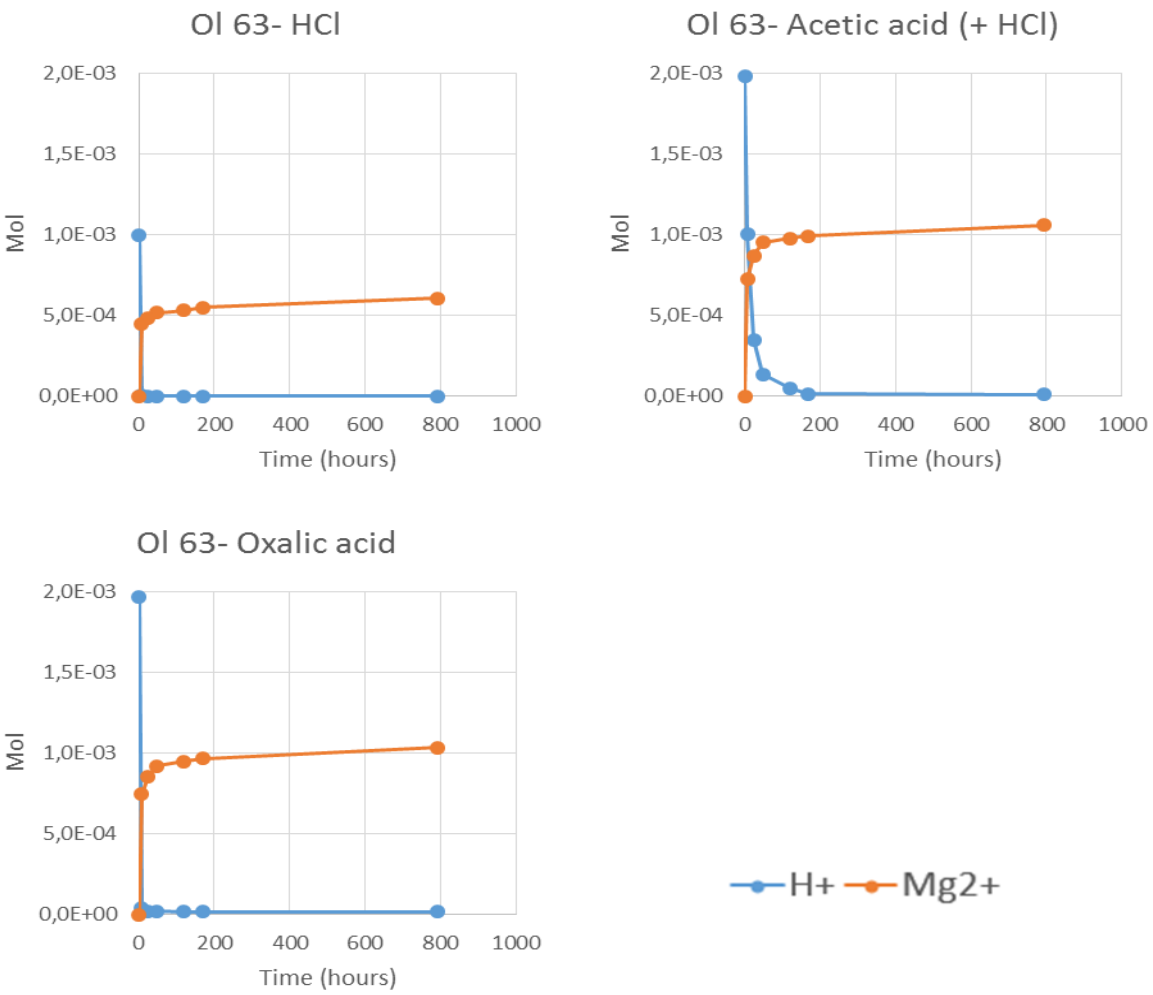

Fig. 4.11 Moles Mg^{2+} released (red symbols) and moles H^+ consumed during experiment 3 for Ol 63- in the HCl, acetic acid (+ HCl) and oxalic acid solution.

For dolomite, nepheline syenite, eclogite and norite the Ca concentration was lowest in the oxalic acid solution. For dolomite the consumption of two mole H^+ corresponds to the release of approximately one mole Ca in the HCl and acetic acid (+ HCl) solutions (Fig. 3.14). However, in the oxalic acid the apparent H^+ consumption was much higher than the release of Ca. The release of Mg was constant in all acid solutions. These observations indicate that oxalic acid inhibit dolomite release of Ca. Similar observations were made from plots with nepheline syenite, eclogite and norite also.

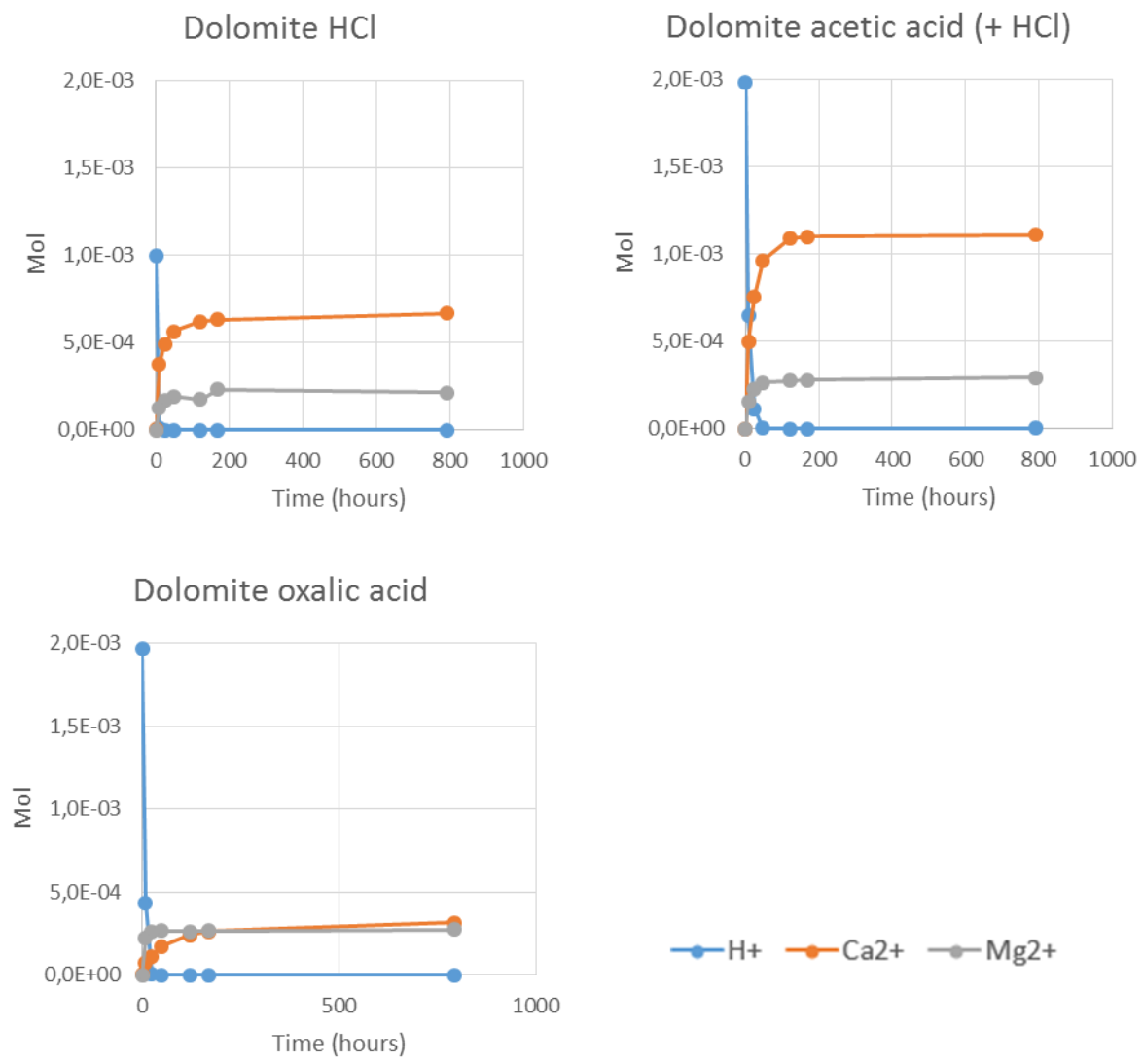

Fig. 4.12 Mol Ca^{2+} and Mg^{2+} released and mol H^{+} consumed during experiment 3 for dolomite in the HCl, acetic acid (+ HCl) and oxalic acid solution.

For larvikite the Ca concentrations are similar in all acid solutions. This indicate that the Ca release is not significantly inhibited or enhanced by organic acids, which could also be related to a generally low pH in the larvikite acid solutions, as organic acids are anticipated to have a larger impact at higher pH > 5.

When comparing the release of cations with acid consumption it is obvious that the organic acids have a different effect on the different samples. In the olivine treatments (Ol 63-125 and Ol 63-) the oxalic acid and acetic acid (+ HCl) solutions have Mg concentrations twice the amount in the HCl solution.

4.5 Grain size

The results suggest, as expected that the grain size is an important factor for pH increase capacity. The two olivine fractions (<63 µm and 63-125 µm) have comparable dissolution rates (which is a measure on area basis), however the Ol 63- increased the pH with 0.9 pH units more than Ol 63-125 during the experiments. Initially the norite material have a dissolution rate similar to the olivine material and since it has a larger surface area, pH increase with 1.3 pH units more than Ol 63-125. For practical use of crushed rocks in the field pH management, it is thus important to consider the combination of surface area of the available material, the area specific dissolution rate of the material and the H^+ consumption of the specific material by dissolution. The effect of the practicalities involved in handling and spreading the material (which may change with grains size) and the eventual monetary and energy cost of crushing if needed.

4.6 Content and release of heavy metals

In the following we have focused on Cr and Ni as relevant for heavy metal pollution, as they are major trace elements in several of the materials in these experiments. The Norwegian classification system for fresh water and sediments establish limits for contamination in these systems for Cr and Ni (Table 4.3). Comparing the materials (rock/mineral samples) to sediment data and solutions from experiment 3 to limits for fresh water contamination (Table 4.4). Since the experiment were with highly artificial conditions, a direct comparison to water quality standards are not too relevant, but it gives an indication of the contamination potential of the materials even after shorter periods on dissolution.

Eclogite, larvikite and nepheline syenite materials have Ni and Cr contents in class I and II. Norite have class II on Cr and IV on Ni (Table 3.1). Olivine have class II on Cr and class V on Ni, and would be considered a toxic sediment following this system. On the other side, olivine is DEBIO approved for agricultural purposes (Vold, 2006). Release of Ni in experiment 3 reveal several water concentrations that fall in class V for Ol 63- in peat soil (+ HCl) and norite in oxalic acid, acetic acid and peat soil (+ HCl) (Fig. 4.4). In class IV for Ni are Ol 63- in oxalic acid. Leachate of Ni from Ol 63- in oxalic acid falls into class IV. For Cr leaching there are no concentrations in class V, but there are a few in class IV: Ol 63-125 in peat soil (+ HCl), larvikite in oxalic acid and peat soil (+ HCl) and norite in peat soil (+ HCl).

Table 4.3 Environmental classification of Cr and Ni concentrations in fresh water and sediment. Table modified from Weideborg et al. (2012).

	I Background	II Good	III Moderate	IV Poor	V Very poor
	Background	No effects	Chronic effects from long time exposure	Acute toxic effects of short term exposure	Extensive toxicity
Fresh water					
Ni (ppb)	0.5	1.7	34	67	>67
Cr- tot[1] (ppb)	0.2	3.4	3.4	360	>360
Sediment					
Ni (mg/kg)	30	43	270	500	>500
Cr- tot (mg/kg)	60	620	6000	60000	>60000

1 There are not done specific analysis of Cr III and Cr IV. See calculations in Weideborg et al. (2012)

Table 4.4 Ni and Cr concentrations (ppb) leached into solution from experiment 3. Classified from information in (Table 4.3). No colour indicates class I or II. ND = not detected.

	Ol 63-		Ol 63-125		Dolomite		Nepheline syenite		Larvikite		Eclogite		Norite	
	Cr	Ni	Cr	Ni	Cr	Ni	Cr	Ni	Cr	Ni	Cr	Ni	Cr	Ni
1	0.72	ND	ND	4.85	0.87	ND	0.17	ND	0.62	18.5	0.86	0.18	1.26	27.1
2	0.008	58.1	3.11	224	0.27	ND	0.91	1.46	25.4	20.5	1.06	3.21	0.5	249
3	ND	3.22	0.75	24.6	ND	ND	0.14	ND	1.87	14.9	ND	ND	0.32	253
4	99.5	3836	7.83	247	1.58	ND	0.62	12.9	5.76	7.72	1.39	ND	49.1	552

1 HCl 2 Oxalic acid 3 Acetic acid (+ HCl) 4 Peat soil (+ HCl)

We have also observed that Ni and Cr concentrations tend to decrease as the solution pH exceeds 5 (Fig. 3.13). Cr and Ni solubility are very pH dependent and if pH is kept close to neutral concentrations it will most likely be lower than maximum values observed from these data. At pH 3 (start pH in experiment 3) Cr and Ni are more soluble and this could explain the high values we have measured. The drop in concentrations due to increasing pH was, however, seemingly counteract by the organic acids (Fig. 3.13). There is a rapid increase for Ni in solution from the olivine in all acid treatments, however the drop in concentrations were lower in the organic acids than in the HCl solution and in the peat soils the content increases throughout the experiment. This is probably due to the chelating effect of oxalic acid or other organic acids in the peat soil slurry, keeping Cr and Ni in solution even if pH increases and could greatly affect the dissolution rate and bioavailability of these toxic elements in soil-groundwater systems. Trends were present but less clear for the other materials as well (Appendix A).

All organic soil from the soil incubation experiment (Table 3.3) can be classified as a class I sediment for Cr. The Ni concentrations in the control (quartz) soil is class I; dolomite, An 63 and An 450 are class II; Ol 450 and Ol 63 are class V. The Ol 450 has a higher Ni concentration and lower pH than Ol 63, further indicating that pH is an important factor for Ni solubility.

Ten Berge et al. (2012) observed low concentrations of Ni from an olivine pot experiment at pH >4.9 and concluded that a long time build-up Ni from olivine dissolution does not necessary lead to toxic levels. Further the use of olivine in agricultural systems have been done for years in Japan and New Zealand (Erstad et al., 2000).

Solubility and bioavailability of the heavy metals are complex topics and it is beyond the scope of this thesis. The classifications of materials and released concentrations of Ni and Cr indicate that especially olivine and norite should be further investigated for Ni and Cr release. We also note that use of olivine and norite might be restricted because they are per definition contamination (naturally contamination).

4.7 Weathering of silicates in soils; the potential for pH management

This work have focused on a few aspects of the potential use for silicate as soil amendments. We have on one side attempted to measure dissolution rates of a set of rocks under controlled conditions, to compare their dissolution rates and ability to increase pH, and heavy metal release. We approached soil conditions by adding organic acids and peat soil solution to see how these would affect rock dissolution. On the other hand we used SEM to investigate the dissolution of rocks incubated for 1.5 years in organic peat soil to make a quantitative assessment of the degree of dissolution in these rocks.

From the SEM examination classification we found that olivine grains in general were more weathered than anorthosite grains. These observations correlated with higher pH in the olivine soil and from observations in experiment 1, where olivine ended at higher pH.

From the pH trajectories in experiment 2 (Fig. 3.11) and 3 (Fig. 3.12) we saw that ranking of material did not change much by changing the type of acid. However the peat soil (+ HCl) treatments (from experiment 3) resulted in lower pHs than in the other acid solutions but still higher concentrations of M and Ca, which indicate an internal buffer capacity keeping the pH lower and thus increasing the total dissolution of the materials. This is compatible with laboratory dissolution rates being several orders of magnitude faster than field scale weathering (White and Brantley, 1995). One reason for this could

be large inhomigenities as we found in the soil incubated samples. The olivine grains varied from having large parts of their surface totally dominated by dissolution to being nearly unaffected by the soil incubation. There are many variables that affect mineral dissolution , e.g. soil type, crop, climate characteristics, mineral grain size, microbial activity, inhibiting processes, etc. e.g. (Berner and Holdren Jr, 1979; Ehrlich, 1996; Hodson, 2006; Ten Berge et al., 2012). Recently it is suggested that soil bacteria and fungi might cause a long term inhibition of forsterite dissolution at surface conditions due to growth of biotic communities at mineral surfaces (Oelkers et al., 2015).

The initial dissolution rates in experiment 3 varied between 2 orders of magnitude (Fig. 3.14). Olivine initially had dissolution rates from 10^{-9} to $10^{-9.5}$ M/m^2/s, larvikite and norite had rates from $10^{-9.4}$ to 10^{-10} M/m^2/s, while dolomite, nepheline syenite and eclogite initially had rates around 10^{-8} (at least for some acid treatments). There is apparent significant uncertainty in the rates estimates below 10^{-11} M/m^2/s, probably due to the experimental design, however for all materials and acid solutions the rates decreased as pH increased. It seems as a close to linear relationship between log H^+ (pH) and log rate below pH 7 and above 10^{-11} M/m^2/s. As dissolution rates decreases with increasing pH it is imminent that the dissolution rates will be relatively low if applied to a moderately acidic soil (e.g. pH 5.5) and that the subsequent pH management effect will most likely not be as efficient as observed in the dissolution rate experiments in this study.

Even though the experimental results are not necessarily identical to dissolution in soil, it gives an idea of how the materials might weather, change the pH, dissolve, etc. And this information may be applied to find relevant application areas. Besides olivine and norite, there is no significant heavy metal leaching, which means that they may be used in nature without an imminent contamination hazard.

Dissolution of olivine in the peat soil incubation experiments increased pH by up to 1.4 pH units, which Liu et al. (2010) suggest to be relevant for reducing N2O emissions in soil. In the dissolution rate experiments olivine, norite and nepheline syenite show the highest potential for pH increase. Out of these materials, nepheline syenite had the highest dissolution rates, approximately 1 log unit faster than olivine and norite at pH 3. In addition olivine and norite contain and release significant amounts of Cr and Ni which potentially can cause contamination problems. Based on these observations nepheline syenite seems the best choice of material for pH management.

4.8 Conclusions

Grain dissolution quantification

- Fractures, etch-pits and silica-layers were present on both olivine and anorthosite grains, in addition olivine display aluminium layers (possibly gibbsite or diaspore) and serpentinization features.
- The olivine grains were in general more weathered than anorthosite grains. E.g. 48% of the olivine grains had more that 50% of the surface covered by cracking or etching pits, whereas none of the anorthosite had 50 % coverage.
- There was relatively high heterogeneity in how much of the surface of the different grains that were covered by dissolution surfaces**.** E.g. 48% of olivine grains had > 50% of the surface influenced by dissolution features, whereas for 10% less than 20% of the surface was influenced.
- The formation of silicate layers will inhibit dissolution, however it seems like the silicate coating crack and spell of over time. 20% of the olivine and 14% of the anorhtosite had parts of the visible surface covered by silica layers. The Si coatings on olivine grains were typically at surfaces normal to those where pitting was found, if this is a general feature, would not be expected to decrease the dissolution rate much.
- Fractures and etch-pits will increase the grain surface area, however there are some uncertainties if the formation etch-pits increase the reactive surface area. This is particularly relevant in anorthosite as the etching occurs as narrow lamella following the mineral structure. We expect more weathering resistant minerals remains at the surface as dissolution progresses.

Dissolution rate experiments

- Olivine, norite and nepheline syenite show the highest potential for increasing pH.
- At pH 3 olivine initially had dissolution rates from 10^{-9} to $10^{-9.5}$ mol/m^2/s, larvikite and norite had rates from $10^{-9.4}$ to 10^{-10} mol/m^2/s, while dolomite, nepheline syenite and eclogite initially had rates around 10^{-8} (at least for some acid treatments).
- All materials showed a non-stoichiometric dissolution and release more Mg^{2+} or Ca^{2+} than Si^{4+} compared to their parental materials. Dissolution in the organic acids was in general closer to stoichiometric dissolution than in HCl.
- Dissolution rates were as expected very pH dependent and decreased with increasing pH.

- The observed dissolution rates were in some cases lower than reported in the literature. This is most likely linked to the experimental setup and possible due to increased concentrations of the major cations in solution as the experiment progresses.
- The different organic acids did not significantly change the pH specific dissolution rates of olivine, however the net Mg^{2+} release increased in oxalic acid and acetic acid compared to HCl. The oxalic acid decreased dissolution rates dolomite, nepheline syenite, eclogite and larvikite.
- The olivine and norite contain and release significant amounts of Ni and Cr to potentially be problematic in an agricultural context. We also note that use of olivine and norite might be restricted because they are per definition contamination (naturally contamination).
- In solution from experiment 3 the Cr and Ni concentrations dropped as pH exceeded 5, the drop in concentrations were lower in the organic acids than in HCl, and in the peat soil treatments the content increased throughout the experiment.
- Estimating how crushed rocks will dissolve in soils based on incubations in water solutions is difficult as numerous factors limiting and accelerating dissolution may be present in soils. However, we do not have any indication that the presence of organic acids or soil slurry will alter the relative order of dissolution rates between the different rock types.
- Based on a high pH increase in the dissolution experiments, high dissolution rates, low contents and release of Cr and Ni, nepheline syenite is proposed to be the best option for agricultural pH management.

5 Further work

Further investigation considering the formation of dissolution features on mineral grains in soils are needed, especially considering the formation of silica layers. Laboratory and/or field experiments are needed. Another way of assessing the problem could possibly be field samplings of the desired material in natural soils containing the minerals. Soils from these areas could also be sampled for investigation of heavy metal release over time. Better assessment of long term stoichiometry dissolution could be achieved in flow through experiments, where dissolution rates could be measured at constant pH over time.

The election of rock/mineral sample best suited for agricultural use might vary with soil, crop and climate. Field and lab experiments have to be done in relevant agricultural system as it is very difficult to anticipate how the reactions will take place by extrapolation from dissolution in acid solutions. Modelling of soil dissolution as proposed by Sverdrup (2009) maybe one way to assess the issue or perhaps soil incubation experiments as by Ten Berge et al. (2012) or Renforth et al. (2015).

6 References

Agency, N. E. (2015). Nordic Mining – søknad om gruvevirksomhet i Engebøfjellet. Oslo: Norwegian Environmental Agency (2013/4983). 79 pp.

Amrhein, C., & Suarez, D. L. (1992). Some factors affecting the dissolution kinetics of anorthite at 25 C. *Geochimica et Cosmochimica Acta, 56*(5), 1815-1826.

Awad, A., Koster van Groos, A., & Guggenheim, S. (2000). Forsteritic olivine: effect of crystallographic direction on dissolution kinetics. *Geochimica et Cosmochimica Acta, 64*(10), 1765-1772.

Baggs, E. M., Smales, C. L., & Bateman, E. J. (2010). Changing pH shifts the microbial source as well as the magnitude of N2O emission from soil. *Biology and fertility of soils, 46*(8), 793-805.

Barman, A. K., Varadachari, C., & Ghosh, K. (1992). Weathering of silicate minerals by organic acids. I. Nature of cation solubilisation. *Geoderma, 53*(1), 45-63.

Bennett, P. C., Hiebert, F. K., & Choi, W. J. (1996). Microbial colonization and weathering of silicates in a petroleum-contaminated groundwater. *Chemical Geology, 132*, 45-53.

Bergaust, L., Mao, Y., Bakken, L. R., & Frostegård, Å. (2010). Denitrification response patterns during the transition to anoxic respiration and posttranscriptional effects of suboptimal pH on nitrogen oxide reductase in Paracoccus denitrificans. *Applied and environmental microbiology, 76*(19), 6387-6396.

Berner, R. A., & Holdren Jr, G. R. (1979). Mechanism of feldspar weathering—II. Observations of feldspars from soils. *Geochimica et Cosmochimica Acta, 43*(8), 1173-1186.

Bernhard, A. (2010). The nitrogen cycle: Processes, players, and human impact. *Nature Education Knowledge, 2*(2), 12.

Brantley, S. L. (2008a). Appendix: Compilation of Mineral Dissolution Rate. In: Brantley S. L, Kubicki J. D, White A. F (eds), Kinetics of water-rock interaction. New York: Springer. P. 737-823.

Brantley, S. L. (2008b). Kinetics of mineral dissolution. In: Brantley S. L, Kubicki J. D, White A. F (eds), Kinetics of water-rock interaction. New York: Springer. P. 151-210.

Bye, A. S., Aarstad, P. A., Løvberget, A. I., & Høie, H. (2014). Jordbruk og miljø. Tilstand og utvikling 2013. Oslo-Kongsvinger: Statistics Norway (2014.10). 134 pp.

Carswell, D., Cuthbert, S., Krabbendam, M., Medaris Jr, L., & Brueckner, H. (2003). Guidebook to the Field Excursions in the Nordfjord—Stadlandet—Almklovdalen Area. Trondheim: Geological Survey of Norway (2003.056). 137 pp.

Charlier, B., Skår, Ø., Korneliussen, A., Duchesne, J.-C., & Vander Auwera, J. (2007). Ilmenite composition in the Tellnes Fe–Ti deposit, SW Norway: fractional crystallization, postcumulus evolution and ilmenite–zircon relation. *Contributions to Mineralogy and Petrology, 154*(2), 119-134.

Chen, Y., & Brantley, S. L. (1998). Diopside and anthophyllite dissolution at 25° and 90°C and acid pH. *Chemical Geology, 147*(3–4), 233-248.

Cordellier, F., Boudier, F., & Boullier, A. M. (1981). Structural study of the Almklovdalen peridotite massif (southern Norway). *Tectonophysics, 77*(3–4), 257-281.

Declercq, J., Bosc, O., & Oelkers, E. H. (2013). Do organic ligands affect forsterite dissolution rates? *Applied Geochemistry, 39*(0), 69-77.

DeMaio, T., & Grandstaff, D. (1996). The effects of dilute organic acids on calcite dissolution. *Oceanographic Literature Review, 4*(43), 355.

Dove, P. M., & Crerar, D. A. (1990). Kinetics of quartz dissolution in electrolyte solutions using a hydrothermal mixed flow reactor. *Geochimica et Cosmochimica Acta, 54*(4), 955-969.

Drever, J., & Stillings, L. (1997). The role of organic acids in mineral weathering. *Colloids and Surfaces A: Physicochemical and Engineering Aspects, 120*(1), 167-181.

Ehrlich, H. L. (1996). How microbes influence mineral growth and dissolution. *Chemical Geology, 132*(1), 5-9.

Erstad, K.-J., Konovalov, N. Y., & Farstad, B. (2000). Bioavailability of nickel in olivine and serpentine, and use of olivine in agriculture and nature management. A litterture review. Korssund: Rådgivende Agronomer AS (1/2000). 46 pp.

Faure, G. (1998). *Principles and applications of geochemistry (Second ed). New Jersey: Prentice Hall. P. 172-199*

Fischer, C., Arvidson, R. S., & Lüttge, A. (2012). How predictable are dissolution rates of crystalline material? *Geochimica et Cosmochimica Acta, 98*(0), 177-185.

Furrer, G., & Stumm, W. (1986). The coordination chemistry of weathering: I. Dissolution kinetics of δ-Al2O3 and BeO. *Geochimica et Cosmochimica Acta, 50*(9), 1847-1860.

Futter, M., Klaminder, J., Lucas, R., Laudon, H., & Köhler, S. (2012). Uncertainty in silicate mineral weathering rate estimates: source partitioning and policy implications. *Environmental Research Letters, 7*(2), 024025.

Gautelier, M., Oelkers, E. H., & Schott, J. (1999). An experimental study of dolomite dissolution rates as a function of pH from− 0.5 to 5 and temperature from 25 to 80 C. *Chemical Geology, 157*(1), 13-26.

Gautier, J.-M., Oelkers, E. H., & Schott, J. (1994). Experimental study of K-feldspar dissolution rates as a function of chemical affinity at 150°C and pH 9. *Geochimica et Cosmochimica Acta, 58*(21), 4549-4560.

Gautneb, H., Ihlen, P., & Boyd, R. (2009). Review of the geology and the distribution of phosphorus in the Lillebukt Alkaline Complex, and adjacent areas, Stjernøy Northern Norway. Trondheim: Geological Survey of Norway (2009.060). 42 pp.

Golubev, S. V., Pokrovsky, O. S., & Schott, J. (2005). Experimental determination of the effect of dissolved CO 2 on the dissolution kinetics of Mg and Ca silicates at 25 C. *Chemical Geology, 217*(3), 227-238.

Gregory, P. J. (2012). *Soils and food security: challenges and opportunities. In: Hester R.E, Harrison R. M (eds), Soils and food security. London: RSC Publishing. P. 1-30.*

Gudbrandsson, S., Wolff-Boenisch, D., Gislason, S. R., & Oelkers, E. H. (2014). Experimental determination of plagioclase dissolution rates as a function of its composition and pH at 22° C. *Geochimica et Cosmochimica Acta, 139*(0), 154-172.

Hamilton, J. P., Brantley, S. L., Pantano, C. G., Criscenti, L. J., & Kubicki, J. D. (2001). Dissolution of nepheline, jadeite and albite glasses: toward better models for aluminosilicate dissolution. *Geochimica et Cosmochimica Acta, 65*(21), 3683-3702.

Hangx, S. J., & Spiers, C. J. (2009). Coastal spreading of olivine to control atmospheric CO2 concentrations: A critical analysis of viability. *International Journal of Greenhouse Gas Control, 3*(6), 757-767.

Harley, A., & Gilkes, R. (2000). Factors influencing the release of plant nutrient elements from silicate rock powders: a geochemical overview. *Nutrient Cycling in Agroecosystems, 56*(1), 11-36.

Heier, K. (1964). Geochemistry of the nepheline syenite on Stjernøy, North Norway. *Norsk Geologisk Tidsskrift 44*, 205-215.

Heldal, T., Kjølle, I., Meyer, G. B., & Dahlgren, S. (2008). National treasure of global significance. Dimension-stone deposits in larvikite, Oslo igneous province, Norway. *Geology for society, 11*, 5-18.

Hellevang, H., Declercq, J., Kvamme, B., & Aagaard, P. (2010). The dissolution rates of dawsonite at pH 0.9 to 5 and temperatures of 22, 60 and 77 C. *Applied Geochemistry, 25*(10), 1575-1586.

Hellmann, R., Wirth, R., Daval, D., Barnes, J.-P., Penisson, J.-M., Tisserand, D., Epicier, T., Florin, B., & Hervig, R. L. (2012). Unifying natural and laboratory chemical weathering with interfacial dissolution–reprecipitation: A study based on the nanometer-scale chemistry of fluid–silicate interfaces. *Chemical Geology, 294–295*(0), 203-216.

Hodson, M. E. (2006). Does reactive surface area depend on grain size? Results from pH 3, 25 °C far-from-equilibrium flow-through dissolution experiments on anorthite and biotite. *Geochimica et Cosmochimica Acta, 70*(7), 1655-1667.

Inskeep, W. P., Nater, E. A., Bloom, P. R., Vandervoort, D. S., & Erich, M. S. (1991). Characterization of laboratory weathered labradorite surfaces using X-ray photoelectron spectroscopy and transmission electron microscopy. *Geochimica et Cosmochimica Acta, 55*(3), 787-800.

Jochum, K. P., Nohl, U., Herwig, K., Lammel, E., Stoll, B., & Hofmann, A. W. (2005). GeoReM: A New Geochemical Database for Reference Materials and Isotopic Standards. *Geostandards and Geoanalytical Research, 29*(3), 333-338.

Johnson, C. L., Hÿtch, M. J., & Buseck, P. R. (2004). Displacement and strain fields around a [100] dislocation in olivine measured to sub-angstrom accuracy. *American Mineralogist, 89*(10), 1374-1379.

Korneliussen, A., Braathen, A., Erambert, M., Lutro, O., & Ragnhildstveit, J. (1998). The geology of the Engebøfjell eclogite deposit and its regional setting. Trondheim: Geological Survey of Norway (98.081). 121 pp.

Kump, L. R., Brantley, S. L., & Arthur, M. A. (2000). Chemical weathering, atmospheric CO2, and climate. *Annual Review of Earth and Planetary Sciences, 28*(1), 611-667.

Lackner, K. S. (2002). Carbonate chemistry for sequestering fossil carbon. *Annual review of energy and the environment, 27*(1), 193-232.

Lasaga, A. C. (1984). Chemical kinetics of water-rock interactions. *Journal of Geophysical Research: Solid Earth (1978–2012), 89*(B6), 4009-4025.

Lasaga, A. C., & Blum, A. E. (1986). Surface chemistry, etch pits and mineral-water reactions. *Geochimica et Cosmochimica Acta, 50*(10), 2363-2379.

Lasaga, A. C., Soler, J. M., Ganor, J., Burch, T. E., & Nagy, K. L. (1994). Chemical weathering rate laws and global geochemical cycles. *Geochimica et Cosmochimica Acta, 58*(10), 2361-2386.

Liu, B., Mørkved, P. T., Frostegård, Å., & Bakken, L. R. (2010). Denitrification gene pools, transcription and kinetics of NO, N2O and N2 production as affected by soil pH. *FEMS microbiology ecology, 72*(3), 407-417.

Liu, Y., Olsen, A. A., & Rimstidt, J. D. (2006). Mechanism for the dissolution of olivine series minerals in acidic solutions. *American Mineralogist, 91*(2-3), 455-458.

Luce, R. W., Bartlett, R. W., & Parks, G. A. (1972). Dissolution kinetics of magnesium silicates. *Geochimica et Cosmochimica Acta, 36*(1), 35-50.

Lüttge, A., Arvidson, R. S., & Fischer, C. (2013). A stochastic treatment of crystal dissolution kinetics. *Elements, 9*(3), 183-188.

Marshak, S., & Prothero, D. R. (2008). *Earth: portrait of a planet (Fourth ed). London: WW Norton. P. 141-183*

Martinez, R. E., Weber, S., & Bucher, K. (2014). Quantifying the kinetics of olivine dissolution in partially closed and closed batch reactor systems. *Chemical Geology, 367*(0), 1-12.

Medaris Jr, L. (1984). A geothermobarometric investigation of garnet peridotites in the Western Gneiss Region of Norway. *Contributions to Mineralogy and Petrology, 87*(1), 72-86.

Meheruna, A., & Akagi, T. (2006). Role of fine roots in the plant-induced weathering of andesite for several plant species. *Geochemical Journal, 40*(1), 57-67.

Moore, A. C., & Qvale, H. (1977). Three varieties of alpine-type ultramafic rocks in the Norwegian Caledonides and basal gnesis complex. *Lithos, 10*(2), 149-161.

Nesse, D. W. (2009). *Introduction to mineralogy (International ed). New York: Oxford University Press. P. 184-185*

Nömmik, H. (1956). Investigations on denitrification in soil. *Acta Agriculturae Scandinavica, 6*(2), 195-228.

Oelkers, E. H. (2001a). An experimental study of forsterite dissolution rates as a function of temperature and aqueous Mg and Si concentrations. *Chemical Geology, 175*(3), 485-494.

Oelkers, E. H. (2001b). General kinetic description of multioxide silicate mineral and glass dissolution. *Geochimica et Cosmochimica Acta, 65*(21), 3703-3719.

Oelkers, E. H., Benning, L. G., Lutz, S., Mavromatis, V., Pearce, C. R., & Plümper, O. (2015). The efficient long-term inhibition of forsterite dissolution by common soil bacteria and fungi at earth surface conditions. *Geochimica et Cosmochimica Acta, 168*, 222-235.

Oelkers, E. H., & Gislason, S. R. (2001). The mechanism, rates and consequences of basaltic glass dissolution: I. An experimental study of the dissolution rates of basaltic glass as a function of aqueous Al, Si and oxalic acid concentration at 25 C and pH= 3 and 11. *Geochimica et Cosmochimica Acta, 65*(21), 3671-3681.

Oelkers, E. H., & Schott, J. (1995). Experimental study of anorthite dissolution and the relative mechanism of feldspar hydrolysis. *Geochimica et Cosmochimica Acta, 59*(24), 5039-5053.

Oelkers, E. H., & Schott, J. (2001). An experimental study of enstatite dissolution rates as a function of pH, temperature, and aqueous Mg and Si concentration, and the mechanism of pyroxene/pyroxenoid dissolution. *Geochimica et Cosmochimica Acta, 65*(8), 1219-1231.

Oelkers, E. H., Schott, J., & Devidal, J.-L. (1994). The effect of aluminum, pH, and chemical affinity on the rates of aluminosilicate dissolution reactions. *Geochimica et Cosmochimica Acta, 58*(9), 2011-2024.

Okland, I., Huang, S., Dahle, H., Thorseth, I. H., & Pedersen, R. B. (2012). Low temperature alteration of serpentinized ultramafic rock and implications for microbial life. *Chemical Geology, 318*, 75-87.

Olsen, A. A., & Rimstidt, J. D. (2008). Oxalate-promoted forsterite dissolution at low pH. *Geochimica et Cosmochimica Acta, 72*(7), 1758-1766.

Palandri, J. L., & Kharaka, Y. K. (2004). A compilation of rate parameters of water-mineral interaction kinetics for application to geochemical modeling. Menlo Park, California: U.S. Geological Survey (2004-1068). 70 pp.

Pokrovsky, O. S., Golubev, S. V., & Jordan, G. (2009). Effect of organic and inorganic ligands on calcite and magnesite dissolution rates at 60 °C and 30 atm pCO2. *Chemical Geology, 265*(1–2), 33-43.

Pokrovsky, O. S., Golubev, S. V., & Schott, J. (2005). Dissolution kinetics of calcite, dolomite and magnesite at 25 C and 0 to 50 atm pCO 2. *Chemical Geology, 217*(3), 239-255.

Pokrovsky, O. S., & Schott, J. (2000). Forsterite surface composition in aqueous solutions: A combined potentiometric, electrokinetic, and spectroscopic approach. *Geochimica et Cosmochimica Acta, 64*(19), 3299-3312.

Pokrovsky, O. S., & Schott, J. (2001). Kinetics and mechanism of dolomite dissolution in neutral to alkaline solutions revisited. *American Journal of Science, 301*(7), 597-626.

Power, I. M., Harrison, A. L., Dipple, G. M., Wilson, S. A., Kelemen, P. B., Hitch, M., & Southam, G. (2013). Carbon mineralization: from natural analogues to engineered systems. *Reviews in Mineralogy and Geochemistry, 77*(1), 305-360.

Qu, Z., Wang, J., Almøy, T., & Bakken, L. R. (2014). Excessive use of nitrogen in Chinese agriculture results in high N2O/(N2O+ N2) product ratio of denitrification, primarily due to acidification of the soils. *Global change biology, 20*(5), 1685-1698.

Raut, N., Dörsch, P., Sitaula, B. K., & Bakken, L. R. (2012). Soil acidification by intensified crop production in South Asia results in higher N 2 O/(N 2+ N 2 O) product ratios of denitrification. *Soil Biology and Biochemistry, 55*, 104-112.

Renforth, P., Pogge von Strandmann, P. A. E., & Henderson, G. M. (2015). The dissolution of olivine added to soil: Implications for enhanced weathering. *Applied Geochemistry, 61*, 109-118.

Rimstidt, J. D., Brantley, S. L., & Olsen, A. A. (2012). Systematic review of forsterite dissolution rate data. *Geochimica et Cosmochimica Acta, 99*, 159-178.

Roberts, D., & Zwaan, K. B. (2007). Marble dykes emanating from marble layers in an amphibolite-facies, multiply-deformed carbonate succession, Troms, northern Norway. *Geological Magazine, 144*(05), 883-888.

Roberts, R. J., Corfu, F., Torsvik, T. H., Hetherington, C. J., & Ashwal, L. D. (2010). Age of alkaline rocks in the Seiland Igneous Province, Northern Norway. *Journal of the Geological Society, 167*(1), 71-81.

Rosso, J. J., & Rimstidt, J. D. (2000). A high resolution study of forsterite dissolution rates. *Geochimica et Cosmochimica Acta, 64*(5), 797-811.

Ruiz-Agudo, E., Putnis, C. V., & Putnis, A. (2014). Coupled dissolution and precipitation at mineral–fluid interfaces. *Chemical Geology, 383*(0), 132-146.

Ruiz-Agudo, E., Putnis, C. V., Rodriguez-Navarro, C., & Putnis, A. (2012). Mechanism of leached layer formation during chemical weathering of silicate minerals. *Geology, 40*(10), 947-950.

Sanderman, J. (2012). Can management induced changes in the carbonate system drive soil carbon sequestration? A review with particular focus on Australia. *Agriculture, Ecosystems & Environment, 155*, 70-77.

Schott, J., Pokrovsky, O. S., Spalla, O., Devreux, F., Gloter, A., & Mielczarski, J. A. (2012). Formation, growth and transformation of leached layers during silicate minerals dissolution: The example of wollastonite. *Geochimica et Cosmochimica Acta, 98*(0), 259-281.

Schuiling, R., & Krijgsman, P. (2006). Enhanced weathering: an effective and cheap tool to sequester CO2. *Climatic Change, 74*(1-3), 349-354.

Smith, P., Martino, D., Cai, Z., Gwary, D., Janzen, H., Kumar, P., McCarl, B., Ogle, S., O'Mara, F., Rice, C., Scholes, B., Sirotenko, O., Howden, M., McAllister, T., Pan, G., Romanenkov, V., Schneider, U., & Towprayoon, S. (2007). Policy and technological constraints to implementation of greenhouse gas mitigation options in agriculture. *Agriculture, Ecosystems & Environment, 118*(1–4), 6-28.

Sognnes, L. S., Fystro, G., Øpstad, S. L., Arstein, A., & Børresen, T. (2006). Effects of adding moraine soil or shell sand into peat soil on physical properties and grass yield in western Norway. *Acta Agriculturae Scandinavica Section B-Soil and Plant Science, 56*(3), 161-170.

Stehfest, E., & Bouwman, L. (2006). N2O and NO emission from agricultural fields and soils under natural vegetation: summarizing available measurement data and modeling of global annual emissions. *Nutrient Cycling in Agroecosystems, 74*(3), 207-228.

Stillings, L. L., & Brantley, S. L. (1995). Feldspar dissolution at 25 C and pH 3: Reaction stoichiometry and the effect of cations. *Geochimica et Cosmochimica Acta, 59*(8), 1483-1496.

Stumm, W., & Wollast, R. (1990). Coordination chemistry of weathering: Kinetics of the surface-controlled dissolution of oxide minerals. *Reviews of Geophysics, 28*(1), 53-69.

Sverdrup, H. (2009). Chemical weathering of soil minerals and the role of biological processes. *Fungal Biology Reviews, 23*(4), 94-100.

Sverdrup, H. U. (1990). The kinetics of base cation release due to chemical weathering. *Lund University Press*.

Swoboda-Colberg, N. G., & Drever, J. I. (1993). Mineral dissolution rates in plot-scale field and laboratory experiments. *Chemical Geology, 105*(1), 51-69.

Ten Berge, H. F., Van der Meer, H. G., Steenhuizen, J. W., Goedhart, P. W., Knops, P., & Verhagen, J. (2012). Olivine weathering in soil, and its effects on growth and nutrient uptake in ryegrass (Lolium perenne L.): A pot experiment. *PloS one, 7*(8), e42098.

Tole, M. P., Lasaga, A. C., Pantano, C., & White, W. B. (1986). The kinetics of dissolution of nepheline (NaAlSiO 4). *Geochimica et Cosmochimica Acta, 50*(3), 379-392.

Ullman, W. J., Kirchman, D. L., Welch, S. A., & Vandevivere, P. (1996). Laboratory evidence for microbially mediated silicate mineral dissolution in nature. *Chemical Geology, 132*(1), 11-17.

Van Hees, P., Lundström, U., & Mörth, C. (2002). Dissolution of microcline and labradorite in a forest O horizon extract: the effect of naturally occurring organic acids. *Chemical Geology, 189*(3), 199-211.

Van Straaten, P. (2006). Farming with rocks and minerals: challenges and opportunities. *Anais da Academia Brasileira de Ciências, 78*(4), 731-747.

Varadachari, C., Barman, A. K., & Ghosh, K. (1994). Weathering of silicate minerals by organic acids II. Nature of residual products. *Geoderma, 61*(3), 251-268.

Velbel, M. A. (2009). Dissolution of olivine during natural weathering. *Geochimica et Cosmochimica Acta, 73*(20), 6098-6113.

Velbel, M. A., & Ranck, J. (2008). Etch pits on naturally altered olivine from dunites of the Appalachian Blue Ridge Mountains, North Carolina, USA. *Mineralogical Magazine, 72*(1), 145-148.

Vitousek, P. M., Aber, J. D., Howarth, R. W., Likens, G. E., Matson, P. A., Schindler, D. W., Schlesinger, W. H., & Tilman, D. G. (1997). Human alteration of the global nitrogen cycle: sources and consequences *Ecological Applications, 7*(3), 737-750.

Vold, O. (2006). Steinmel i landbruket: Kvalitetskrav og godkjenningsordninger. *Seminar om bruk av steinmel i landbruk, UMB, Ås: Debio*.

Wanvik, J. E. (2000). Norwegian anorthosites and their industrial uses, with emphasis on the massifs of the Inner Sogn-Voss area in western Norway. Geological Survey of Norway Bulletin 436, 103-112

Wanvik, J. E. (2010). Summary of knowledge about Norwegian anorthosite prospecting - in relation to Greenland anorthosites. Trondheim: Geological Survey of Norway (2010.020). 21 pp.

Weideborg, M., Blytt, L. D., Stang, P., Henninge, L. B., & Vik, E. A. (2012). Versjon 1 Bakgrunnsdokument for utarbeidelse av miljøkvalitetsstandarder og klassifisering av miljøgifter i vann, sediment og biota *Klima- og forurensings-direktoratet (Klif)* (pp. 105).

Weissbart, E. J., & Rimstidt, J. D. (2000). Wollastonite: Incongruent dissolution and leached layer formation. *Geochimica et Cosmochimica Acta, 64*(23), 4007-4016.

Welch, S. A., & Ullman, W. J. (1996). Feldspar dissolution in acidic and organic solutions: Compositional and pH dependence of dissolution rate. *Geochimica et Cosmochimica Acta, 60*(16), 2939-2948.

White, A. F., & Brantley, S. L. (1995). Chemical weathering rates of silicate minerals: an overview. *Chemical Weathering Rates of Silicate Minerals, 31*, 1-22.

Wilmart, E., Demaiffe, D., & Duchesne, J.-C. (1989). Geochemical constraints on the genesis of the Tellnes ilmenite deposit, Southwest Norway. *Economic Geology, 84*(5), 1047-1056.

Wilson, M. J. (2004). Weathering of the primary rock-forming minerals: processes, products and rates. *Clay Minerals, 39*(3), 233-266.

Wogelius, R. A., & Walther, J. V. (1991). Olivine dissolution at 25 °C: effects of pH, CO2, and organic acids. *Geochimica et Cosmochimica Acta, 55*(4), 943-954.

7 Appendices

Appendix A – Element concentrations from experiment 3

Mg, Si, Cr and Ni concentrations and pH in the different acid solutions vs time (hours) for olivine.

Ca, Mg, Si, Cr and Ni concentrations and pH in the different acid solutions vs time (hours) for dolomite, nepheline syenite, larvikite, eclogite and norite.

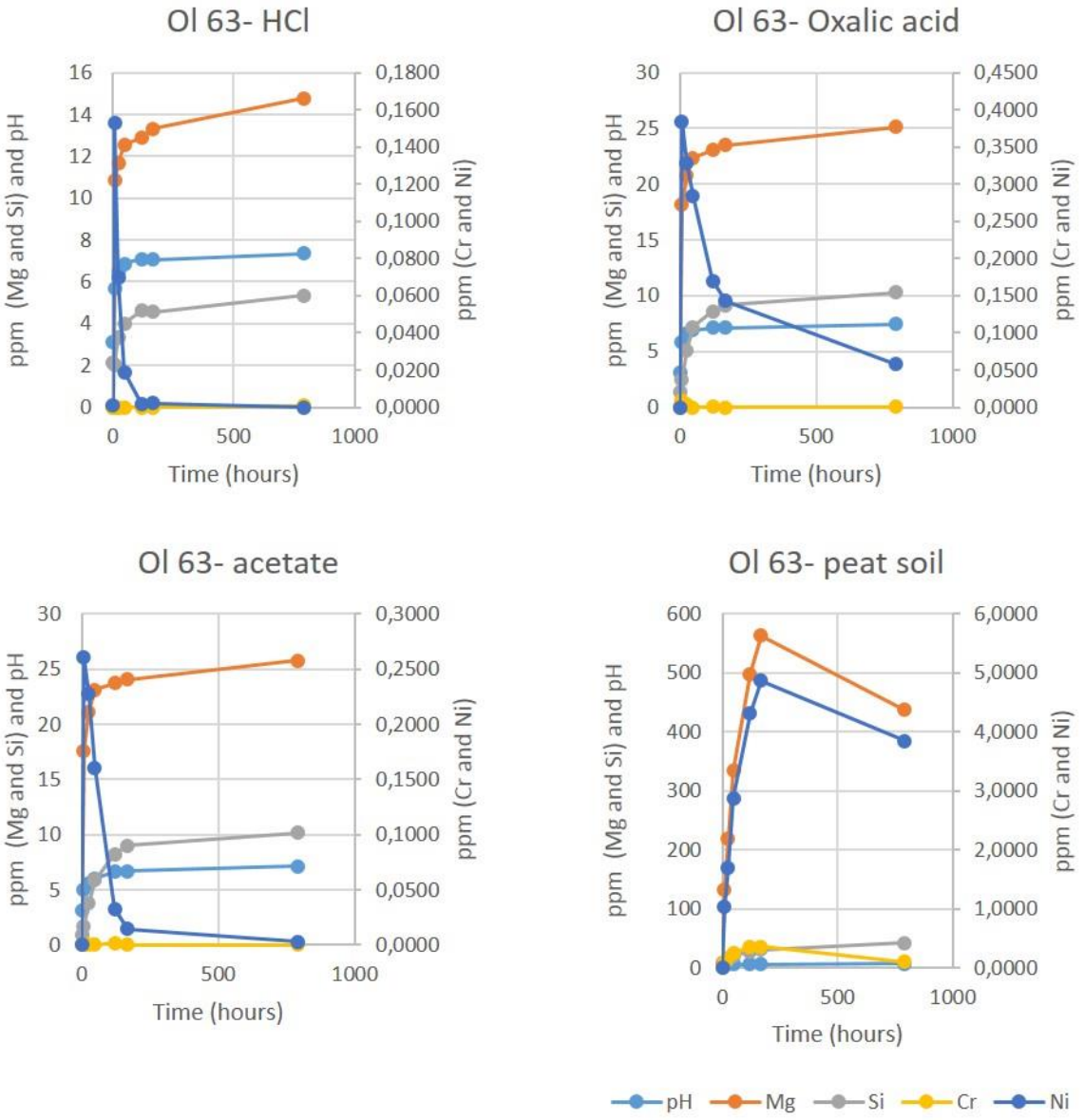

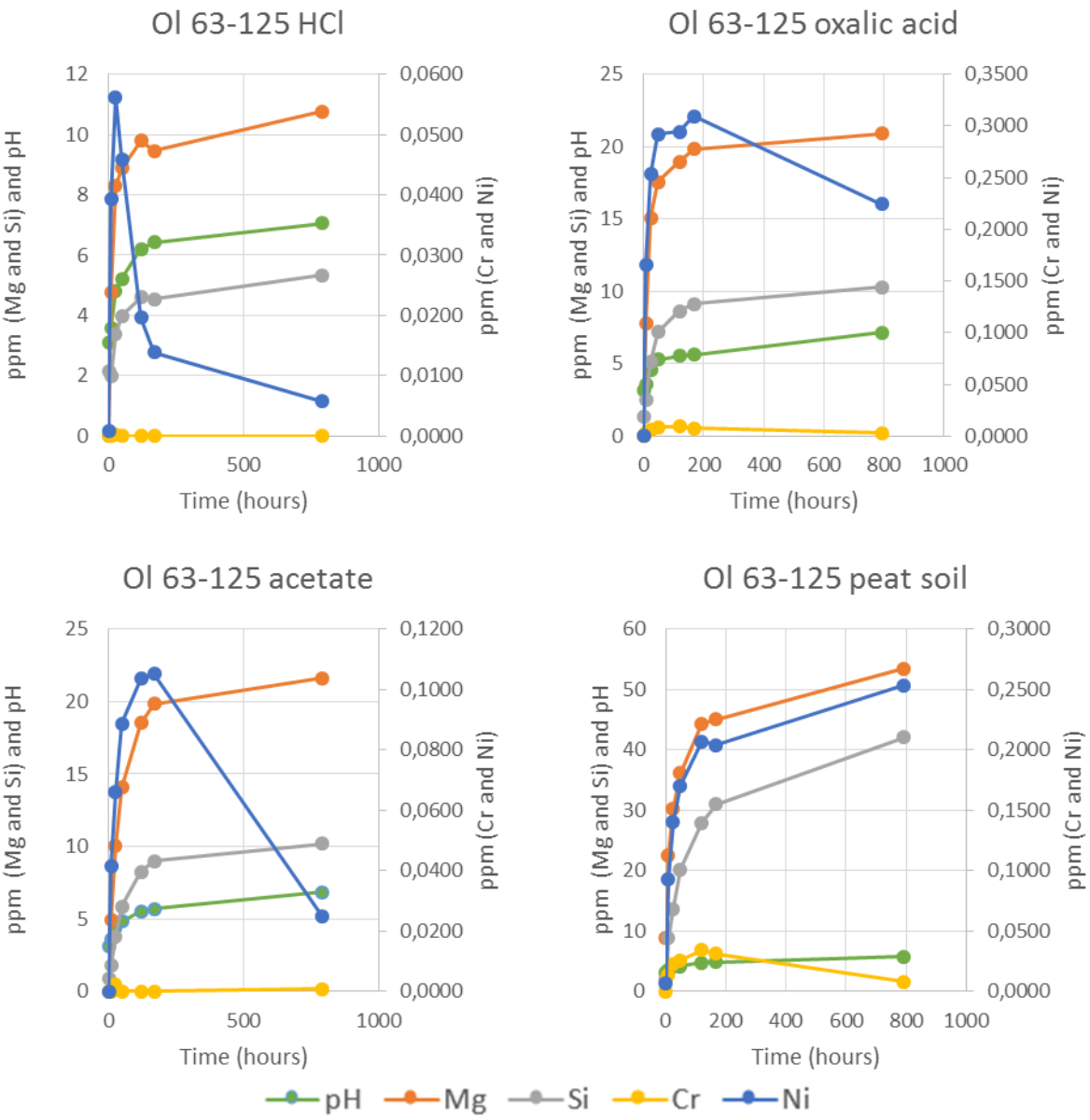
Ol 63-125 HCl
ppm (Mg and Si) and pH
ppm (Cr and Ni)
Time (hours)
Ol 63-125 oxalic acid
ppm (Mg and Si) and pH
ppm (Cr and Ni)
Time (hours)
Ol 63-125 acetate
ppm (Mg and Si) and pH
ppm (Cr and Ni)
Time (hours)
Ol 63-125 peat soil
ppm (Mg and Si) and pH
ppm (Cr and Ni)
Time (hours)
pH
Mg
Si
Cr
Ni

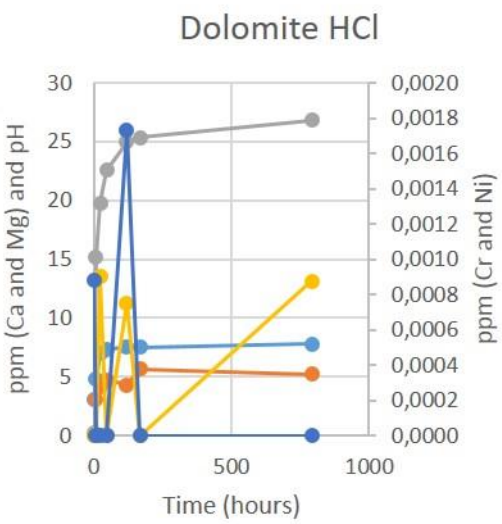
Dolomite HCl
ppm (Ca and Mg) and pH
ppm (Cr and Ni)
Time (hours)
30
25
20
15
10
5
0
0,0020
0,0018
0,0016
0,0014
0,0012
0,0010
0,0008
0,0006
0,0004
0,0002
0,0000
0
500
1000

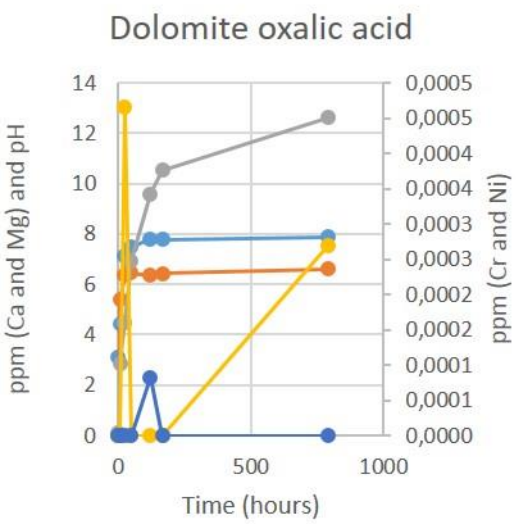
Dolomite oxalic acid
ppm (Ca and Mg) and pH
ppm (Cr and Ni)
Time (hours)
14
12
10
8
6
4
2
0
0,0005
0,0005
0,0004
0,0004
0,0003
0,0003
0,0002
0,0002
0,0001
0,0000
0
500
1000

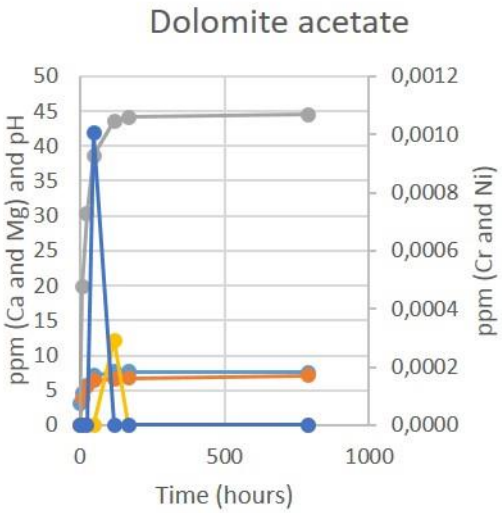
Dolomite acetate
ppm (Ca and Mg) and pH
ppm (Cr and Ni)
Time (hours)
50
45
40
35
30
25
20
15
10
5
0
0,0012
0,0010
0,0008
0,0006
0,0004
0,0002
0,0000
0
500
1000

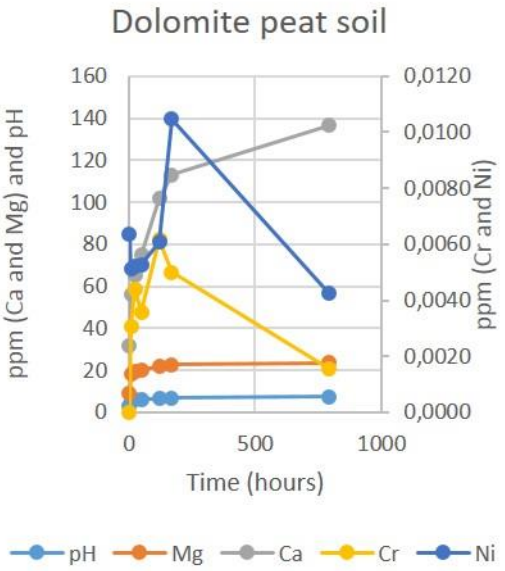
Dolomite peat soil
ppm (Ca and Mg) and pH
ppm (Cr and Ni)
Time (hours)
160
140
120
100
80
60
40
20
0
0,0120
0,0100
0,0080
0,0060
0,0040
0,0020
0,0000
0
500
1000
pH
Mg
Ca
Cr
Ni

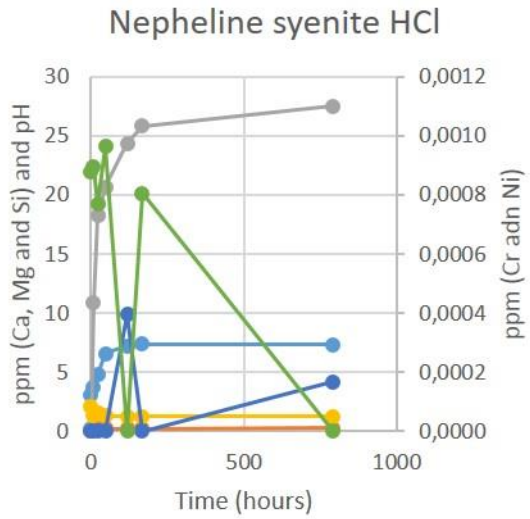
Nepheline syenite HCl
ppm (Ca, Mg and Si) and pH
ppm (Cr adn Ni)
Time (hours)
0
5
10
15
20
25
30
0,0000
0,0002
0,0004
0,0006
0,0008
0,0010
0,0012
0
500
1000

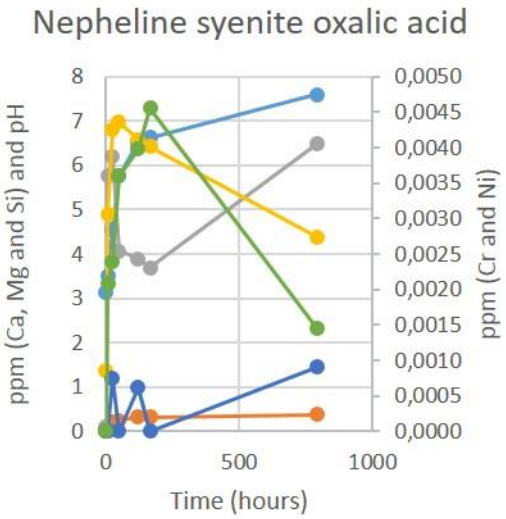
Nepheline syenite oxalic acid
ppm (Ca, Mg and Si) and pH
ppm (Cr and Ni)
Time (hours)
0
1
2
3
4
5
6
7
8
0,0000
0,0005
0,0010
0,0015
0,0020
0,0025
0,0030
0,0035
0,0040
0,0045
0,0050
0
500
1000

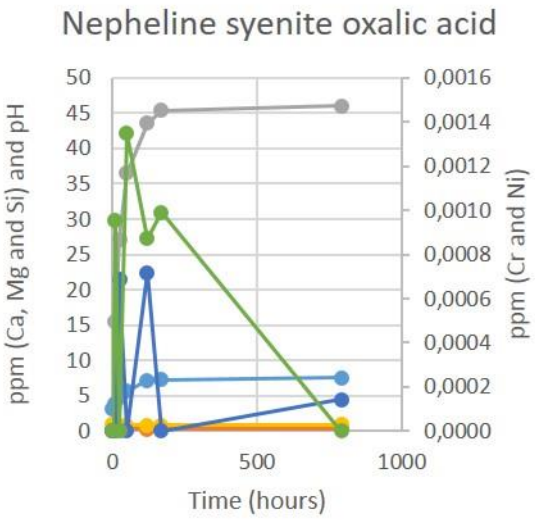
Nepheline syenite oxalic acid
ppm (Ca, Mg and Si) and pH
ppm (Cr and Ni)
Time (hours)
0
5
10
15
20
25
30
35
40
45
50
0,0000
0,0002
0,0004
0,0006
0,0008
0,0010
0,0012
0,0014
0,0016
0
500
1000

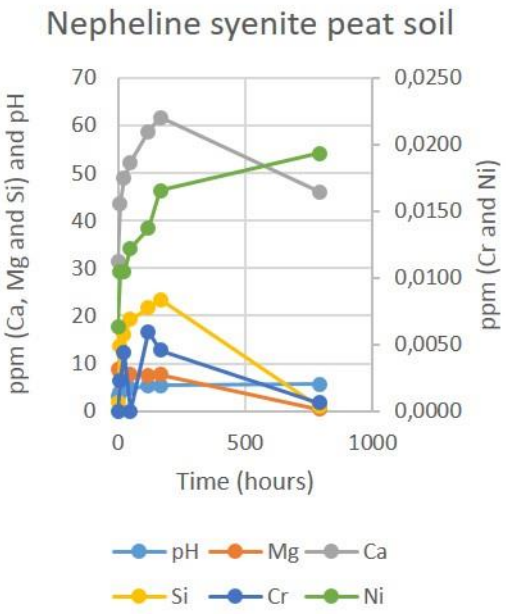
Nepheline syenite peat soil
ppm (Ca, Mg and Si) and pH
ppm (Cr and Ni)
Time (hours)
0
10
20
30
40
50
60
70
0,0000
0,0050
0,0100
0,0150
0,0200
0,0250
0
500
1000
pH
Mg
Ca
Si
Cr
Ni

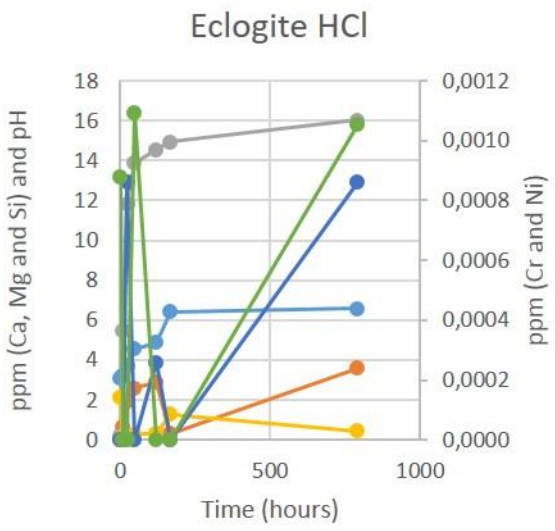
Eclogite HCl
ppm (Ca, Mg and Si) and pH
ppm (Cr and Ni)
Time (hours)
0
500
1000
0
2
4
6
8
10
12
14
16
18
0,0000
0,0002
0,0004
0,0006
0,0008
0,0010
0,0012

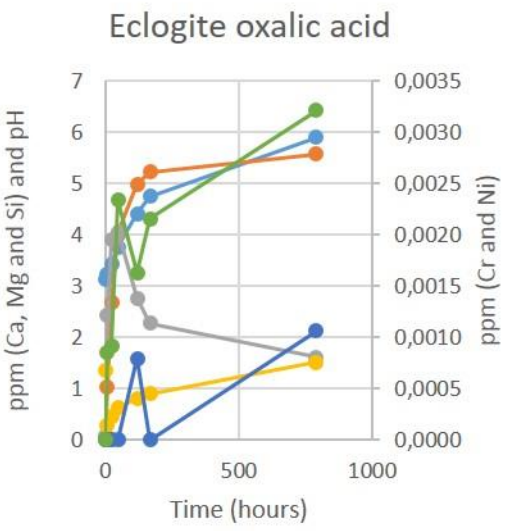
Eclogite oxalic acid
ppm (Ca, Mg and Si) and pH
ppm (Cr and Ni)
Time (hours)
0
500
1000
0
1
2
3
4
5
6
7
0,0000
0,0005
0,0010
0,0015
0,0020
0,0025
0,0030
0,0035

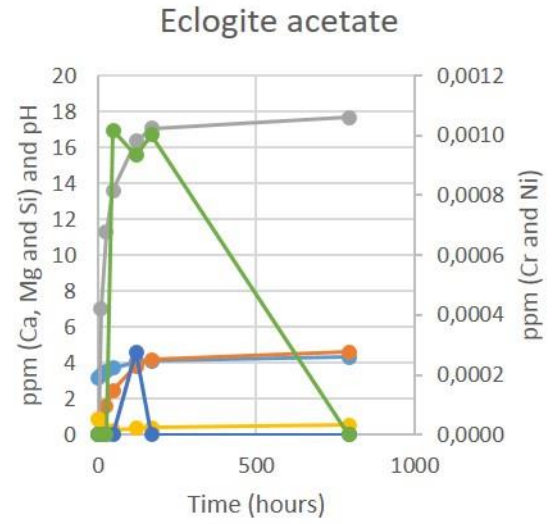
Eclogite acetate
ppm (Ca, Mg and Si) and pH
ppm (Cr and Ni)
Time (hours)
0
500
1000
0
2
4
6
8
10
12
14
16
18
20
0,0000
0,0002
0,0004
0,0006
0,0008
0,0010
0,0012

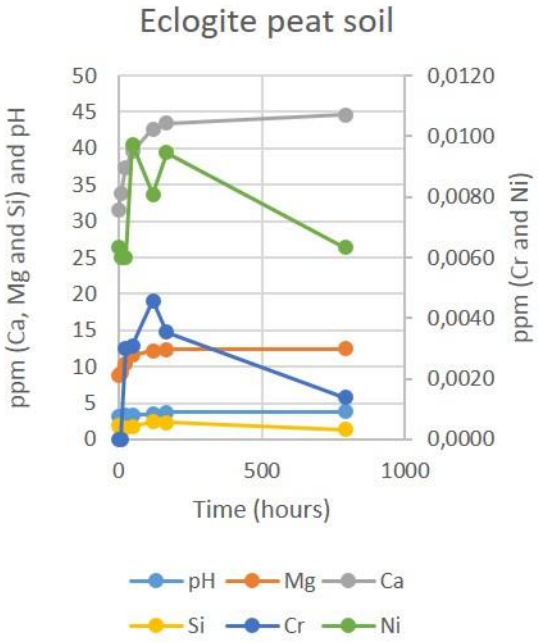
Eclogite peat soil
ppm (Ca, Mg and Si) and pH
ppm (Cr and Ni)
Time (hours)
0
500
1000
0
5
10
15
20
25
30
35
40
45
50
0,0000
0,0020
0,0040
0,0060
0,0080
0,0100
0,0120
pH
Mg
Ca
Si
Cr
Ni

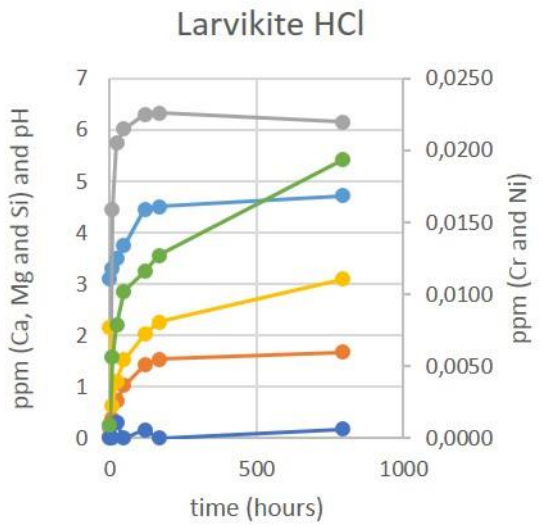
Larvikite HCl
ppm (Ca, Mg and Si) and pH
ppm (Cr and Ni)
time (hours)
0
500
1000
0,0250
0,0200
0,0150
0,0100
0,0050
0,0000

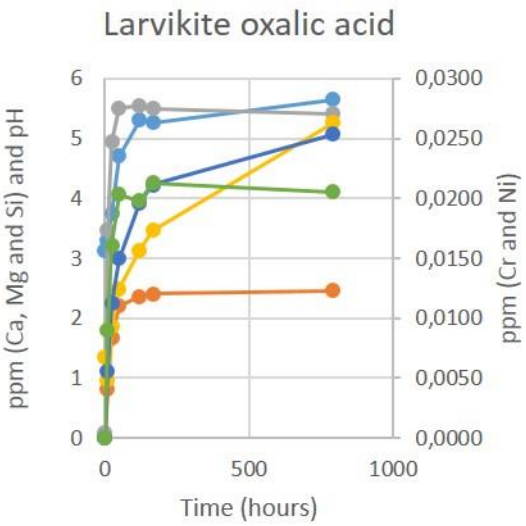
Larvikite oxalic acid
ppm (Ca, Mg and Si) and pH
ppm (Cr and Ni)
Time (hours)
0
500
1000
0,0300
0,0250
0,0200
0,0150
0,0100
0,0050
0,0000

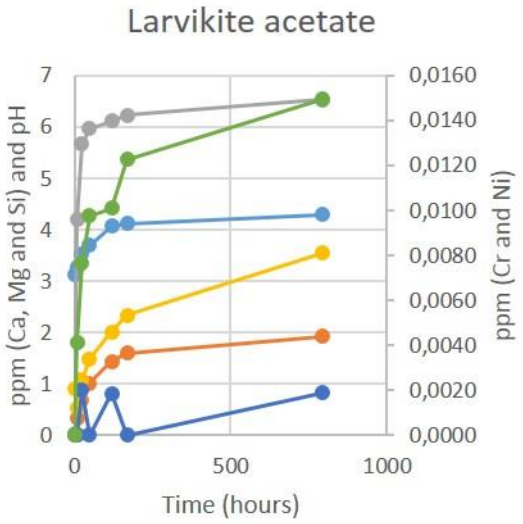
Larvikite acetate
ppm (Ca, Mg and Si) and pH
ppm (Cr and Ni)
Time (hours)
0
500
1000
0,0160
0,0140
0,0120
0,0100
0,0080
0,0060
0,0040
0,0020
0,0000

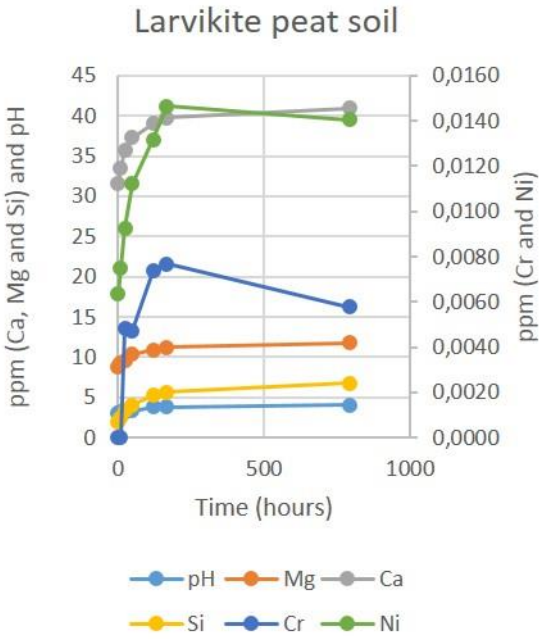
Larvikite peat soil
ppm (Ca, Mg and Si) and pH
ppm (Cr and Ni)
Time (hours)
0
500
1000
0,0160
0,0140
0,0120
0,0100
0,0080
0,0060
0,0040
0,0020
0,0000
pH
Mg
Ca
Si
Cr
Ni

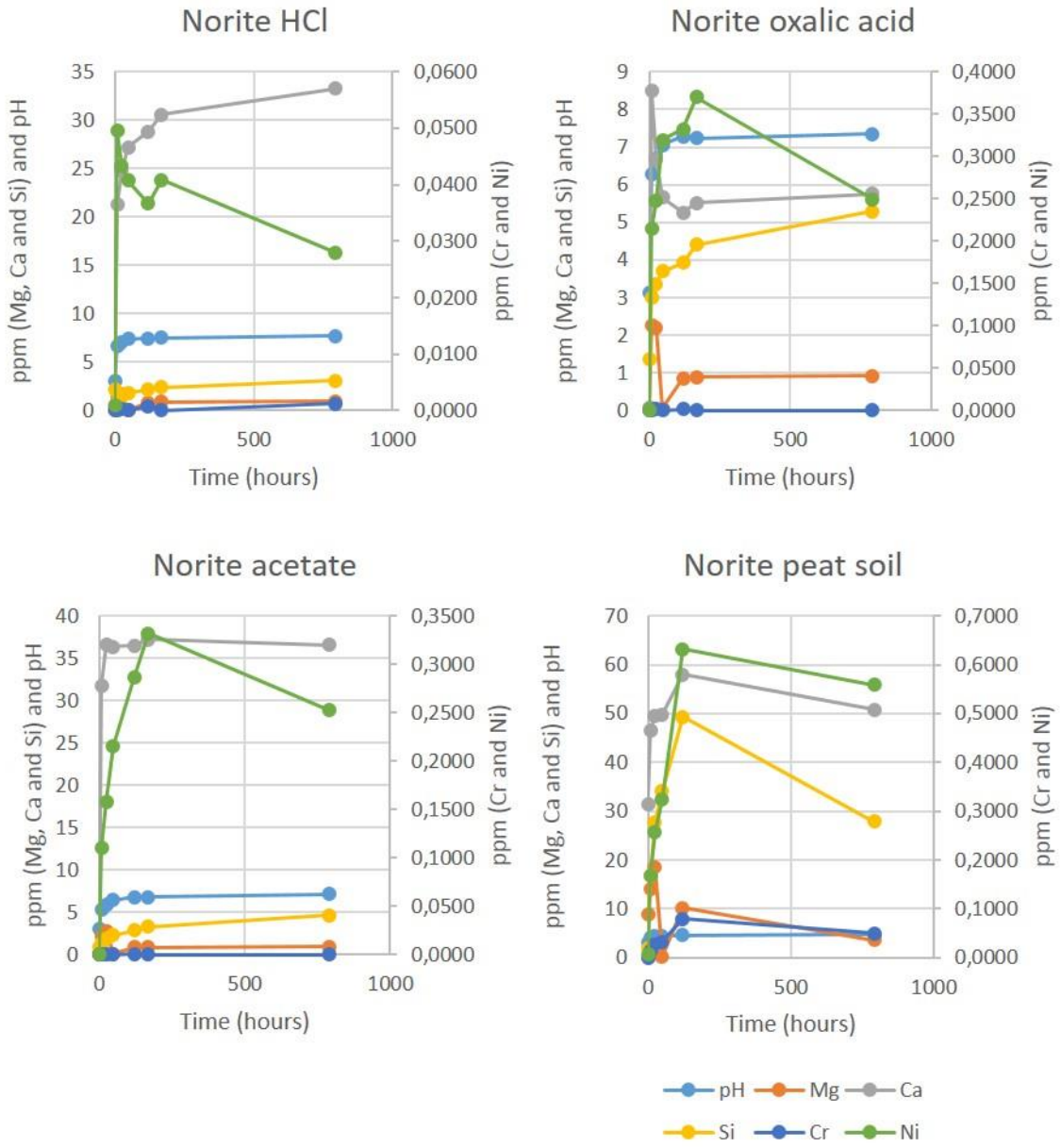
Norite HCl
ppm (Mg, Ca and Si) and pH
ppm (Cr and Ni)
Time (hours)
Norite oxalic acid
ppm (Mg, Ca and Si) and pH
ppm (Cr and Ni)
Time (hours)
Norite acetate
ppm (Mg, Ca and Si) and pH
ppm (Cr and Ni)
Time (hours)
Norite peat soil
ppm (Mg, Ca and Si) and pH
ppm (Cr and Ni)
Time (hours)
pH
Mg
Ca
Si
Cr
Ni

Appendix B – Dissolution rates from experiment 3

This appendix contains mineral dissolution rate data collected from dissolution rate experiment 3. The experiments are conducted at 25°C. The minerals included here are: olivine 63-, olivine 63-125, dolomite, altagro, larvikite, eclogite and norite. Each table contains information on fluid composition, specific surface area, experimental duration, element release (Mg and Si for olivine, Mg and Ca for dolomite, Ca and Si for the other samples), surface area normalized dissolution rates. The dissolution rates are based on moles released per surface area per time unit, mole/m^2/s.

Sample	Fluid composition	Surface area (m^2/g)	Output ppm Mg	Output ppm Si	pH	Time (sec)	Rate Mg	Rate Si
Olivine 63-	0.001 MHCl	8.42	0.0	2.1	3.1	0		
		8.42	10.8	2.0	5.7	28800	1.8E-10	-2.3E-12
		8.42	11.7	3.4	6.5	86400	6.9E-12	1.0E-11
		8.42	12.6	4.0	6.9	172800	5.0E-12	3.0E-12
		8.42	12.9	4.6	7.1	432000	6.1E-13	9.6E-13
		8.42	13.3	4.5	7.1	604800	1.2E-12	-1.4E-13
		8.42	14.8	5.3	7.3	2246400	3.9E-13	1.9E-13
Olivine 63-	0.001 M Oxalic acid	8.42	0.0	1.4	3.1	0		
		8.42	18.1	2.5	5.9	28800	3.1E-10	1.6E-11
		8.42	20.8	5.1	6.6	86400	2.2E-11	1.9E-11
		8.42	22.3	7.2	6.9	172800	8.8E-12	1.0E-11
		8.42	23.0	8.6	7.1	432000	1.3E-12	2.2E-12
		8.42	23.5	9.1	7.2	604800	1.2E-12	1.2E-12
		8.42	25.1	10.3	7.5	2246400	4.5E-13	2.7E-13
Olivine 63-	0.001 M Acetic acid	8.42	0.0	0.9	3.1	0		
		8.42	17.6	1.7	5.0	28800	3.0E-10	1.2E-11
		8.42	21.1	3.8	5.6	86400	3.0E-11	1.5E-11
		8.42	23.1	5.8	6.1	172800	1.1E-11	9.9E-12
		8.42	23.7	8.2	6.6	432000	1.2E-12	3.7E-12
		8.42	24.1	9.0	6.7	604800	8.7E-13	1.8E-12
		8.42	25.8	10.2	7.1	2246400	4.7E-13	2.8E-13
Olivine 63-	Peat soil (+ HCl)	8.42	8.9	1.9	3.1	0		
		8.42	133.4	8.8	5.3	28800	2.1E-09	1.0E-10
		8.42	219.2	13.6	6.0	86400	7.2E-10	3.5E-11
		8.42	334.3	20.2	6.2	172800	6.4E-10	3.1E-11
		8.42	497.7	27.9	6.4	432000	3.0E-10	1.2E-11
		8.42	562.8	31.0	6.4	604800	1.8E-10	7.1E-12
		8.42	437.5	42.1	6.8	2246400	-3.4E-11	2.6E-12

Sample	Fluid composition	Surface area (m^2/g)	Output ppm Mg	Output ppm Si	pH	Time (sec)	Rate Mg	Rate Si
Olivine 63-125	0.001 MHCl	1.59	0.02	2.14	3.1	0		
		1.59	4.75	1.55	3.58	28800	4.3E-10	-4.6E-11
		1.59	8.28	1.44	4.81	86400	1.6E-10	-4.1E-12
		1.59	8.88	1.41	5.22	172800	1.8E-11	-8.0E-13
		1.59	9.79	1.28	6.2	432000	8.7E-12	-1.1E-12
		1.59		1.25		604800		-4.5E-13
		1.59	10.76	1.26	7.05	2246400	1.4E-12	2.2E-14
	0.001 M Oxalic acid	1.59	0.01	1.36	3.13	0		
		1.59	7.76	3.51	3.6	28800	7.0E-10	1.7E-10
		1.59	15.08	3.50	4.55	86400	3.3E-10	-5.5E-13
		1.59	17.57	3.32	5.31	172800	7.4E-11	-4.7E-12
		1.59	18.98	2.95	5.55	432000	1.4E-11	-3.1E-12
		1.59	19.83	2.89	5.64	604800	1.2E-11	-7.1E-13
		1.59	20.91	2.77	7.14	2246400	1.6E-12	-1.6E-13
	0.001 M Acetic acid (+ HCl)	1.59	0.00	0.91	3.13	0		
		1.59	4.89	2.97	3.58	28800	4.4E-10	1.6E-10
		1.59	10.06	3.54	4.33	86400	2.3E-10	2.2E-11
		1.59	14.08	3.74	4.82	172800	1.2E-10	5.1E-12
		1.59	18.52	3.58	5.53	432000	4.3E-11	-1.4E-12
		1.59	19.87	3.46	5.67	604800	1.9E-11	-1.4E-12
		1.59	21.63	2.93	6.84	2246400	2.6E-12	-6.7E-13
	Peat soil (+ HCl)	1.59	8.86	1.85	3.08	0		
		1.59	22.56	54.79	3.46	28800	1.2E-09	4.1E-09
		1.59	30.34	73.16	4.05	86400	3.5E-10	7.1E-10
		1.59	36.17	89.45	4.13	172800	1.7E-10	4.2E-10
		1.59	44.40	95.78	4.72	432000	7.9E-11	5.3E-11
		1.59	45.04	101.86	4.85	604800	9.1E-12	7.5E-11
		1.59	53.48	148.90	5.71	2246400	1.2E-11	5.9E-11
Sample	**Fluid composition**	**Surface area (m^2/g)**	**Output ppm Mg**	**Output ppm Ca**	**pH**	**Time (sec)**	**Rate Mg**	**Rate Ca**
Dolomite	0.001 MHCl	0.13647	0.02	0.21	3.1	0		
		0.13647	3.08	15.20	4.8	28800	3.2E-09	9.5E-09
		0.13647	4.17	19.78	6.95	86400	5.7E-10	1.4E-09
		0.13647	4.72	22.58	7.31	172800	1.9E-10	5.8E-10
		0.13647	4.28	24.95	7.58	432000	-4.9E-11	1.6E-10
		0.13647	5.65	25.37	7.53	604800	2.3E-10	4.2E-11
		0.13647	5.23	26.82	7.75	2851200	-5.1E-12	1.1E-11
	0.001 M Oxalic acid	0.13647	0.01	0.09	3.13	0		
		0.13647	5.38	2.86	4.45	28800	5.6E-09	1.8E-09
		0.13647	6.39	4.49	7.13	86400	5.2E-10	5.1E-10
		0.13647	6.46	6.95	7.47	172800	2.3E-11	5.1E-10
		0.13647	6.36	9.59	7.81	432000	-1.1E-11	1.8E-10
		0.13647	6.44	10.52	7.78	604800	1.3E-11	9.4E-11
		0.13647	6.61	12.63	7.89	2851200	2.2E-12	1.6E-11
	0.001 M Acetic acid (+ HCl)	0.13647	0.00	0.04	3.13	0		
		0.13647	3.84	19.81	4.54	28800	4.0E-09	1.3E-08
		0.13647	5.49	30.31	5.65	86400	8.6E-10	3.3E-09
		0.13647	6.41	38.64	7.15	172800	3.2E-10	1.7E-09
		0.13647	6.64	43.55	7.67	432000	2.6E-11	3.3E-10
		0.13647	6.74	44.09	7.65	604800	1.5E-11	5.4E-11
		0.13647	7.13	44.52	7.53	2851200	4.9E-12	3.3E-12

	Peat soil (+ HCl)	0.13647	8.86	31.52	3.08	0		
		0.13647	18.35	56.38	5.39	28800	9.9E-09	1.6E-08
		0.13647	19.20	65.27	5.8	86400	4.4E-10	2.8E-09
		0.13647	20.17	74.96	6.26	172800	3.3E-10	2.0E-09
		0.13647	21.84	101.60	6.65	432000	1.9E-10	1.8E-09
		0.13647	22.59	112.93	6.88	604800	1.2E-10	1.1E-09
		0.13647	23.48	136.64	7.28	2851200	1.1E-11	1.8E-10
Sample	**Fluid composition**	**Surface area (m^2/g)**	**Output ppm Ca**	**Output ppm Si**	**pH**	**Time (sec)**	**Rate Ca**	**Rate Si**
Altagro	0.001 MHCl	0.16083	0.2147	2.1444	3.1	0		
		0.16083	10.8538	1.3778	3.68	28800	5.7E-09	-5.9E-10
		0.16083	18.2224	1.5118	4.77	86400	2.0E-09	5.1E-11
		0.16083	20.6761	1.2907	6.59	172800	4.3E-10	-5.6E-11
		0.16083	24.3647	1.2333	7.23	432000	2.1E-10	-4.7E-12
		0.16083	25.8051	1.2703	7.36	604800	1.2E-10	4.5E-12
		0.16083	27.4902	1.2615	7.35	2851200	1.1E-11	-8.0E-14
	0.001 M Oxalic acid	0.16083	0.0891	1.3574	3.13	0		
		0.16083	5.7594	4.8874	3.52	28800	3.1E-09	2.7E-09
		0.16083	6.1854	6.7987	4.54	86400	1.1E-10	7.3E-10
		0.16083	4.0695	6.9683	5.76	172800	-3.7E-10	4.3E-11
		0.16083	3.8863	6.5769	6.53	432000	-1.1E-11	-3.2E-11
		0.16083	3.6898	6.4243	6.63	604800	-1.7E-11	-1.9E-11
		0.16083	6.4768	4.3900	7.59	2851200	1.8E-11	-1.8E-11
	0.001 M Acetic acid (+ HCl)	0.16083	0.0391	0.9054	3.13	0		
		0.16083	15.5477	0.7604	3.88	28800	8.4E-09	-1.1E-10
		0.16083	27.1290	0.8189	4.77	86400	3.1E-09	2.2E-11
		0.16083	36.4504	0.8523	5.62	172800	1.6E-09	8.4E-12
		0.16083	43.5277	0.8352	7.2	432000	4.1E-10	-1.4E-12
		0.16083	45.3476	0.8404	7.31	604800	1.6E-10	6.3E-13
		0.16083	46.0227	0.9628	7.55	2851200	4.3E-12	1.1E-12
	Peat soil + (HCl)	0.16083	31.5249	1.8532	3.08	0		
		0.16083	43.6688	13.6678	3.84	28800	6.5E-09	9.1E-09
		0.16083	48.9183	15.9802	4.36	86400	1.4E-09	8.8E-10
		0.16083	52.2384	19.2768	4.69	172800	5.9E-10	8.3E-10
		0.16083	58.6657	21.6458	5.36	432000	3.7E-10	2.0E-10
		0.16083	61.6305	23.3503	5.36	604800	2.5E-10	0.0E+00
Sample	**Fluid composition**	**Surface area (m^2/g)**	**Output ppm Ca**	**Output ppm Si**	**pH**	**time (sec)**	**Rate Ca**	**Rate Si**
Larvikite	0.001 MHCl	1.22	0.21	2.14	3.10	0		
		1.22	4.46	0.63	3.29	28800	4.2E-11	-1.5E-10
		1.22	5.76	1.11	3.51	86400	2.0E-11	2.4E-11
		1.22	6.01	1.52	3.75	172800	1.1E-11	1.4E-11
		1.22	6.31	2.02	4.46	432000	5.0E-12	5.4E-12
		1.22	6.33	2.25	4.51	604800	2.0E-12	3.7E-12
		1.22	6.15	3.10	4.72	2246400	2.0E-13	1.0E-12

	0.001 M Oxalic acid	1.22	0.09	1.36	3.13	0		
		1.22	3.48	0.96	3.29	28800	9.3E-11	-4.0E-11
		1.22	4.94	1.86	3.74	86400	5.1E-11	4.5E-11
		1.22	5.51	2.49	4.71	172800	2.0E-11	2.1E-11
		1.22	5.55	3.14	5.31	432000	2.0E-12	7.1E-12
		1.22	5.50	3.47	5.27	604800	7.1E-13	5.3E-12
	0.001 M Acetic acid (+ HCl)	1.22	5.42	5.27	5.65	2246400	8.5E-14	2.2E-12
		1.22	0.04	0.91	3.13	0		
		1.22	4.19	0.52	3.27	28800	3.9E-11	-3.9E-11
		1.22	5.67	1.07	3.52	86400	2.0E-11	2.7E-11
		1.22	5.96	1.48	3.70	172800	1.2E-11	1.4E-11
		1.22	6.11	2.01	4.07	432000	5.2E-12	5.7E-12
		1.22	6.23	2.33	4.12	604800	3.0E-12	5.1E-12
		1.22	6.53	3.55	4.30	2246400	4.5E-13	1.5E-12
	Peat soil (+ (HCl)	1.22	31.52	1.85	3.08	0		
		1.22	33.43	2.33	3.15	28800	3.9E-11	4.8E-11
		1.22	35.80	3.38	3.16	86400	2.7E-11	5.2E-11
		1.22	37.29	4.05	3.30	172800	2.7E-11	2.2E-11
		1.22	39.06	5.21	3.82	432000	6.3E-12	1.3E-11
		1.22	39.79	5.67	3.81	604800	6.0E-12	7.5E-12
		1.22	40.97	6.77	4.07	2246400	8.3E-13	1.3E-12
Sample	**Fluid composition**	**Surface area (m^2/g)**	**Output ppm Ca**	**Output ppm Si**	**pH**	**Time (sec)**	**Rate Ca**	**Rate Si**
Eclogite	0.001 MHCl	0.065852	0.2147	2.1444	3.1	0		
		0.065852	5.4998	0.1166	3.25	28800	7.0E-09	-3.8E-09
		0.065852	11.8425	0.2165	3.75	86400	4.1E-09	9.3E-11
		0.065852	13.8719	0.2732	4.55	172800	8.7E-10	3.5E-11
		0.065852	14.5337	0.3126	4.88	432000	9.3E-11	7.9E-12
		0.065852	14.9274	1.2829	6.42	604800	8.3E-11	2.9E-10
		0.065852	16.0215	0.4368	6.57	2246400	1.7E-11	-1.9E-11
	0.001 M Oxalic acid	0.065852	0.0891	1.3574	3.13	0		
		0.065852	2.4358	0.2789	3.22	28800	3.1E-09	-2.0E-09
		0.065852	3.8906	0.4469	3.43	86400	9.5E-10	1.6E-10
		0.065852	4.0612	0.6252	3.76	172800	7.3E-11	1.1E-10
		0.065852	2.7546	0.8080	4.41	432000	-1.8E-10	3.7E-11
		0.065852	2.2693	0.9024	4.75	604800	-1.0E-10	2.8E-11
		0.065852	1.6167	1.5149	5.9	2246400	-1.0E-11	1.4E-11
	0.001 M Acetic acid (+ HCl)	0.065852	0.0391	0.9054	3.13	0		
		0.065852	7.0178	0.1282	3.27	28800	9.2E-09	-1.5E-09
		0.065852	11.2902	0.2046	3.52	86400	2.8E-09	7.1E-11
		0.065852	13.5913	0.2521	3.7	172800	9.9E-10	2.9E-11

		0.065852	16.3270	0.3521	4.07	432000	3.9E-10	2.0E-11
		0.065852	17.0501	0.3773	4.12	604800	1.5E-10	7.5E-12
		0.065852	17.6489	0.5294	4.3	2246400	9.3E-12	3.4E-12
	Peat soil (+ HCl)	0.065852	31.5249	1.8532	3.08	0		
		0.065852	33.7170	1.3086	3.14	28800	2.9E-09	-1.0E-09
		0.065852	37.3275	1.6090	3.26	86400	2.4E-09	2.8E-10
		0.065852	39.5955	1.7931	3.37	172800	9.8E-10	1.1E-10
		0.065852	42.6680	2.4166	3.44	432000	4.3E-10	1.3E-10
		0.065852	43.4680	2.3101	3.71	604800	1.7E-10	-3.2E-11
		0.065852	44.5726	1.3266	3.84	2246400	1.7E-11	-2.2E-11
Sample	**Fluid composition**	**Surface area (m^2/g)**	**Output ppm Ca**	**Output ppm Si**	**pH**	**Time (sec)**	**Rate Ca**	**Rate Si**
Norite	0.001 MHCl	6.93	0.2147	2.1444	3.1	0		
		6.93	21.2492	0.9949	6.7	28800	2.6E-10	-2.0E-11
		6.93	24.7647	1.4435	7.09	86400	2.2E-11	4.0E-12
		6.93	27.2203	1.8236	7.37	172800	1.0E-11	2.2E-12
		6.93	28.8354	2.1556	7.43	432000	2.2E-12	6.3E-13
		6.93	30.5454	2.3993	7.5	604800	3.4E-12	6.9E-13
		6.93	33.2316	3.0811	7.68	2246400	4.0E-13	1.4E-13
	0.001 M Oxalic acid	6.93	0.0891	1.3574	3.13	0		
		6.93	8.4956	2.9994	6.28	28800	1.1E-10	2.9E-11
		6.93	6.6707	3.3593	6.7	86400	-1.1E-11	3.2E-12
		6.93	5.6627	3.7078	7.05	172800	-4.1E-12	2.0E-12
		6.93	5.2638	3.9247	7.28	432000	-5.3E-13	4.1E-13
		6.93	5.5079	4.4122	7.24	604800	4.9E-13	1.4E-12
		6.93	5.7521	5.2838	7.35	2246400	3.6E-14	1.8E-13
	0.001 M Acetic acid (+ HCl)	6.93	0.0391	0.9054	3.13	0		
		6.93	31.7805	1.3665	5.4	28800	4.0E-10	8.2E-12
		6.93	36.5979	1.9540	5.98	86400	3.0E-11	5.2E-12
		6.93	36.3392	2.3321	6.43	172800	-1.1E-12	2.2E-12
		6.93	36.4743	2.8964	6.83	432000	1.8E-13	1.1E-12
		6.93	37.2216	3.3423	6.79	604800	1.5E-12	1.3E-12
		6.93	36.5661	4.6407	7.14	2246400	-9.7E-14	2.7E-13
	Peat soil (+ HCl)	6.93	31.5249	1.8532	3.08	0		
		6.93	46.6374	16.8593	4.12	28800	1.9E-10	2.7E-10
		6.93	49.4437	27.7648	4.3	86400	1.7E-11	9.6E-11
		6.93	49.8107	34.0104	4.41	172800	1.5E-12	3.6E-11
		6.93	58.0196	49.3664	4.59	432000	1.1E-11	2.9E-11
		6.93			4.6	604800		
		6.93	50.8208	27.8572	4.65	2246400	7.5E-12	5.9E-12

Appendix C – Trace element concentrations

All trace element concentrations (ppm) for starting materials.

ppm	Norite	Eclogite	Olivine	Vulcanic glass	Larvikite	Nepheline syenite
Li7(MR)	4,768	6,606	0,948	5,312	18,438	4,359
Sc45(MR)	9,237	60,228	7,223	30,232	4,468	6,012
V51(MR)	398,521	301,657	12,062	230,726	57,292	131,890
Cr52(MR)	340,406	9,609	928,363	261,126	30,735	66,237
Cr53(MR)	342,277	9,951	943,853	255,901	31,133	66,160
Mn55(MR)	713,711	1598,942	592,256	972,469	1041,433	1577,170
Co59(MR)	93,190	55,920	99,922	33,422	7,122	16,534
Ni60(MR)	483,297	12,304	2306,578	106,306	10,688	28,177
Cu63(MR)	179,115	26,517	7,514	54,845	11,518	7,294
Zn66(MR)	129,526	127,843	25,475	58,622	115,531	86,813
Zn67(MR)	130,269	133,730	24,452	66,363	110,661	86,489
Zn68(MR)	117,224	125,751	25,438	58,335	115,006	85,628
Rb85(MR)	7,561	5,845	0,886	8,243	36,495	27,369
Sr86(MR)	512,509	119,365	46,094	151,578	612,395	1499,696
Sr88(MR)	483,042	117,218	44,158	152,022	575,760	1418,908
Y89(MR)	6,312	18,548	0,163	24,204	25,142	17,551
Zr90(MR)	50,112	6,197	0,370	96,158	369,247	205,903
Zr91(MR)	48,077	6,491	0,378	95,851	370,282	202,279
Nb93(MR)	13,975	2,219	0,420	9,139	128,004	168,646
Cs133(MR)	0,095	0,352	0,115	0,212	1,010	0,117
Hf178(MR)	1,783	0,299	0,015	2,606	9,829	5,047
Ta181(MR)	1,411	0,265	0,013	0,766	8,996	10,539
Pb206(MR)	3,097	1,522	1,241	1,133	7,642	1,150
Pb208(MR)	3,392	1,647	1,386	1,291	7,947	1,242
Th232(MR)	0,511	0,736	0,143	0,901	12,055	1,496
U238(MR)	0,180	0,200	0,108	0,265	4,611	0,469

Appendix D -SEM images

A compilation of images from the grain dissolution quantification. The quantification presented in the results were based on 15-40 images, several EDS analysis and observations during examination, however all data are not included here. Four to six images of each grain was included to illustrate the main features.

Olivine

Olivine ID.1

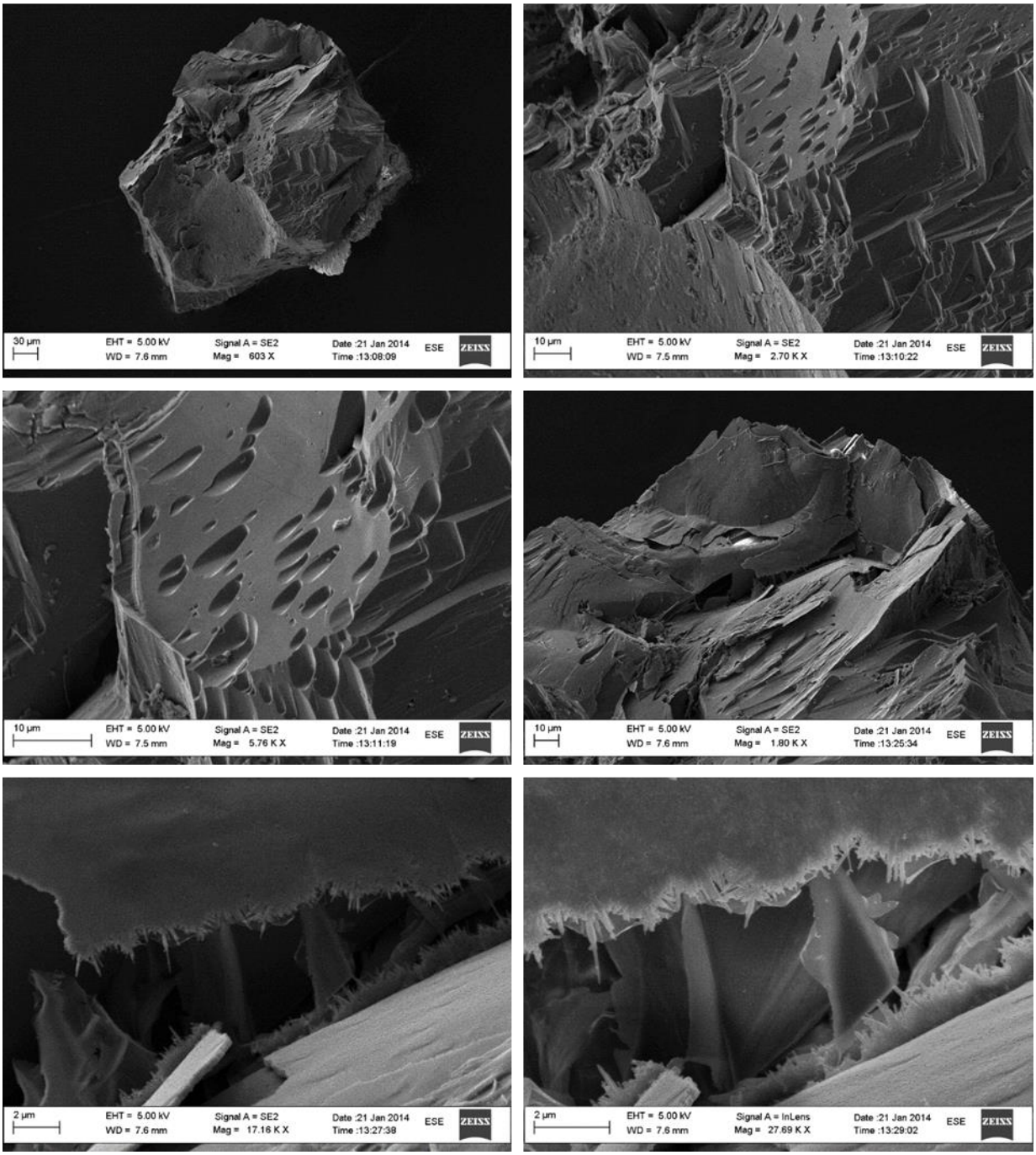

Olivine ID.2

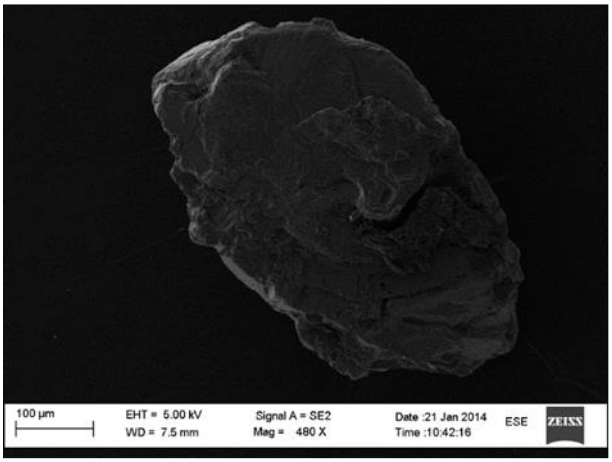
100 µm
EHT = 5.00 kV
WD = 7.5 mm
Signal A = SE2
Mag = 480 X
Date :21 Jan 2014
Time :10:42:16
ESE
ZEISS

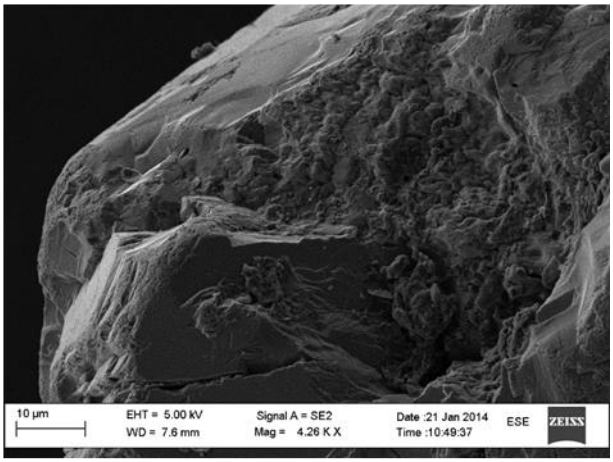
10 µm
EHT = 5.00 kV
WD = 7.6 mm
Signal A = SE2
Mag = 4.26 K X
Date :21 Jan 2014
Time :10:49:37
ESE
ZEISS

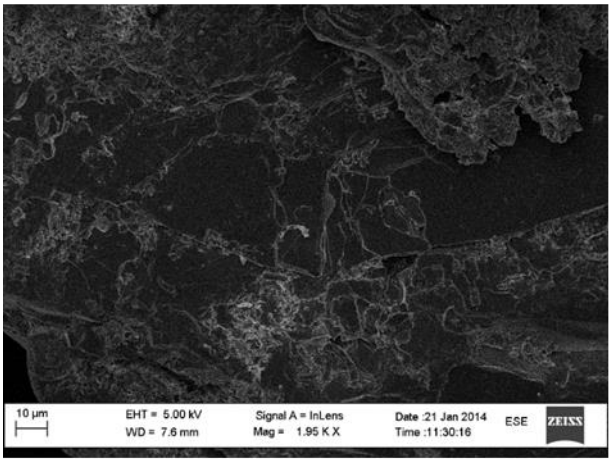
10 µm
EHT = 5.00 kV
WD = 7.6 mm
Signal A = InLens
Mag = 1.95 K X
Date :21 Jan 2014
Time :11:30:16
ESE
ZEISS

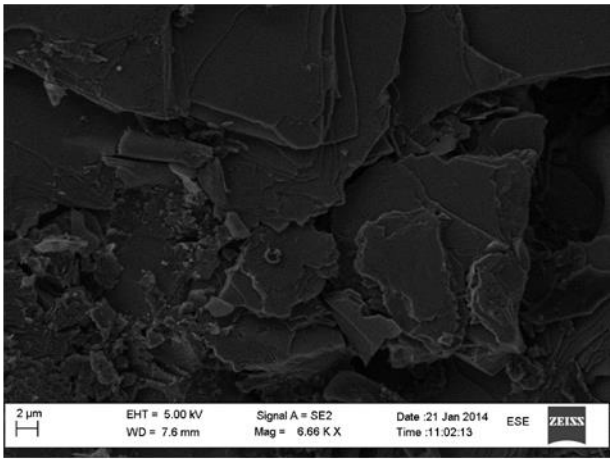
2 µm
EHT = 5.00 kV
WD = 7.6 mm
Signal A = SE2
Mag = 6.66 K X
Date :21 Jan 2014
Time :11:02:13
ESE
ZEISS

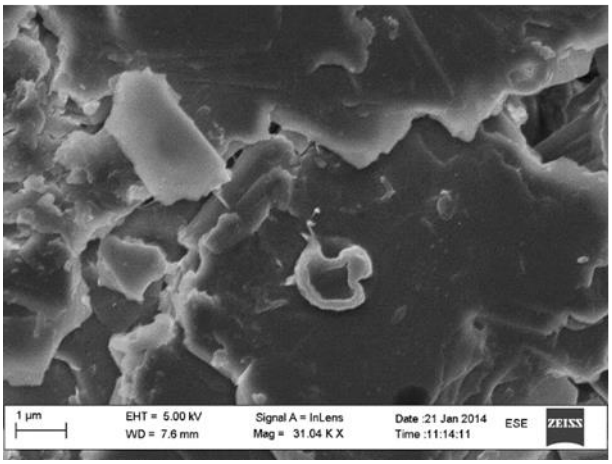
1 µm
EHT = 5.00 kV
WD = 7.6 mm
Signal A = InLens
Mag = 31.04 K X
Date :21 Jan 2014
Time :11:14:11
ESE
ZEISS

Olivine ID.3

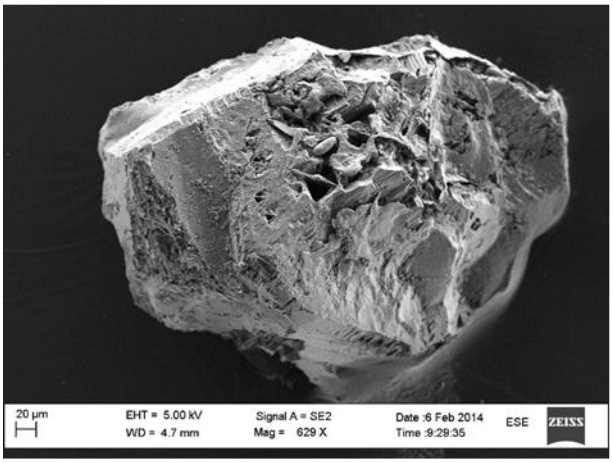
20 µm
EHT = 5.00 kV
WD = 4.7 mm
Signal A = SE2
Mag = 629 X
Date :6 Feb 2014
Time :9:29:35
ESE
ZEISS

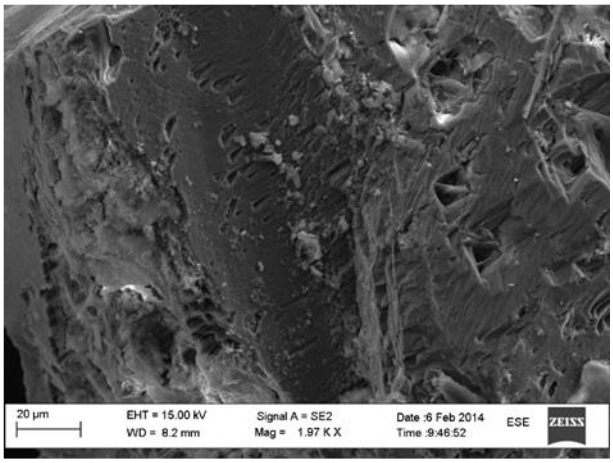
20 µm
EHT = 15.00 kV
WD = 8.2 mm
Signal A = SE2
Mag = 1.97 K X
Date :6 Feb 2014
Time :9:46:52
ESE
ZEISS

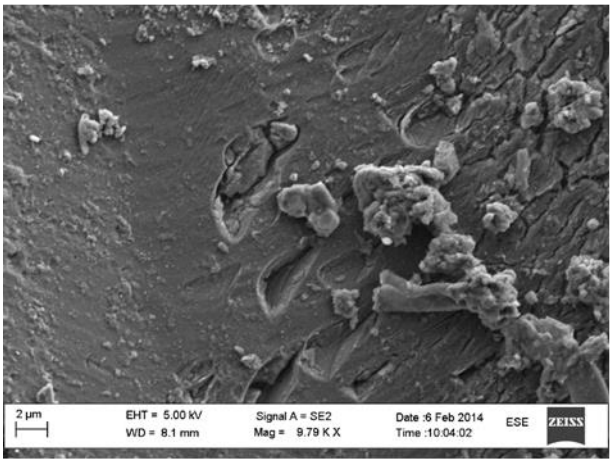
2 µm
EHT = 5.00 kV
WD = 8.1 mm
Signal A = SE2
Mag = 9.79 K X
Date :6 Feb 2014
Time :10:04:02
ESE
ZEISS

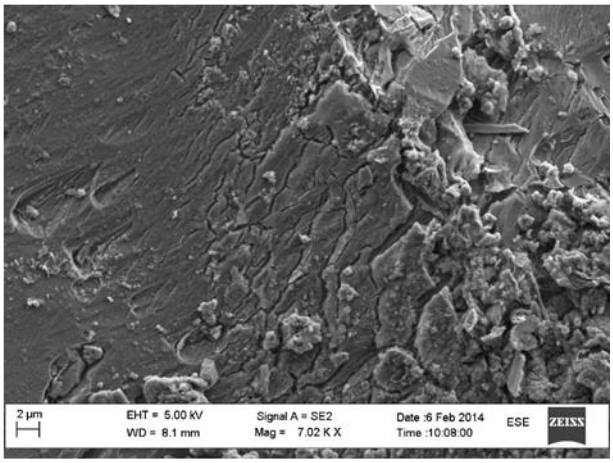
2 µm
EHT = 5.00 kV
WD = 8.1 mm
Signal A = SE2
Mag = 7.02 K X
Date :6 Feb 2014
Time :10:08:00
ESE
ZEISS

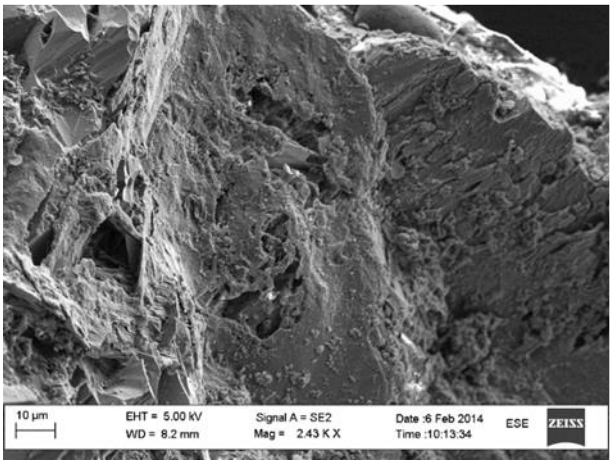
10 µm
EHT = 5.00 kV
WD = 8.2 mm
Signal A = SE2
Mag = 2.43 K X
Date :6 Feb 2014
Time :10:13:34
ESE
ZEISS

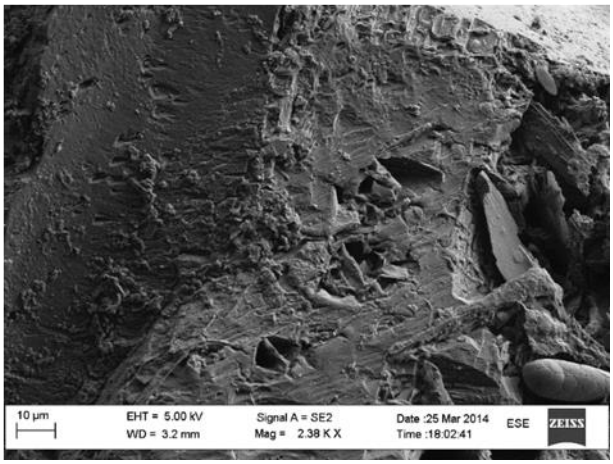
10 µm
EHT = 5.00 kV
WD = 3.2 mm
Signal A = SE2
Mag = 2.38 K X
Date :25 Mar 2014
Time :18:02:41
ESE
ZEISS

Olivine ID.4

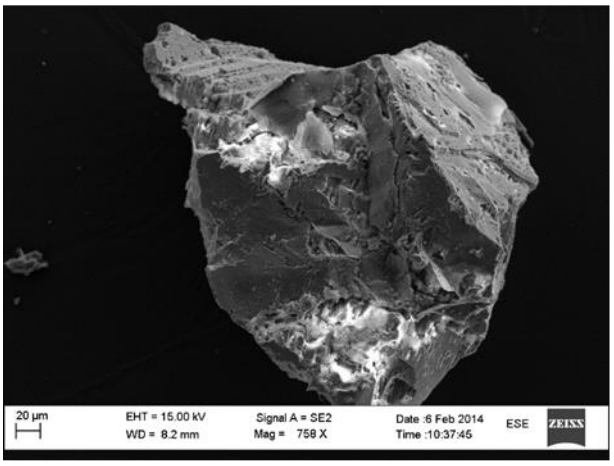
20 µm
EHT = 15.00 kV
WD = 8.2 mm
Signal A = SE2
Mag = 758 X
Date :6 Feb 2014
Time :10:37:45
ESE
ZEISS

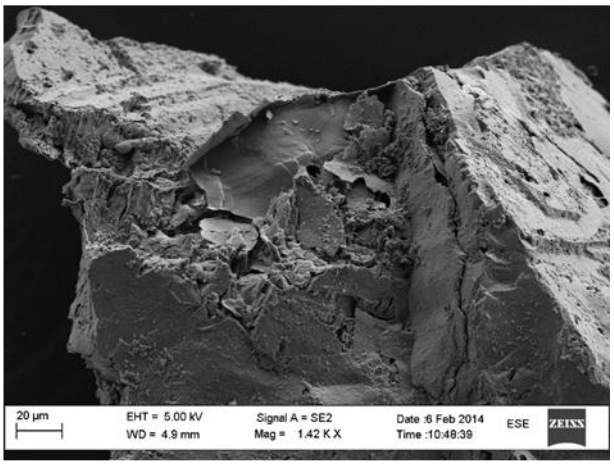
20 µm
EHT = 5.00 kV
WD = 4.9 mm
Signal A = SE2
Mag = 1.42 K X
Date :6 Feb 2014
Time :10:48:39
ESE
ZEISS

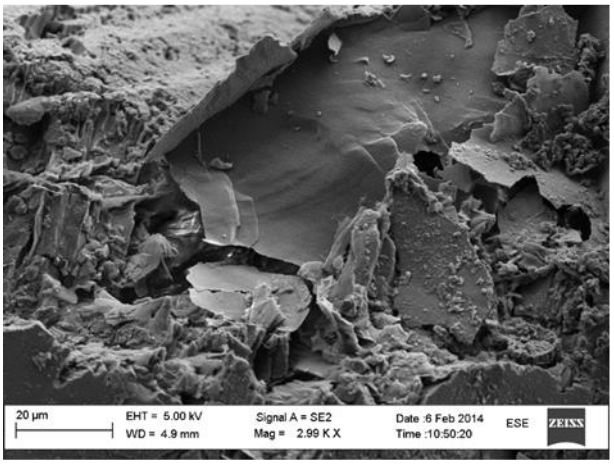
20 µm
EHT = 5.00 kV
WD = 4.9 mm
Signal A = SE2
Mag = 2.99 K X
Date :6 Feb 2014
Time :10:50:20
ESE
ZEISS

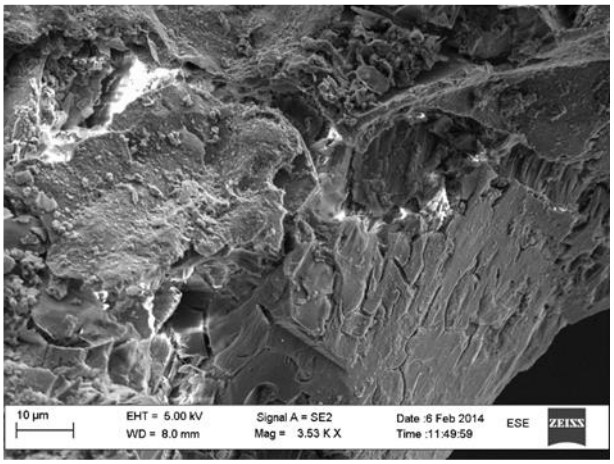
10 µm
EHT = 5.00 kV
WD = 8.0 mm
Signal A = SE2
Mag = 3.53 K X
Date :6 Feb 2014
Time :11:49:59
ESE
ZEISS

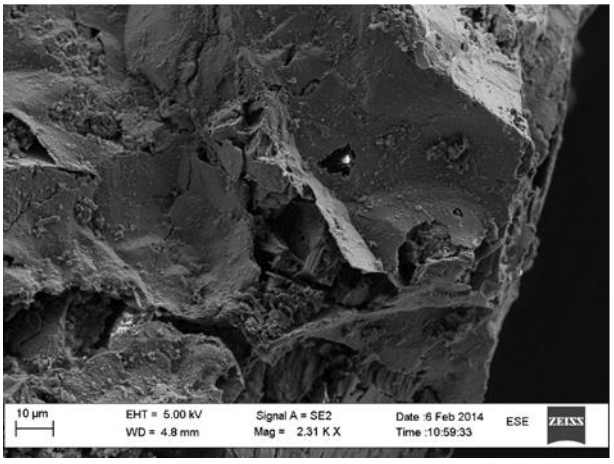
10 µm
EHT = 5.00 kV
WD = 4.8 mm
Signal A = SE2
Mag = 2.31 K X
Date :6 Feb 2014
Time :10:59:33
ESE
ZEISS

Olivine ID.5

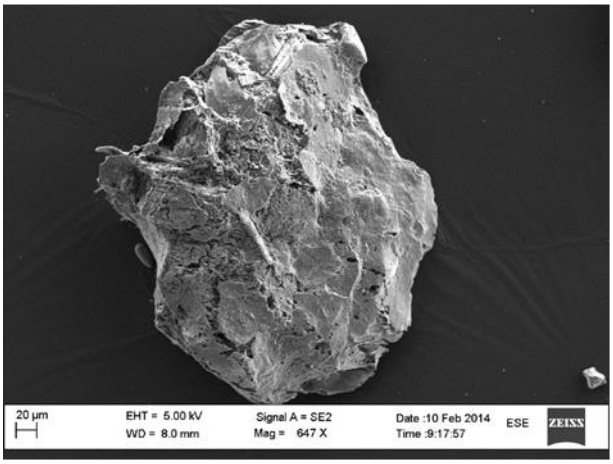
20 µm
EHT = 5.00 kV
WD = 8.0 mm
Signal A = SE2
Mag = 647 X
Date :10 Feb 2014
Time :9:17:57
ESE
ZEISS

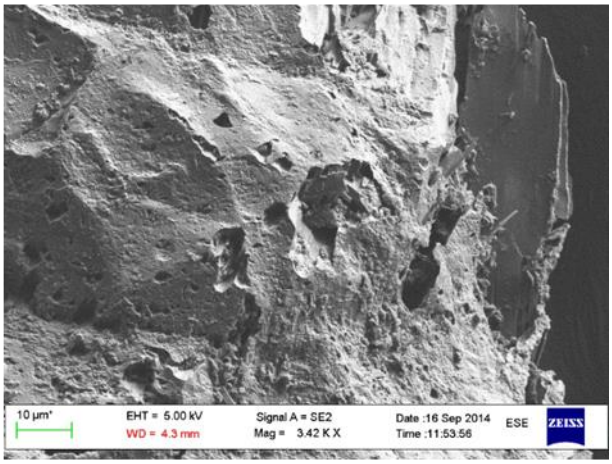
10 µm*
EHT = 5.00 kV
WD = 4.3 mm
Signal A = SE2
Mag = 3.42 K X
Date :16 Sep 2014
Time :11:53:56
ESE
ZEISS

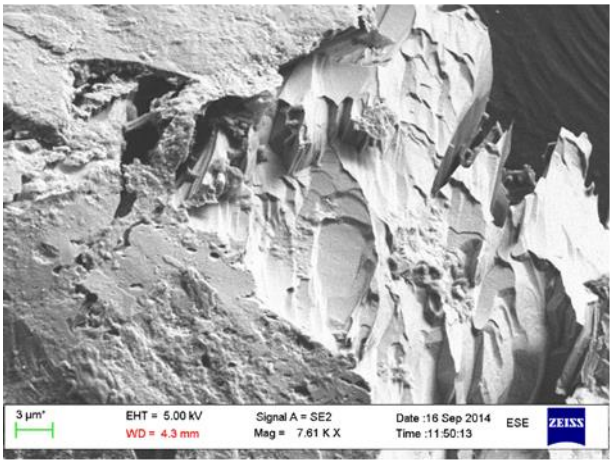
3 µm*
EHT = 5.00 kV
WD = 4.3 mm
Signal A = SE2
Mag = 7.61 K X
Date :16 Sep 2014
Time :11:50:13
ESE
ZEISS

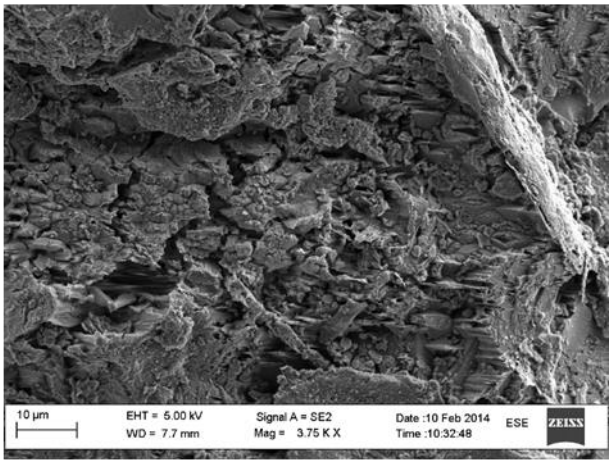
10 µm
EHT = 5.00 kV
WD = 7.7 mm
Signal A = SE2
Mag = 3.75 K X
Date :10 Feb 2014
Time :10:32:48
ESE
ZEISS

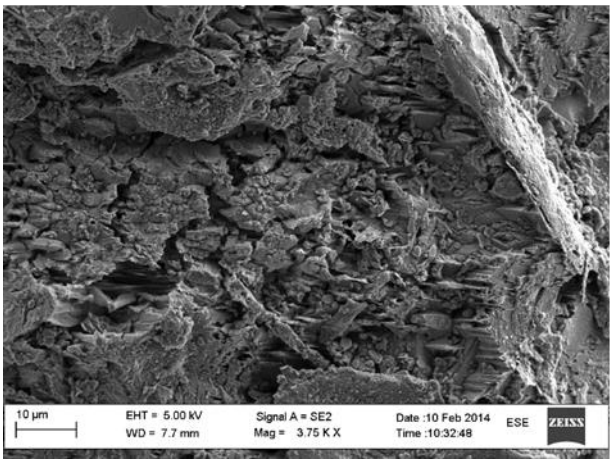
10 µm
EHT = 5.00 kV
WD = 7.7 mm
Signal A = SE2
Mag = 3.75 K X
Date :10 Feb 2014
Time :10:32:48
ESE
ZEISS

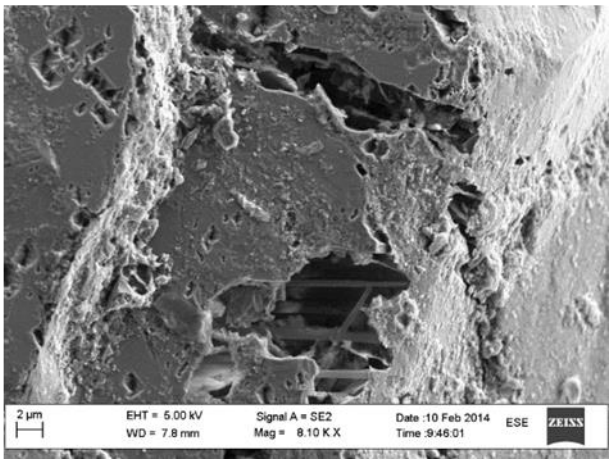
2 µm
EHT = 5.00 kV
WD = 7.8 mm
Signal A = SE2
Mag = 8.10 K X
Date :10 Feb 2014
Time :9:46:01
ESE
ZEISS

Olivine ID.6

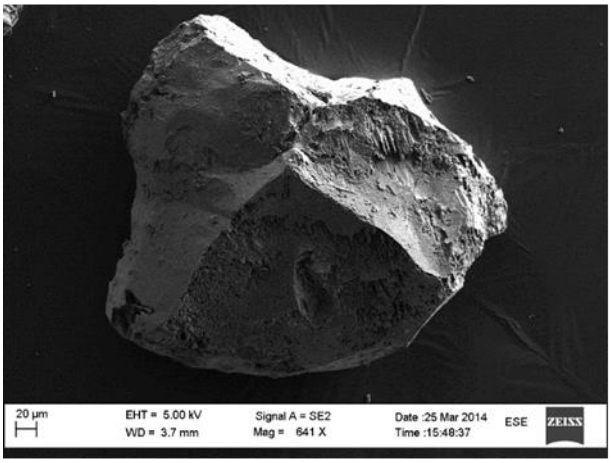
20 µm
EHT = 5.00 kV
WD = 3.7 mm
Signal A = SE2
Mag = 641 X
Date :25 Mar 2014
Time :15:48:37
ESE
ZEISS

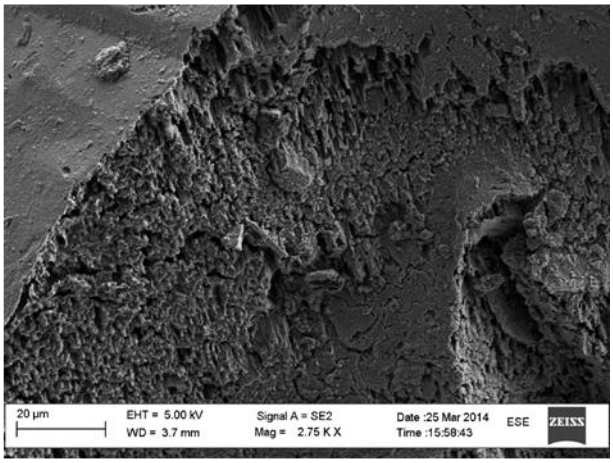
20 µm
EHT = 5.00 kV
WD = 3.7 mm
Signal A = SE2
Mag = 2.75 K X
Date :25 Mar 2014
Time :15:58:43
ESE
ZEISS

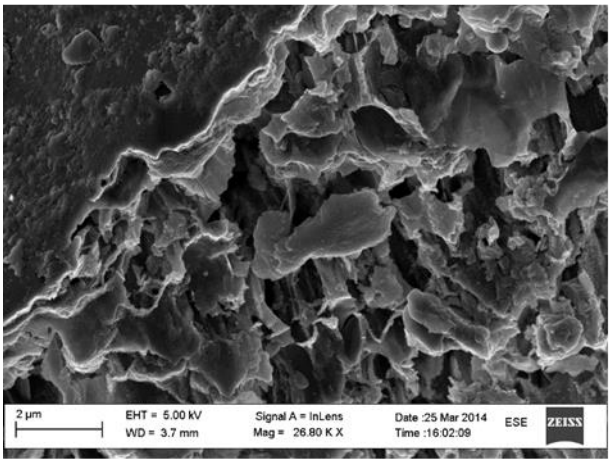
2 µm
EHT = 5.00 kV
WD = 3.7 mm
Signal A = InLens
Mag = 26.80 K X
Date :25 Mar 2014
Time :16:02:09
ESE
ZEISS

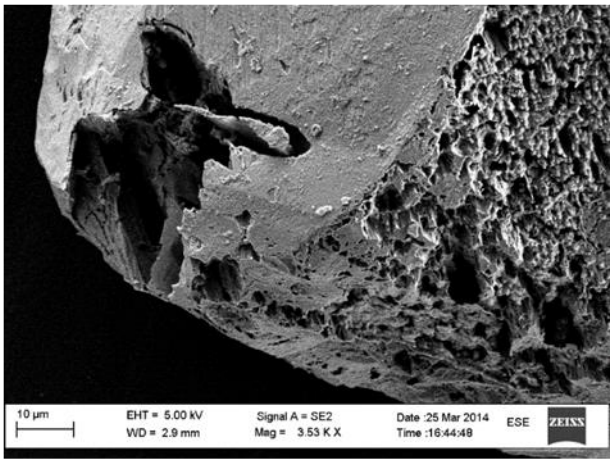
10 µm
EHT = 5.00 kV
WD = 2.9 mm
Signal A = SE2
Mag = 3.53 K X
Date :25 Mar 2014
Time :16:44:48
ESE
ZEISS

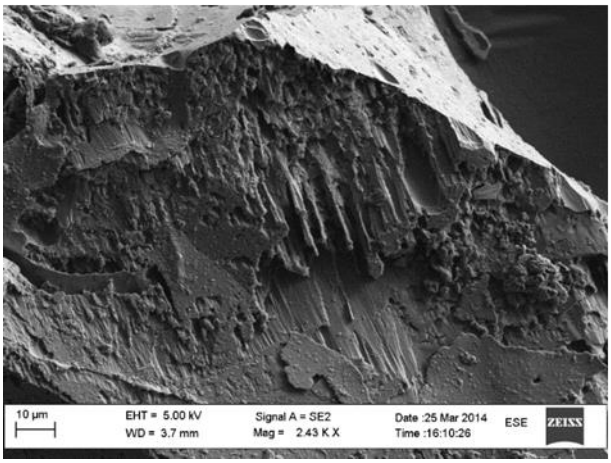
10 µm
EHT = 5.00 kV
WD = 3.7 mm
Signal A = SE2
Mag = 2.43 K X
Date :25 Mar 2014
Time :16:10:26
ESE
ZEISS

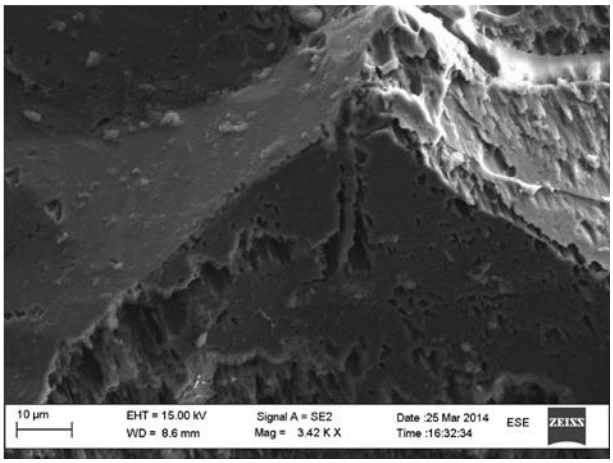
10 µm
EHT = 15.00 kV
WD = 8.6 mm
Signal A = SE2
Mag = 3.42 K X
Date :25 Mar 2014
Time :16:32:34
ESE
ZEISS

Olivine ID. 7

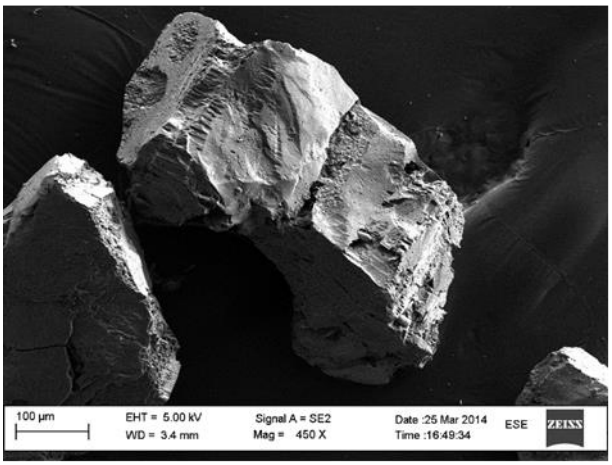
100 µm
EHT = 5.00 kV
WD = 3.4 mm
Signal A = SE2
Mag = 450 X
Date :25 Mar 2014
Time :16:49:34
ESE
ZEISS

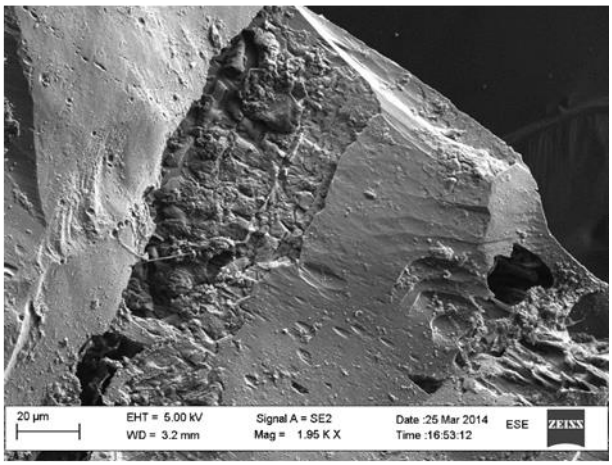
20 µm
EHT = 5.00 kV
WD = 3.2 mm
Signal A = SE2
Mag = 1.95 K X
Date :25 Mar 2014
Time :16:53:12
ESE
ZEISS

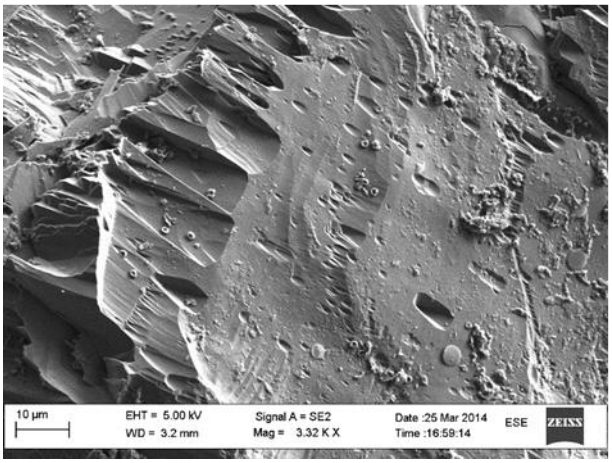
10 µm
EHT = 5.00 kV
WD = 3.2 mm
Signal A = SE2
Mag = 3.32 K X
Date :25 Mar 2014
Time :16:59:14
ESE
ZEISS

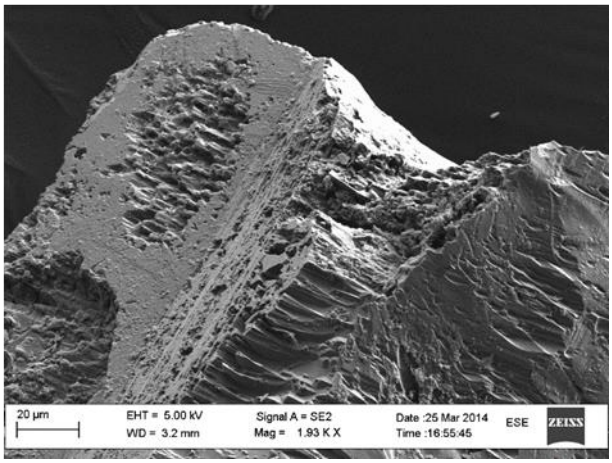
20 µm
EHT = 5.00 kV
WD = 3.2 mm
Signal A = SE2
Mag = 1.93 K X
Date :25 Mar 2014
Time :16:55:45
ESE
ZEISS

Olivine ID. 8

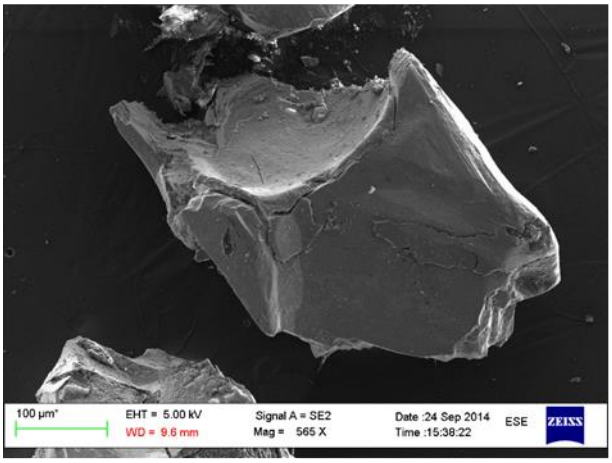
100 µm*
EHT = 5.00 kV
WD = 9.6 mm
Signal A = SE2
Mag = 565 X
Date :24 Sep 2014
Time :15:38:22
ESE
ZEISS

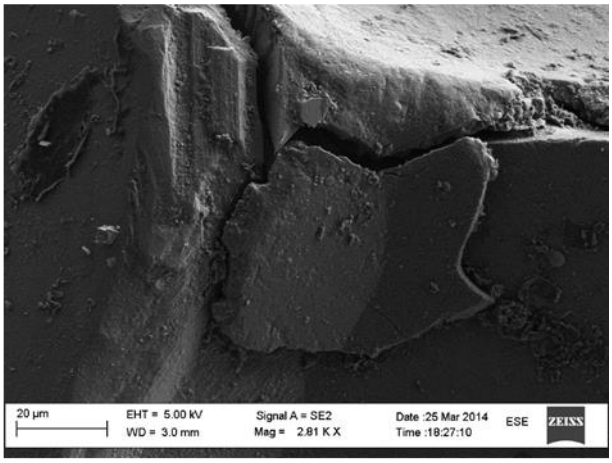
20 µm
EHT = 5.00 kV
WD = 3.0 mm
Signal A = SE2
Mag = 2.81 K X
Date :25 Mar 2014
Time :18:27:10
ESE
ZEISS

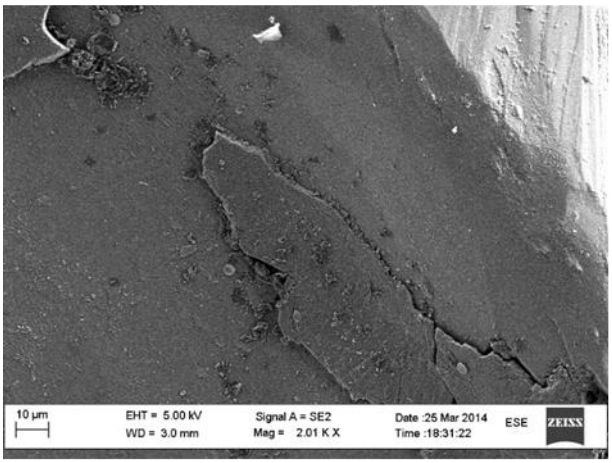
10 µm
EHT = 5.00 kV
WD = 3.0 mm
Signal A = SE2
Mag = 2.01 K X
Date :25 Mar 2014
Time :18:31:22
ESE
ZEISS

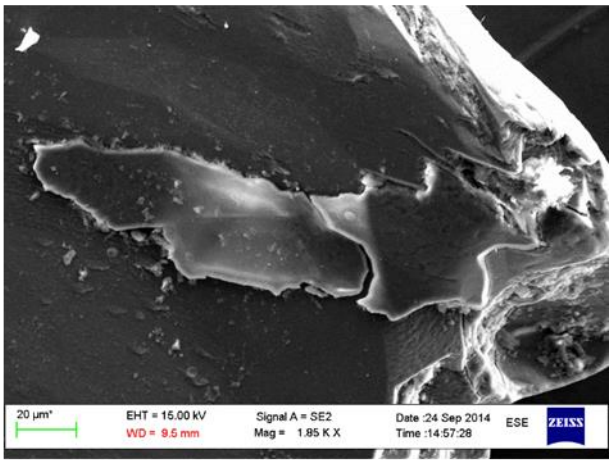
20 µm*
EHT = 15.00 kV
WD = 9.5 mm
Signal A = SE2
Mag = 1.95 K X
Date :24 Sep 2014
Time :14:57:28
ESE
ZEISS

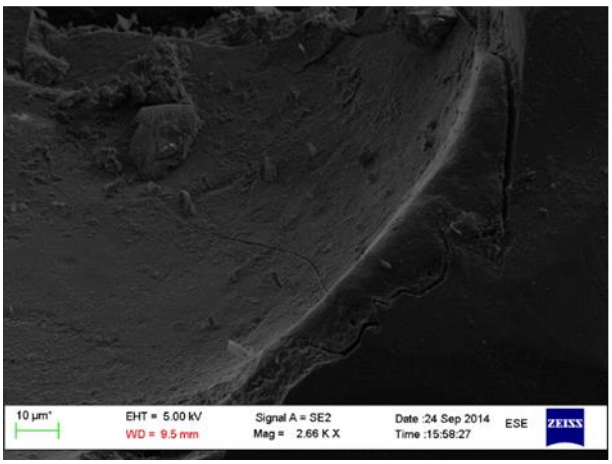
10 µm*
EHT = 5.00 kV
WD = 9.5 mm
Signal A = SE2
Mag = 2.66 K X
Date :24 Sep 2014
Time :15:58:27
ESE
ZEISS

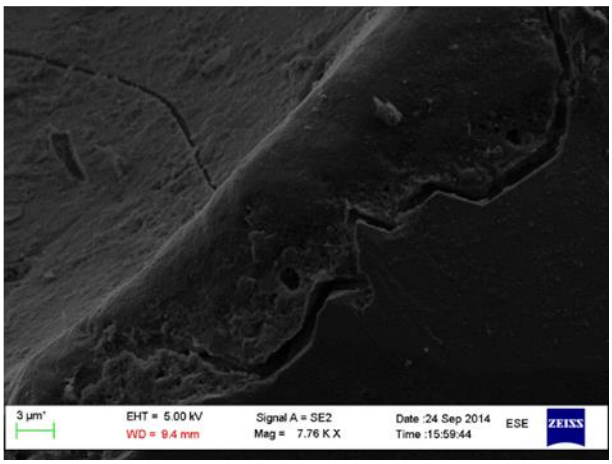
3 µm*
EHT = 5.00 kV
WD = 9.4 mm
Signal A = SE2
Mag = 7.76 K X
Date :24 Sep 2014
Time :15:59:44
ESE
ZEISS

Olivine ID. 9

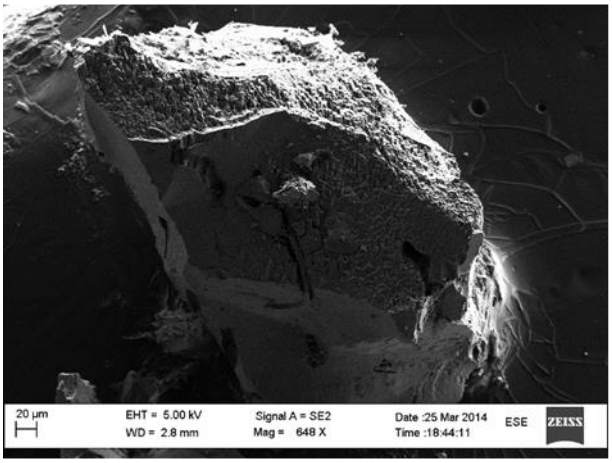
20 µm
EHT = 5.00 kV
WD = 2.8 mm
Signal A = SE2
Mag = 648 X
Date :25 Mar 2014
Time :18:44:11
ESE
ZEISS

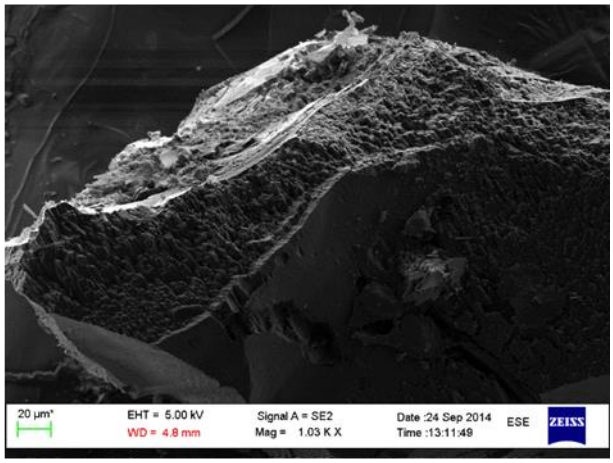
20 µm
EHT = 5.00 kV
WD = 4.8 mm
Signal A = SE2
Mag = 1.03 K X
Date :24 Sep 2014
Time :13:11:49
ESE
ZEISS

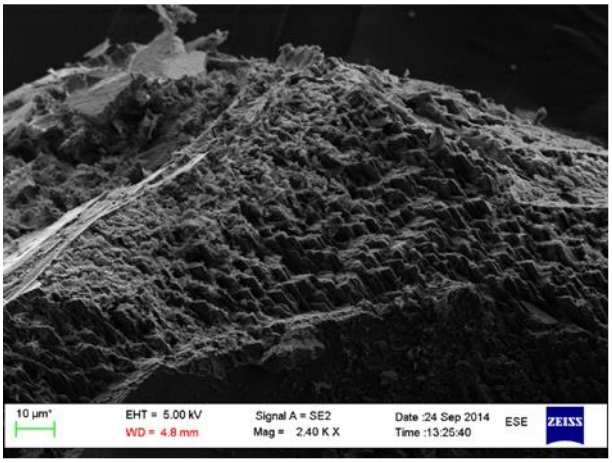
10 µm
EHT = 5.00 kV
WD = 4.8 mm
Signal A = SE2
Mag = 2.40 K X
Date :24 Sep 2014
Time :13:25:40
ESE
ZEISS

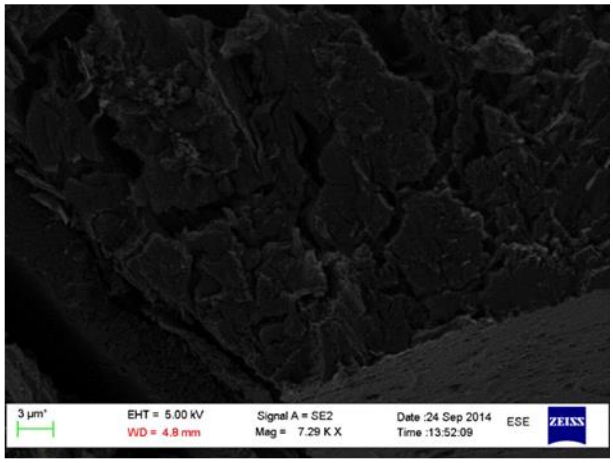
3 µm
EHT = 5.00 kV
WD = 4.8 mm
Signal A = SE2
Mag = 7.29 K X
Date :24 Sep 2014
Time :13:52:09
ESE
ZEISS

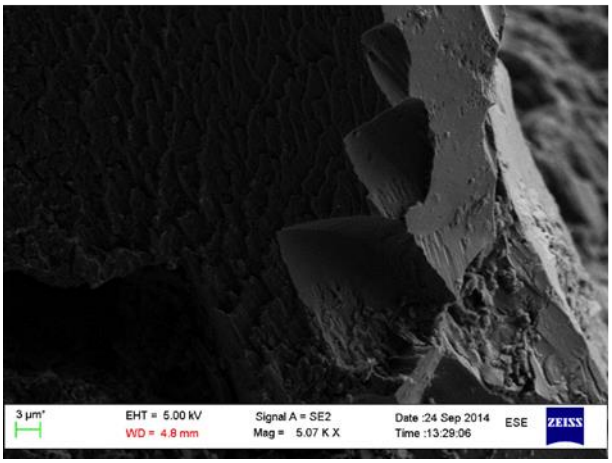
3 µm
EHT = 5.00 kV
WD = 4.8 mm
Signal A = SE2
Mag = 5.07 K X
Date :24 Sep 2014
Time :13:29:06
ESE
ZEISS

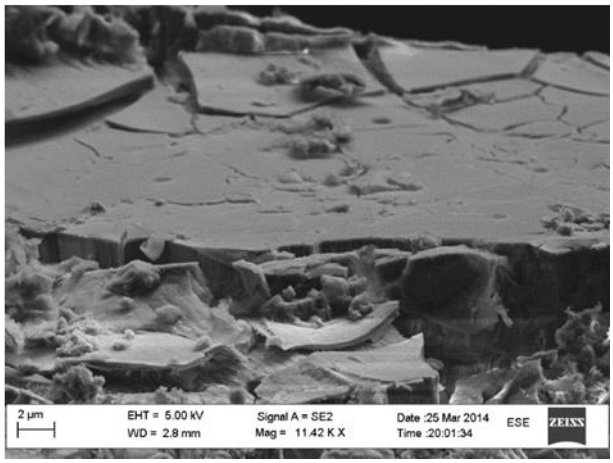
2 µm
EHT = 5.00 kV
WD = 2.8 mm
Signal A = SE2
Mag = 11.42 K X
Date :25 Mar 2014
Time :20:01:34
ESE
ZEISS

Olivine ID. 10

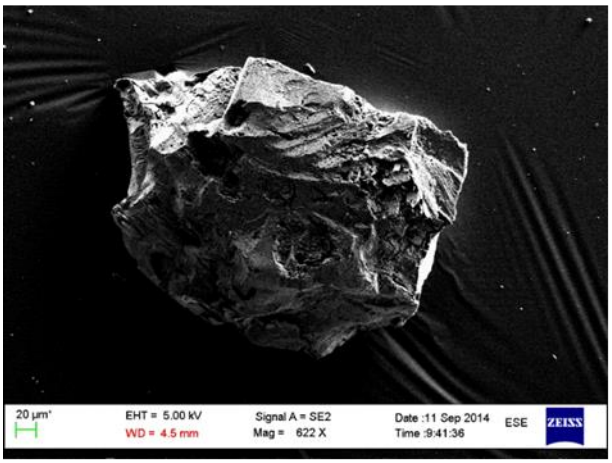

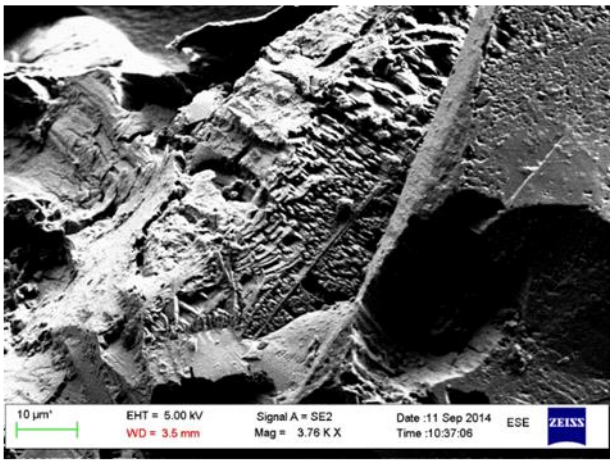

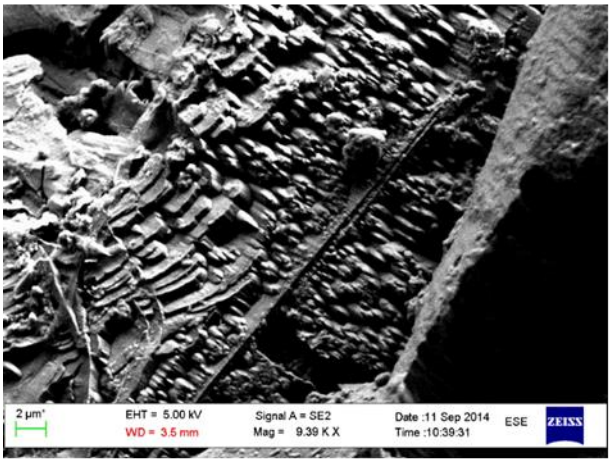

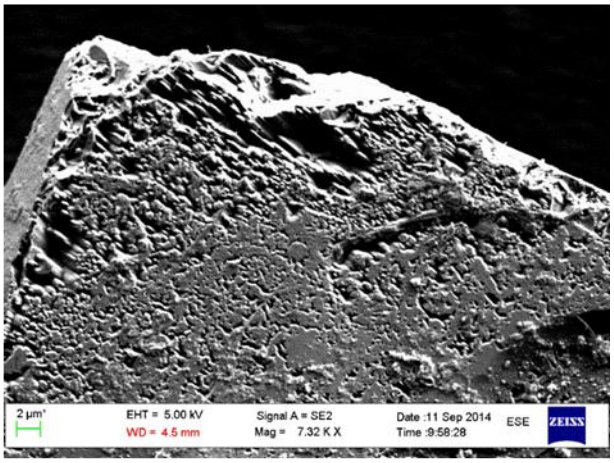

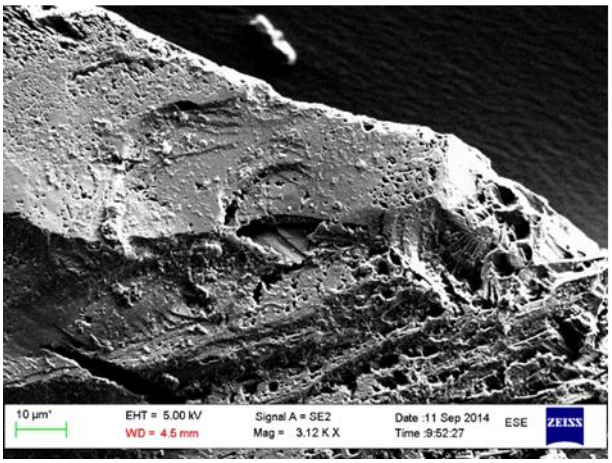

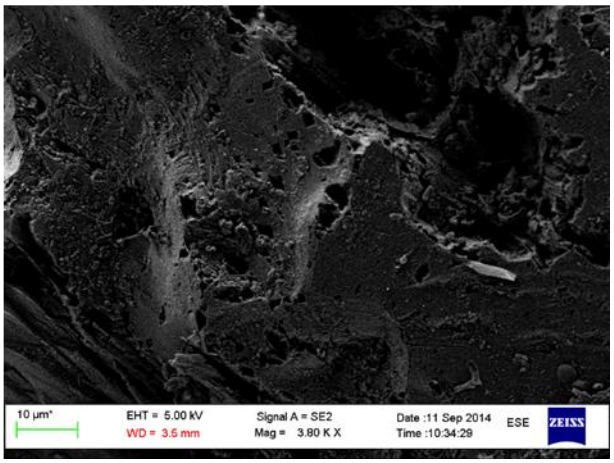

Olivine ID. 11

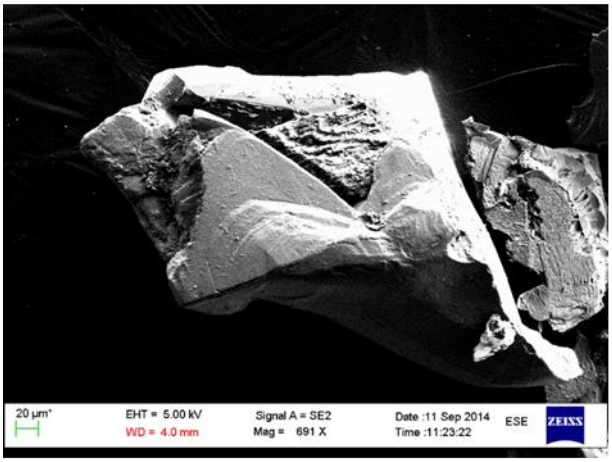

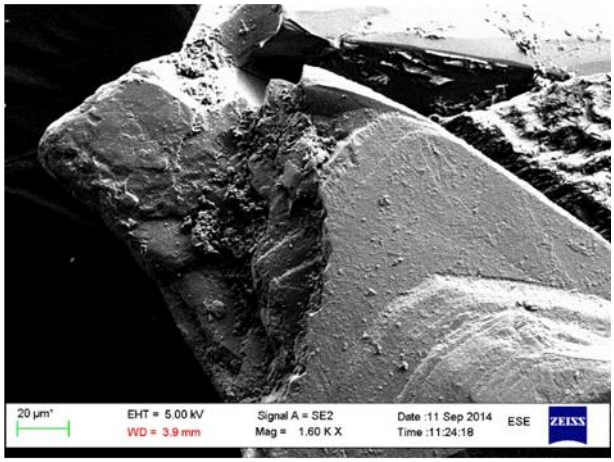

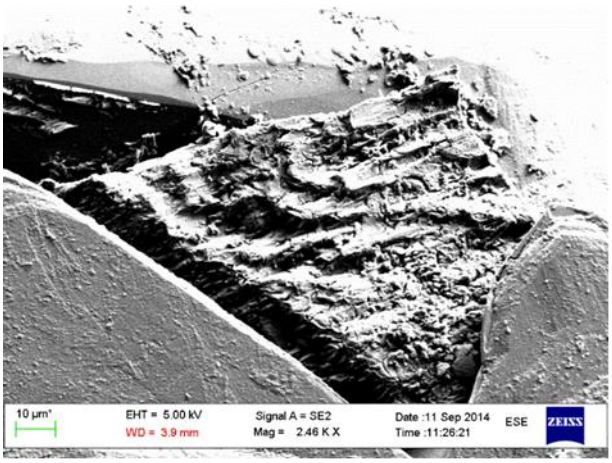

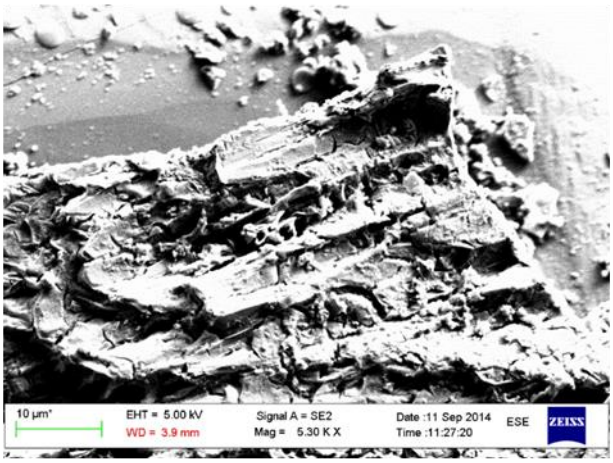

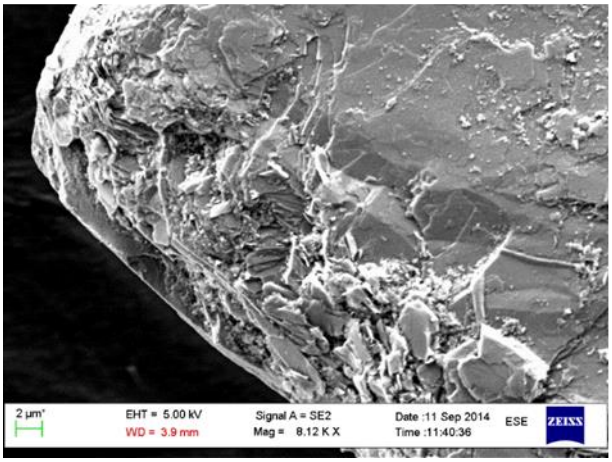

Olivine ID. 12

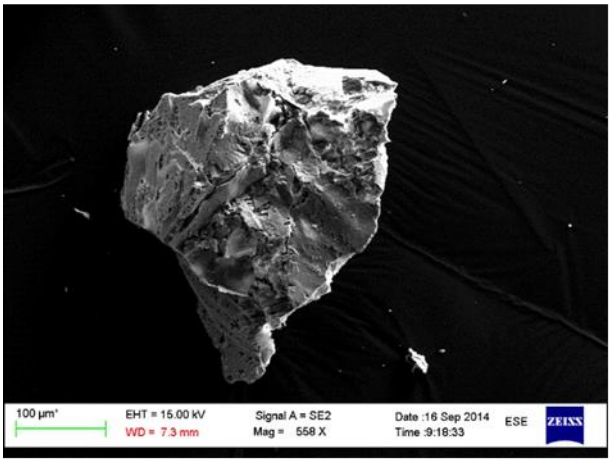

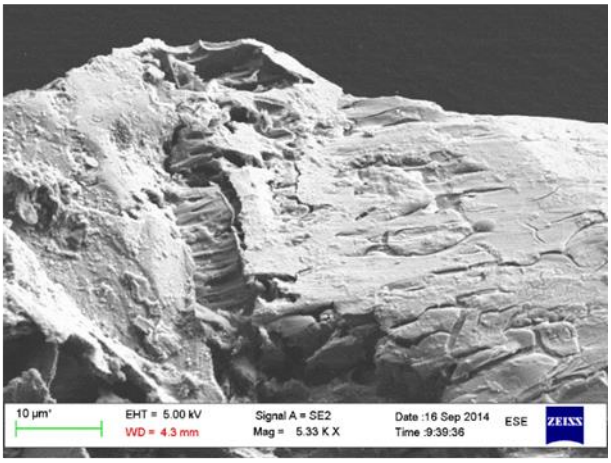

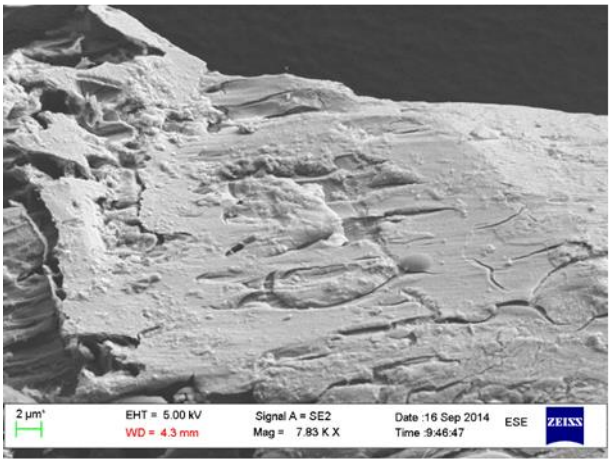

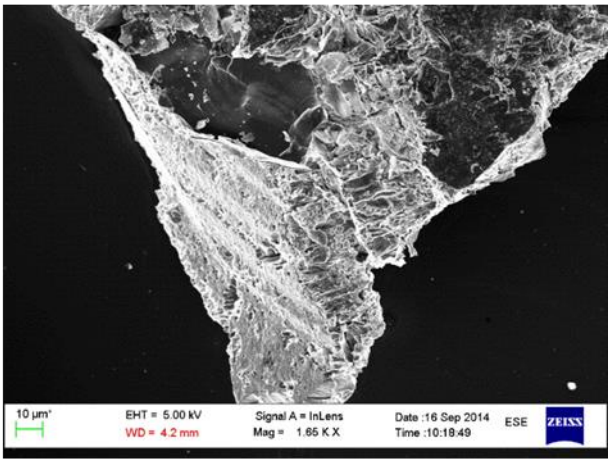

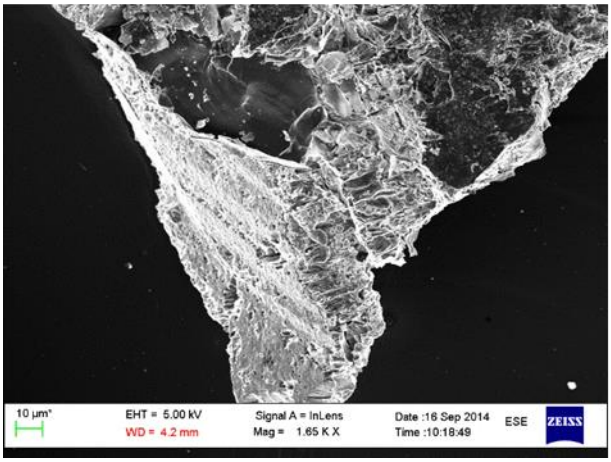

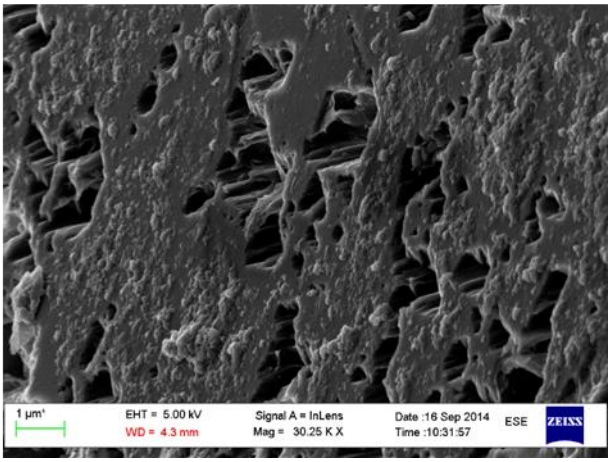

Olivine ID. 13

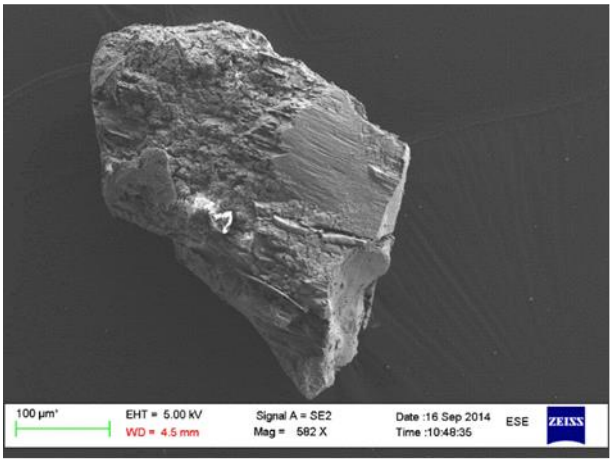

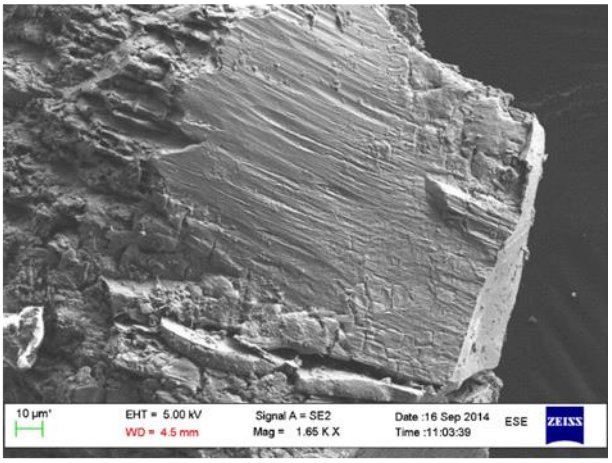

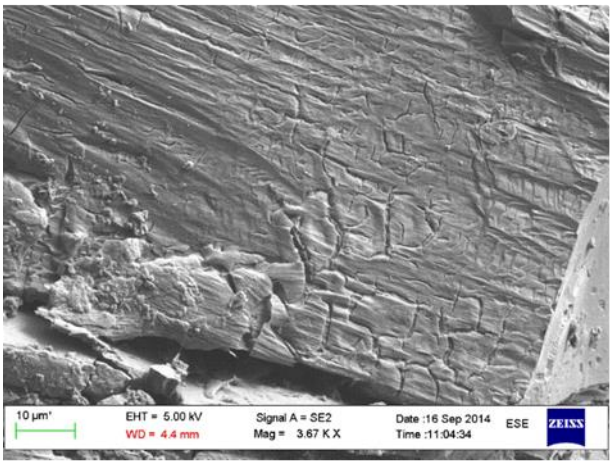

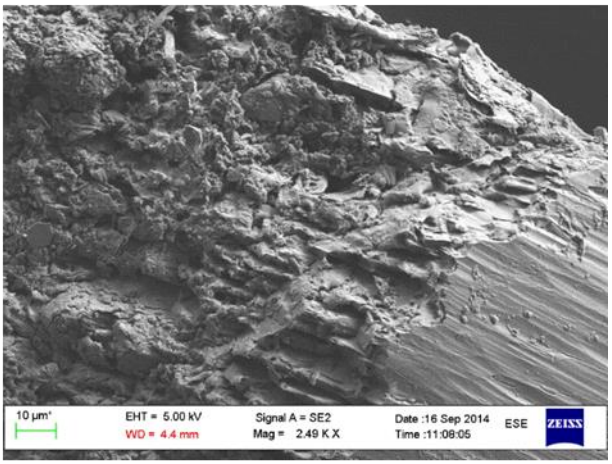

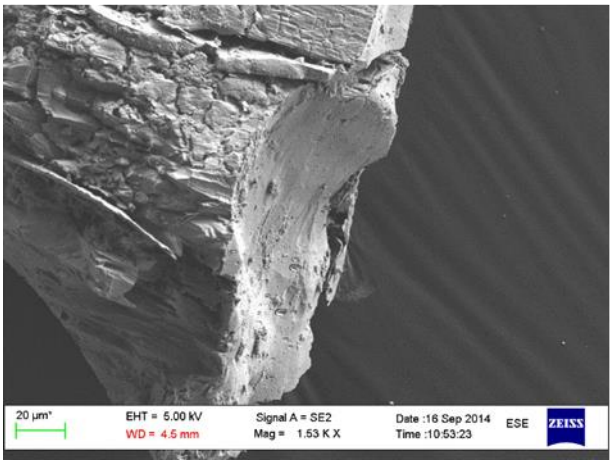

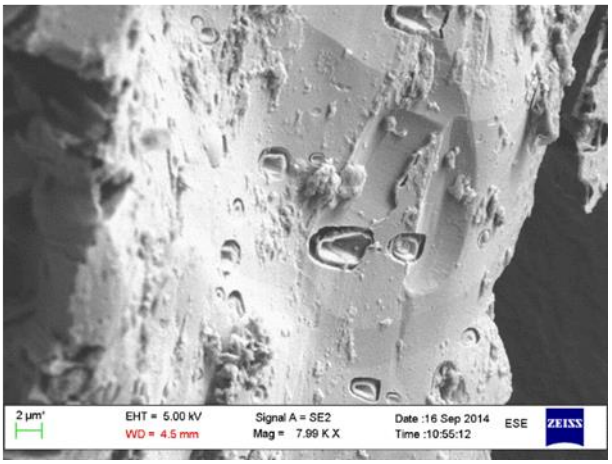

Olivine ID. 14

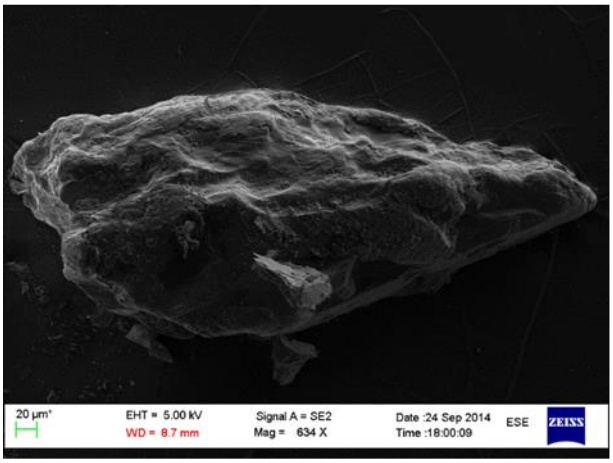

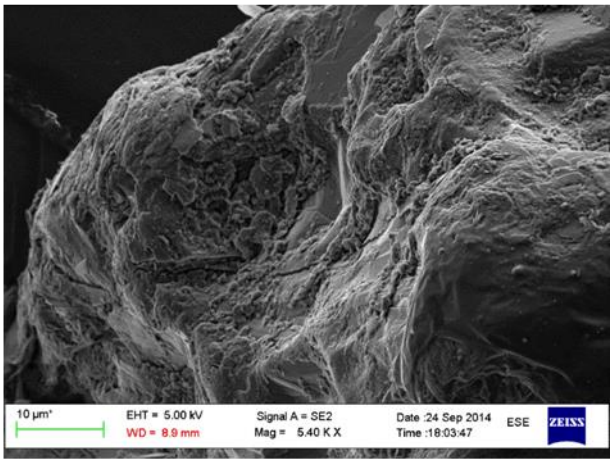

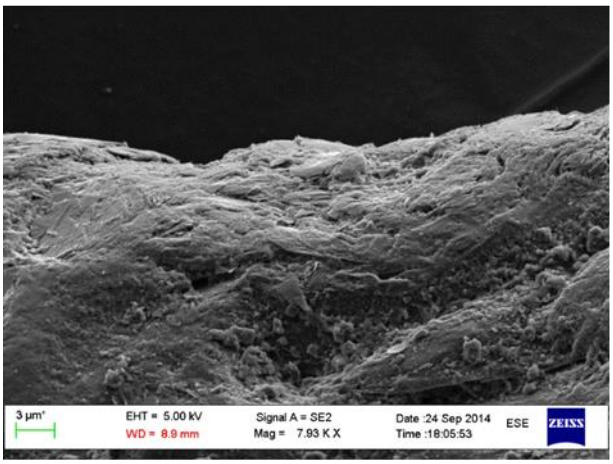

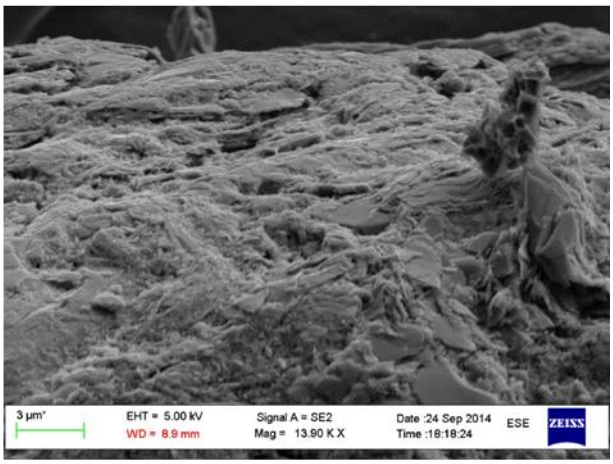

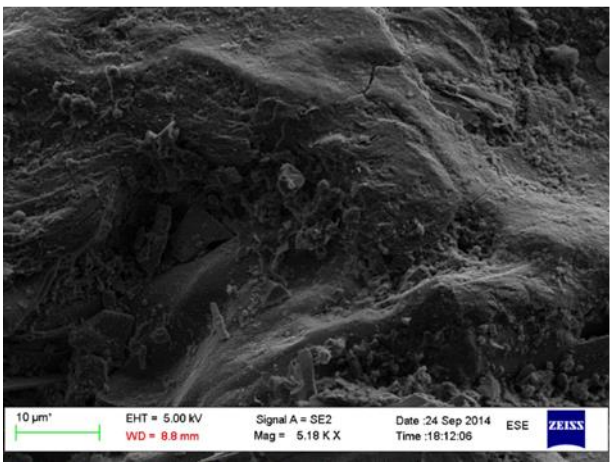

Olivine ID. 15

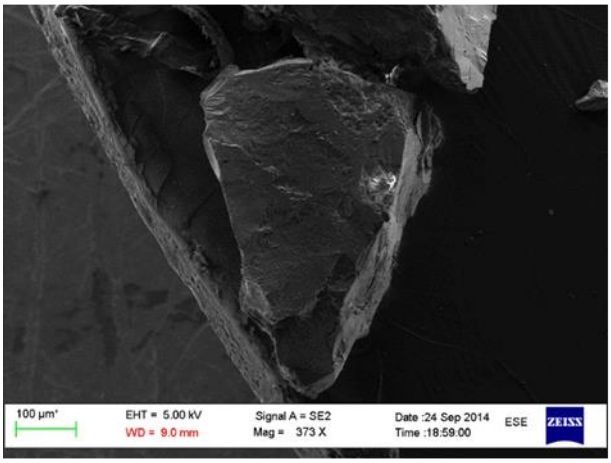

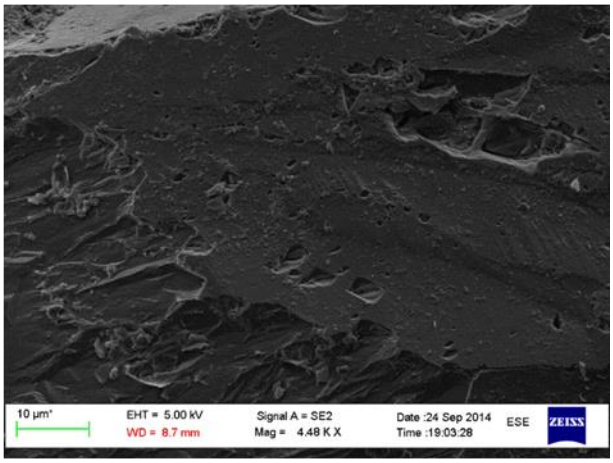

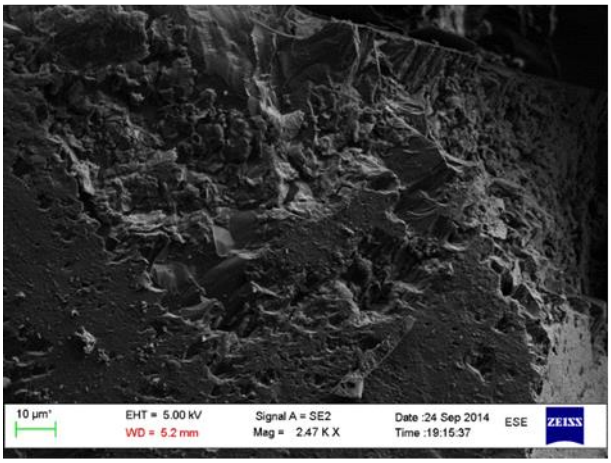

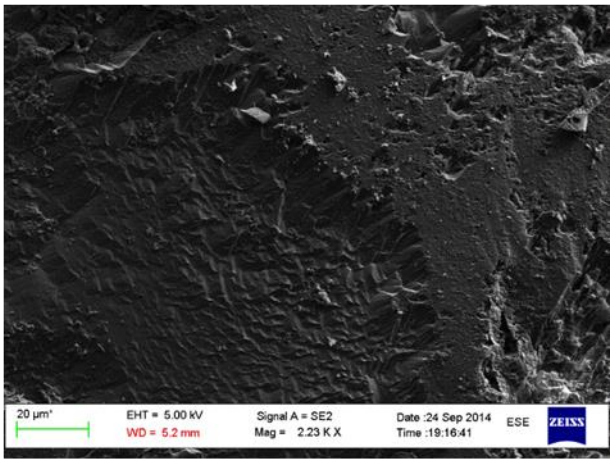

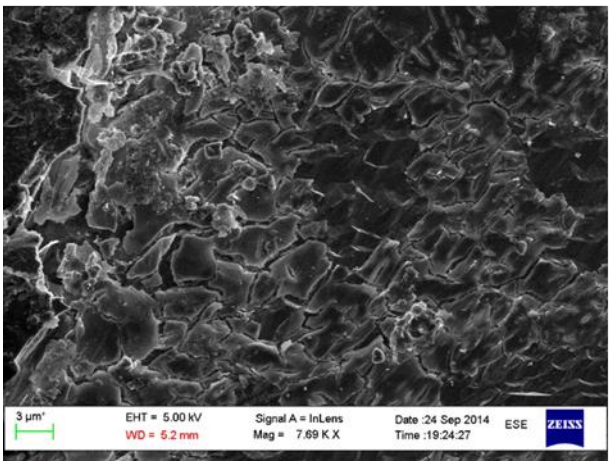

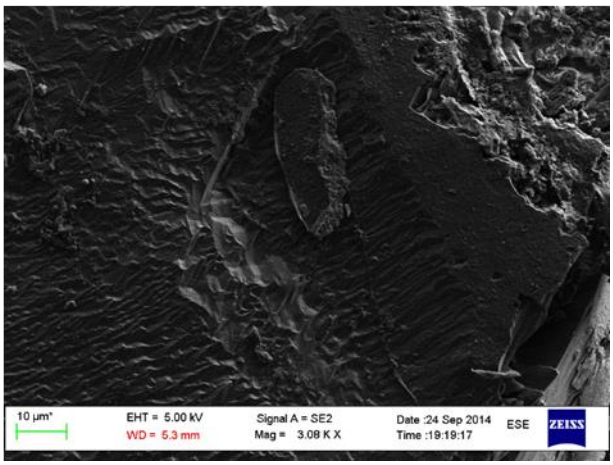

Olivine ID. 16

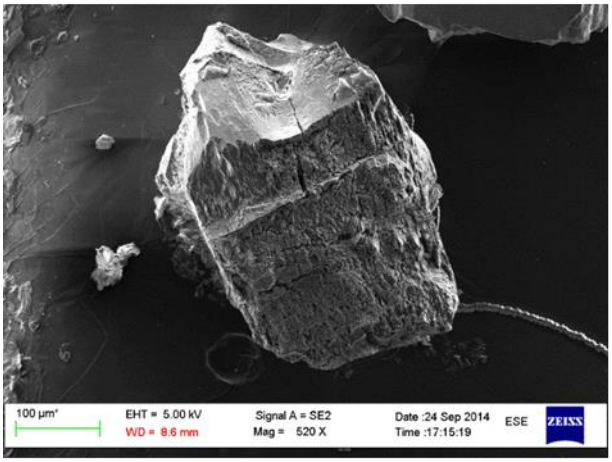

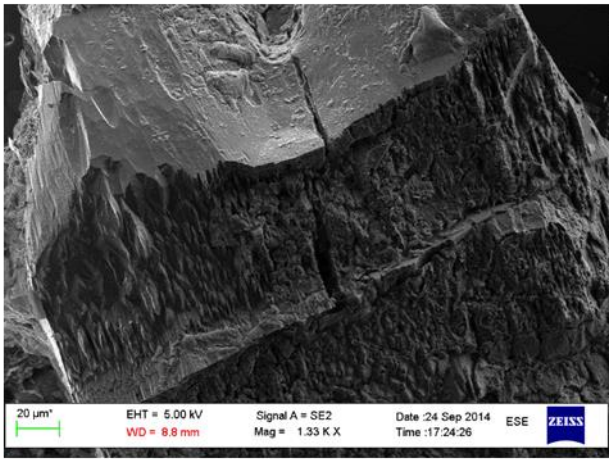

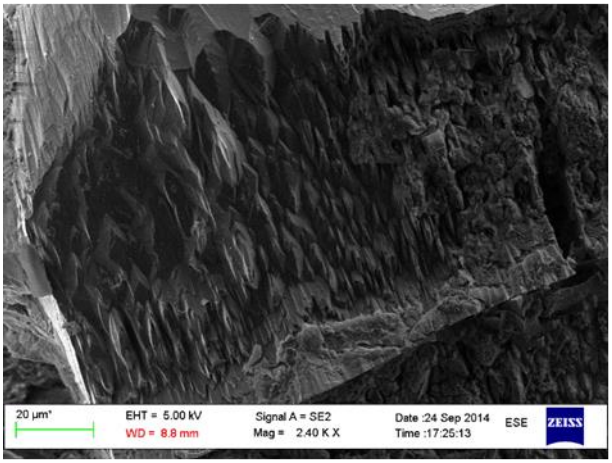

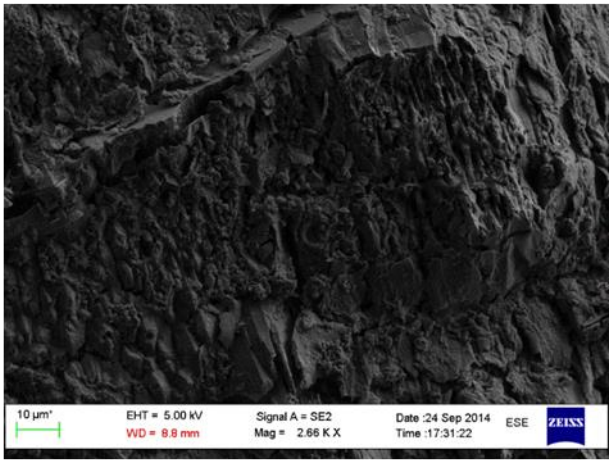

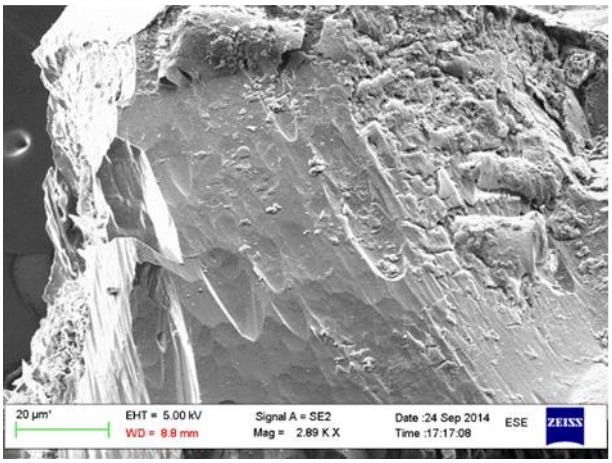

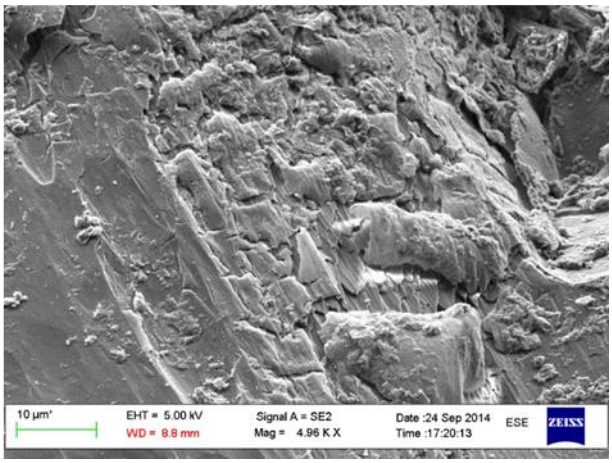

Olivine ID. 17

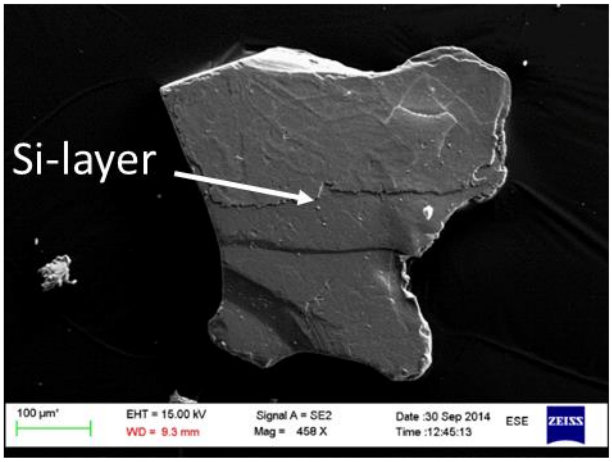

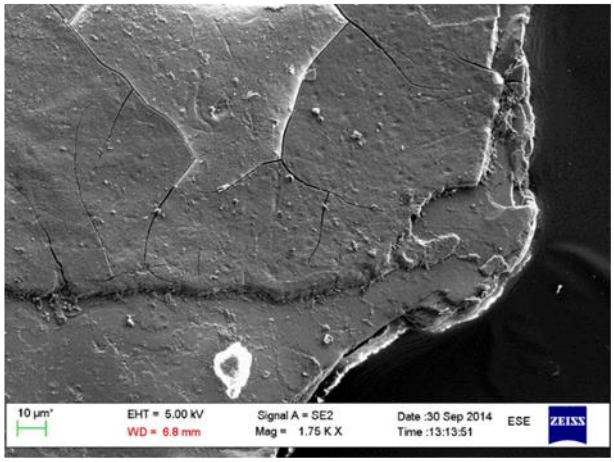

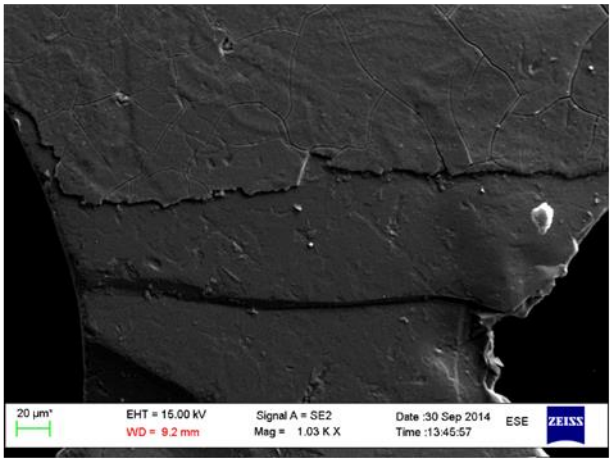

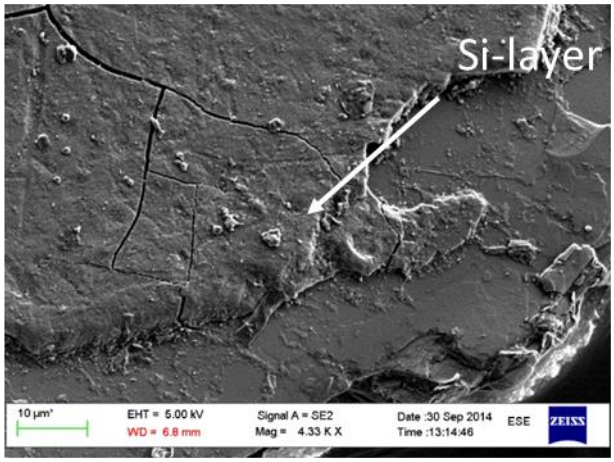

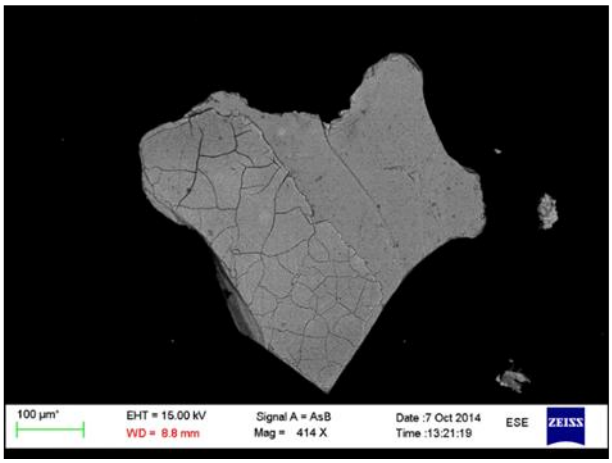

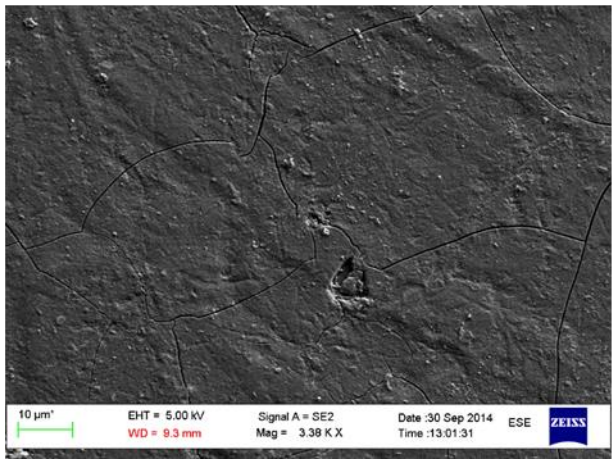

Olivine ID. 18

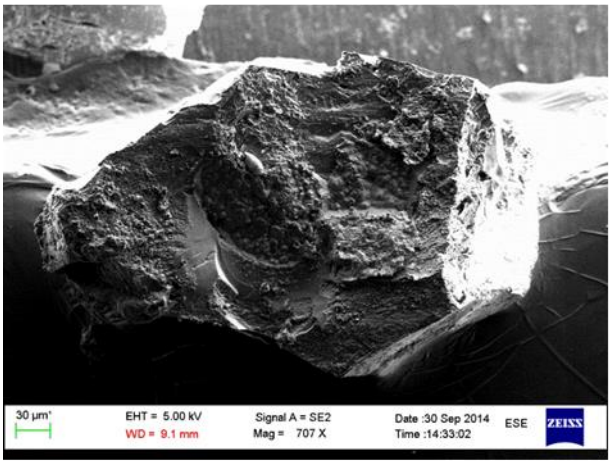

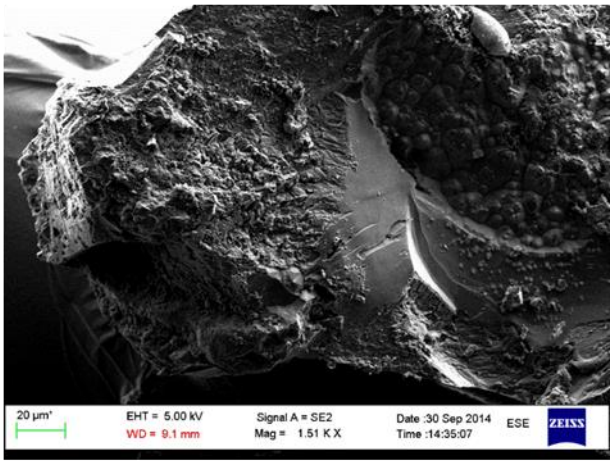

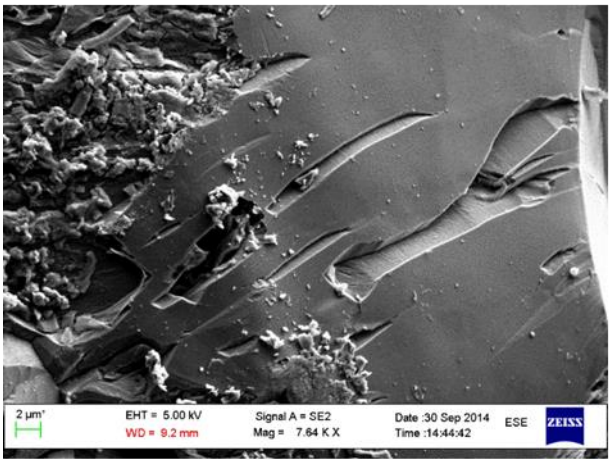

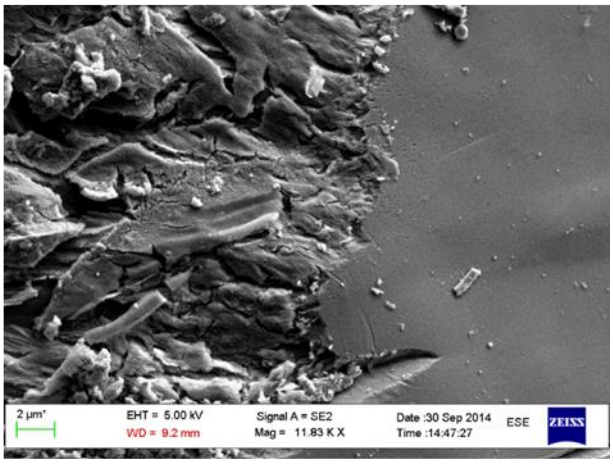

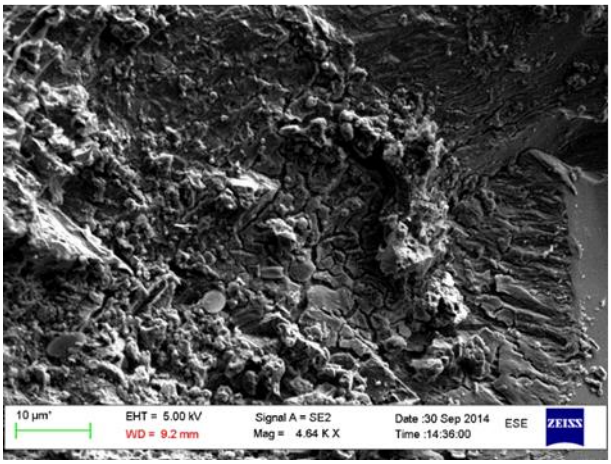

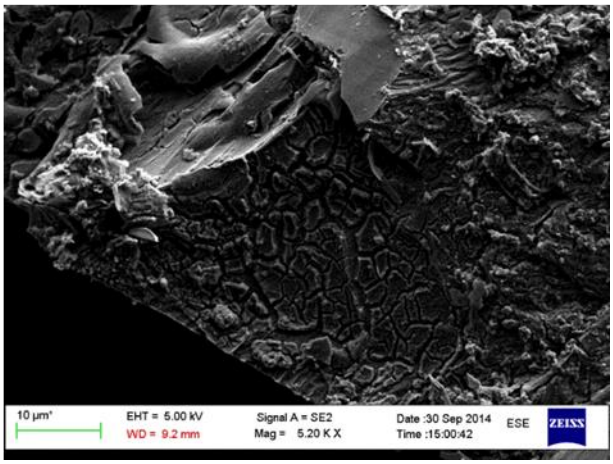

Olivine ID. 19

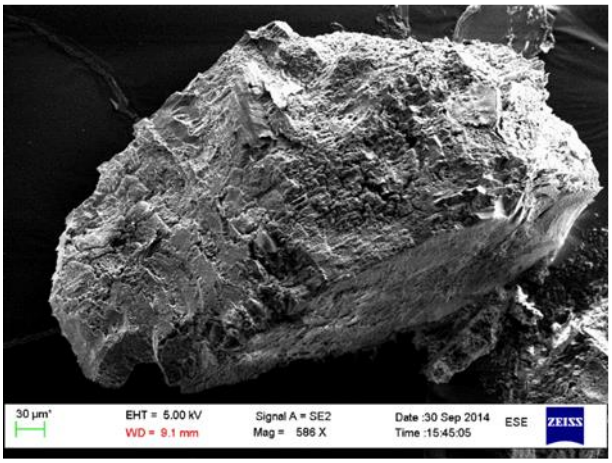

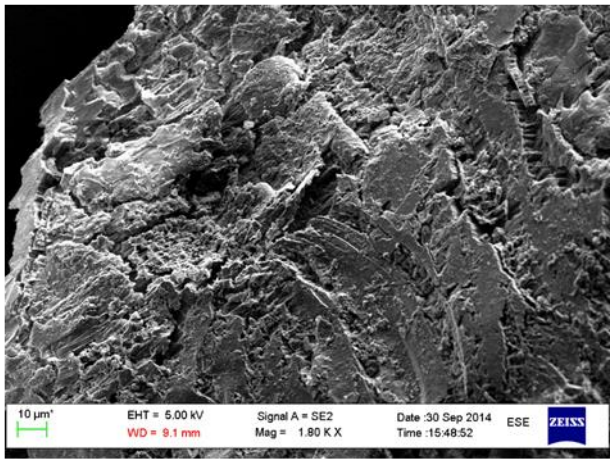

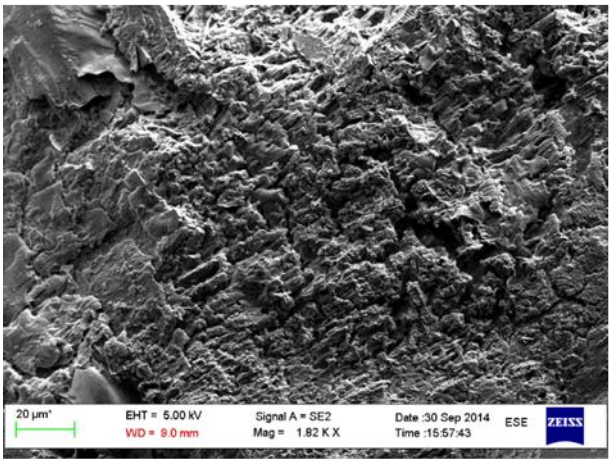

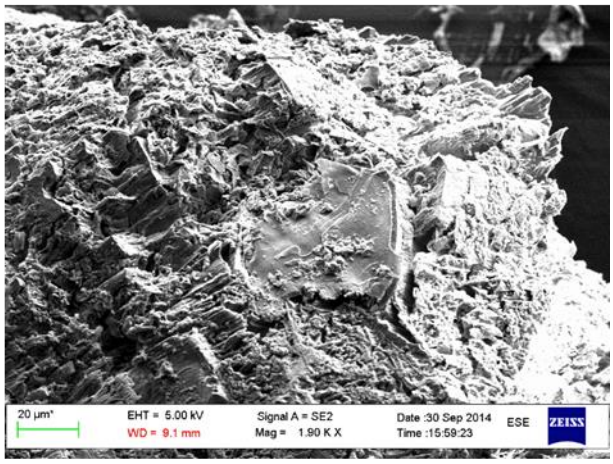

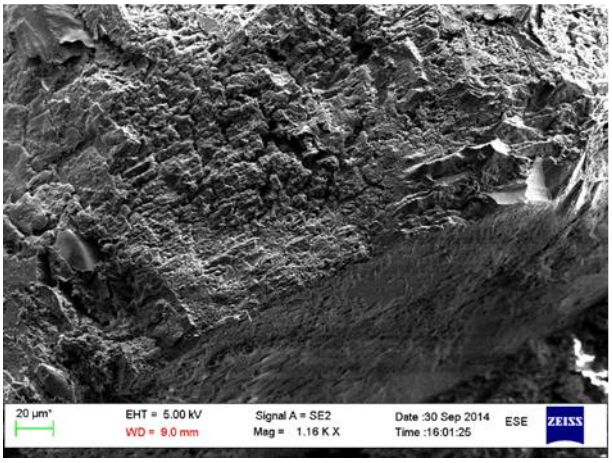

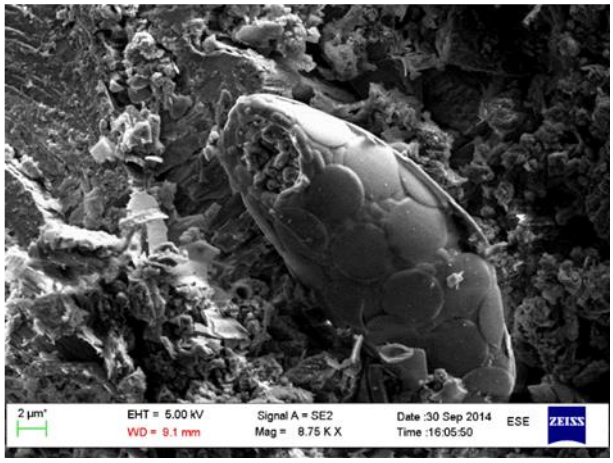

Olivine ID. 20

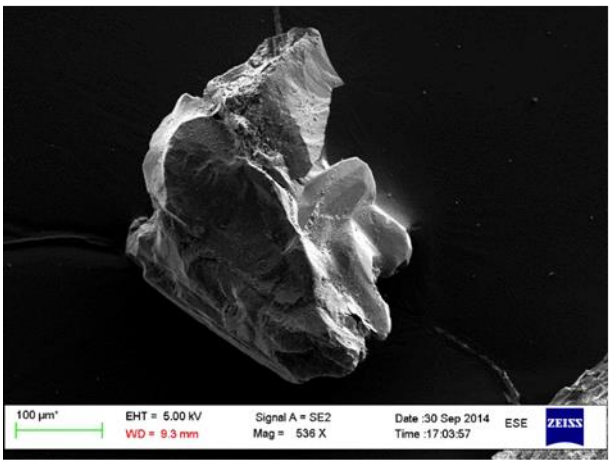

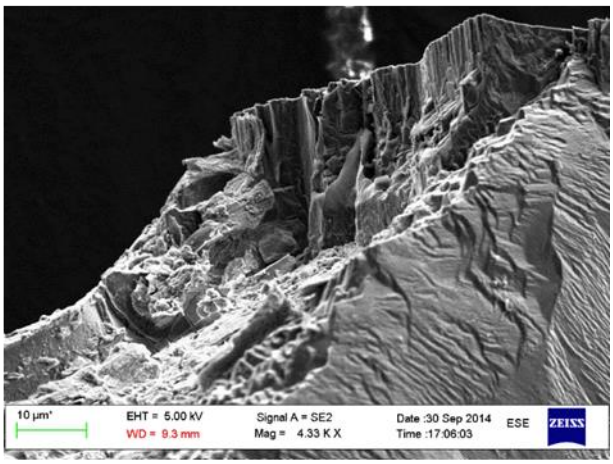

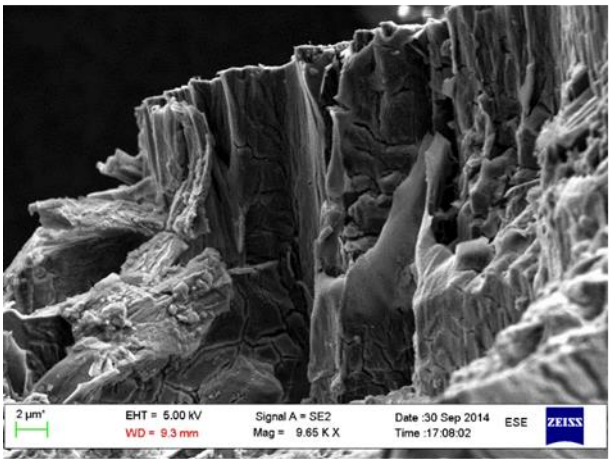

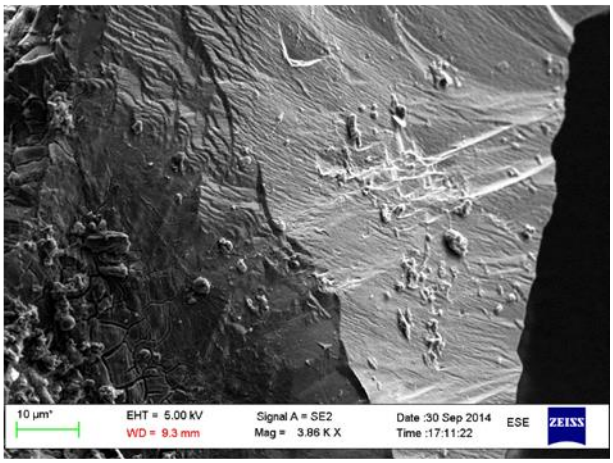

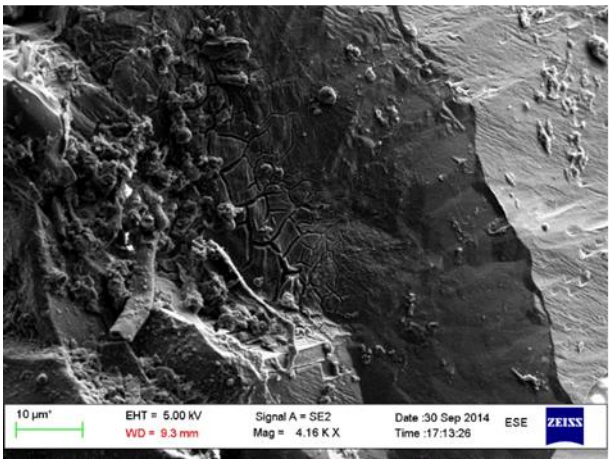

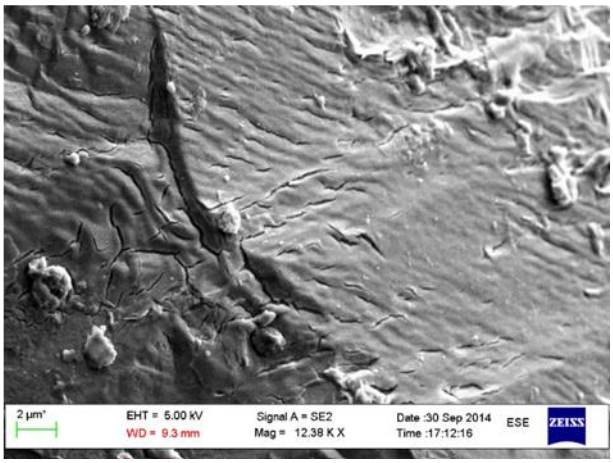

Olivine ID. 21

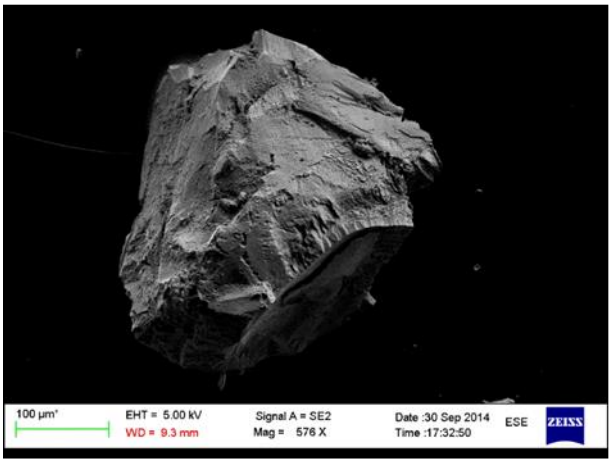

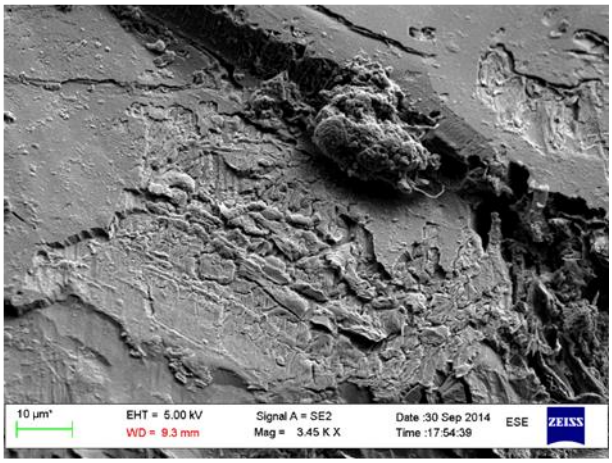

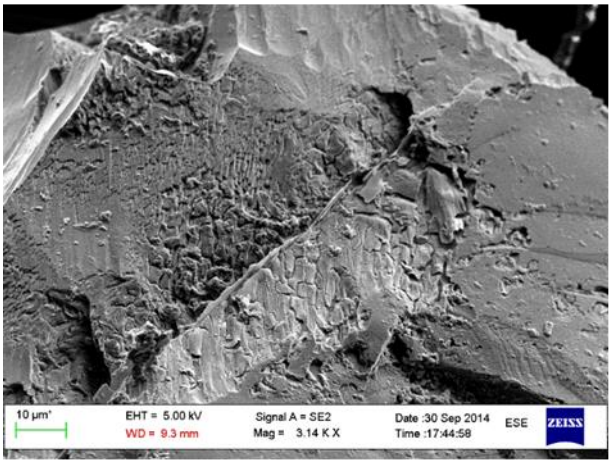

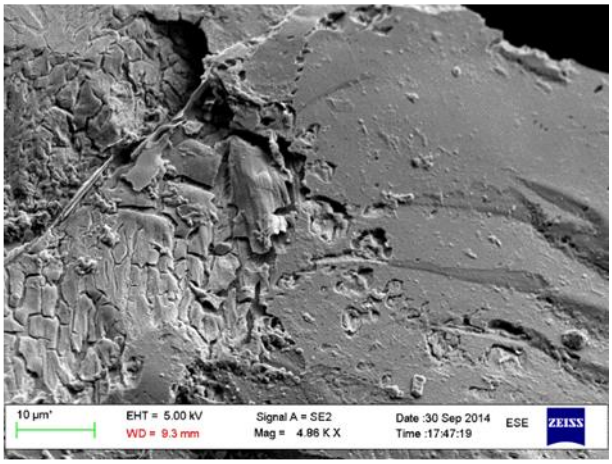

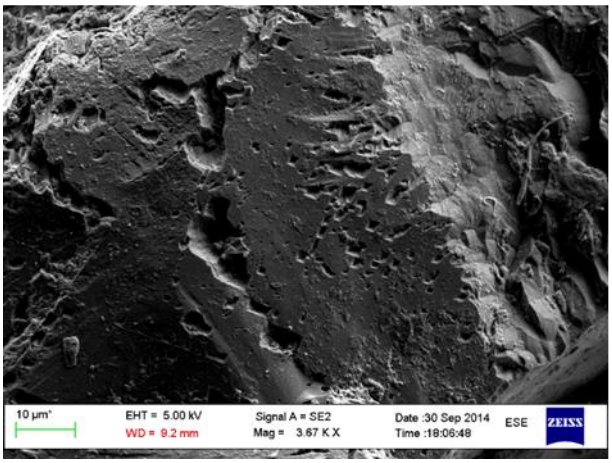

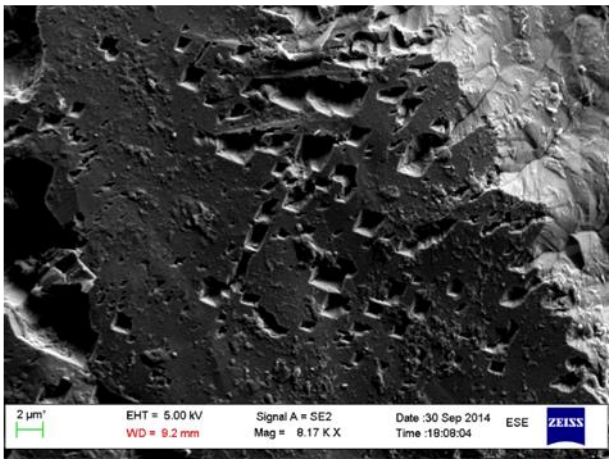

Anorthosite ID.1

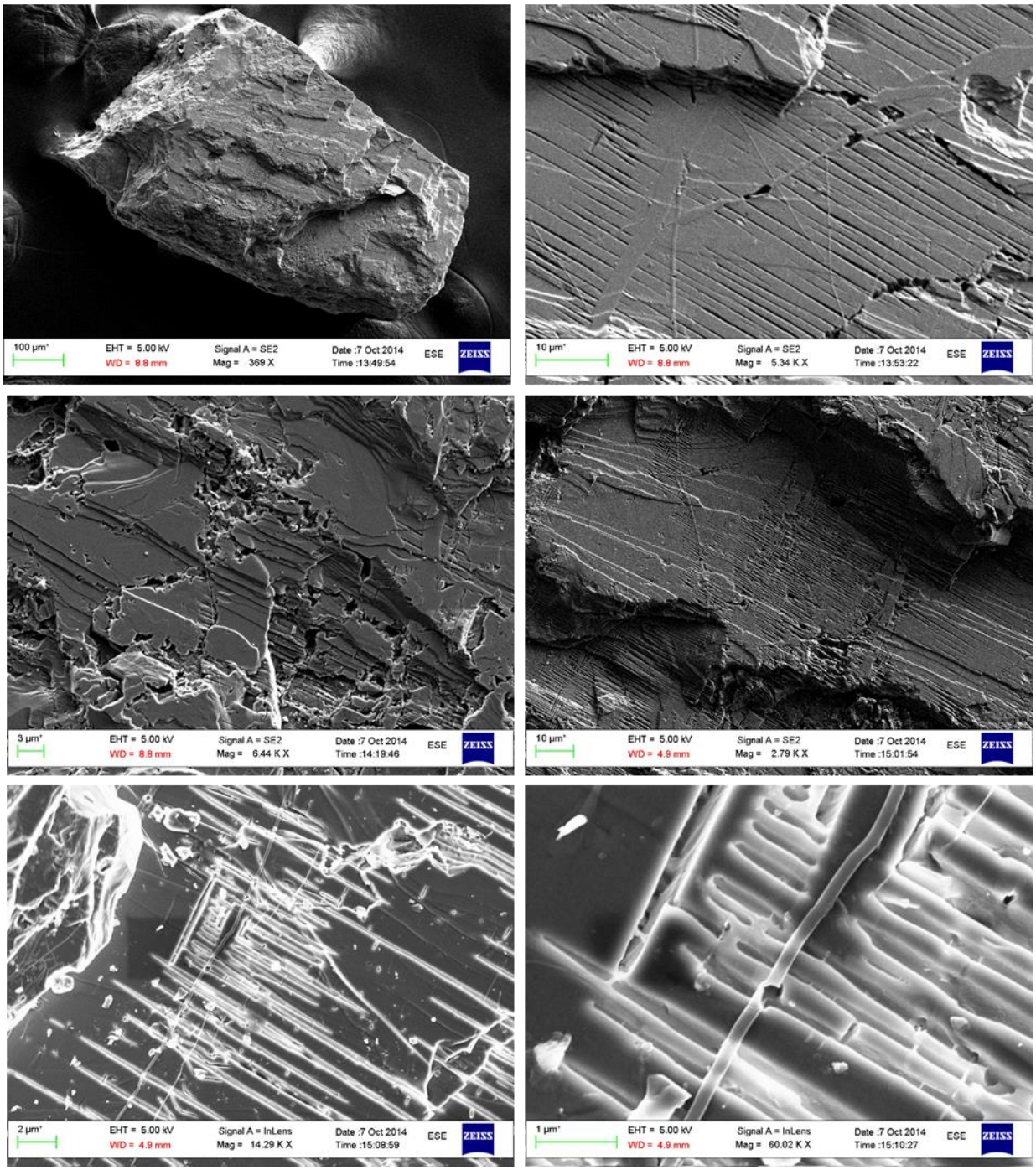

Anorthosite ID. 2

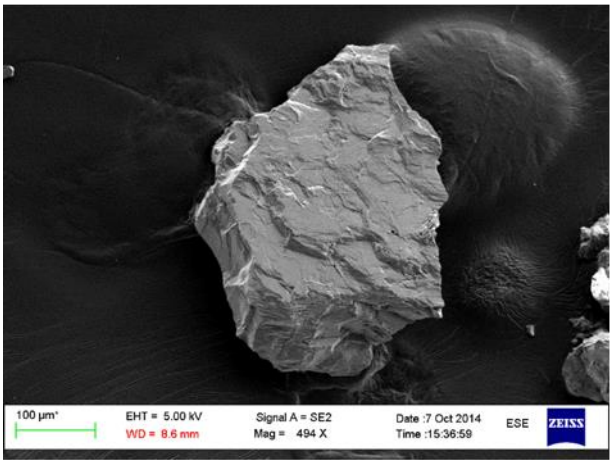

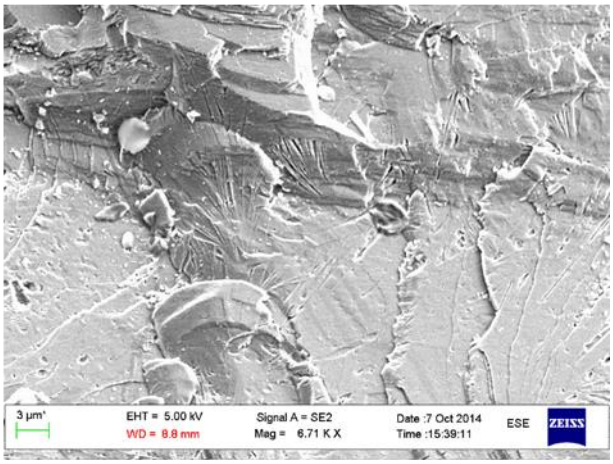

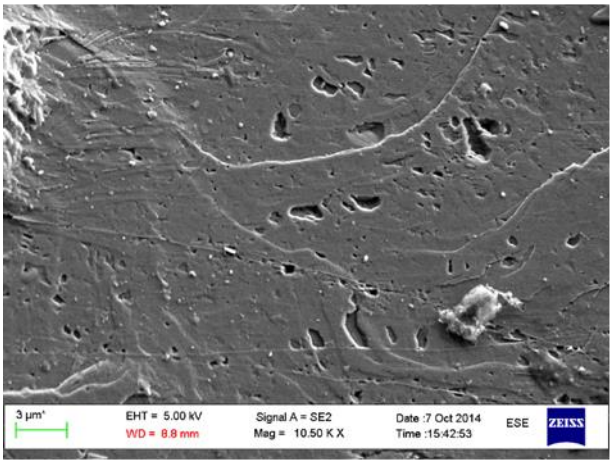

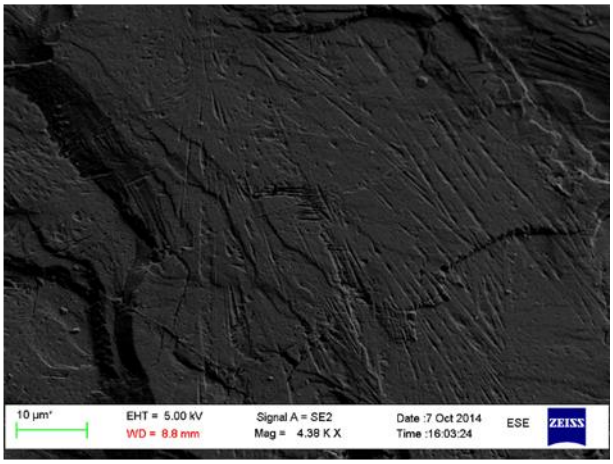

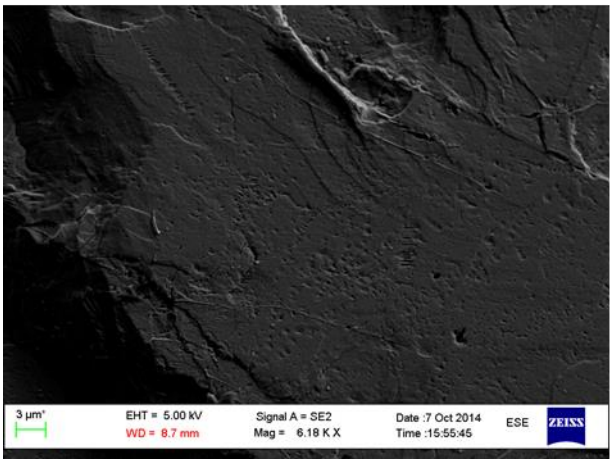

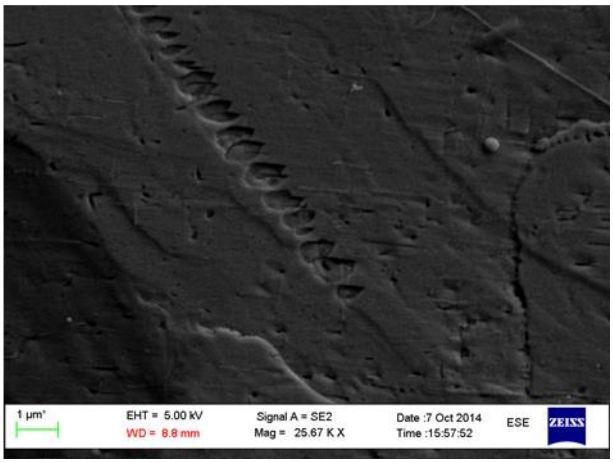

Anorthosite ID. 3

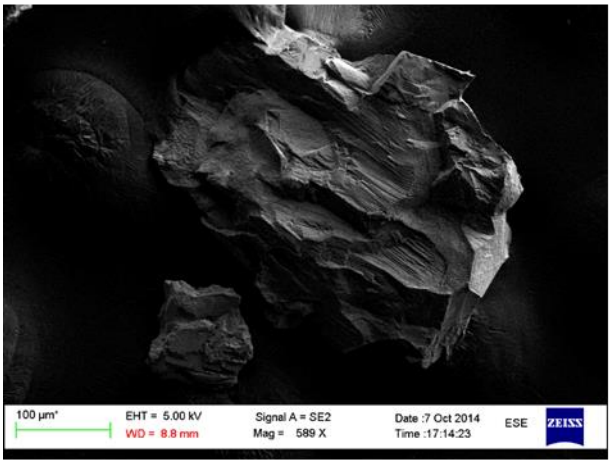

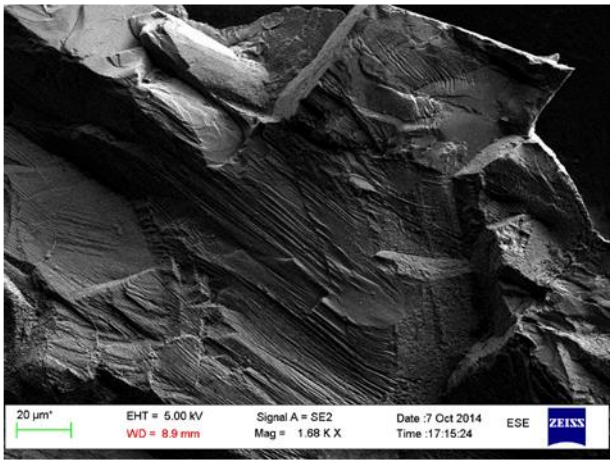

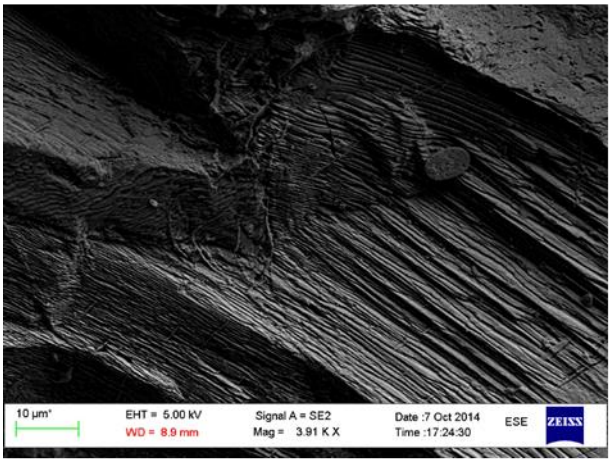

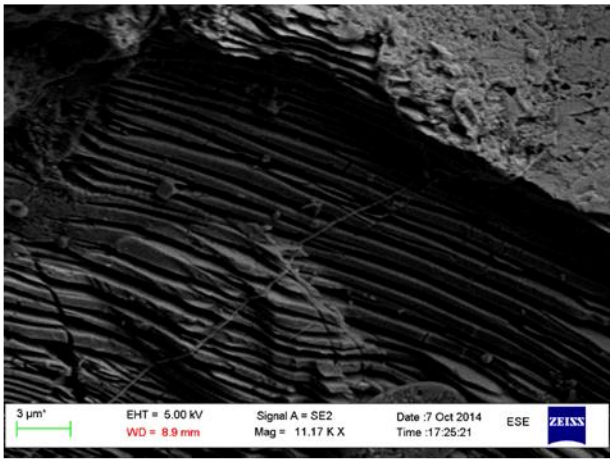

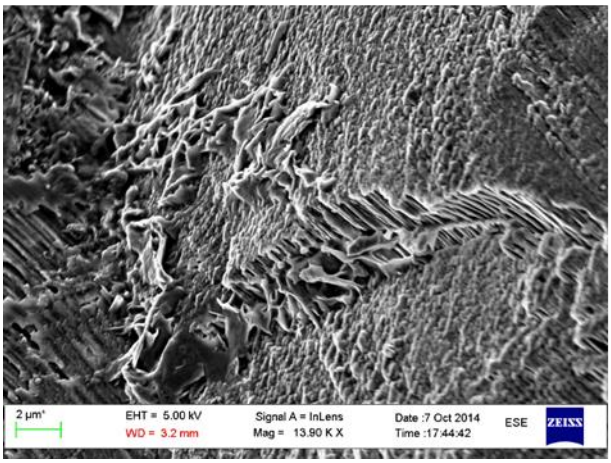

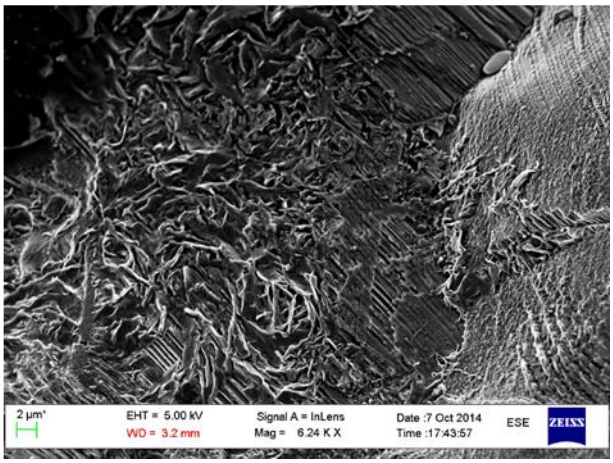

Anorthosite ID. 4

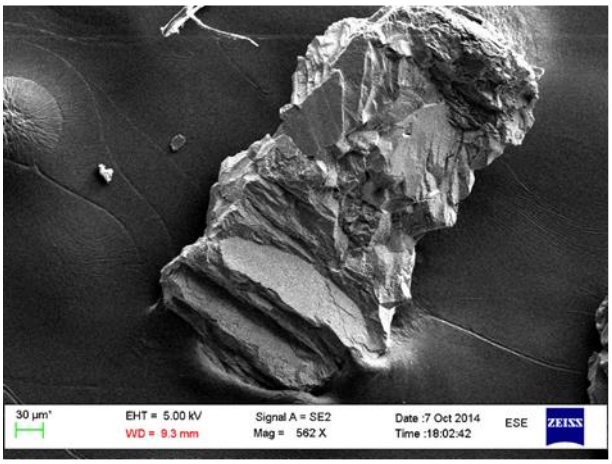

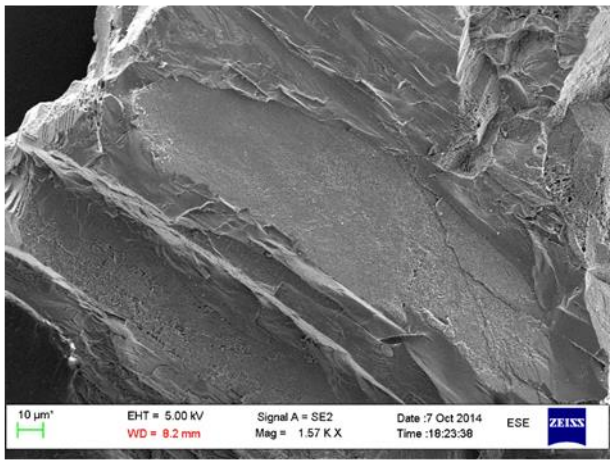

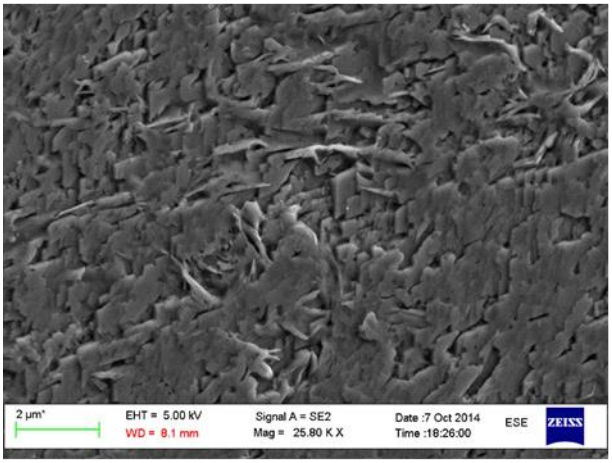

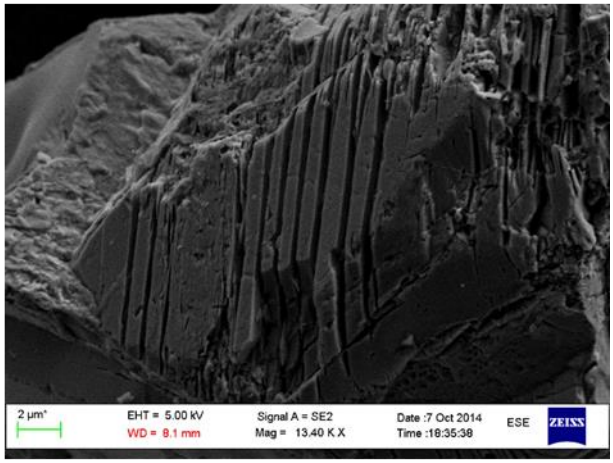

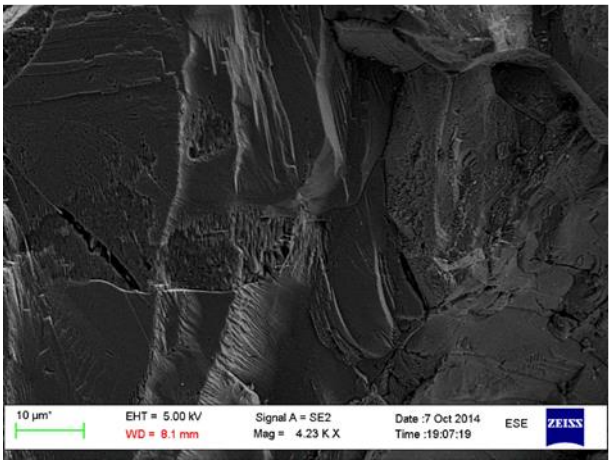

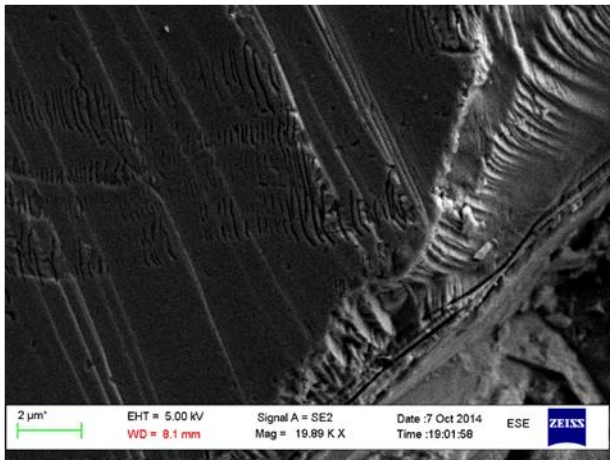

Anorthosite ID. 5

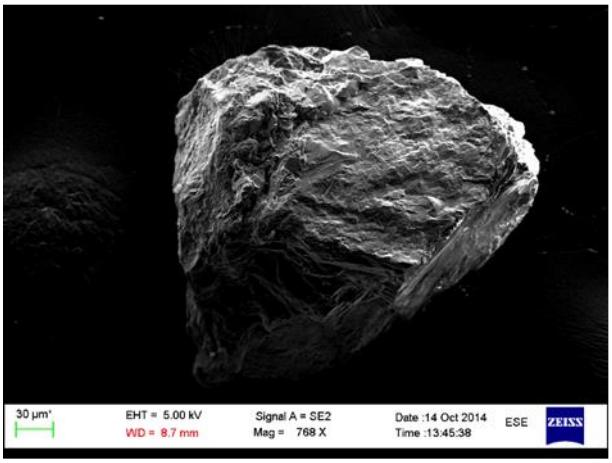

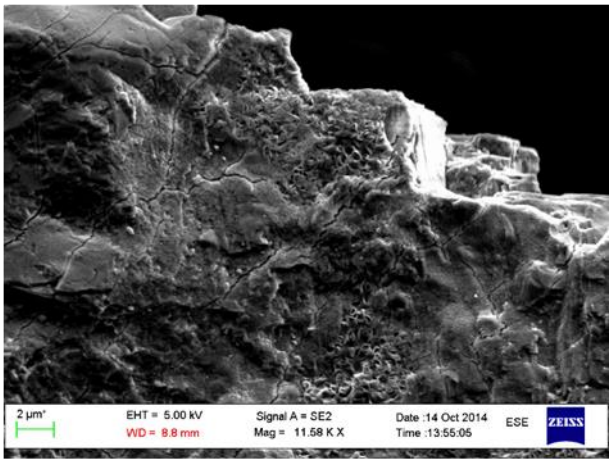

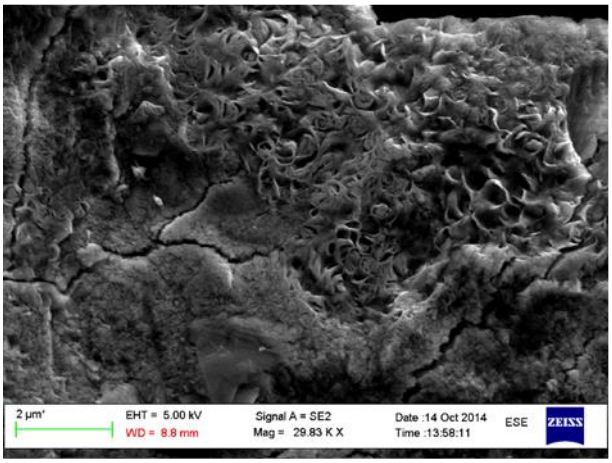

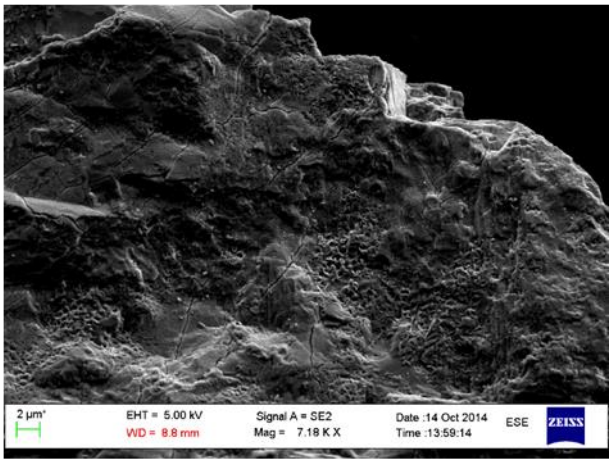

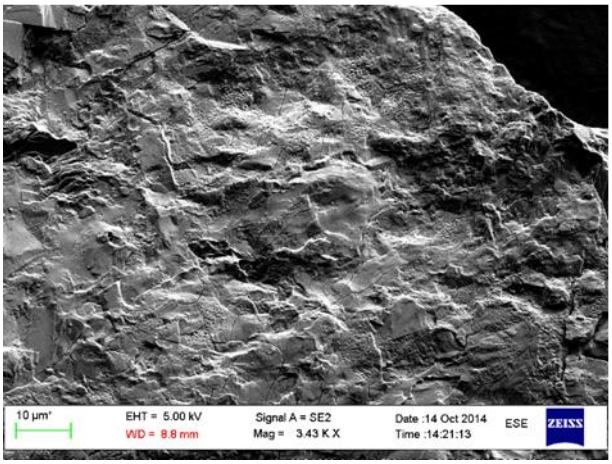

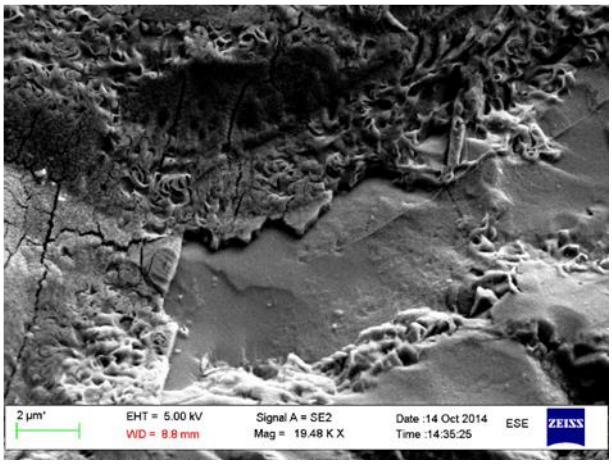

Anorthosite ID. 6

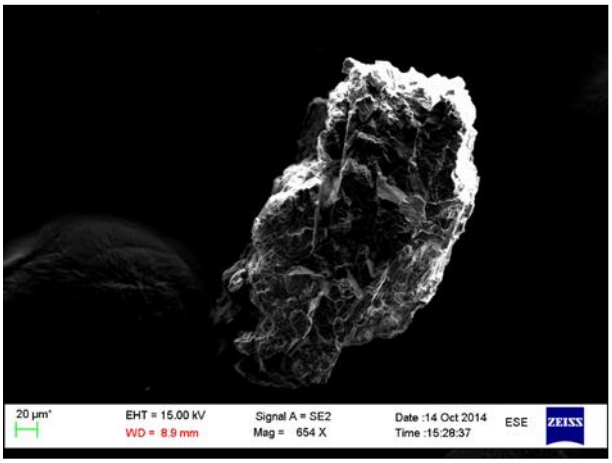

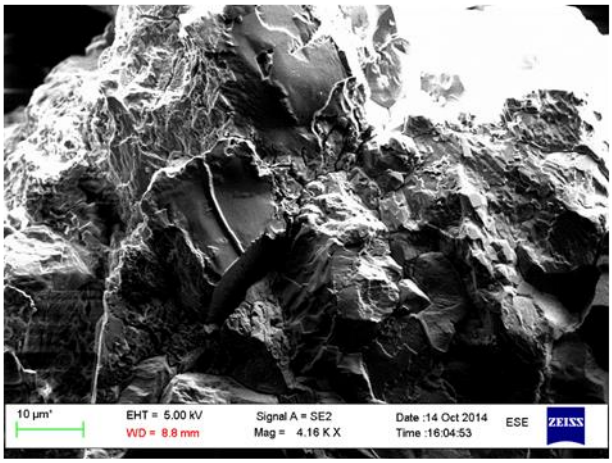

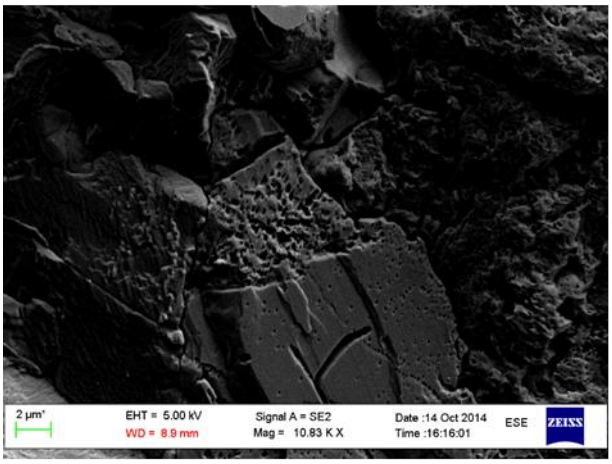

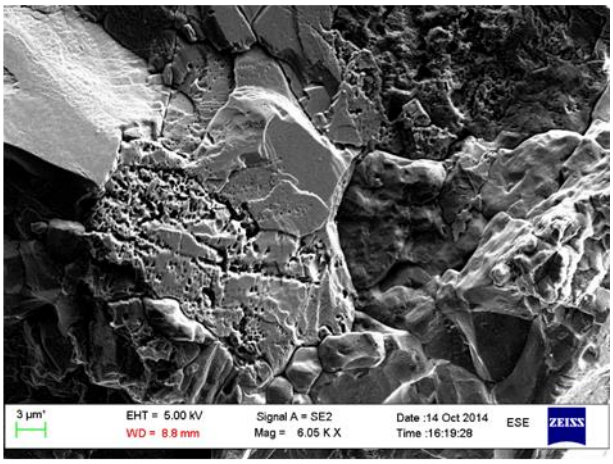

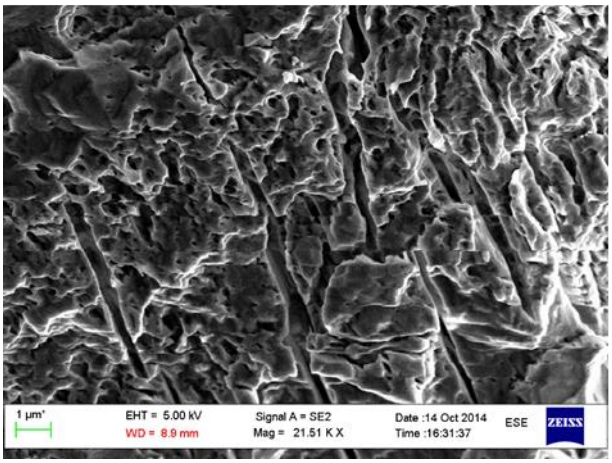

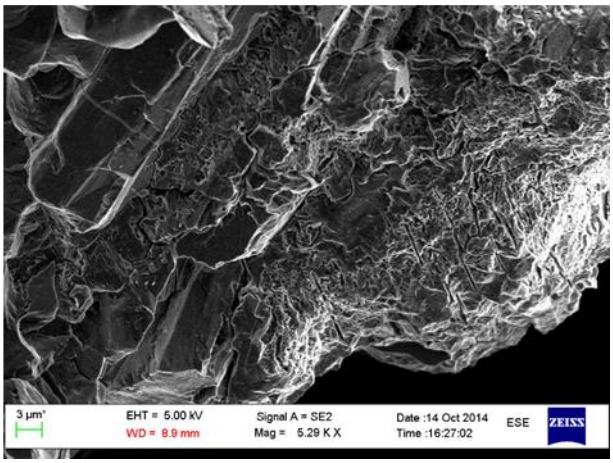

Anorthosite ID. 7

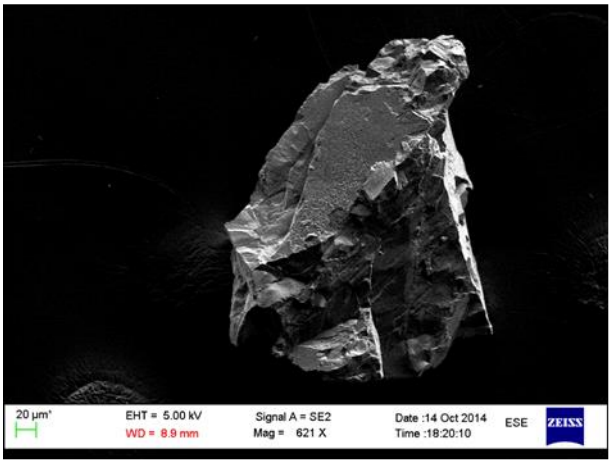

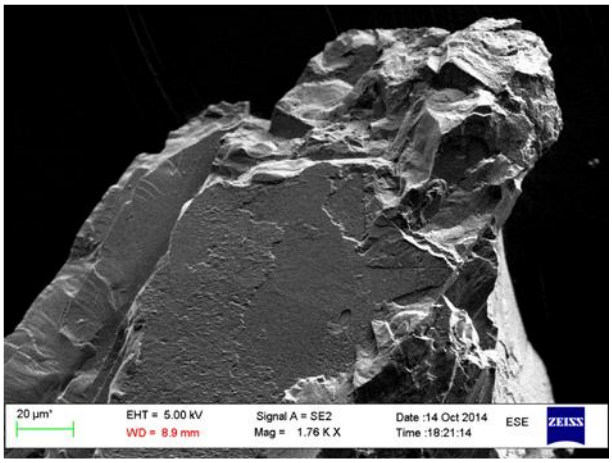

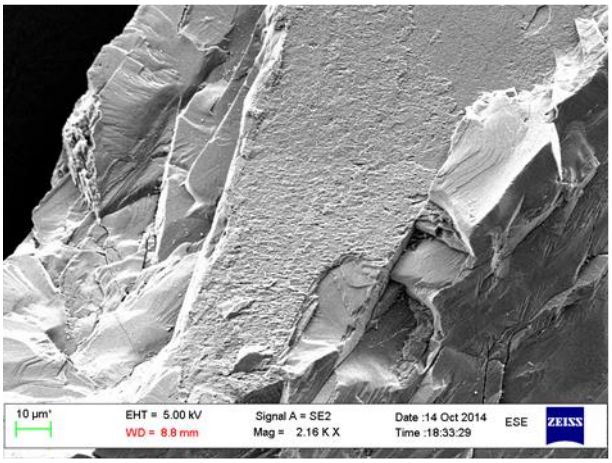

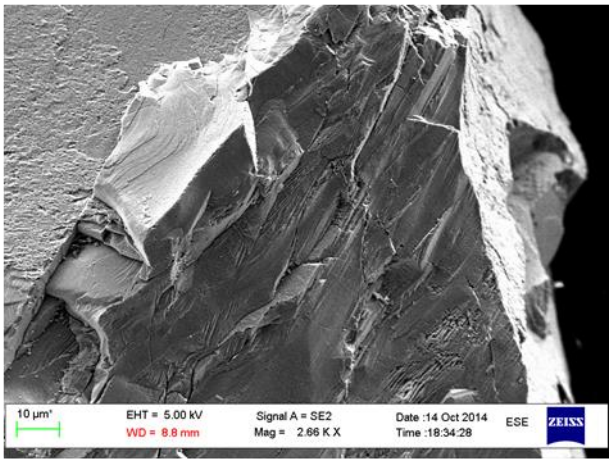

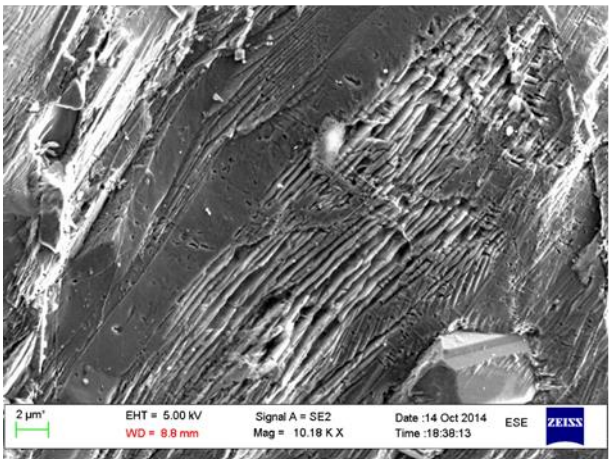

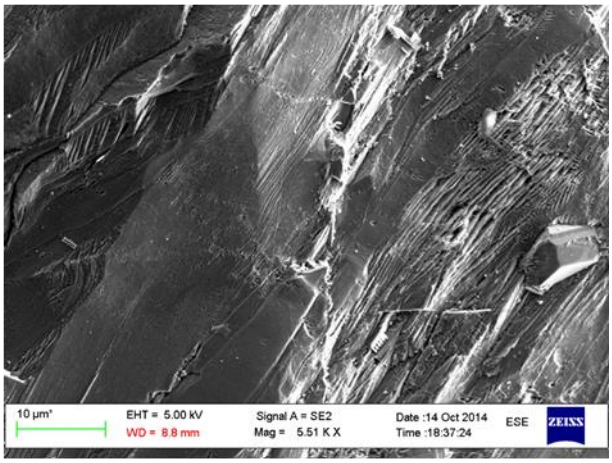

Anorthosite ID. 8

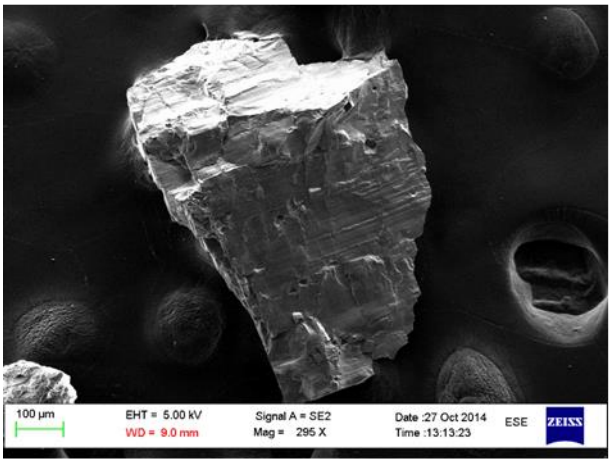

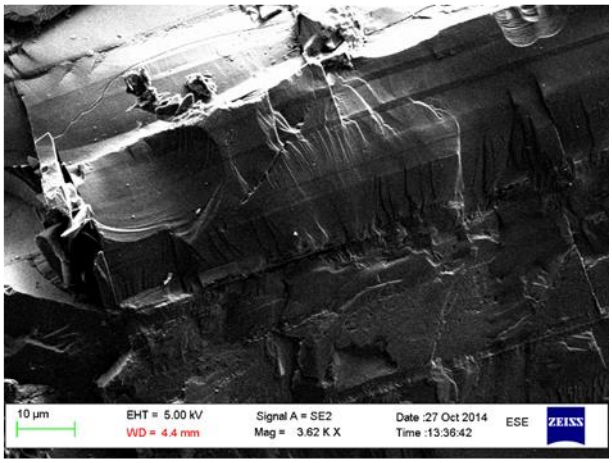

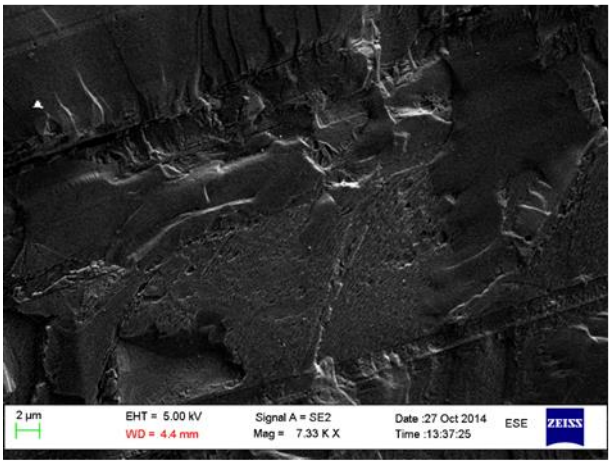

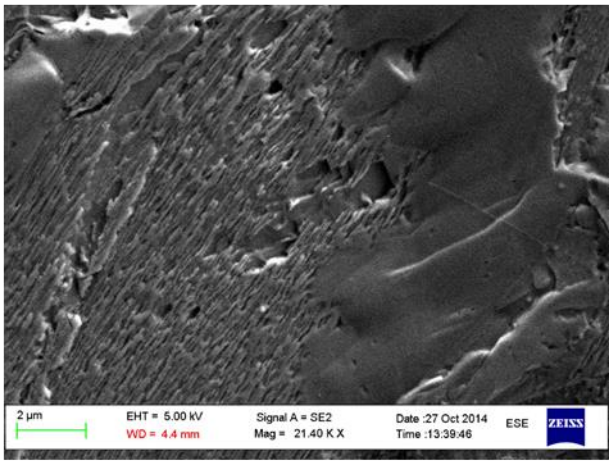

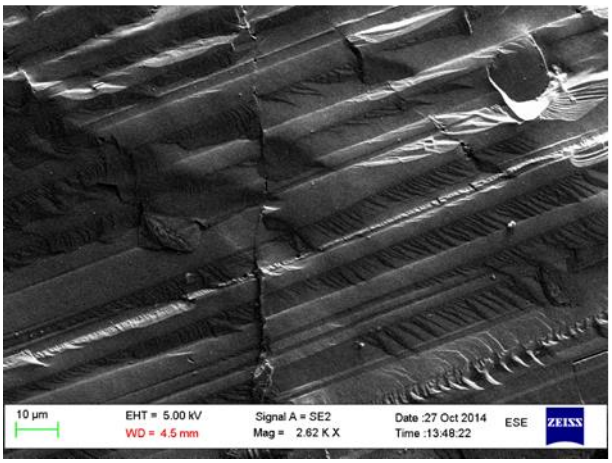

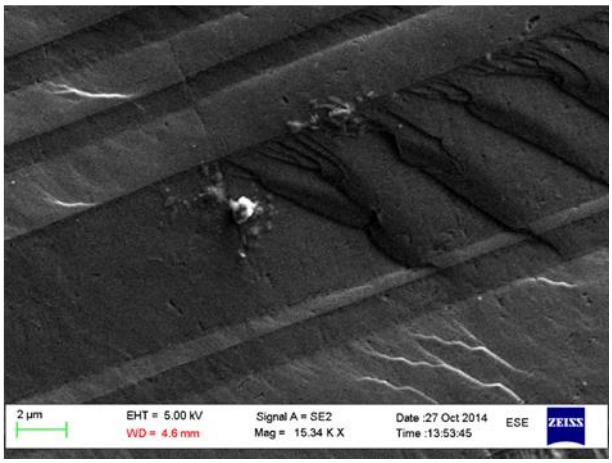

Anorthosite ID. 9

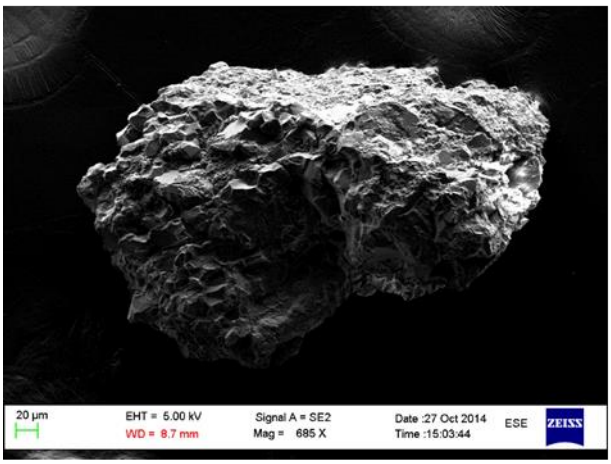

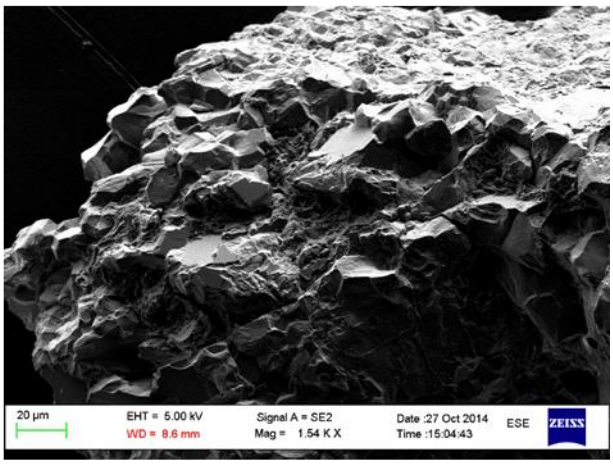

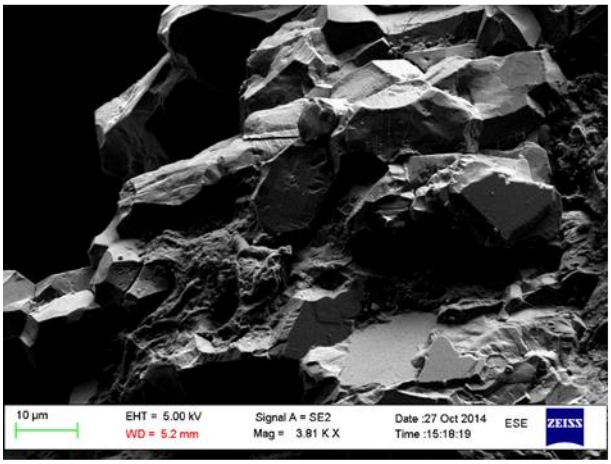

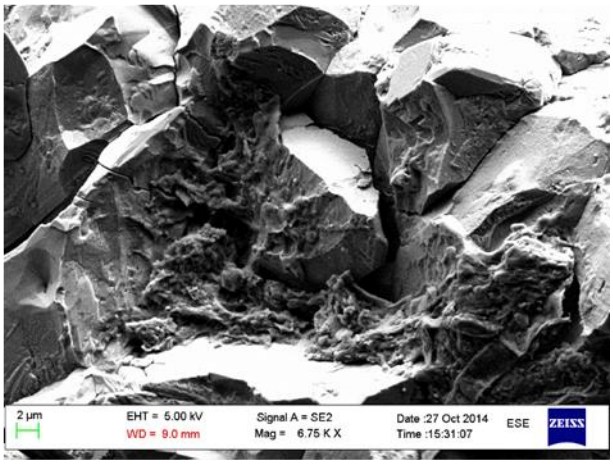

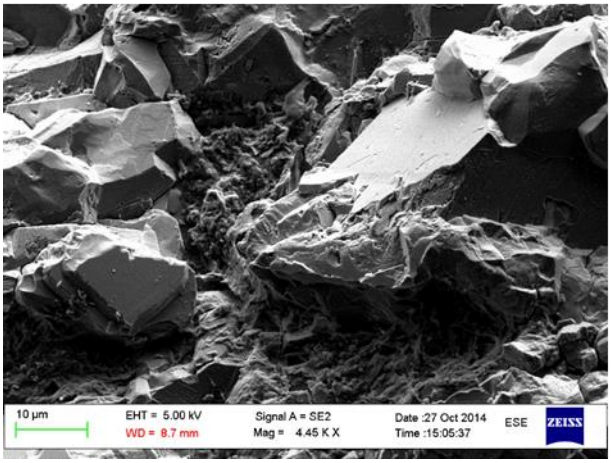

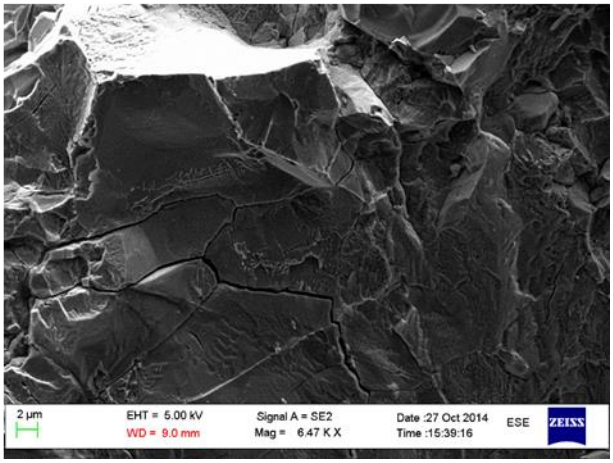

Anorthosite ID. 10

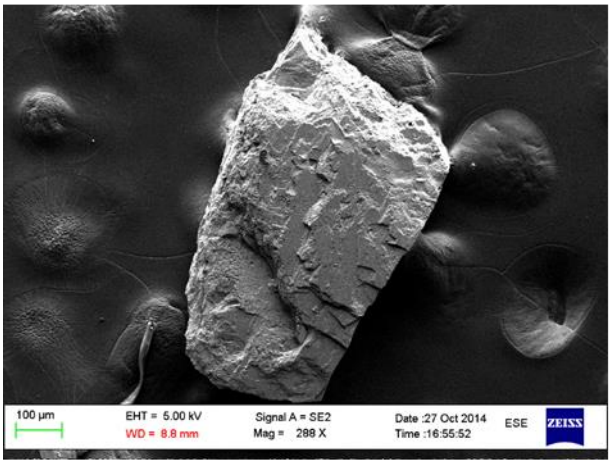

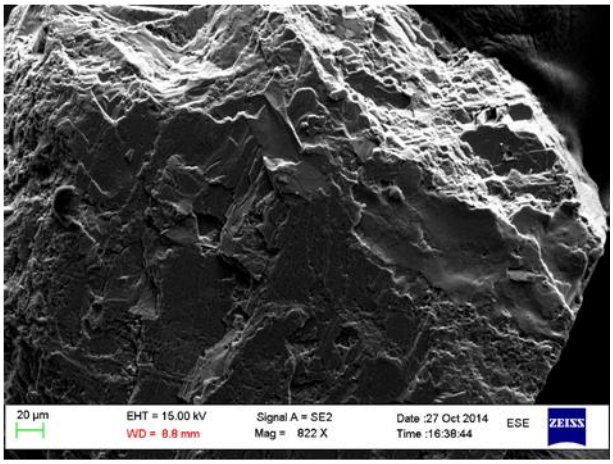

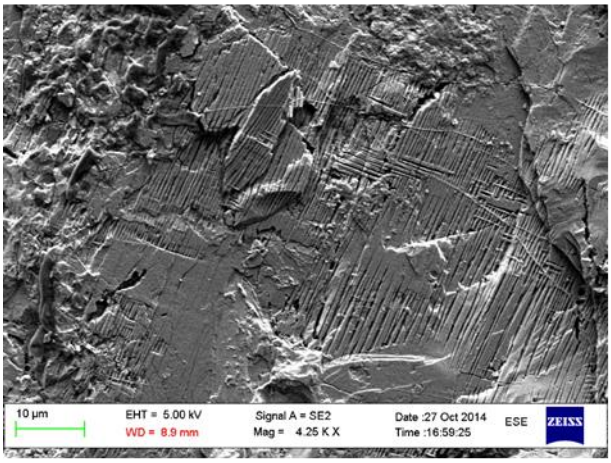

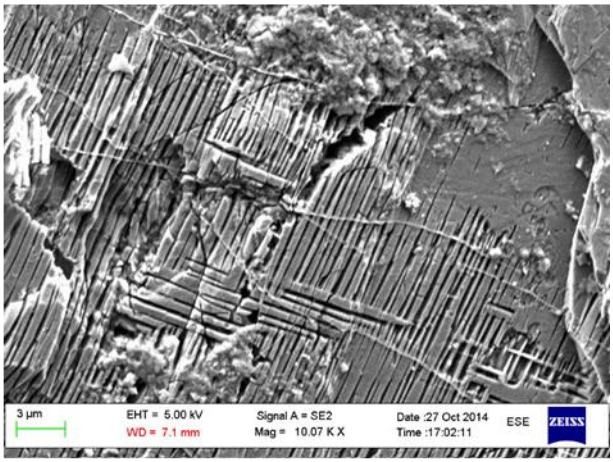

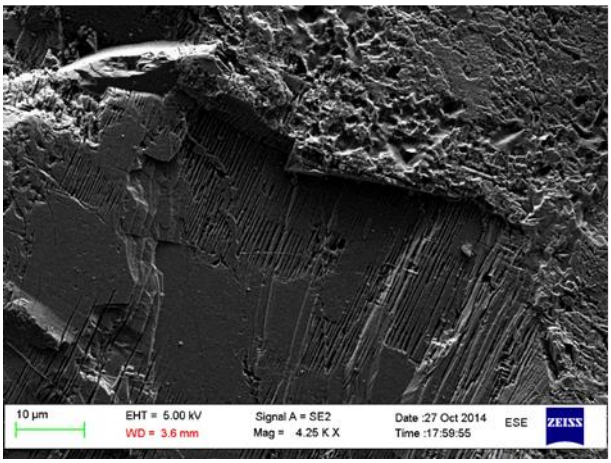

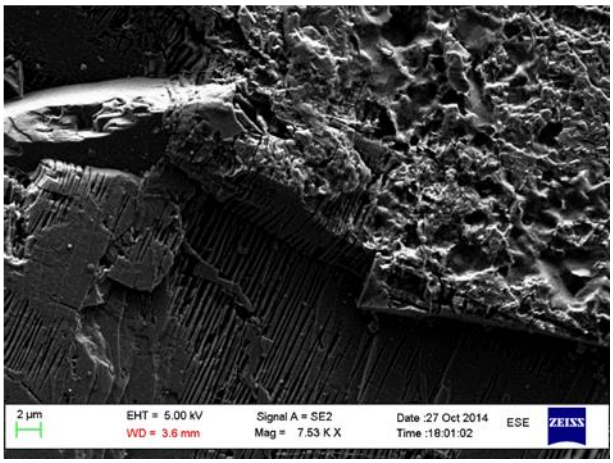

Anorthosite ID. 11

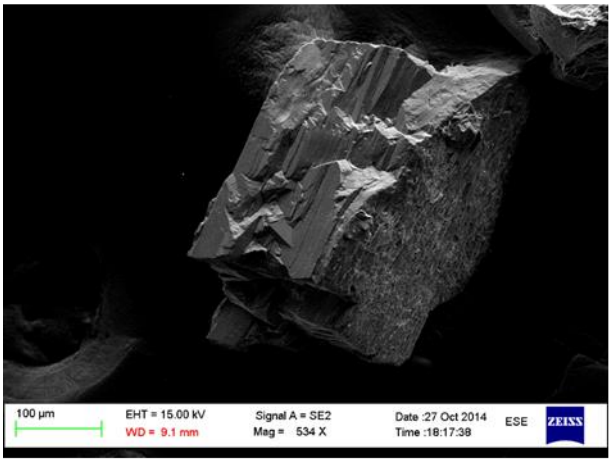

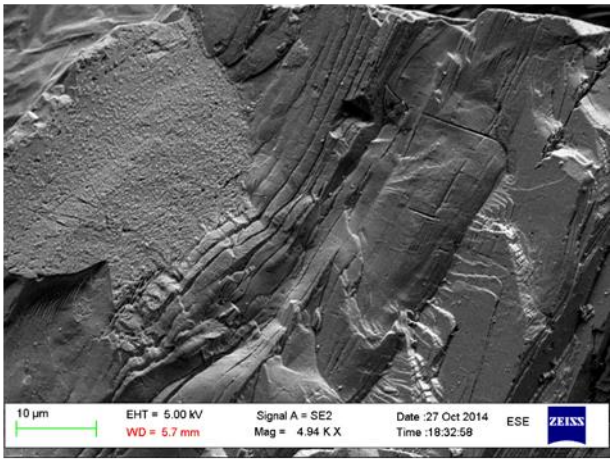

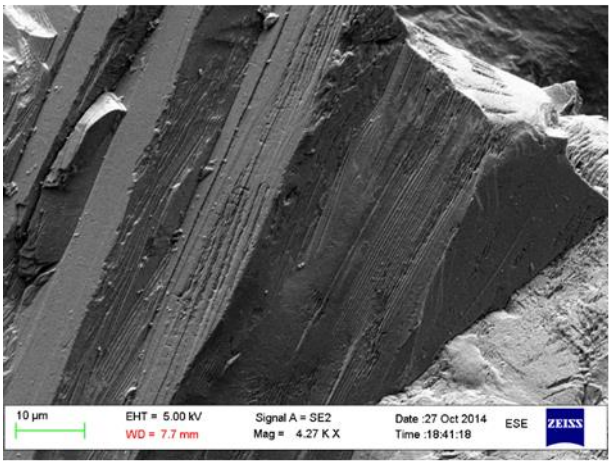

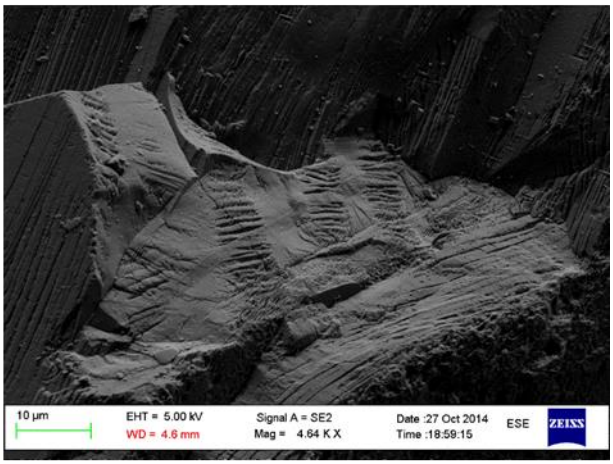

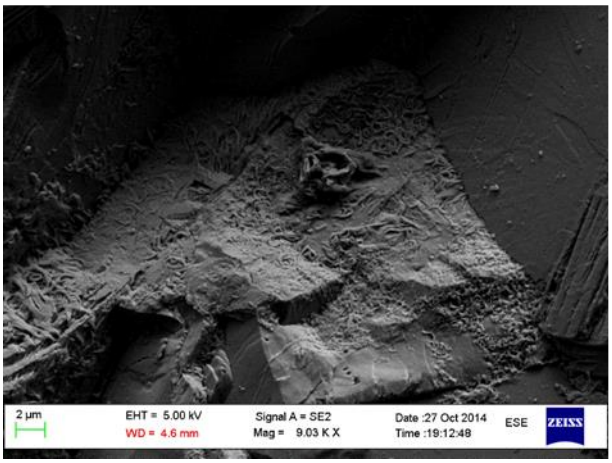

Anorthosite ID. 12

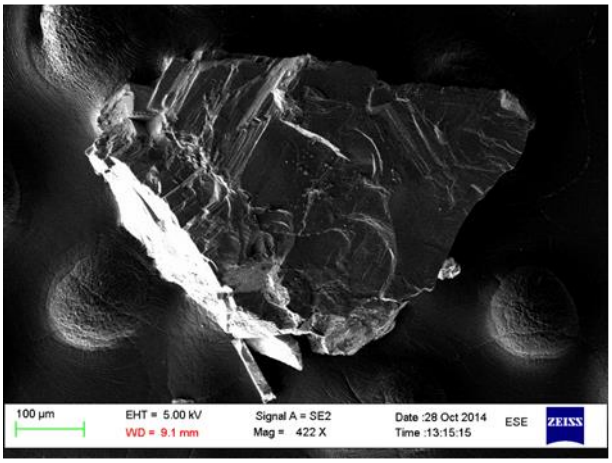

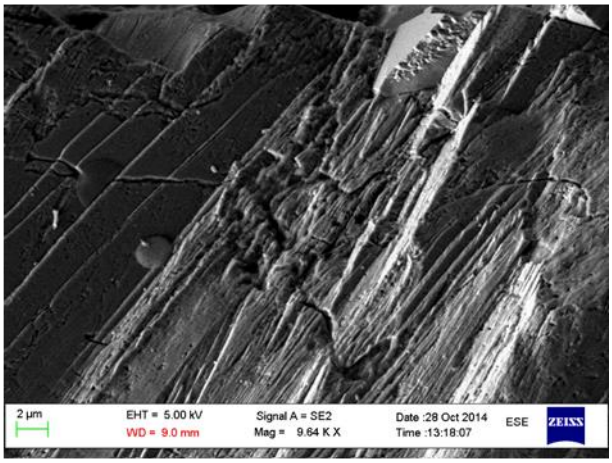

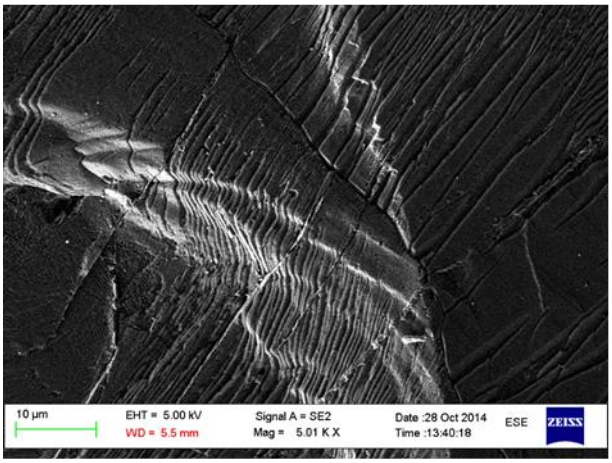

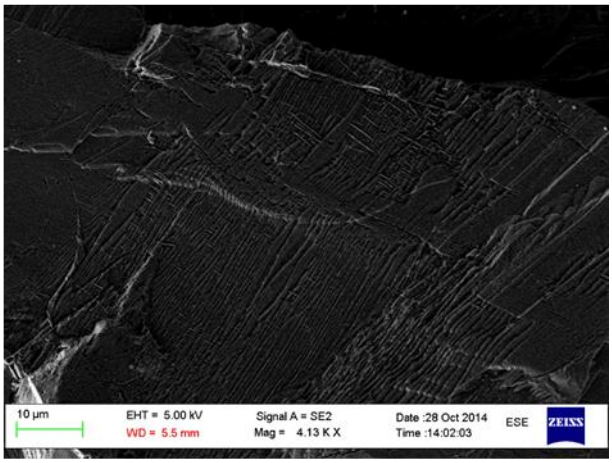

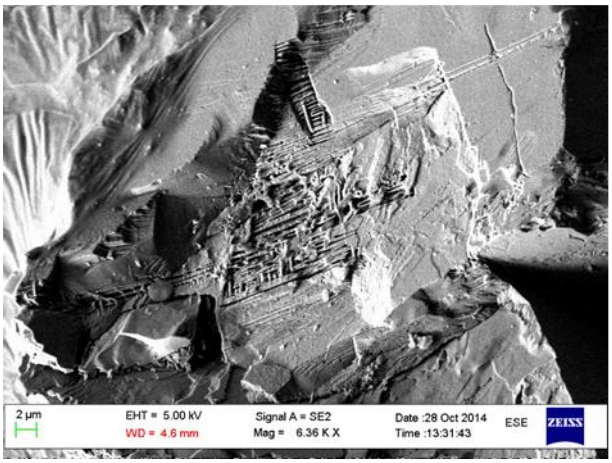

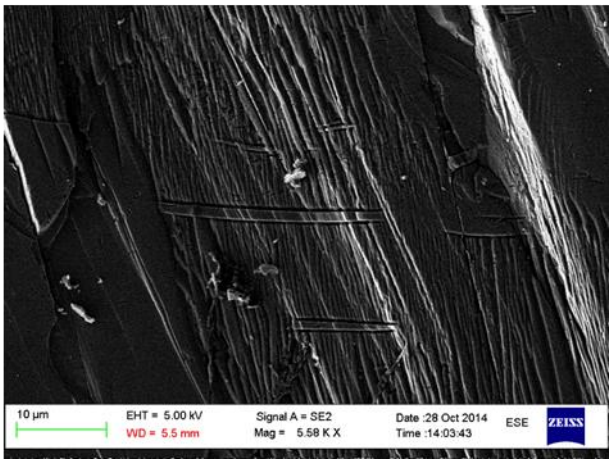

Anorthosite ID. 12

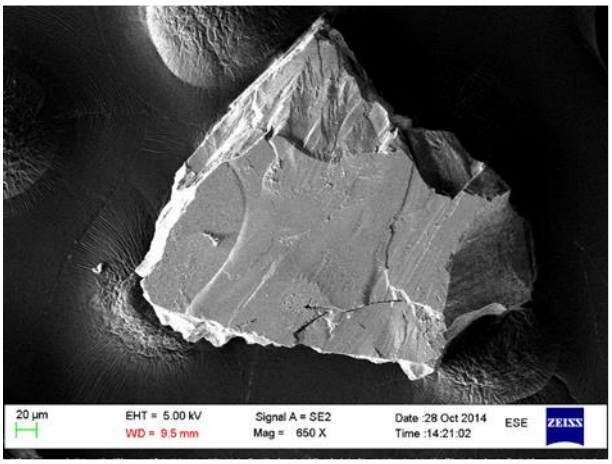

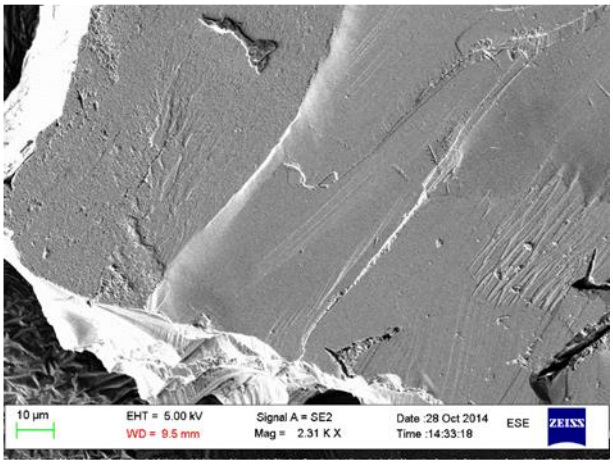

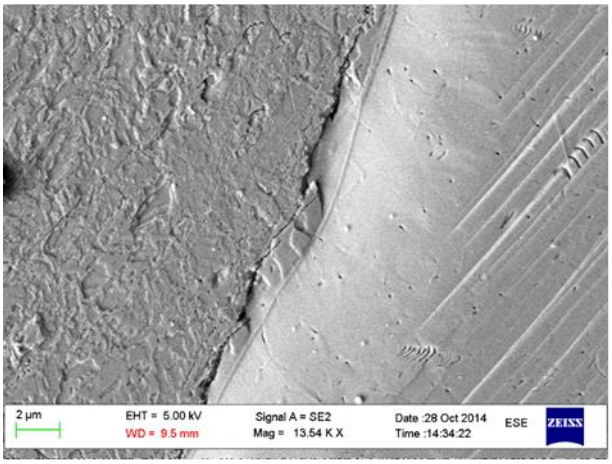

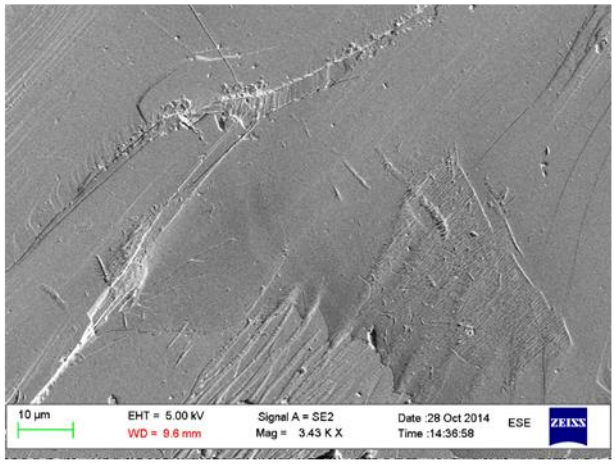

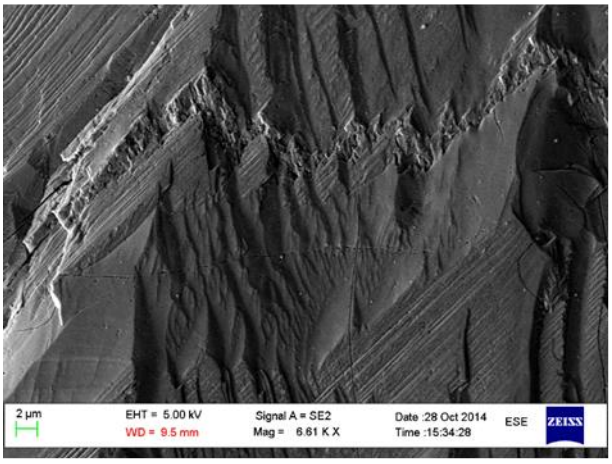

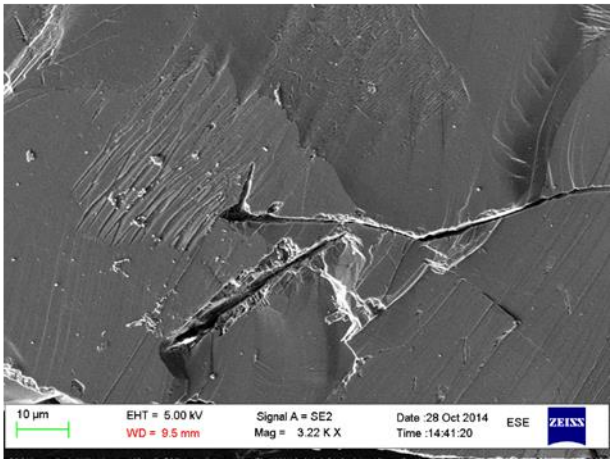

Anorthosite ID. 14

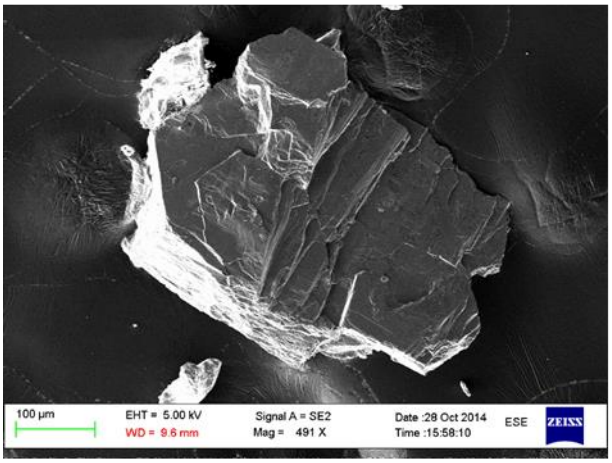

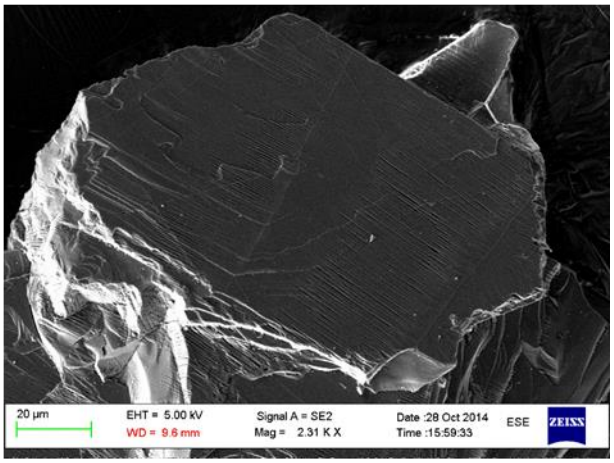

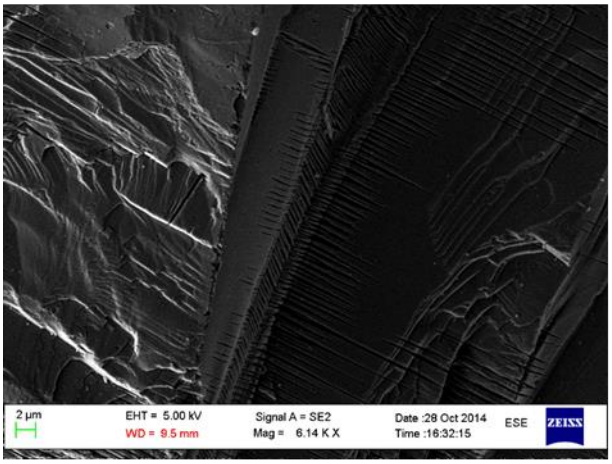

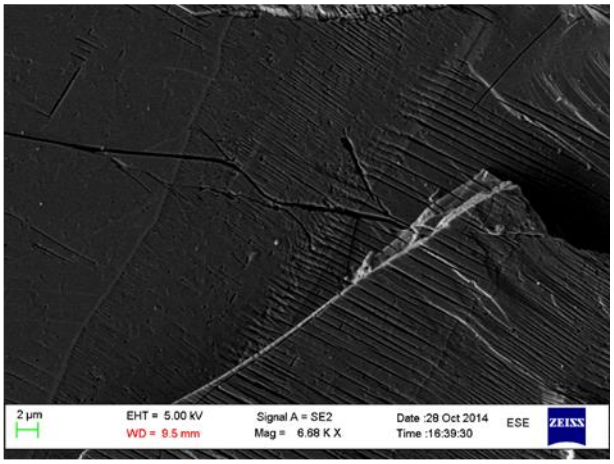

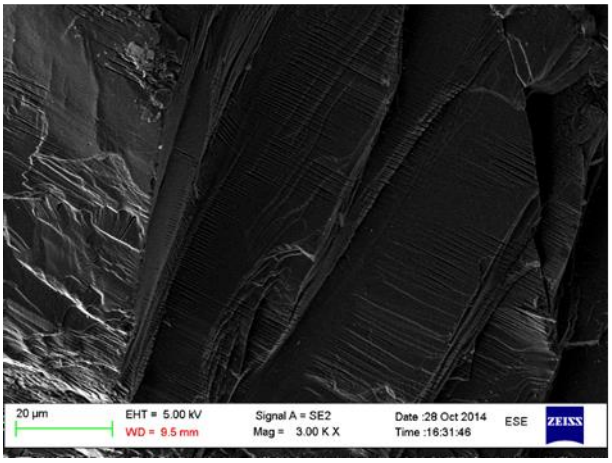

Anorthosite ID. 15

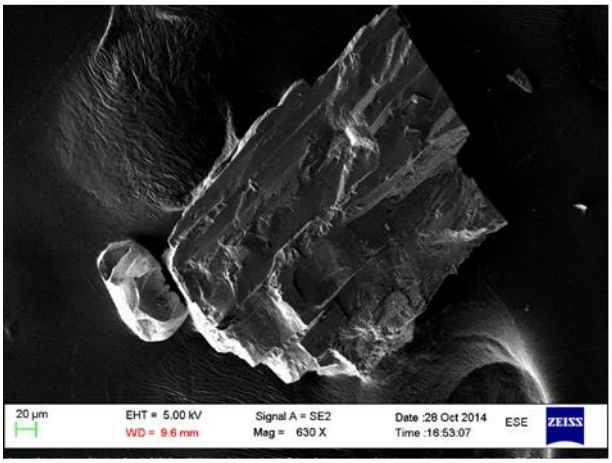

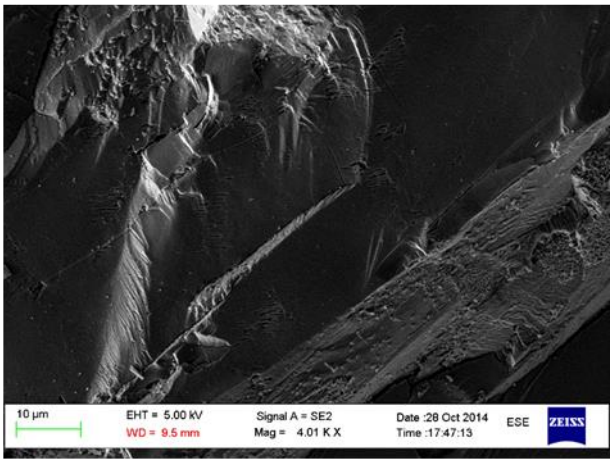

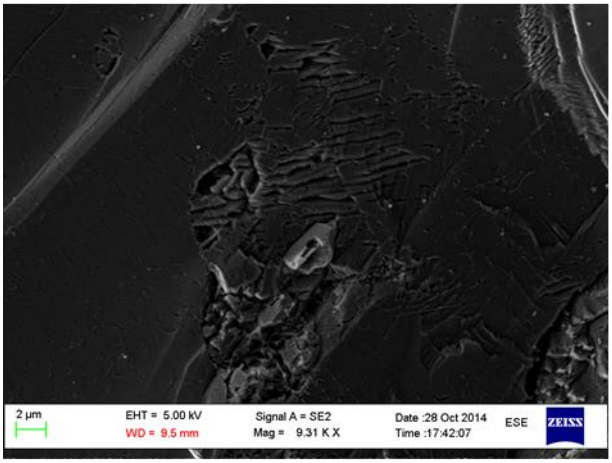

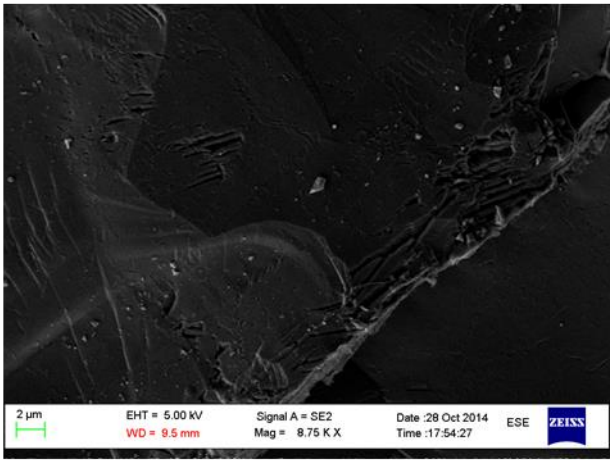

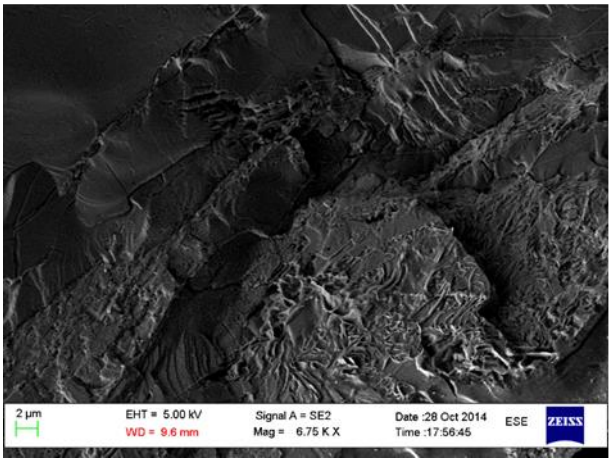

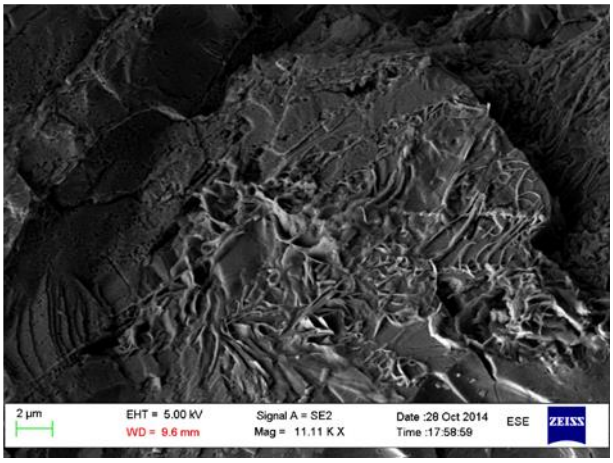

Anorthosite ID. 16

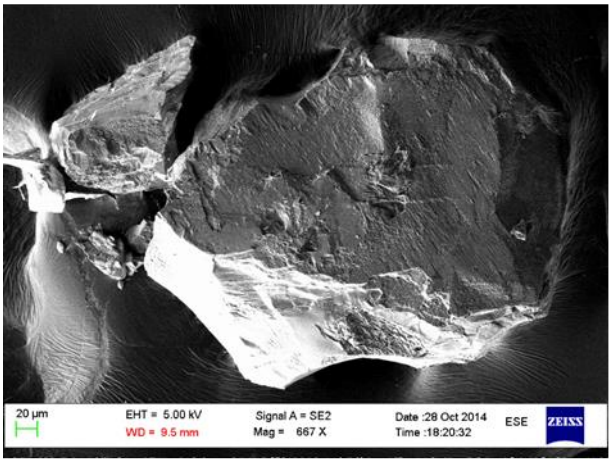

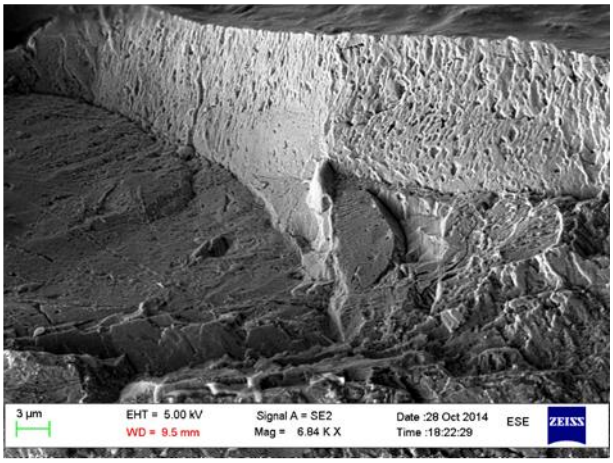

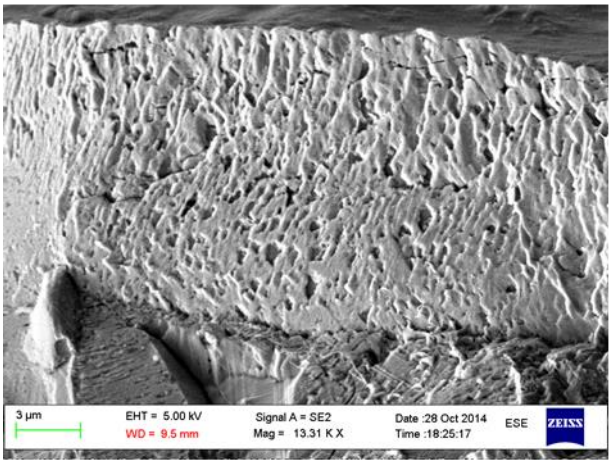

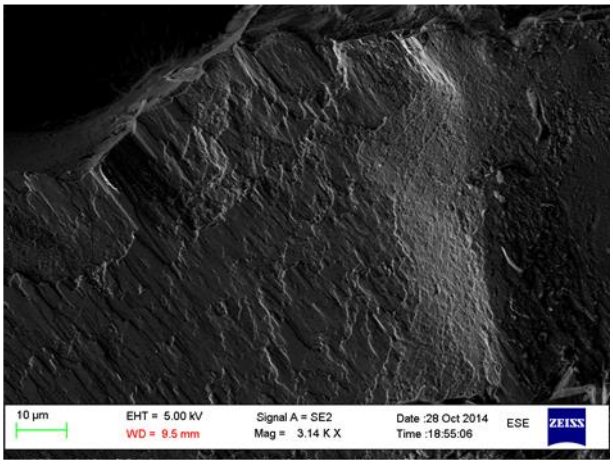

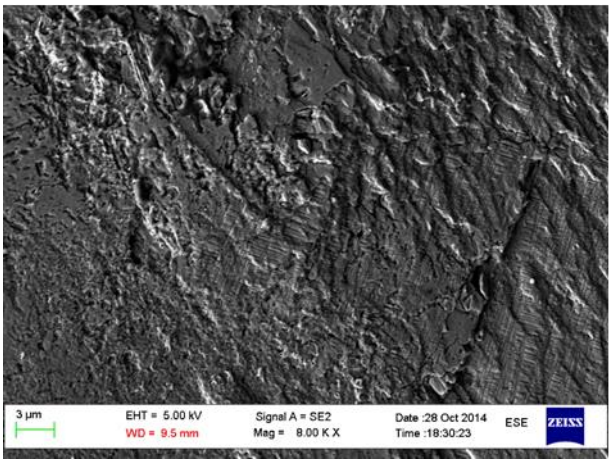

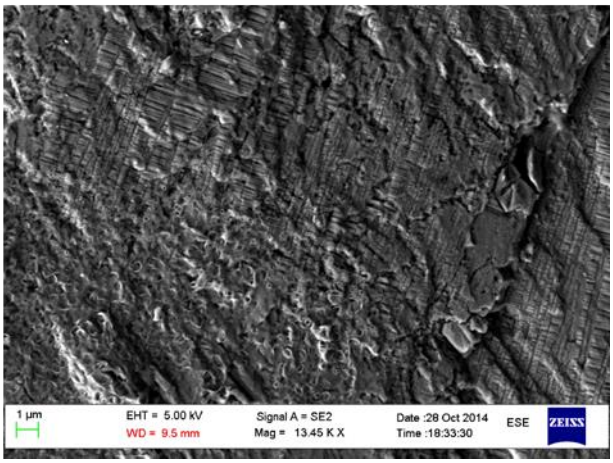

Anorthosite ID. 17

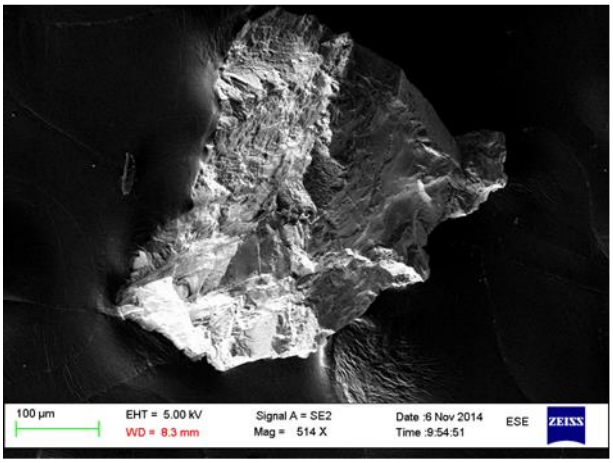

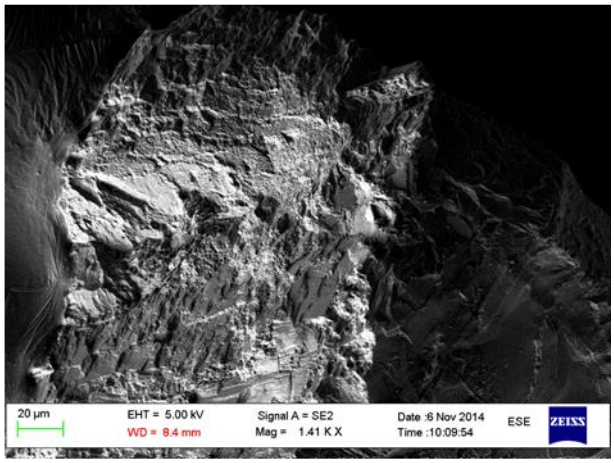

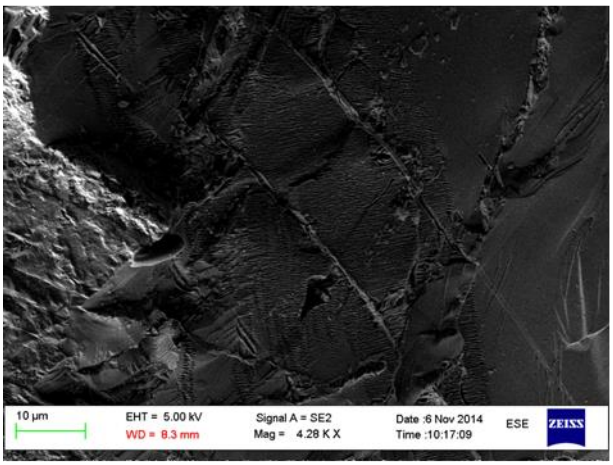

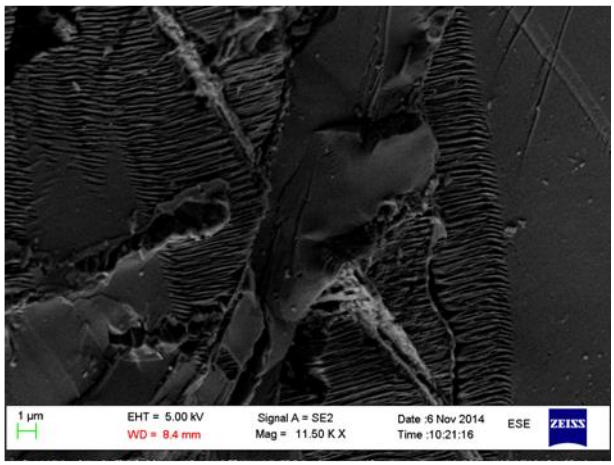

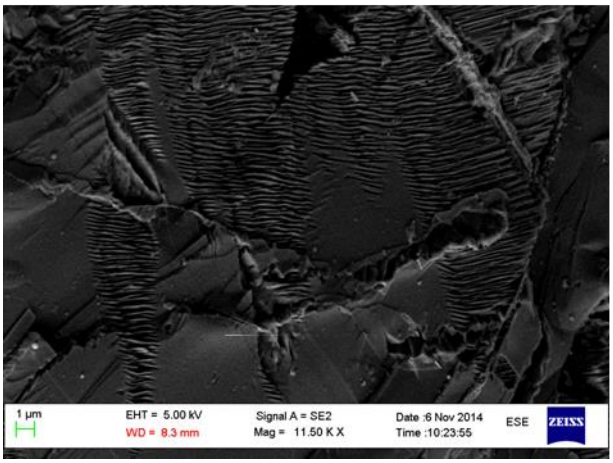

Anorthosite ID. 18

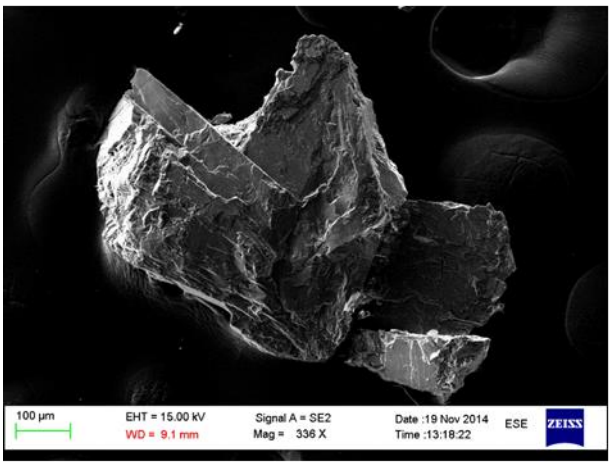

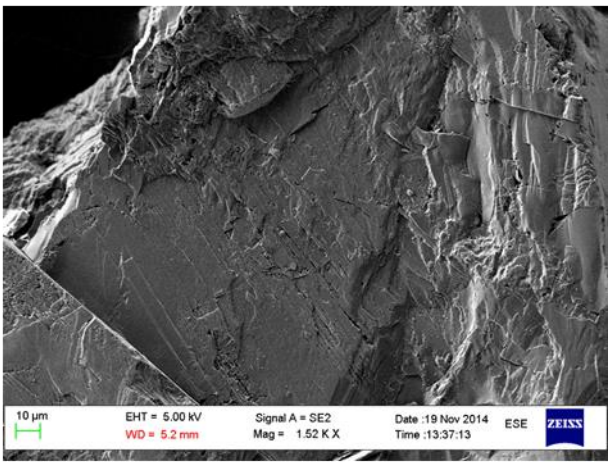

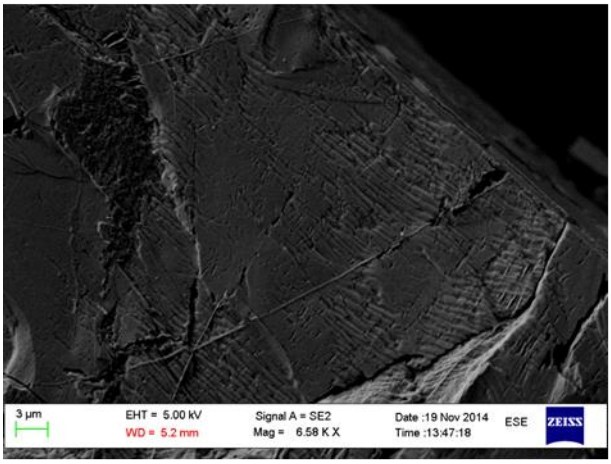

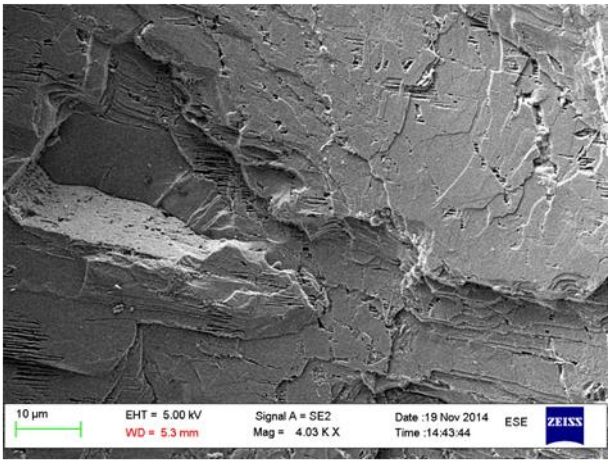

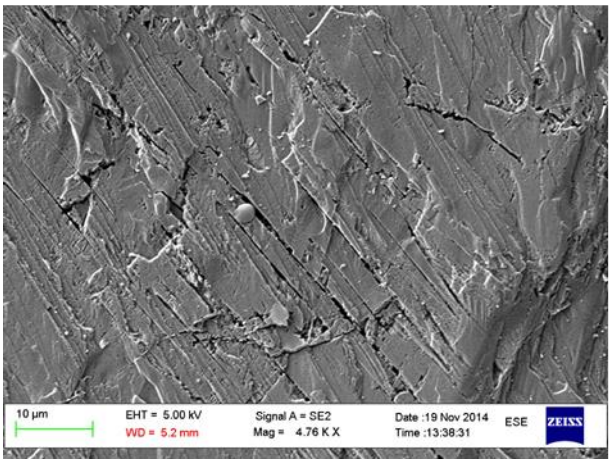

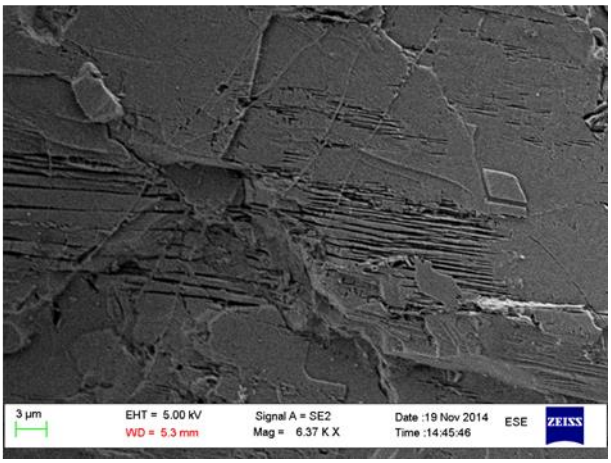

Anorthosite ID. 19

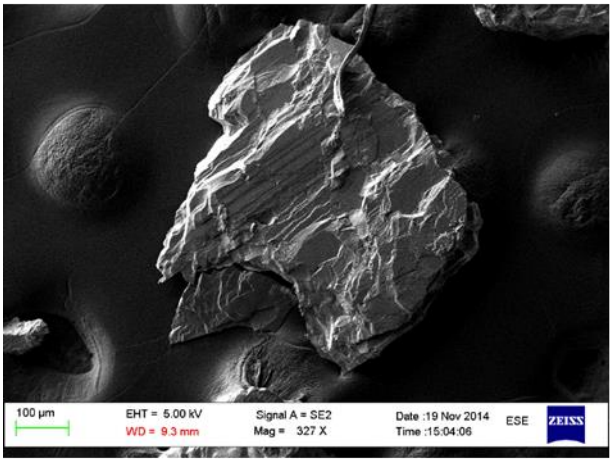

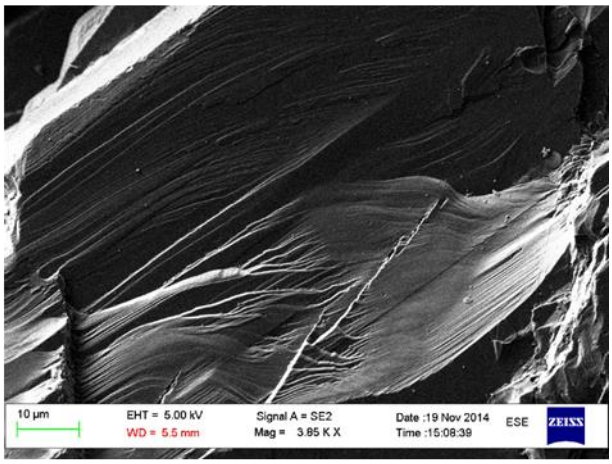

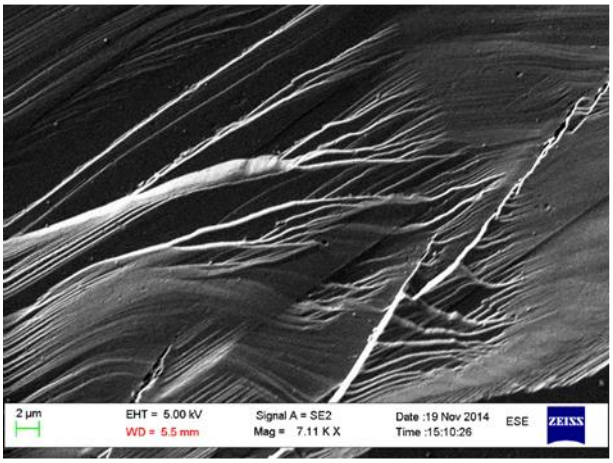

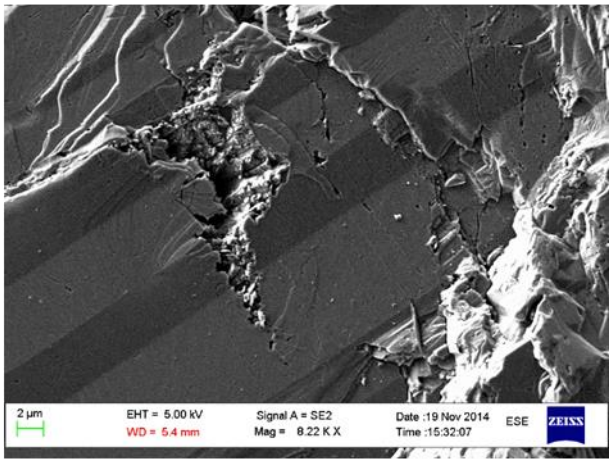

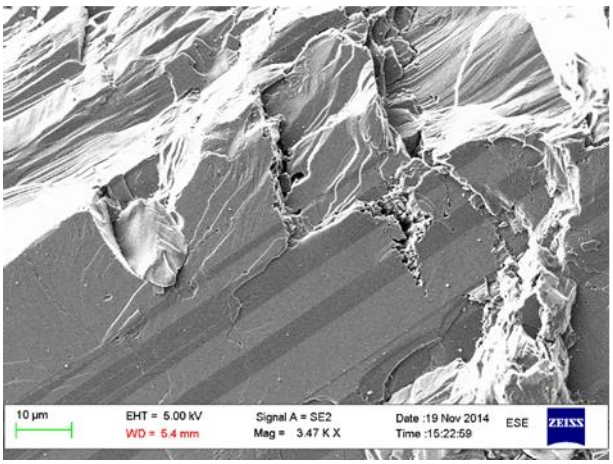

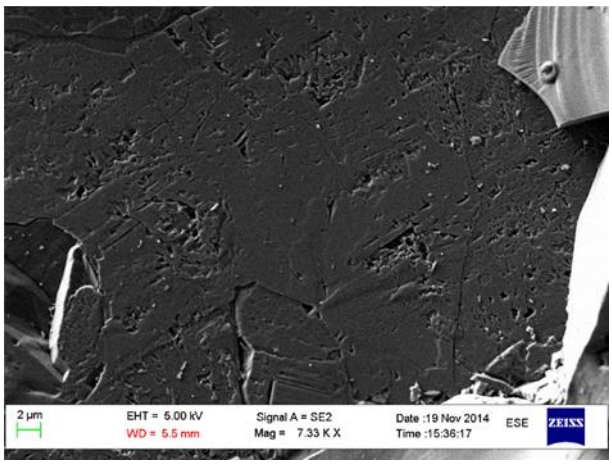

Anorthosite ID. 20

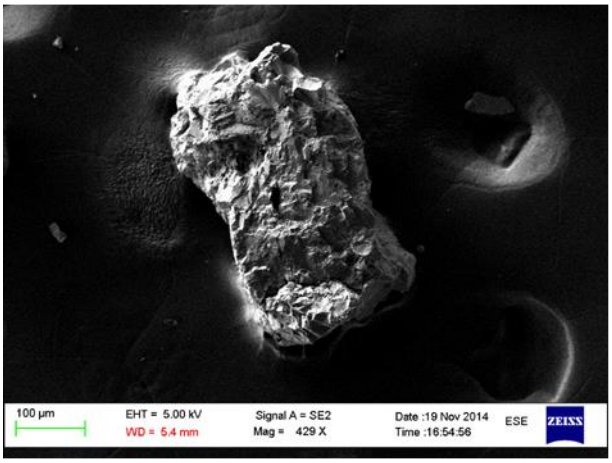

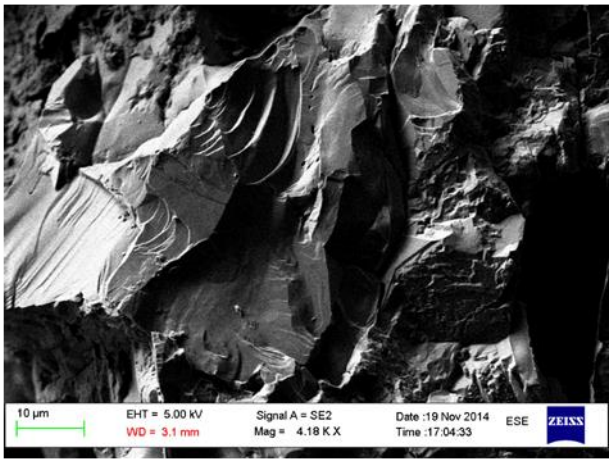

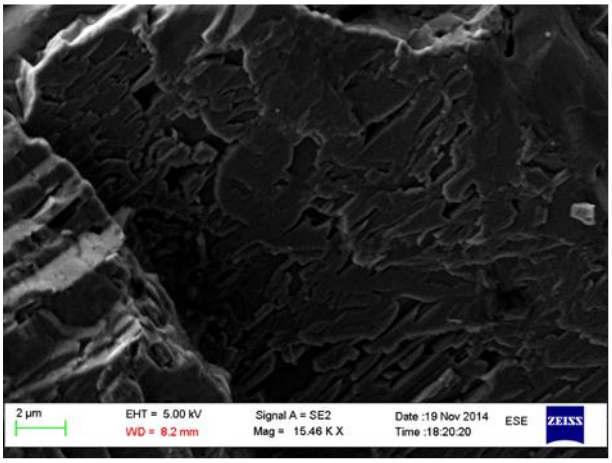

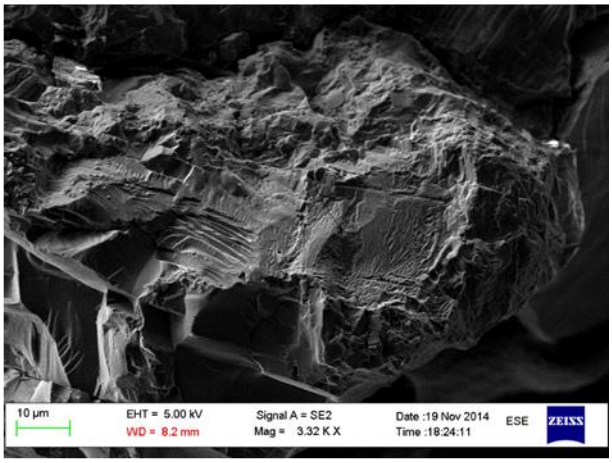

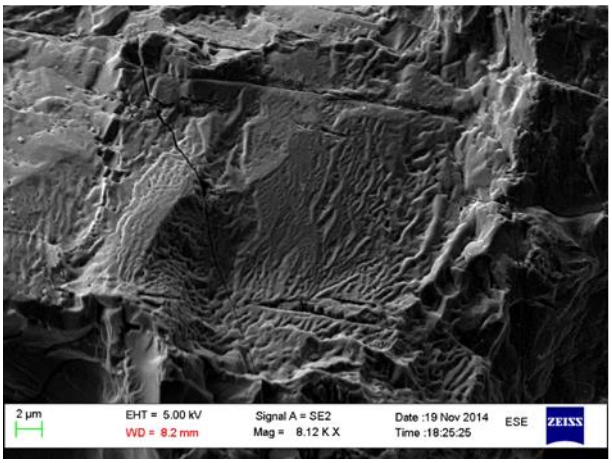

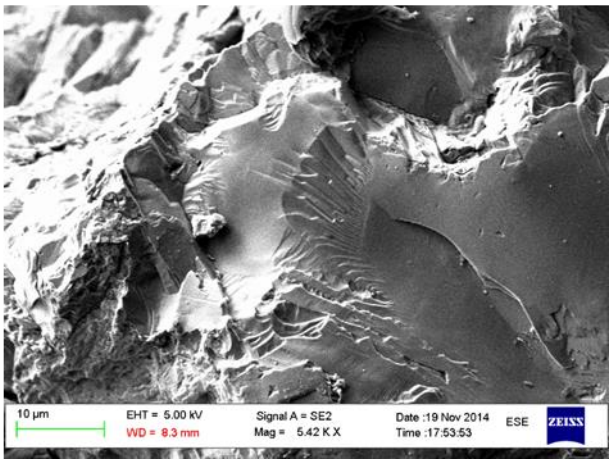

Anorthosite ID. 21